# ESTIMATION OF SOIL LOSS IN TUIRIAL WATERSHED

**A THESIS SUBMITTED IN PARTIAL FULFILLMENT OF THE REQUIREMENTS FOR THE DEGREE OF DOCTOR OF PHILOSOPHY**


**IMANUEL LAWMCHULLOVA**

**MZU REGISTRATION NO.: 3189 of 2014**

**Ph.D. REGISTRATION NO.: MZU/Ph.D. /1793 of 28.08.2021**




**DEPARTMENT OF GEOGRAPHY AND RESOURCE MANAGEMENT**

**SCHOOL OF EARTH SCIENCES AND NATURAL RESOURCE MANAGEMENT**


**MARCH, 2025**

# ESTIMATION OF SOIL LOSS IN TUIRIAL WATERSHED

**BY**

**IMANUEL LAWMCHULLOVA**

**DEPARTMENT OF GEOGRAPHY AND RESOURCE MANAGEMENT**

**Supervisor**

**Prof. VISHWAMBHAR PRASAD SATI**

**Submitted**

**In partial fulfillment of the requirement of the Degree of Doctor of Philosophy in Geography and Resource Management of Mizoram University, Aizawl**

**MIZORAM UNIVERSITY (A Central University)**

**Dr. Vishwambhar Prasad Sati**, ***D.Litt. Ph.D.***
**Senior Professor**
**Visiting Professor, IMPRI, New Delhi**
CAS-PIFI Fellow; VS-TWAS; VS-CAS; GF-ICSSR; VS-INSA
*Department of Geography and Resource Management*
*School of Earth Sciences*

Visiting Professor-Lviv University, Ukraine
Tanhril, Aizawl,
Mizoram- 796 004, India
Phone: (M) 090899 04889
E-mail: vpsati@mzu.edu.in
sati.vp@gmail.com

## CERTIFICATE

This is to certify that the thesis entitled "**Estimation of Soil Loss in Tuirial Watershed**", submitted by Imanuel Lawmchullova, under Registration No.: MZU/Ph. D./1793 of 28.08.2021, embodies the record of the original research endeavour carried out by him under my supervision. He has been duly registered and has fulfilled all the requirements laid down in the Ph. D. regulations of Mizoram University. I further certify that the thesis presented is worthy of being considered for the award of the Ph. D. degree. This research has not been submitted for the attainment of any research degree at any other university.

Place: Tanhril, Aizawl
Dated:

(PROF. VISHWAMBHAR PRASAD SATI)
Supervisor

**Formerly:** Professor of Geography in MPHE; **Scientific Editor:** Journal of Mountain Science, A Springer Publication; **Member Editorial Board:** (1) SAR, A Journal of Canadian Centre for Education and Research; (2) International Journal of Agricultural and Food Research (3) International General of Geosciences; **Expert Member:** ENVIS on Himalayan Ecology; **Corresponding Member:** International Geographical Union (IGU) **Ex-Chairman:** Board of Studies in Geography, Jiwaji University, Gwalior

**DECLARATION**

**MIZORAM UNIVERSITY**

**MARCH, 2025**

I **IMANUEL LAWMCHULLOVA**, hereby declare that the subject matter of this thesis is the record of work done by me, that the contents of this thesis did not form basis of the award of any previous degree to me or to do the best of my knowledge to anybody else, and that the thesis has not been submitted by me for any research degree in any other University/Institute.

This is being submitted to the Mizoram University for the **Degree of Doctor Philosophy in Geography and Resource Management**

(IMANUEL LAWMCHULLOVA)

Candidate

(Prof. BENJAMIN L. SAITLUANGA)
Head

(Prof. VISHWAMBHAR PRASAD SATI)
Supervisor

## ACKNOWLEDGEMENT

Firstly, I thanks to almighty GOD for the guidance, shower of blessings and healthy life that have enabled me to successfully complete this prestigious research work.

I really grateful to my supervisor Senior Professor Vishwambhar Prasad Sati, Department of Geography and Resource Management, Mizoram University for his expertise, patience, dedication, guidance, valuable time spare and support to complete my thesis

I would like to express my deepest gratitude to my previous beloved Supervisor, Professor Ch. Udaya Bhaskara Rao (L) Department of Geography and Resource Management, Mizoram University, who has passed away on 20th September, 2024 for his remarkable guidance, support and mentorship to fulfill my thesis objectives.

I really appreciate to Ministry of Tribal Affairs (MoTA) Scholarship Division for providing financial assistance through National Fellowship and Scholarship for Higher Education of Schedule Tribe Student (NFST) during the course of my research.

I thanks to all the teaching and non-teaching faculty of the Department of Geography and Resource Management, Mizoram University, for their kind inspiring assistance, co-operation and valuable recommendation to improve my research.

I extend sincere gratitude to the Mizoram State Remote Sensing and Application Centre (MIRSAC), Government of Mizoram, providing for their valuable information of Soil map and watershed boundary and shape file of Tuirial drainage system.

I thanks to Geological Survey of India (GSI) Kolkata, for their freely accessible valuable geo-spatial data of geology, lithology, lineament and geomorphic features. I extend my gratitude to the Alaska Satellite Facility for their free of cost ALOS PALSAR DEM. In addition, European Space Agency (ESA) Sentinel 2B satellite imagery free of cost. I kindly acknowledge NASA POWER for their climatic data free of cost.

I kindly acknowledge Joseph Lalngaihawma of Ph. D student at Department of Geography and Resource Management, Mizoram University, with the help of his, GPS survey at the source of Tuirial river successfully conducted. I also thanks to my cousin Lalramropuia of Saipum village for his valuable time spare the Bathymetry survey can be completed. I would like to express my gratitude to my student Lalnunpui of 4th Semester, Department of Geography and Resource Management, Mizoram University, for his help bathymetry survey can be fulfilled.

I in debt to my beloved parent Lalzawmliana and Lalrimawii for their financial assistantship, praying and mentally support along with their belief and hope in my journey of education, without them this research would never been accomplish. My sister Lalthazovi and her husband Lalrothanga, also my second eldest sister Lallunghnemi and her husband Larinmawia for their kind support really meant to this research accomplishment. I really thanks to my brother Lalhmahruaia for his taken care of family during my absence. To my beloved wife Lalrinkimi, your understanding, motivation and patience really means to fulfillment of this prestigious research. Also, during the course of Ph. D. program your sacrifice for taking care of our beloved first born Raphael Lawmchullova Varte. I thanks to Lalhriatrengi, Lalramsanga, Lalhlunmawii, Pentecosthanga, Ruthi Lalringheti, and Lalmalsawmi for their unwavering support and continuous encouragement which have been the source of inspiration.

This thesis is a culmination of the efforts and support of many and I am grateful for each one of you who has played a part in this endeavor.

IMANUEL LAWMCHULLOVA

Research Scholar

## CONTENTS

## List of figures

## List of tables

## List of Plates

## Abbreviations

| | |
|---|---|
| º | Degree |
| ºC | Degree Celsius |
| % | Percentage |
| $\lambda$ | flow accumulation |
| $m$ | variable length-slope exponent |
| $\beta$ | slope gradient |
| $\theta$ | slope angle |
| A | Reservoir Catchment |
| AASL | Average Annual Soil Loss |
| ALOS PALSAR | Advanced Land Observing Satellite Phased Array Type L-Band Synthetic Aperture Radar |
| AHP | Analytical Hierarchy Process |
| ArcGIS | Aeronautical Reconnaissance Coverage Geographic Information System |
| AWC | Available Water Holding Capacity |
| BM | Bench Mark |
| C | Cover Management |
| $C_c$ | Compactness Constant |
| CHAID | Chi-Squared Automatic Interaction Detector |
| CLM | Community Land Model |
| CRT | Classification and Regression Trees |
| GLM | Global Climate Model |
| dBD | Dry Bulk Density |
| $D_d$ | Drainage Density |

| | |
|---|---|
| $D_i$ | Dissection Index |
| DEM | Digital Elevation Model |
| E | Area Average Gross Soil Loss Rate |
| EQ | Ecological Quality |
| Eq. | Equation |
| ESA | European Space Agency |
| ESs | Ecosystem Services |
| ESV | Ecosystem Service Values |
| EUROSEM | European Soil Erosion Model |
| FAO | Food and Agriculture Organization |
| GIS | Geographic Information System |
| GPS | Global Positioning System |
| $G_r$ | Gradient ratio |
| GSI | Geological Survey of India |
| Ha | Hectare |
| H | Basin Relief |
| HCA | Hierarchical Cluster Analysis |
| HI | Hypsometric Integral |
| IC | Instrument Capacity |
| IDW | Inverse Distance Weighted |
| i.e. | That is |
| IMD | Indian Meteorological Department |
| InVEST | Integrated Valuation of Ecosystem Services and Tradeoffs |
| IRS | Indian Remote Sensing Satellite |
| IW | Instrument Weight |
| K | Soil Erodibility Factor |
| Kg | Kilogram |

| | |
|---|---|
| *L* | slope length |
| LANDSAT | Land Satellite |
| LE | Economic life time |
| LISS | Linear Image Self Scanning |
| $L_o$ | length of overflow land |
| LPF | Local Polynomial Function |
| LS | Steepness and length of the slope |
| $L_u$ | Stream Length |
| LU/LC | Land Use and Land Cover |
| $m^3$ | cubic metre |
| $m^3/yr$ | cubic metre per year |
| $Mm^3$ | Million cubic metre |
| MARS | Multivariate Adaptive Regression Splines |
| MIRSAC | Mizoram State Remote Sensing Application Centre |
| MNDWI | Modified Normalized Difference Water Index |
| Mg $ha^{-1}yr^{-1}$ | Mega gram per hectare per year |
| MJ.mm $ha^{-1}$ $hr^{-1}$ $yr^{-1}$ | Mega-joule millimeter per hectare per hour per year |
| m/s | Metre per Second |
| MSI | Multi-Spectral Instrument |
| MSL | Mean Sea Level |
| MUSLE | Modified Universal Soil Loss Equation |
| MW | Megawatt |
| NASA POWER | National Aeronautic Space Application Prediction of Worldwide Energy Resources |
| NDAI | Normal Difference Area Index |
| NDVI | Normalized Difference Vegetation Index |
| NDWI | Normalized Difference Water Index |

| | |
|---|---|
| NE-SW | Northeast to Southwest |
| NIR | Near Infrared Red |
| NH | National Highway |
| NNW-SSE | North-Northwest to South-Southeast |
| NSR | Night Storage Reservoir |
| NW | Net Weight |
| NWM | National Water Model |
| NW-SE | Northwest to Southeast |
| OLI–TIRS | Operational Land Imager and Thermal Infrared Sensors |
| OTB | Orfeo Tool Box |
| P | Conservation Practice Factor |
| P | perimeter of basin |
| PCA | Principal Component Analysis |
| PDAI | Percentage Difference Area Index |
| PWD | Public Worker Department |
| Qgis | Quantum Geographic Information System |
| R | Rainfall Erosivity Factor |
| R | Red |
| $R_b$ | Bifurcation Ratio |
| $R_c$ | Circularity Ratio |
| $R_e$ | Elongation Ratio |
| $R_f$ | Form Factor |
| $R_{hp}$ | Relative Relief |
| $R_n$ | Ruggedness Number |
| RPI | River Pollution Index |
| $R_r$ | Relief Ratio |
| RMSE | Root Mean Square Error |

| | |
|---|---|
| RS | Remote Sensing |
| RS | Rate of Sediment |
| RSC | Current Reservoir Storage Capacity |
| RUSLE | Revised Universal Soil Loss Equation |
| S | steepness of slope |
| SAC | Space Application Centre |
| SCS-CN | Soil Conservation Service - Curve Number |
| SDGs | Sustainable Development Goals |
| SDR | Sediment Delivery Ratio |
| $S_f$ | Stream Frequency |
| SOI | Survey of India |
| SPANS | Spatial Analysis Systems |
| SPR | Sediment Production Rate |
| SS | Suspended Solids |
| SSY | Specific Sediment Yield |
| STI | Sediment Transport Index |
| SV | Sediment Volume |
| SVM | Support Vector Machine |
| SW | Sediment Weight |
| SWC | Soil and Water Conservation |
| SWAT | Soil and Water Assessment Tools |
| SWS | Sub-watersheds |
| SY | Sediment Yield |
| SYI | Sediment Yield Index |
| T | Time |
| t $ha^{-1}$ $yr^{-1}$ | Ton per hectare per year |
| tons/$km^2$/$yr^{-1}$ | Ton per square kilometre per year |

| | |
|---|---|
| t hr. $MJ^{-1}mm^{-1}$ | Ton per hour per mega-joule per millimeter |
| TE | Trap Efficiency |
| TGA | Total Geographical Area |
| TIN | Triangulation Irregular Network |
| TN | Total Nitrogen |
| TM | Thematic Mapper |
| TP | Total Phosphorus |
| $T_r$ | Texture Ratio |
| UN | United Nation |
| USLE | Universal Soil Loss Equation |
| UTM | Universal Transverse Mercator |
| $V_s$ | volumes |
| VR-CESM | Variable-Resolution Global Climate Model |
| WGS | World Geodetic System |
| WRI | Water Ratio Index |
| Yr | Year |

# CHAPTER – 1

# INTRODUCTION

## 1.1 General Introduction

Soil erosion is defined as the removal of topsoil from the surface and transported through the external agencies such as running water, wind, solar energy and tillage (FAO, 2020). In addition, soil erosion is a natural process that continues depending on natural factors and is accelerated by anthropogenic factors (Wischmeier and Smith, 1978). Soil erosion can take place under various natural climatic environments and anthropogenic activities. Soil erosion occurs naturally when soil particles are disintegrated, transported, and deposited at different places by various erosion agents like wind, running water, surface run-off and solar energy. On the other hand, various anthropogenic activities such as intensive agricultural, practices, deforestation, overgrazing and improper land use planning, rapid urbanization which could have led extensive soil erosion (Lawmchullova and Rao, 2024). The rate of soil erosion is rigorously higher than the rate of soil formation. Soil is the exhaustible resource. The average amount of soil loss in the natural process of erosion is estimated at 0.1 – 1ton $ha^{-1}yr^{-1}$, while the soil loss by anthropogenic factors is 10-1000 times higher than this value (Bleu, 2003).

Soil erosion decreases with agricultural productivity, degrades ecosystem functions, increases hydrogeological risk by landslides, floods, significant losses of biodiversity and infrastructures, also in severe cases, leads to displacement of human populations. Furthermore, soil erosion causes problems such as food security risk, decrease in aesthetic landscape beauty, increase in flood risk, decrease in water quality, pollution in rivers and lakes, eutrophication, loss of biodiversity, decrease in capacity and lifetime of water reservoirs (Uzuner and Dengiz, 2020; Wuepper *et al.,* 2020). Similarly, natural and anthropogenic activities further accelerate erosion on both on-site and off-site consequences. The on-site effect refers to the extensive removal of valuable topsoil and

vital soil nutrients in-situ. Essential soil nutrients like nitrogen, phosphorus, potassium, calcium and soil organic matter are carried away by erosion (Pimentel, 2006). For instance, soil erosion and land degradation are the major threats to global food security and the failure of Sustainable Development Goals (SDGs) (UN, 2015; FAO, 2020). On the other hand, the off-site impact mainly arises from sedimentation downstream. Soil removed from the upper catchments is deposited in the downstream parts of the river. It gives rise to numerous problems, among which sedimentation of reservoirs downstream is reported to be the most prominent (Kothyari, 1996). This has remarkably reduced the reservoirs water storage and hydroelectric power generation capacity. Furthermore, sedimentation in the streams also disrupt the riverine ecosystem and its recreational value, depleting water quality and enhancing the chances of floods (Gelagay, 2016). Hence, sedimentation is the consequence of accelerated soil erosion on the hillslopes and an increase or decrease in the amount of soil loss consequently influence the amount of sedimentation in a drainage basin (Dewanjan and Ahmad, 2020).

Soil erosion is one of the most important environmental problems because it causes soil and land degradation (Dutal and Reis, 2020). Soil loss is common issue faced by agricultural land, especially tropical and semi-arid regions of Africa, south America, and south east Asia. Agricultural productivity has decreased by 23% of the global terrestrial area due to land degradation and as a result, 3.2 billion people have been directly and indirectly affected by it (Scholes *et al*., 2018). Worldwide, the rate of land degradation due to soil erosion is estimated as 70 – 90% (Chalise et al. 2018). In humid sub-tropical region, particularly Himalaya region of India soil erosion is highly influenced by surface run-off. In addition, the rugged mountainous terrain of these humid climate zones undergoes significant impact of soil removal (Markose and Jayappa, 2016; Rajbanshi and Bhattacharya, 2020). About 29.77% of the total geographical area experiences land degradation of which 36.20 M ha is affected by water-induced soil loss in India (SAC, 2021). The predicted amount of 5334 million tons of soil loss is induced by surface run-off at a rate of 16.35 ton $ha^{-1}yr^{-1}$, where 61% of the total sediments are deposited in new places, 29% are deposited at the bottom of sea and the remaining 10% are deposited in reservoirs.

The Eastern Indian Himalayan region as a whole is experiencing serious problem of soil erosion and the rivers flowing through this region carries huge quantities of sediments and finally discharge into the Bay of Bengal. About 25% of the dissolved load is supplied to the World oceans by the Himalayan and Tibetan regions (Raymo and Ruddiman, 1992). The foot hills of Himalayas, which extends in the northeastern part of Indian states like Arunachal Pradesh, Nagaland, Manipur, Mizoram, Meghalaya and Assam and this region, are no exception to huge soil loss. The sediment load in the Himalayan rivers is increased due to loss of forest cover, indiscriminate exploitation of other natural resources, intense monsoonal precipitations and the fragile river catchments of low water retention capacity (Valdiya, 1985; Rawat and Rawat, 1994). Geologically the region is very weak and fragile due to its soil structure mostly composed of sandstones, siltstones and shales. Erosion worsens the physical, chemical and biological properties of soil by removing of natural nutrients, humus and top soil and the soil is left unproductive for crop growth. Anthropogenic disturbances such as deforestation, expansion of agricultural land from forest cover, shifting cultivation (locally known as Jhum) on steep slopes, construction of roads, rapid urbanization and other developmental activities coupled with high rainfall, poor soil conservation and high soil erosivity induced by shallow soil depths, low structural stability are the main reasons for high rate of soil loss (Markose and Jayappa, 2016). High seismicity is yet another factor in the region for high soil erosion and sedimentation in river reaches (Jain *et al*., 2001). Soil erosion is nevertheless a major problem which affects the agricultural production (Al-Abadi *et al*., 2016), soil fertility (Blanco and Lal, 2008; Verheijen *et al*., 2009), excessive siltation (Wilkinson and McElroy, 2007; Dutta, 2016), and sedimentation in lakes and rivers, water quality and recreation. Each year, due to soil erosion, million tons of soil is eroded off mostly from agricultural lands in mountainous terrain (Dabral *et al*., 2008; Pandey *et al*., 2009; Adornado *et al*., 2009; Naqvi *et al*., 2013; Zonunsanga, 2016; Kisan *et al*., 2016). Recent estimates indicate that nearly 39% of the Indian Himalayas has potential soil erosion rate of more than 40 Mg $ha^{-1}yr^{-1}$ (Mandal and Sharda, 2013). Thus soil erosion is

a major setback to the sustainable development of natural resources and environment and thus calls for urgent quantification (Barman *et al*., 2020).

### 1.2 Statement of the Problem

Soil erosion and siltation are the most problems experiencing in hilly region which receives high rainfall like in Mizoram the eastern extension of Himalayas. In addition, this problem is expected to be widespread, continued and significant issue on water resource planning, shorten of reservoir life span, shallow water, natural ecosystem, sustainable land and environment management. Despite knowing the significant issues of soil erosion and siltation, there has been lack of adequate comprehensive research on estimate of total soil loss at sub-watershed level and silted at reservoir with minimization of the strategic action planning. Therefore, a precise and timely assessment is essential for understanding the spatial distribution, degree and amount of erosion and siltation with developing effective control measures.

The conventional methods of determining soil erosion rate and siltation in a watershed include field survey and based on experimental plots as well as acquiring run-off and sediment data from stream gauging stations, which require a lot of equipment, huge capital investment, time consuming and involvement of large labourers, also it has a limitation in terms of spatial representation for dynamic environments in a wide area (Lu *et al*., 2004; Pradeep *et al*., 2015; Ganasri and Ramesh, 2015; Kucuker and Giraldo, 2022). Moreover, actual field measurements are exceptional to mountainous and agricultural land throughout the country, and the recorded data for run-off, and sediment influx is not readily available at the watershed level since most of the river basins are still ungauged (Prasannakuma *et al*., 2012; Rajbhanshi and Bhattacharya, 2020). Due to the fact this limitation it is difficult to comprehensively evaluate the complex spatial patterns, varying magnitude, and temporal dynamics of soil erosion processes within a watershed (Vijith *et al*., 2012; Bhat *et a*l., 2017; Kalambukattu and Kumar, 2017). Considering the absence of extensive evaluation in this region and lack of secondary data, coupled with limitations of

conventional methods to comprehend this complex phenomenon, the purpose of the present study is to fill this knowledge gap, generating synoptic information through the application of geospatial technology-based modeling in a watershed.

## 1.3 Objectives of the study

`The present study aimed at estimation of total soil loss at Tuirial watershed, Mizoram using bathymetry survey, soil erosion model with the integration of geo-spatial data in geographic information system (GIS) along with the application of other pioneering formulae. The study aims to achieve the following specific objectives:

1.3.1 To estimate the total soil loss at Tuirial watershed

1.3.2 To estimate the siltation level at Tuirial dam

1.3.3 To analyze the morphometry of Tuirial watershed

1.3.4 To suggest the remedial measures of soil loss and siltation level at watershed and dam.

## 1.4 Significance of the study

The research being undertaken encompasses significant implications for sustainable watershed management, soil erosion control and environmental conservation recently, the advanced techniques of remote sensing (RS) and GIS has gained universal approval as a dominant tool for ecological hazard assessment and for developing effective resource conservation and management strategies (Pham *et al*., 2018; Sujatha and Sridhar, 2018; Halefom and Teshome, 2019; Makaya *et al*., 2019; Rashid *et al*., 2020). This advancement in geo-informatics has also successfully ensured an adequate manifestation and modelling of various earth phenomena (Anbazhagan *et al*., 2011). With RS and GIS technique-based modelling approaches, the present study attempts to assess soil erosion comprehensively. Moreover, this study was intended to provide reliable, cost effective, and

spatially explicit information on erosion and siltation in a watershed. This valuable insight into the complex processes and problems will be helpful for sustainable watershed management that focuses on the formulation of feasible erosion and siltation mitigation plans, strategic land use planning, and appropriate land and water management policies.

In addition, this research will showcase the potential advantages of RS and GIS techniques regarding the problems associated with assessing accelerated erosion rate in a hilly watershed. By demonstrating the reliability and applicability of these technologies, this study can help promote wider adoption of geospatial modelling techniques and their practical implications for motoring and analyzing soil erosion along with its on-site and off-site consequences in the future, consequently, this will result in a better understanding and improved application of environmental management practices at a watershed scale.

### 1.5 Scope and Limitations of the study

The most feasible micro-level planning region i.e., a watershed has been selected for assessing soil erosion and siltation in this research. This study integrated several soil loss modelling approaches to estimate total soil loss with extensive field survey for justification of the results. One of the most popular robust techniques for soil loss model is revised universal soil loss equation (RUSLE), in this approach various erosion influencing factors such as soil texture, steepness of slope, length of the slope, rainfall erosivity, land use and land covers were integrated through ArcGIS environment. This study result can be used for minimization of action planning and management of watershed. Beside this, the study utilizes various scientific methods related with siltation at reservoir such as dry bulk density (dBD), bathymetry survey, sediment yield (SY), specific sediment yield (SSY), sediment volume (SV), geo-statistical, Trap efficiency (TE), rate of sediment accumulation, estimation of sediment thickness, estimation of storage capacity and reservoir economic lifespan are also included. The study encompasses the satellite image processing technique with classification of land use and land cover for detecting the erosion points like agricultural lands and roads. Digital elevation models (DEM) were also used

for the computation of Tuirial river basin morphometry. In this research the morphometric linear parameters such as the bifurcation ratio ($R_b$) drainage density ($D_d$), stream length ($L_u$) (stream frequency ($S_f$), texture ratio ($T_r$) and length of overflow land ($L_o$) have direct influence on erosion in the basin. Similarly, areal aspects such as the circularity ratio ($R_c$, form factor ($R_f$), elongation ratio ($R_e$) and compactness constant ($C_c$) also affect soil erosion. Additionally, relief parameters such as basin relief (H) relief ratio ($R_r$), relative relief ($R_{hp}$) ruggedness number ($R_n$) (dissection index ($D_i$) and hypsometric integral (HI) has varied influences on spatial magnitude of erosion. All the above mentioned morphometric parameters were analyzed with respect to empirical pioneering works and geographic information systems (GIS). To understand the geometry of landforms is critical criteria for erosion points identification along with cycle of erosion.

However, the present study has certain limitations on application of digital elevation model (DEM) with low resolution 12.5 metres ALOS PALSAR was employed to estimate LS factor and steepness of slope analysis, it may lead the distortion of length and steepness of slope. Similarly, the topographic map of the year 1987 was found not suitable to calculate the initial storage of the Tuirial dam due to the dynamic change in elevation induced by the excavation of the landmass at the bottom and utilized for embankment fills to dam construction. Again, the landuse land cover of the present study also classified it from Sentinel image with 10 metres resolution, which may lead false positive error in classification. But in future this issue can be fixed with the help of good quality satellite images and DEM. In addition, validation of soil loss, sediment yield and siltation at the dam is impossible from the field survey, since Tuirial watershed is un-gauged and the absence of field based erosion measurement. The previous studies are also modeling based which needs field verification.

## 1.6 Organization of the Thesis

The whole thesis is divided into eight chapters. Chapter 1 includes the introduction, overview of the contextual information, statement of the problems, research objectives, significance of the study, and scope and limitations of the thesis.

Chapter 2 deals with a rigorous review of a wide range of relevant existing literature such as sedimentation processes factors and affecting along with siltation at dam and total soil loss at watershed from various international, national and regional levels.

In the chapter 3 presented the details research methodology which deals with data collection, data mining, analyzing and generation of geo-spatial modeling framework.

Chapter 4 highlighted the geo-environmental setting of Tuirial watershed which consists of physical characteristics of slope, elevation, geomorphology, lithology, geology, climate, drainage, and vegetation.

Chapter 5 deals with erosion susceptibility of Tuirial watershed by revised universal soil loss (RUSLE). In addition, interpretation of various prone to soil loss and comparing with other works.

Chapter 6 focusing assessment of siltation in Tuirial dam with the help of bathymetry survey and various scientific techniques.

In chapter 7 the morphometric characteristics such linear, areal and relief parameters of the Tuirial watershed were analyzed and describe the intensity of erosion at various sub-watersheds.

In Chapter 8, conclusion with findings and recommendations to minimize further erosion risk are presented.

# CHAPTER – 2

# REVIEW OF LITERATURE

## 2.1 Introduction

This chapter provides the valuable information of research methodologies of the conducted studies on soil erosion, siltation and drainage morphometry on the basis of international, national and regional level findings and critics. A number of studies have been carried out on various aspects of drainage morphometry characteristics to understand nature of landforms, hydrological cycle and associated erosion and siltation at the reservoirs. The following sections examined different aspects of the multifaceted approaches, at international, national and regional levels constituting an extensive exploration of soil loss and siltation estimation studies. Generally, the present review focuses on contemporary research approaches accomplished through the collaboration of advanced techniques encompassing remote sensing and geographic information system (GIS).

## 2.2 General

Kothari (1996) examined soil erosion and sedimentation condition in different parts of India after extensive literature review on soil and sedimentation. The study found out that Himalaya region which is the most affected by severe soil loss due to fragile geological setting and anthropogenic activities. The study identified more erosion in upper catchment while huge volume of siltation in reservoirs. The study recommended the detailed examination of the catchment to address soil loss and siltation in affected regions and effective conservation techniques.

Recently, Chilika Lake was studied by Rajan (2019), substituting multiple equations like Pine biomass volume $b(t)$ (Nautiyal and Babor, 1985), the stock abundance, $x$ $(t)$ (Clark, 1985), species '$\rho x$' and carrying capacity $kx(t)$, variable $hx(t)$ and $l(t)$ (Newcombe and Jensen,1996) etc., by evaluating the PES and estimation of erosion.

General algebraic modelling systems (GAMS 24.7.4) software, which revealed that the encompassing forest reduces the speed of sedimentation influx within the lake. During the monsoon, the rate of sedimentation is higher than in the winter season. The common annual rate of sediment load is 85.77 mg/l and the rate of sedimentation depends on the existing land use pattern. But this study incorporates number of model algebraic equations which is not universally accepted.

Diaz-Gonzalez *et al*., (2022) performed a review on "Machine learning and remote sensing techniques applied to estimate soil indicators." The prediction of crop production based on the approximation of chemical, physical, and biological soil quality indicators (SQI), which includes different machine learning (ML) techniques to exercise data from remote sensing (RS) systems. Machine Learning technique is useful for adjustment of crop management application and as a result to boost crop yield.

By focusing on land use/land cover (LU/LC) change inter link with ecosystem service was examined for more than three decades at Fincha watershed due to government implemented Hydroelectric Dam and Sugarcane Plantation. ArcGIS software for land use/land cover dataset, Estimation of ecosystem service values and Elasticity of ESV change in relation to LU/LC were the methods employed for the study. The study reveals that cultivated land, water body, settlement and sugar cane plantation were increased per year, whereas wetland, forest land and bare land were reduced per year and the total values of the natural capital were also decreased (Tolessa *et al*., 2021). The limitation of the study is based on single data set which is Landsat-5 TM 1987 and Landsat-8 OLI–TIRS 2015. Notable and ground verification is indispensable to clarify the genuine character of land use and land cover change.

Tsai *et al*., (2021) attempting to set up the watershed health indicator and health check of reservoirs on 95 public water supply, irrigation reservoir and watershed in Taiwan. The methodology which incorporates health indicators of the watershed identified are forest coverage rate, soil erosion depth, sediment accumulation rate, and suspended solids (SS) concentration. The three wellbeing markers identified with water quality

improvement are river pollution index (RPI), point source contamination decrease, and non-point source contamination potential. In this study it was found that the water supply reservoirs have high forest coverage and a low soil disintegration profundity; be that as, these reservoirs have a low water quality because of a depressed spot source contamination was dealt with (9.1%–17.7%) and 44–65.8 kg non-point source contamination per sq.km. Most irrigation reservoirs are situated in the flat plains, which have forest coverage (50.5%) and high sediment gathering (36.7%). However, this observation does not specify the time of test taken, where it very well may be fluctuated water quality as far as seasons.

On the basis of water pollution, water quality and land use in the central Nepal Himalayan watershed study performed by applying Eigenvector model, Watershed delineation and predictor variables extraction, Exploratory data analysis, Regression analysis, Spatial regression models were the methods they used to explore the connection between water quality and different social, segment, and geological components in an urbanizing watershed of Nepal with an examine of various availability frameworks to conceptualize spatial interrelationships (Mainali and Chang, 2021). But, this analysis does not specify accurate water quality level and the water quality inspecting like-wise took uniquely in winter, it very well may be differed on during monsoon season.

Osman *et al*., (2021) carried out Flood modeling of Sungai Pinang Watershed under the impact of urbanization based on Liuxihe modelling and Support Vector Machine (SVM). Resulting of Urbanization extraordinarily impacted land use/land cover including increased overflow volumes, peak discharges and flow concentrations. Liuxihe model can give specialized reference to flood control and fiasco decrease. Yet, it doesn't specify where flood control and Liuxihe model is just reference of flood admonitions.

To highlight hydrological analysis in watersheds based on variable-resolution global climate model (VR-CESM), which discovered that effects of environmental change on hydrology fluctuate in snow-ruled diminishing snowpack and early snowmelt shifts overflow tops prior and decreases their size. While in rain-dominated watersheds increasing precipitation in the projection period, peak runoff increases in the wet season.

In regional-scale watersheds in the western United States and China, VRCESM generally, projects increasing precipitation and runoff through the middle of this century, particularly in the coastal watersheds that receive more moisture from the ocean. A bigger variation between yearly changeability and higher recurrence of wet and dry years are anticipated for the future for most of the watersheds, showing that environmental change could influence the event of outrageous hydrological occasions consequently conceivably expanding the dangers of emerging Geo_hazards. Variable Resolution Global Climate Model (VR-CESM), Community Land Model (CLM), Global Climate Model (GCM), National Water Model (NWM) are the models applied to fulfill the study (Xu and Di, 2021). Be that as it may, impediment of these models were it require loads of cycle and phases of refinement of satellite picture to fit in it, so it lessen the actual satellite resolution like in VR-CESM.

Lin *et al*., (2021) creating lake nutrient enrichment (SLRs) based on Chaohu Lake Basin. Understanding that both TN and TP in watershed yield is expanding throughout the previous ten years. The SLRs for TN are essentially situated in metropolitan development regions while SLRs for TP primarily found in major influent streams. An ideal time of SLRs identification of TP and TN is Spring and Summer respectively. SWAT and Arc-SWAT model is the primary programming to recognize the significant substance change in watersheds. Other measurable information's were determined and assembled dependent on the co-efficient of correlation strategy. Impediments of the review; green growth and lake biomass is the important index of SLRs. SWAT model is generally utilized for distinguishing a substance change in agriculture dominated watershed, while they applied for Chaohu Lake which encompassed by the city.

Nemunas river watershed, river course, hydrologic regime, sediment (SS), Total Nitrogen (TN) and Total Phosphorus (TP) stack from the stream to the Curonian Lagoon under the influence of climate change using SWAT model. Watershed become drier in long run, TN increase in winter while loss of phosphorus. Predicted nutrient stack changes during winter season show a two-fold multiple rise of residue. The theoretical framework used to evaluate future climate change indicators were precipitation, temperature and

carbon dioxide (Cerkasova *et al*., 2021). However, significant side stone anthropogenic activities impact is excluded.

Zhu *et al*., (2021) analyze the interlinking between ecological standard and ecosystem services in a red soil high terrain watershed. The methodological framework which employs for achieving in this research were; The remote sensing ecological index and the ecosystem service index, were utilized to show Ecological Quality (EQ) and Ecosystem Services (ESs), i.e., water yield, soil conservation, carbon storage and food supply. The outcome shows that the relationship between EQ and ES by applying Spearmen correlation, while EQ was diminishing at the watershed. Limitations of the study includes several indicators like vegetation cover, soil, parameters, including evapotranspiration correlation coefficient, and management factor, soil, carbon thickness and so on, were taken from the literature review, which might emerge future possible mistakes. Multi-dimensional and spatial tempo scales observation are expected to additionally discover the relationship between EQ and ESs, and work on the precision and enduring nature of the findings.

### 2.3 Morphometry

The analysis of landforms, shape and earth's surface configuration with a quantitative and mathematical approach is known as morphometry (Clarke, 1996). The morphometric study reveals the characteristics of the river catchment, hydrological and geomorphic processes, including the drainage system. In addition, it plays a significant role in the studies of hydrologic modeling, prioritization of subwatersheds, and soil and water degradation management (Fallah *et al*., 2016; Choudhari *et al*., 2018). A number of environmental factors directly affect soil loss, and those controlling factors should be checked to minimize erosion-vulnerable zones and undesirable effects on the environment (Kumar *et al*., 2011). Similarly, it is essential to comprehend the morphometric characteristics of hydrological regimes, terrain features, and soil erosion (Patel *et al*., 2013). Additionally, it also helps to understand the interactions between humans and the environment through economic activity leading to soil erosion (Patel *et al*., 2013; Gajbhiye

*et al*., 2014; Arulbalaji and Padmalal, 2020). Morphometric parameters have a significant influence on examining erosion-susceptible zones (Horton, 1945; Schumm, 1963; Yadav *et al*., 2014; Kadam *et al*., 2019). It includes linear, aerial and relief features, which show one- and two-dimensional properties of the basin, respectively (Chauhan *et al*., 2016; Sharma and Mahajan, 2020). These morphometric parameters are associated with different physical and geomorphological aspects of a river basin that have significant impacts either by indirect or direct erosion, which is essential to identify soil loss-prone areas (Abboud and Nofal, 2017; Umrikar, 2017; Sarkar *et al*., 2020).

Horton (1932, 1945) introduced the quantitative measurement of drainage basin to analyze drainage system. Later, adjustment and further analysis were performed by Strahler (1952, 1964). Pioneering Horton (1932, 1945) works concentrated on stream number, stream length, drainage density, channel frequency. Strahler (1952, 1964) adjusted the Horton works to perform further analysis like stream order, form factor ratio, bifurcation ratio, relief basin, circularity ratio, stream length ratio. Likewise, other various researchers developed the new parameters such as elongated ratio, relief ratio (Schumm, 1956), relative relief ratio (Melton, 1958), hypsometric integration (Pike and Wilson, 1971), ruggness number (Patton and Baker, 1976), hypsometric curve (Kouli *et al*, 2007), gradient ratio (Sreedevi *et al*. 2009).

Earlier, the river basin and sub-watershed level of the drainage characteristics were performed by conventional methods at global scale. The advancement of information technologies in geographic information system and spatial remote sensing data (RS and GIS) provides a powerful tool for computation and assessment of various hydrological characteristics at global level. Systematically using geo-spatial approach to perform morphometric analysis of drainage basin has been conducted by various researchers (Rao, 2015; Sreedevi *et al*. 2009). Their result revealed that, morphometric analysis using remote sensing and geographic information system provides the principle information of landforms, hydrogeological features of the watershed. The advantage of geo-spatial approach has low in capital investment, expenditure and time saved. In this study of the Middle Tuirial river basin the linear, areal and relief morphometric parameters were

computed by applying pioneering works and equations with geospatial data and GIS techniques. Because no significant study was found in this area with an attempt of the relationship of relief and hydrological aspect. This study aims to highlight the quantitative analysis of Middle Tuirial watershed for proper soil and water conservation. In addition, to understanding landscape evolution and hydrological characteristics of the river basin.

Additionally, some authors have minimized morphometric parameters using principal component analysis (PCA), which is closely associated with a significant impact on erosion (Meshram and Sharma, 2018; Arefin *et al*., 2020; Pathare and Pathare, 2021). Furthermore, some of the studies compared morphometric parameters are based on hierarchical cluster analysis (HCA) (Meshram and Sharma, 2017; Chauhan *et al*., 2022). However, the PCA and HCA techniques remove the less effective parameters, which are also included in the erosion susceptibility criteria. Additionally, usage of single criteria to identify erosion proneness yields low accuracy because erosion was led by multiple driver agents that require inclusive examination. Drainage system, surface runoff, land use/land cover, soil texture, and physical setting are considered as factors that influence vulnerable to soil loss at the river basins and are also useful for the identification and prioritization of sub-watersheds (Harsha *et, al*., 2020; Sutradhar, 2020; Haokip *et al*., 2022; Hembram and Saha, 2020). These studies reveal a positive relation between the all-inclusive approach and soil loss prone zone within the watershed. However, they exclude the soil texture and rainfall, which are critical parameters and agents of erosion. Furthermore, comprehending topsoil instability is essential due to variations in soil properties with different amounts of soil (Kulimushi *et al*., 2021). Likewise, a clay soil texture with high solidity resist infiltration resulted in a high intensity of surface runoff and low permeability but less erosion, while a silt soil texture with high permeability but limited holding capacity led to more erosion (Bhattacharya *et al*., 2019; Kadam *et a*l., 2022). Geology and geomorphology also influence the hydrological system because the landform patterns and structure affect the drainage system with erodibility of the basin (Nookaratnam *et al*., 2005; Sreedevi *et al*., 2009). Similarly, the terrain, slope, elevation, rainfall characteristics and land use and land cover patterns of the basin accelerate the surface run-off with enormous fragile topsoil

wash away (Sutradhar, 2020; Haokip *et al*., 2022; Ebrahimi and Sadeghi, 2023). However, the above studies are ignoring the total soil loss and its area coverage which are crucial factors for determining susceptible of soil loss in geo-environment parameter. As best of the conducted literature studied, it is revealed that no authors have employed the integrated geo-environment parameters such as morphometric, average annual soil loss (AASL), sediment transport index (STI) and sediment production rate (SPR) approach to identify prioritization of watershed. But, in this study the new parameter of average annual soil loss (AASL) was included for determining the prioritization of watershed. The analytical hierarchy process (AHP) technique permits the determination of the weight of each erosional parameter based on their significant level (Chitsaz and Malekian, 2016; Siddiqui *et al*., 2009; Shelar *et al*., 2022; Hailu *et al*., 2023). It also efficient and simplicity with reducing the chances of bias in decision making (Saaty, 1980). This method is widely utilized worldwide for the identification of priority zones to initiate measures of soil and water conservation with minimized risk.

Morphometry of drainage network in volcanic landforms (Altın and Altın, 2011) was done by applying morphometric parameters (Strahler, 1964) like drainage map; ordering streams; and measuring the catchment area and perimeter, the length of drainage channels, drainage density and frequency, and bifurcation ratio (Kumar *et al*., 2000). Also applying Concavity Index (Langbein, 1964; Larue, 2008), deviations from a line (Phillips and Lutz, 2008; Larue, 2008) uncovers that vary in parameter of values implies the volcanic mountains weren't elevated on a similar period and were exposed to various morphologic cycles. However, landform development is long-term process, here during this study neglecting the span of the landform cycle.

The morphometric analysis of alluvial drainage provides understanding into its dynamics, erosion capacity, susceptibility to floods and conceivable genetic relations to tectonic faulting. The results indicate a vulnerability to erosion and flooding events, and these intense phenomena concentrate mostly on third-order catchments. Two dissimilar drainage network systems are shown: an older drainage network system with a main NW-SE direction, which includes fourth- and fifth-order branches, and a recent drainage

network system, which includes new, smaller order branches with a main NE-SW direction. The major tectonic fault orientations are NNW-SSE. The study reveals that the hydrographic network and faults present different directions, which shows that the hydrographic pattern is not impacted by tectonics (Charizopoulos *et al.,* 2019).

Delineation of the drainage basin is largely performed based on the GIS approach; the main purpose of delineation is prioritization for the management of sub-watershed. Recently many researchers made an attempt to figure out morphometry, permeability within sub-soil, aerial and relief parameters of every sub-watershed based on their influences of soil erosion and other degradation. Based on the result, the authority implemented immediate action to formulate conservation of sub-watershed (Bharath *et al*., 2021; Shrivatra *et al*., 2021). However, how to formulate conservation of the watershed is neglected.

An attempt was made on morphometric drainage and its influence on landforms using the conventional method (for eg: Horton, 1945; Strahler, 1952, 1957, 1964; Leopold and Miller, 1956; Krishnamurthy *et al*., 1996) and Remote Sensing data and Geographic Information Systems (GIS) technique (for eg: Srinivasan, 1988; Biswas *et al*., 1999; Jain *et al*., 1995). Remote Sensing and Geographic Information System techniques are more accurate rather than the conventional approaches (Reddy *et al.*, 2004; Bharath *et al.*, 2021). Because remote sensing data and GIS approach were convenient for delineation of drainage morphometry of distinct geological units, landforms, properties of soil and eroded lands.

Reddy *et al*., 2004 examined the drainage morphometry and its influence on landform processes, soil physical and land erosion characteristics in Vena river basin of basaltic terrain (Deccan traps), Nagpur district, Maharashtra, Central India. Indian Remote Sensing Satellite (IRS)-ID Linear Image Self Scanning (LISS)-III sensor with Survey of India (SOI) topographical sheets (1:50,000 scale) were used for systematic analysis of various morphometric, lithological and landform characteristics of the river basin. Morphometric analysis was carried out at sub basin level using Spatial Analysis System steepness of slope (SPANS ver. 7.0). GIS system to analyze the influence of drainage

morphometry on landforms, soil depth, drainage, available water holding capacity (AWC) and land erosion characteristics. They identified ten distinct landforms in the basin based on visual interpretation of satellite image such are dissected ridges, isolated mounds, linear ridges, escarpments, plateau spurs, subdued plateau, rolling plains, foot slopes, narrow valleys and main valley floor. Very shallow soils exist on dissected ridges, isolated mounds, linear ridges, escarpments and plateau spurs are associated with high drainage density (Dd), impermeable geology and high runoff conditions. High drainage density, high bifurcation ratio (Rb) and steep slopes are the main causative factors for the development of well- drained soils. The AWC is low in the soils of higher elevations whereas, it is very high at lower elevation in the sub basins. On the other hands, high drainage density, stream frequency (Fu) and texture ratio (T) are associated with severe erosion. The analysis reveals that the influence of drainage morphometry is very significant in understanding the landform processes, soil physical properties and erosional characteristics. The study demonstrates that remotely sensed data and GIS based approach is found to be more appropriate than the conventional methods in evaluation and analysis of drainage morphometry, landforms and land resources and to understand their inter-relationships for planning and management at river basin level.

Krishnan and Ramasamy, (2022) conducted a research on morphometric assessment and prioritization of watershed through the morphometric parameter characteristics of the Moyar river basin, Nilgiris district of Tamil Nadu in Southern India. The morphometric appraisal was carried out based on DEM and GIS. The drainage patterns clearly exposed effective regional tectonics, and the stream orders of the basin are primarily controlled by physiographic and tectonic structure in the study area. The bifurcation ratio was recorded from 3.8 to 6.2, and the higher values of the mean bifurcation of the all stream orders revealed that the geological and tectonic control of the river basin. Furthermore, the novelty of the study revealed that the three SWS (SWS3, SWS7, and SWS6) are highly susceptible and it requires appropriate sustainable soil and water conservation.

Hema *et al*., 2021 performed prioritization of sub-watersheds in the Kanakapura watershed, of Ramanagara district, Karnataka, using multi-criteria ranking method.

Priorities indexing of each of the parameters such as rainfall, lithology, drainage density, slope, lineament, hydro geomorphology, land-use, and land-cover are done, based on their impact significance, and overlay analysis was performed to identify critical sub-watersheds. They found out that the priority needs to be given to the Bannimukudlu and Kodihalli sub-watersheds followed by remaining sub-watersheds to regulate surface water flow thereby improving water table level. Some of the strategies proposed for effective conservation and management of water resources are the construction of a check dam, implementation of water harvesting methods, identification of artificial recharge sites.

Govarthanambikai and Sridhar (2024) carried out prioritization of sub-watersheds in Noyyal river basin using the geospatial technique with to recommend control soil erosion and water conservation measures. Thirteen fundamental morphometric parameters classified as linear, areal, and relief aspects were considered for the Noyyal river basin. Principal component analysis (PCA) was performed to correlate the morphometric parameters along with more significance impact on erosion. PCA analysis is appropriate and robust technique with widely employed in selecting more significant parameters (correlated parameters) that are responsible for watershed prioritization. The sub-watershed with the lowest compound value is ranked first in priority. They found out that the sub-watershed SW-8 was the highest priority due to high risk to soil loss, while sub-watershed SW-17 is low priority.

AgnihotriI *et al*., 2020 examined the current study, the geospatial technique was utilized to prioritize the sub-watershed of the Noyyal River Basin to control soil erosion and propose water conservation measures. The study describes the importance of using a digital elevation model to evaluate the drainage pattern and to extract relevant parameters. The river basin was categorized into 17 sub-watersheds, designated as SW1–SW17. The stream order of watershed ranges first to fifth order and possesses a dendritic drainage pattern. Thirteen fundamental morphometric parameters classified as linear, areal, and relief aspects were considered for the Noyyal River Basin. Principal component analysis (PCA) was performed in the current study for categorization and the morphometric parameters were correlated. PCA analysis is a more appropriate, well-known, commonly

used method for having versatility in selecting more significant parameters (correlated parameters) that are responsible for watershed prioritization. The sub-watershed with the lowest compound value is ranked first in priority. It reveals that sub-watershed SW8 has a high priority while low priority is given to sub-watershed SW17. According to the results, more water and soil-conserving measures are suggested in the respective sub-watersheds.

**2.4 Estimation of Soil loss**

Kovac *et al*., (2012) examined erosion and reservoir siltation in ungauged Mediterranean catchments by the Phosphate model (Stone *et al*., 1995; de Vicente *et al*., 2010). Soil loss was estimated using Universal Soil Loss Equation (USLE) (Wischmeier and Smith, 1965, 1978; Wang *et al*., 2001; Bagarello *et al*., 2012; Zhang *et al*., 2008; Addis *et al*., 2015; Pham *et al*., 2018). Parameters of USLE are associated with meteorological data (rainfall intensities and heights within the simulation period) and various maps it regards catchment properties (topography, slope, physical soil type, topsoil humus content, land use classes, land management practices). Area-specific annual soil loss values were calculated for each cell. Sediment suspended (SS) is evaluated by joining the individual cells in keeping with the flow tree. High sediment concentration hot pot is merely focused the land use management zone viz., Source controls (land use conversions, nutrient management, cultivation method changes) are planned to scale back emissions at their source by reducing the soil contamination or the quantity of the runoff and soil loss. Transport-controlling measures (buffer zones, swales and constructed wetlands) are implemented to retain SS and particulate P during their transport within the field and also along the riverbed. But, the phosphate model is restricted for estimation of erosion risk.

Erosion susceptibility indicators like soil loss factor (USLE-K) (Römkens *et al*., 1997; Vaezi *et al*., 2010; Alaboz *et al*., 2021) dispersion ratio, and aggregate stability by applying various algorithms CHAID (Chi-Squared Automatic Interaction Detector), Exhaustive CHAID, CRT (Classification and Regression Trees), and MARS (Multivariate Adaptive Regression Splines) in decision trees and assessing the spatial distribution of those properties using multiple interpolation methods (Albayrak and Yilmaz, 2009).

However, it does not seem to be many estimation studies of erosion susceptibility parameters using the choice tree estimation approach.

Integrated Valuation of Ecosystem Services and Tradeoffs (InVEST) Sediment Delivery Ratio (SDR) (Gashaw *et al*., 2021) model are used for estimating soil loss and sediment export. They discovered that InVEST SDR can be used for identifying high risk erosion zone and prioritizations of sub-watersheds for soil and water conservation (SWC) planning.

Revised Universal Soil Loss Equation (RUSLE) (Renard, 1997; Römkens *et al*., 1997; Wang *et al*., 2001; Zhang *et al*., 2008; Parras-Alcántara *et al*., 2016; Zerihun *et al*., 2018; Kayet *et al*., 2018) model and Geographic information system (GIS) approach (Pham *et al*., 2018; Mohammed *et al*., 2020) and SCS-CN (Soil Conservation Service - Curve Number) estimates soil loss by applying rainfall passivity and runoff erosivity (R), soil erodibility (K), slope length and steepness (LS), cover management (C) and conservation practice (P) factors. Clearly drawn out that the RULSE method is one of the most widely applied models for the estimation of soil – water erosion.

The Universal Soil Loss Equation (USLE) and also the Revised USLE (RUSLE) the initial USLE nomograph (Knomo) and EPIC (KEPIC) (Wischmeier and Smith, 1978; Renard,1997) were employed to evaluate the following soil properties, organic matter content, soil texture, soil structure, and permeability for estimating soil loss by the entire country of Brazil. With this result, the rate of soil loss is extremely found within the western Amazon (de Faria Godoi, *et al*. 2021). However, RUSLE/USLE models are the foremost widely used method for soil loss and erodibility estimation and prediction, data acquisition which is critical for determining prediction relies on secondary, ground verification or field survey is necessary for proving the rate of erosion whether it's correct or wrong.

Many researchers emphasize to substitute multiples of techniques for finding a new model to carry out better result, which want to clarify. Like, specific sediment yield (SSY) (Bussi *et al*., 2013; Jolly, 1982) involves the determination of the volume ($V_s$) and dry bulk

density (dBD) (Verstraeten and Poesen, 2001), of reservoir deposits that accumulated throughout a specific period of time ($T_R$) (Rowan *et al*., 1995) deposited in the reservoir basin defines the reservoir sediment trap efficiency (TE) (Brown, 1944), the size of the reservoir catchment is (A) (Verstraeten and Poesen, 2002). The then, a new equation is ready for substituting all these formulae by evaluating the specific sediment yield (SSY), hence $SSY = V_{s*}\, dBD/T_{R*}TE*A$, (Bussi *et al*., 2013; Reinwarth *et al*., 2018). The sediment delivery ratio (SDR) (USDA-SCS, 1983) describes the interrelationship between erosion by water and fluvial sediment delivery and is defined as the ratio of SSY to the catchment-area average gross soil loss rate (E) (Glymph, 1954; Roehl, 1962). By substituting the formula, it enables to figure out catchment-area average gross erosion rate (E), therefore, E = SSY/SDR, (Walling, 1983).

Erosion risk analysis was performed by Gürtekin and Gökçe (2021) at Harebakayış sub-watershed of Elazig, Turkey using RUSLE model based on GIS. GIS integration at raster calculator was utilized in order to estimate total soil loss and rate of soil erosion. They found out that the high erosion risk was estimated as 68% in grasslands with 70% in sparse forest. Similarly, the results depicted that 43.2% of TGA was high in erosion risk, while the erosion risk was low and normal level in 56.8% of the TGA of sub-watershed. Furthermore, the regions with high erosion are relatively distributed in the western part of the sub-watershed. The study concludes that the high risk of erosion in Harebakayış sub-watershed of Elazig is due to steepness of slope and sparse vegetation cover.

Kumar *et al*., 2022 has been conducted prediction of soil erosion and prioritization of sub-watersheds in Nainital district Uttarakhand, India using the combination of revised universal soil loss equation (RUSLE) with remote sensing (RS) and geographical information system (GIS) techniques. The parameters influencing soil loss such as rainfall-runoff erosivity (R) factor, soil erodibility (K) factor, slope length steepness (LS) factor, cover management (C) factor, and the erosion control practices (P) factor are integrated using GIS environment. Similarly, the geo-spatial aspects such as land use/land cover (LU/LC), the digital elevation model (DEM), slope, contours, drainage network, soil texture, organic matter, and rainfall were integrated using raster calculator. They found out

that the annual average soil loss ranges between 20 to 80 t $ha^{-1}$ $yr^{-1}$ in the Nainital. Furthermore, 7 out of 50 sub-watersheds were required immediate action for conserving natural resources, while only 4 sub-watersheds of the total were given lowest priority. Moreover, the major portions of Nainital district falls under the severe prone category of soil erosion, and therefore required immediate action plans to check soil erosion and evade the possibility of landslides.

The universal soil loss equation (USLE), modified universal soil loss equation (MUSLE) (Wischmeier and Smith, 1978), revised universal soil loss equation (RUSLE) (Renard *et al*., 1997), soil and water assessment tool (SWAT) (Arnold *et al*., 1998), and European soil erosion model (EUROSEM) (Morgan *et al*., 1998) are the most popular empirical methods available for predicting soil erosion. The utmost extensively used models to assess soil loss among empirical approaches are RUSLE and USLE. The empirical approaches, RUSLE and USLE techniques are the same (Vanlalchhuanga et al. 2021). However, RUSLE has a few advantages over USLE. The RUSLE empirical approach is modified and upgraded, such as monthly rainfall factors (R), slope length and steepness of slope (LS) factor (Renard *et al*., 1997).

In this study, RUSLE (Renard *et al*., 1997) empirical approach was employed to compute soil loss in the Tuirial basin of Mizoram by incorporating five parameters, such as soil erodibility factor (K), rainfall erosivity factor (R), cover management factor (C), conservation practice (P) factor, slope length and steepness factor (LS) (Renard *et al*., 1997). The advantage of RULSE model is it can accurately estimate annual soil loss (Tessema, 2020). A number of scientific investigations have been performed to estimate annual soil loss using RUSLE and geospatial techniques globally, such as the upper Tuirial watershed (Barman *et al*., 2020), in the northeastern part of India, at Mahadevpur block (Vanlalchhuanga *et al*., 2021), the western Ghats of Kerala (Thomas *et al*., 2018), the lower Kulsi basin of Northeast India (Thakuriah, 2023) and also in other countries, like Sri Lanka, at the Sabaragamuwa basin (Senanayake *et al*., 2020), and in Malaysia, at the Pansoon sub-basin (Yusof *et al*., 2019). Thus, this method is commonly used to estimate and prediction of future soil loss. The present study includes the details of thematic layer

to compute LS factor like flow accumulation ($\lambda$), variable length-slope exponent ($m$), factor that varies with slope gradient ($\beta$), slope angle ($\theta$), slope length ($L$), and the steepness of slope ($S$). These parameters give the accurate result of LS factor.

### 2.5 Estimation of siltation

Rãdoane and Radoane (2005), examined 138 dam the sediment sources and reservoir siltation in Romania. They found out that the 15 dams are in very serious condition with average sediment accumulation of 8 million $m^3$ during the initial 2 to 10 years. Again, 30 dams are experiencing serious siltation issue with about 35 million mc sediment accumulation during 10 to 50 years of dam function. In addition, all these severe siltation dams are situated in Carpathian mountain range. Besides that, the specific sediment yield is over 250 tons/$km^2$/$yr^{-1}$. This study suggests that the controlling factors and sources of sediments are the composition of the lithological structure and the size of the basin.

Endalew and Mulu (2022) investigate the rreservoir sedimentation during 2016 – 2021 at Shumburit earth dam of Ethopia by employing bathymetry survey technique and remote sensing data. They reveal that the total deposited sediment during 5 years is over 0.364 M tons, which reduces about 7.52% of the dam gross storage capacity. In addition, the siltation rate is estimated as 49500 $m^3$/yr and thereby reduced 1.25% of dam storage. Furthermore, this research also identifies Shumburit dam specific sediment yield of 45.46 tons/ha/$yr^{-1}$, which exhibits average sediment production is higher than global and African countries. They also discover that the reservoir will not function more than 15 years if the siltation rate is continued as the previous six years. Sediment accumulation is a major factor in reducing the useful life of irrigation reservoirs. This study also highlighted the key source of extreme sedimentation in the Shumburit reservoir is agricultural areas, no implementation of buffer zone and improper watershed management. Apart from that during the construction of dam, the designer and authority must pay more attention on sediment pit at the bottom of dam for flushing out the accumulated sediment to sustain economic useful lifespan of dam.

Several studies were performed with the approaches of bathymetry survey technique, remote sensing and geographic information system to determine the amount of sediment accumulation, the rate of siltation, trap efficiency, and storage capacity loss at dam site across the globe. The bottom topography changes were estimated by spatio-temporal image analysis and bathymetric survey at Sakuma Dam in Japan (Bilal et al., 2017) and Aswan high dam in Egypt (El-Sersawy, 2005). Geographic information system and remote sensing techniques are useful to determine the storage loss and sediment accumulation (Dadoria *et al*., 2017). Similarly, by analytical method with the integration of bathymetric survey data of Koyna reservoir in the Western Maharashtra (Patil and Shetkar, 2015) and Wonogiri reservoir in Central Java Province (Wulandari *et al*., 2015) the sedimentation was monitored. Moreover, other groups used to estimate sediment accumulation at the bottom of dam by normalized difference water index (NDWI) (Shukla *et al*., 2017; Jagannathan and Krishnaveni, 2021), water ratio index (WRI) and normalized difference vegetation index (NDVI) (Rokni *et al*., 2014; Gautam *et al*., 2015), modified NDWI (Ali *et al*., 2019) and combination of all other above methods (Acharya *et al*., 2017) yielded positive results. However, those methods were applicable only for the estimation of surface volume. Thus, all the above methods were successfully performed at the global level, although remote sensing techniques are found to be more advantageous, even in case of non-availability of ground data (Bhavsar and Gohil, 2015). However, bathymetry survey is useful to validate trap efficiency and other techniques of sedimentation estimation (Issa *et al*., 2015). Besides that, hydrographic surveys and grab sampling methods also useful to estimate siltation level during the rainy season (Godwin *et al*., 2011). This area is witnessing severe erosion due to fragile steep slopes and unconsolidated sedimentary rocks with high intensity of rainfall during monsoon period. So far, no proper scientific investigations were carried out in this area on siltation estimation. The present study is first of its kind to estimate the rate of siltation, sediment thickness and its distribution along with useful life span of Tuirial dam by bathymetry survey, remote sensing and geographic information system.

Kumar *et al*., 2022 conducted estimation of sediment yield assessment, prioritization and control practices in Chambal river basin using SYI model. The Sediment yield index (SYI) method is employed using soil texture, topography, rainfall erosivity, geomorphology and landuse-landcover parameters to compute the spatial distribution of sediment yield rate and plan soil conservation and prioritize watershed in the Chambal river basin. The model does not provide absolute sediment yield value and can be used only for qualitative purposes. The present study estimated the sediment yield rate between 560-2625 ton/ha/yr with an average value of 1608.89 ton/ha/yr and severe, very high, high, moderate, and low priority zones. The priority levels are determined based on average sediment yield values and conservation approaches are proposed for all the catchments.

Darama *et al*., 2019 examined sediment deposition of Hasanlar Dam using bathymetric and remote sensing. The study found out that the analysis of the bathymetry along with RS and GIS technique indicated that storage loss in reservoir active volume between 1974 and 1999 was 24% and between 1974 and 2014 storage loss was 26%. The study reveals dam storage was reduced due to huge volume of sediment deposition. The bathymetry survey depicted dam storage capacity was decreased by 26% of the total dam storage capacity. The sediment accumulation is more close to entrance of the reservoir along with the deepest part of the dam bottom. Besides that, severely deposited sediment is found nearby the spillway. The specific sediment yield during 40 years is estimated as 1.12 ton/$m^3$ and sediment yield is about 1347.5 ton/$km^2/yr^{-1}$. Furthermore, the remote sensing data enabled to estimate surface area and volume of water at the dam. Thus it was depicted as time saving and low financial investment to carry out this type of research using bathymetry and remote sensing technique.

Shiferaw and Abebe, 2021 studied siltation and economic lifespan of the reservoir at Abrajit reservoir in east Gojjam, Amhara region, Ethiopia using bathymetry and toposheets survey. The accumulated sediment volume was estimated by subtracting the TIN raster layer of the initial from the currently measured bed level. They have revealed that 343700.1 $m^3$ bulk of sediment was accumulated which reduces 20% of the total reservoir storage capacity. Similarly, they found out that the amount of sediment

28,641.675 $m^3yr^{-1}$ is the catchments contribution, so that reduces 1.66% of annual reservoir volume. They estimated the economic life span of reservoir is less than 12 years. The estimated specific sediment yield (SSy) was found to be 4733.38 ton/$km^{-2}/yr^{-1}$. For the durability and proper functioning, the dam it is recommended for regular monitoring of sediment accumulation in the reservoir.

Skariah and Suriyakala, 2021 investigated the amount of sediment deposition in Idukki reservoir using satellite remote sensing method. LANDSAT 8 OLI/TIRS satellite images for the period 2017–2019 were used to assess the water spread area using Normalized Difference Water Index (NDWI), determine the sediment deposition and evaluate the revised capacity of the reservoir. They have revealed a reduction of 11.6% between the original base year (1974) and current year (2019). The loss in live storage capacity between the years 1974 and 2019 was 0.10 $km^3$ which is equivalent to 100 $hm^3$. They mentioned the conventional method like bathymetry survey required huge financial investment, similarly time-consuming. Therefore, the satellite image is recommended for accumulation of siltation in reservoir. However, estimation of silted sediment without conducting bathymetry survey the possibility of error is high. For instance, to perform siltation at dam bathymetry survey is a must.

Mekonnen *et al*., 2022 evaluated the rate of sedimentation and storage capacity of Adebra night storage reservoir (NSR) by bathymetric survey. A comparison of original and current reservoir capacity was used to evaluate the quantity of sediment deposition in the reservoir. The Adebra NSR reservoir capacity was decreased by the accumulation of sedimentation from 36,902 $m^3$ in 2012 to 27,722 $m^3$ in 2020. The results of this study showed that the Adebra night storage reservoir had lost on an average 24.8% of its capacity due to sedimentation, during 8 years of operation. The average deposition rate of sedimentation in Adebra NSR was estimated to be 1147.5 $m^3/yr^{-1}$, with a loss rate of 3.1% per year. The value of sedimentation rates found in live storage of the reservoir area was 1147.5 $m^3/yr^{-1}$. In general, the study findings showed that the capacity of NSR was reduced by the accumulation of sedimentation year to year throughout the design period. Therefore, to improve the capacity of NSR should be planned and implemented different techniques

of sediment control and removal, depending on the estimation of sediment production from watersheds of inlets and outlets of reservoirs.

Tesfaye *et al*., 2022 carried out temporal change of dam storage in three reservoirs situated at Nile river basin using toposheets, remote sensing data and bathymetry survey. The Normalized Difference Water Index (NDWI) was used to estimate surface volume temporal change. Again, toposheet was used for initial dam bottom survey and the recent year is performed bathymetry survey. Percentage Difference Area Index (PDAI), Normal Difference Area Index (NDAI) techniques also informed the deviation of storage dam from toposheet bottom elevation, satellite image and bathymetry field survey. This research found out that the 0.33%, 2.53% and 2.13% dam storage loss in Koga, Shina and Selamko reservoirs during 2009-2016. In a span of 9 and 11 $Mm^3$ Koga reservoir storage capacity has reduced from, showing an annual storage loss of (2009–2016), which exhibits the rate of siltation is exceeding global average by 1%. Similarly, this indicates sedimentation issue in these three reservoirs suggests that relatively higher than other reservoir in Ethiopia. To improve the sustainable useful life span of reservoir the implementation of proper water management strategic plan is immediately required. Additionally, to sustain the dam storage capacity adoption of manual and mechanical sediment pit construction is essential for flushing.

## 2.6 Conclusion

The existing literature give more knowledge on research methods, along with the region to region and global research conducted system for the estimation of siltation and erosion at watershed level. In this thesis I have reviewed 89 articles international, 55 national and 4 regional articles regards on estimation of soil loss and siltation at the reservoir.

# CHAPTER – 3

# RESEARCH METHODOLOGY

## 3.1 Introduction

This chapter comprises an extensive collection of materials and a methodological design for the accomplishment of this thesis. However, the study is primarily focused on quantitative approaches to understanding watershed status. This chapter discusses the assessment of soil loss in the Tuirial watershed and siltation in the Tuirial dam. In addition, the study involves an investigation of drainage morphometry to determine the importance of erosion using morphometry parameters. Furthermore, innovative remote sensing and geographic information systems technology has been used with various models to offer useful insights into the processes of soil erosion and siltation in the Tuirial watershed, since this approach is a powerful tool for spatial analysis.

## 3.2 Data Acquisition

The data consists of primary and secondary are employed in the present research. The secondary data are acquired from various geo-spatial website, published articles and extensive field survey. The primary data was obtained from field survey. The topographical maps provided by the survey of India at 1: 50,000 were utilized to generate watershed boundary. Geology, lithology and Geomorphic landforms with tectonics were obtained from geological survey of India (GSI) online data portal, Bhukosh-GSI to generate thematic layers. Advanced land observing satellite (ALOS) phased array type L-band synthetic aperture radar (PALSAR) Dem at 12.5m x 12.5m resolution (Copernicus), soil texture data acquired from Mizoram state remote sensing application centre (MIRSAC) and daily rainfall data (Table 1) from NASA Power at seventeen rain gauge stations (NASA power). Sentinel 2B MSI2C at 10 m resolution was downloaded from Copernicus European Space Agency (ESA).

A number of field surveys were conducted for erosion inventory, and various locations of erosional and non-erosional characteristics were identified and recorded using a Garmin 550 GPS device. The height of the Tuirial River's sources in Chawilung was determined by a GPS survey. Ground truthing was widely utilized in visual observation and verification to establish the validity of theme layers like Lulc. Throughout the study, smart phones were utilized to gather extensive field photographs with high resolution.

### 3.3 Generation of geo-environment thematic layers

The Tuirial watershed is covering large area of about 1414.26 $km^2$ characterised by elongated shape, as it is falling in five topographical sheets. The topographical sheets are scanned using Ao size scanner. Geo-referencing was performed at Qgis software using online base map as a reference. The rectified toposheets are mosaiced as one Toposheet using merge tool. The mosaic Toposheet was projected at WGS 1984 UTM Zone 46N coordinate system. Then, important features such as roads, streams, spot heights, settlement and dam location are digitized using the digitizing tools of point, line, and polygon. Qgis and ArcGIS are the two softwares utilized for generation of thematic layers.

The elevation map was divided into five classes using manual classified symbol. Slope was generated from ALOS PALSAR DEM using spatial analyst tool. Slope and elevation was divided into five classes manually. Then, the raster was done reclassification with conversion into polygon. Again, polygon was dissolved at grid-code. Thus, the area calculation was performed in the attribute table using calculate geometry.

Geology, geomorphic features, lineament features and lithological units were obtained from Bhukosh-GIS. Those features were extracted from the downloaded geo-spatial data through the vector clipping tool. Then, polygon dissolve execution was performed by dissolve algorithm at their specific features. The area calculation was done using calculate geometry. Thus, each of the final thematic layers were generated separately using Qgis 3.22.

Daily rainfall data was acquired from NASA Power at seventeen villages located across the Tuirial basin. The daily rainfall data was converted to monthly rainfall. The yearly rainfall was then approximated using Microsoft Excel by adding all the monthly rainfall data. Similarly, the x and y coordinates of all the village wise rainfall data were used for interpolation. The inverse distance weighted (IDW) method was used to generate the thematic layer representing the spatial distribution of rainfall.

### 3.4 Land use and land cover classification

Satellite imagery, Sentinel 2B MSI2C, featuring 10 m resolution, was downloaded from the Copernicus European Space Agency (ESA). The selection of satellite image-captured date is a crucial task because of cloud cover and atmospheric distortion of the image quality. To avoid this issue, we opted for the image captured date is March 3rd, 2020. Ranganath *et al*., (2000) stated the best months for studying forest and vegetation types in north-east India's wet evergreen and semi-evergreen areas are February and March. The vegetation of the Tuirial watershed was estimated using normalized vegetation index (NDVI) values through the raster calculator in Arc-GIS. The NDVI formula was expressed as under (Eq.) (Rouse *et al.*, 1974). The NDVI output was again classified into five classes based on its distinctive pixel value and existing literature.

$$NDVI = \frac{(NIR - R)}{(NIR + R)} \qquad 3.1$$

Where, NIR indicate near-infrared red, and R signify the red band of the sentinel-2 satellite image.

#### 3.4.1 Layer stacking and sub-setting

For this study, all the band sets of sentinel (4, 5, 7, 8, 9, 10, 11, 12, 13) were merged into a single layer in Qgis 3.22. Each composite layer was assigned a different band (Red, Green, and Blue) with an output of two composite layers of true-color and false-color.

### 3.4.2 Image correction and enhancement

Geometric and radiometric corrections are essential for improving the visibility of satellite images for proper interpretation. The technique of filtering haze and dust reflection to adjust the brightness level of a satellite image is called radiometric correction. This correction helps to enhance the overall precision and makes it easier to contrast, identify, and properly interpret the image features. Geometric correction is another important step in satellite image interpretation. It involves rectification of distortions caused by the satellite's sensor tilt and terrain relief. By precisely aligning the image with its corresponding geographic coordinate system through geometric correction, which permits a more accurate analysis of the image. The present study used only the level 2 satellite images because all the data were corrected to remove geometric distortions (Srivastava *et al*., 2012; Ha *et al*., 2020).

### 3.4.3 Land use and land cover classification using the Orfeo tool box

The false color composite image makes it easier to distinguish different LULC patterns in the study area. This technique is more accurate for the identification of land features based on their tone, texture, shape, and other characteristics. Fifty (50) training samples were taken from different LULC patterns. After the selection of SVM and maximum likelihood, these training samples were input into the Orfeo toolbox, and later the algorithm was performed. The accuracy of the classified output was then assessed by means of comparing ground truth data and the results obtained (Bayarsaikhan *et al*., 2009; Brahmabhatt *et al*., 2000). Fallow land, built-up area, agricultural land, dense forest, and open forest are identified from natural color composite images.

### 3.4.4 Accuracy assessment

Evaluation of the accuracy of the image classified is an essential task in post-image classification. This evaluation helps in the performance of the classification model and the identification of any misclassification errors. Further, the accuracy assessment allows the comparison of different classification algorithms to determine the better image. The Orfeo

Tool Box (OTB) vector machine on the GIS platform and the confusion matrix function are used in this study for accuracy assessment. The confusion matrix function helps in evaluating the performance of the classification algorithm by providing information about the true negative and false positive classifications (Foody, 2002). The generated training samples were overlaid on the classified temporal image. These points represent the locations where the classification algorithm made predictions. By comparing the ground-truth data and the performance of the classification algorithm, potential areas are to be corrected. Additionally, this overlay process helps in visualizing the spatial distribution of different classes within the thematic layer to understand patterns and trends in the data. The "Confusion Matrix" function in Qgis is used to determine the Kappa coefficient for accuracy evaluation. The confusion matrix is used to compare referenced data to classified data and counts the number of observations that fall into each category. Based on the numbers in this confusion matrix, the Kappa coefficient is calculated (Eq. 3.2 - 3.5).

$$Producer's\ Accuracy\ (\%) = \left(\frac{x_{kk}}{x_{+k}}\right) \times 100 \tag{3.2}$$

$$User's\ Accuracy = \left(\frac{x_{kk}}{x_{+k}}\right) \times 100\% \tag{3.3}$$

$$Overall\ Accuracy = \frac{1}{N}\sum_{k=1}^{r} ni \tag{3.4}$$

$$Kappa\ co-efficient\ (K_c) = \frac{N\sum_{k=1}^{r} x_{kk} - \sum_{k=1}^{r}\ (x_{k+} \cdot x_{+k})}{N^2 \sum_{k=1}^{r}\ (x_{k+} \cdot x_{+k})} \tag{3.5}$$

Where $N$ is total number of pixels count, $r$ is number of LULC classes, $x_{kk}$ is total pixels from row "k" and column "$k$," $x_{k+}$ is total training samples in a row "k," and $x_{+k}$ is total training samples in column "k" from the error matrix.

### 3.5 Estimation of total soil loss in Tuirial watershed

Tuirial river basin is prone to soil erosion due to high intensity of rainfall, high surface run-off on the hill slopes, in addition to the human intervention in the thick forest cover to satisfy economic needs. It is extremely crucial to assess soil erosion prone zone at the river basin for suitable enactment of water and land resource controlling and preservation programme. This study aims to estimate the susceptible soil loss zones at the Tuirial river basin. As the majority of the land use and cover patterns were settlement, forest, water bodies, highways, fallow land, present cultivation, and settled cultivation, are associated with undulating topography in this fragile terrain, which promotes accelerated erosion.

The universal soil loss equation (USLE), modified universal soil loss equation (MUSLE) (Wischmeier and Smith, 1978), revised universal soil loss equation (RUSLE) (Renard *et al*., 1997), soil and water assessment tool (SWAT) (Arnold *et al*., 1998), and European soil erosion model (EUROSEM) (Morgan *et al.*, 1998) are the most popular empirical methods for predicting soil erosion. The utmost extensively used models to assess soil loss among empirical approaches are RUSLE and USLE. The empirical approaches, RUSLE and USLE techniques are the same (Vanlalchhuanga *et al*., 2021). However, RUSLE has a few advantages over USLE. The RUSLE empirical approach is modified and upgraded, such as monthly rainfall factors (R), slope length and steepness of slope (LS) factor (Renard *et al*., 1997).

In this study, RUSLE (Renard *et al*., 1997) empirical approach was employed to compute soil loss in the Tuirial basin of Mizoram by incorporating five parameters, such as soil erodibility factor (K), rainfall erosivity factor (R), cover management factor (C), conservation practice (P) factor, slope length and steepness factor (LS) (Renard *et al*., 1997). The advantage of RULSE model can accurately estimate annual soil loss (Tessema, 2020). The number of scientific investigations have been performed to estimate annual soil loss using RUSLE and geospatial techniques globally, such as the upper Tuirial watershed (Barman *et al*., 2020), in the northeastern part of India, at Mahadevpur block

(Vanlalchhuanga *et al*., 2021), the western Ghats of Kerala (Thomas *et al*., 2018), the lower Kulsi basin of Northeast India (Thakuriah, 2023). In other countries, like Sri Lanka, at the Sabaragamuwa basin (Senanayake *et al.,* 2020), and in Malaysia, at the Pansoon sub-basin (Yusof *et al*., 2019). Thus, this method is commonly used to estimate and prediction of future soil loss. The present study includes the details of thematic layer to compute LS factor like flow accumulation ($\lambda$), variable length-slope exponent ($m$), factor that varies with slope gradient ($\beta$), slope angle ($\theta$), slope length ($L$), and the steepness of slope ($S$). These parameters give the accurate result of LS factor.

The RUSLE approach was used to assess average annual soil loss (A) and erosion prone zone at Tuirial river basin which is highlighted in equation 3.6. The detailed methodological flow structure is followed in this approach (Figure 3.1)

$$A = R \times K \times L \times S \times C \times P \tag{3.6}$$

Where, $A$ is average of yearly soil erosion per unit area (t $ha^{-1}yr^{-1}$), $R$ is erosivity of precipitation (MJ mm $ha^{-1}$ $yr^{-1}$), $K$ is erodibility factor of soil (ha hr. $MJ^{-1}$ mm), $L$ is length of incline factor, $S$ is gradient of incline factor (dimensionless), $C$ is protection managing factor (dimensionless), and $P$ is preservation practice factor (dimensionless).

### 3.5.1 Precipitation erosivity factor (R)

Rainfall erosivity depends on the volume and concentration of precipitation (Renard and Foster, 1983), and significant to control soil loss (Thakuriah, 2023). The precipitation erosivity factor is governed by two downpour features like kinetic energy ($E$) and precipitation concentration within 30-minute interval ($I$) (Wischmeier and Smith, 1978). In the current study, thirty (30) years (1992–2022) of NASA power daily rainfall data at 413-metre resolution from seventeen rain gauge stations were taken to figure out $R$ factor. The rainfall data was interpolated using the inverse distance weighted (IDW) tool due to appropriate intended for smooth rainfall scattering and minimum error (Bakis *et al*., 2021). Thus, the precipitation erosivity factor (R) was assessed by applying equation 3.7 with the help of raster calculator in ArcGIS 10.4, (Vanlalchhuanga *et al*., 2021).

$$R = 79 + 0.363\,x \quad (3.7)$$

Where *R* is the precipitation erosivity factor (MJ.mm $ha^{-1}$ $hr^{-1}$ $yr^{-1}$), x is mean yearly precipitation (mm).

### 3.5.2 Soil erodibility factor (K)

The vulnerability of soil erosion is controlled by texture, size, chemical properties of soil, surface run-off, and the quantity and concentration of precipitation (Prasannakumar et al. 2011; Vanlalchhuanga *et al*., 2021; Thakuriah, 2023). Soil texture and the feature data were prepared by the data obtained from the Mizoram Remote Sensing and Application Centre. The *K* factors for each soil texture were accredited after obtaining the soil erodibility value from Barman *et al*., (2020). Then, transformed into a raster thematic layer using conversion tool from ArcGIS 10.4.

### 3.5.3 Steepness and Length of the Slope (LS) Factors

Length of the slope (*L*) is the length of distance between highest and lowest elevation the place where deposition started and to end by entering the river passage (Wischmeier and Smith, 1978). Angle of Inclination (*S*) is the angle of leaning of the slope, beside it is a dimensionless factor. The higher the slope length and the angle of inclination, the higher the possibility to susceptibility to soil erosion (Renard *et al*., 1997; Wischmeier and Smith, 1978). Earlier USLE and RULSE used for computing gentle slopes areas for one dimension however, in the rugged terrain region it becomes two-dimensional, to estimate LS factor is difficult (Van Remortel *et al*., 2004). There are various methods of LS factor calculation, although, in this study it was adopted LS factor computation after Van Remortel *et al*., (2004) and Moore and Wilson, (1992). The LS factor was generated from ALOS PALSAR DEM using equation 3.8 – 3.13.

$$\lambda = \left[\frac{Flow\ Accumulation}{3.1416}\right]^{0.5} \quad (3.8)$$

$$\beta = \frac{\sin\theta}{[3 \cdot (\sin\theta)^{0.8} + 0.56]} \tag{3.9}$$

$$m = \frac{\beta}{(1+\beta)} \tag{3.10}$$

$$L = \left[\frac{\lambda}{22.13}\right]^{m} \tag{3.11}$$

$$S = 10.8 \cdot \sin\theta + 0.03 \quad \theta < 9\%$$
$$S = 16.8 \cdot \sin\theta - 0.5 \quad \theta \geq 9\% \tag{3.12}$$

$$LS = \left[\left(\frac{"\lambda"}{22.13}\right)^{\wedge} "m"\right] \times "S" \tag{3.13}$$

where $\lambda$ is flow accumulation, $m$ is adjustable slope-length exponent, $\beta$ is a factor differs with slope incline, and $\theta$ is the slope angle, $L$ is the slope length (m), $S$ is inclination of slope.

### 3.5.4 Cover management factor (C)

The protection managing factor is defined as the proportion of soil erosion to diverse land use/ land cover. The *P* factor is constant, it ranges from 0 to 1, based on the pattern of land cover and landuse system. An area with vegetation cover slows down the velocity of rainfall, besides that raindrops indirectly hit soil particles resulted to less erosion. On the other hand, an area with bare-land, rocky and cultivation areas have more soil loss due to the uninterrupted raindrops hit on the soil surface (Prasannakumar *et al*., 2011; Rahaman *et al*., 2015). LULC thematic layer was generated from Sentinel 2B MSI2C at 10 m spatial resolution. Settlement, current cultivation, fallow land, water bodies, bamboo, dense, medium, and open forest types were identified as lulc classes in Tuirial watershed. The *C* factors for each lulc classes were accredited after obtaining the *C* value

from Barman *et al*., (2020). Then, transformed into a raster thematic layer using conversion tool from ArcGIS 10.4.

### 3.5.5 Practise management factor (P)

The preservation managing factor is the degree and volume of soil erosion under the conservation of vegetation compared with the up-land and low-land cultivation on the hill slope (Dabra *et al*., 2008; Das *et al*., 2018; Vanlalchhuanga *et al*., 2021; Thakuriah, 2023). Practise management factors such as contouring, terraces, proper drainage, and settled agriculture help to reduce the degree and quantity of soil erosion due to decrease surface run-off (Renard and Foster, 1983). As per the practise management factor, the P value is constant and ranges from 0 to 1. The value close by zero signifies that the preservation practise is good, whereas close to 1 refers to poor practise management (Chatterjee *et al*., 2014; El Jazouli *et al*., 2017; Ozsahin *et al*., 2018). The *P* factors for each lulc classes were accredited after the *P* value acquired from Barman et al. 2020). Then, transformed into a raster thematic layer using conversion tool from ArcGIS 10.4.

### 3.5.6 Thematic layer integration using Spatial Analyst tool

The obtained out values of R, K, C, P, and LS factors are transformed into a thematic raster layer, which was integrated through a raster calculator using ArcGIS 10.4, to derive the soil erosion layer of the Tuirial watershed (Eq.3.6). The thematic layer was reclassified into seven erosion risk zones by spatial analyst tools. Then, the raster layer of the soil erosion map was converted into a polygon to compute each soil loss area.

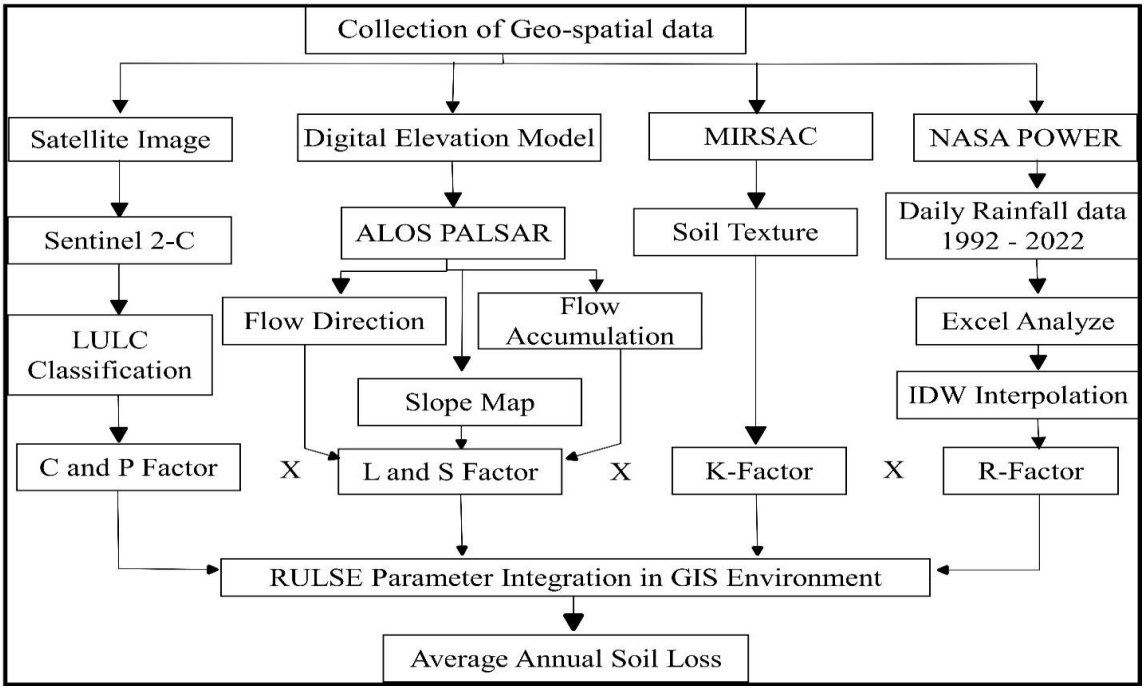


Figure 3.1: Work flow for estimation of average annual soil loss

### 3.6 Estimation of siltation in Tuirial dam

Reservoir sediment is transported by running water, deposited at the reservoir bottom, which is loaded from upstream (Skariah and Suriyakala, 2021). The reservoir sedimentation is a continuous process. It has become a major issue worldwide due to improper management of reservoirs and extensive exploitation of natural forest in the catchment area (Adongo *et al*., 2021). However, the measurement of siltation at the dam does not include statistical models of erosion (Bombino *et al*., 2022). The rate of siltation at the reservoir and the sediment transport index can be computed by measuring sediment pits and using the sediment yield model (Hassan *et al*., 2017; Maina *et al*., 2018). However, the bathymetry survey is the most precise method of evaluation of accumulated sediment at the reservoir than other approaches (Maina *et al*., 2018). These methods determine the sediment thickness at the initial reservoir bed level and the current year of sediment accumulated (Hassan *et al*., 2017). Several studies were performed with the approaches of bathymetry survey technique, remote sensing and geographic information system to determine the amount of sediment accumulation, the rate of siltation, trap efficiency, and

storage capacity loss at dam site across the globe. The bottom topography changes were estimated by spatio-temporal image analysis and bathymetric survey at Sakuma Dam in Japan (Bilal *et al*., 2017) and Aswan high dam in Egypt (El-Sersawy, 2005). Geographic information system and remote sensing techniques are useful to determine the storage loss and sediment accumulation (Dadoria *et al*., 2017). Similarly, by analytical method with the integration of bathymetric survey data of Koyna reservoir in the Western Maharashtra (Patil and Shetkar, 2015) and Wonogiri reservoir in Central Java Province (Wulandari *et al*., 2015) the sedimentation was monitored. Moreover, others groups used to estimate sediment accumulation at the bottom of dam by normalized difference water index (NDWI) (Shukla *et al*., 2017; Jagannathan and Krishnaveni, 2021), water ratio index (WRI) and normalized difference vegetation index (NDVI) (Rokni *et al*., 2014; Gautam *et al*., 2015), modified NDWI (Ali *et al*., 2019) and combination of all other above methods (Acharya *et al*., 2017) yielded positive results. However, those methods were applicable only for the estimation of surface volume. Thus, all the above methods were successfully performed at the global level, although remote sensing techniques are found to be more advantageous, even in case of non-availability of ground data (Bhavsar and Gohil, 2015). However, bathymetry survey is useful to validate trap efficiency and other techniques of sedimentation estimation (Issa *et al*., 2015). Besides that, hydrographic surveys and grab sampling methods also useful to estimate siltation level during the rainy season (Godwin *et al*., 2011). This area is witnessing severe erosion due to fragile steep slopes and unconsolidated sedimentary rocks with high intensity rainfall during monsoon period. So far, no proper scientific investigations were carried out in this area on siltation estimation. The present study is first of its kind to estimate the rate of siltation, sediment thickness and its distribution along with useful life span of Tuirial dam by bathymetry survey, remote sensing and geographic information system.

### 3.6.1 Bathymetry survey

Bathymetry survey was conducted to configure dam bottom topography elevation at 62 selected points. The surface water level of Tuirial dam is 73.35m above MSL (Neepco Bench Mark). The x and y coordinates of all 62 points were obtained by a field survey

using hand held GPS (Garmin Oregon 550) instrument. The z values of bottom elevation were obtained from the Neepco Bench Mark. Similarly, the dam depth was measured at the same points with the help of a timber boat by attaching about 2 kg of stone to the 100 meters long measuring tape at the end.

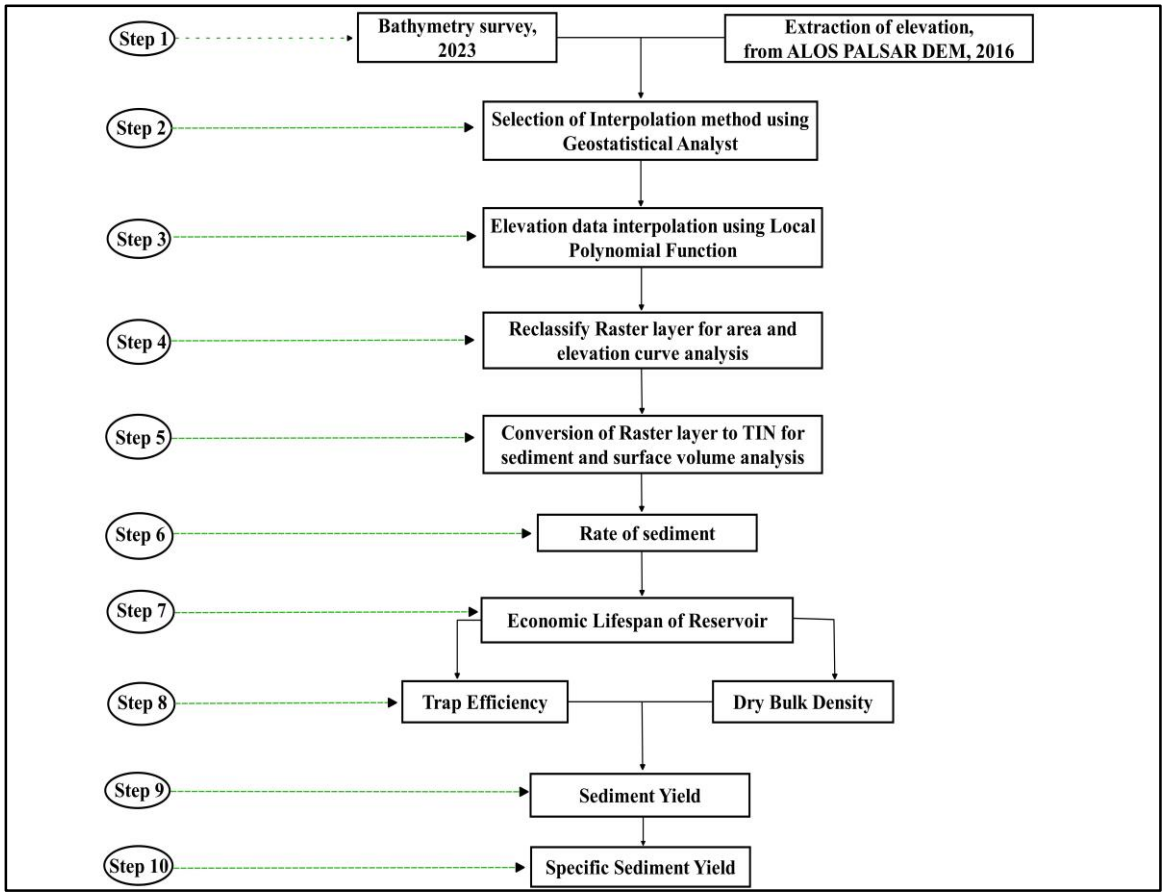


Figure 3.2: Flow chart showing methodology adopted

### 3.6.2 Extraction of elevation values from DEM

By using ALOS PALSAR DEM of the year 2016 at 12.5 × 12.5m resolution, the elevation data was extracted at the same bathymetry survey points for the generation of triangulated irregular network (TIN) (Eq. 3.14).

$$V\{\text{'dem'}, 1, \text{make} - \text{point}\ (1,1)\} \tag{3.14}$$

Where, V = raster value; 1 = latitude and longitude

### 3.6.3 Selection of raster interpolation method

In order to find out the most appropriate interpolation method, for the observed values and the predicted values geo-statistical tools were used. In this approach, the four distinct interpolation methods such as Kringing, local polynomial interpolation, radial base function and inverse distance weighted cross-validation were performed in order to validate the accuracy of each spatial interpolation method. So that each interpolation techniques are expected to give root mean square error (RMSE) (Eq. 3.15) and coefficient of correlation (r) value by applying both observed and interpolated values.

$$RMSE = \sqrt{\frac{1}{n}\sum_{k=1}^{n}[obs - int]^2} \quad \textbf{(}3.15\textbf{)}$$

Where, n is the number of observation points, *obs* is the observed value and *int* is the interpolated value.

### 3.6.4 TIN Interpolation

The z values of the bottom topography were obtained by bathymetry survey and the values were interpolated for the generation of TIN by using TIN interpolation technique. It is essential for the computation of the area and storage capacity of the reservoir. The TIN layer is characterized by three dimensions (x, y, and z) with a set of distinct triangles, signifies a computerized model of the dam bottom area consisting of randomly distributed vertices obtained from contour lines and point extents (Iradukunda *et al*., 2020; Arabkhedri *et al*., 2021; Stoner *et al*., 2022; Mekonnen *et al*., 2022). TIN surface obtained from the topographic survey, and the bathymetry survey was converted into raster layer (DEM). Contours with 1 metre interval were extracted from DEM and also elevation profile was generated by profile tools. Similarly, raster layer was converted into vector format to obtain the area of dam surface and bottom.

### 3.6.5 Estimation of dam storage capacity

The depth of dam and coordinates were measured by a measuring tape and GPS instrument (Garmin Oregon 550) respectively. The surface water level was measured taking Neepco Bench Mark as reference. The measured depth was subtracted from the surface water level (Neepco bench BM) to get the bottom topography. Then, Spatial Analyst tool was used to generate bottom topography using local polynomial function (LPF) interpolation. The interpolated DEM was converted into TIN. Thus, Tuirial surface area and dam storage capacity were computed by bathymetry data using 3D Analyst tools of surface volume in ArcGIS 10.4. This method was used to estimate storage capacity and sediment volume (Eq. 3.16).

$$SV = S_1 - S_2 \tag{3.16}$$

Where, SV = Sediment Volume ($m^3$), $S_1$ = Surface volume in the initial year ($m^3$), $S_2$ = Surface Volume of in the current year ($m^3$)

### 3.6.6 Estimation of sediment volume in Tuirial dam

The sediment volume was computed from the difference between the initial and current storage using the 3D Analyst surface volume tool. The topographic map of the year 1987 was found not suitable to calculate the initial storage of the Tuirial dam due to the dynamic change in elevation induced by the excavation of the landmass at the bottom and utilized for embankment fills to dam construction. In order to extract the elevation data from the ALOS PALSAR DEM the Equation (() was adopted. A local polynomial function was then adopted to interpolate the elevation points between the initial year 2016 and the bathymetry survey year 2023. To determine the surface area and storage capacity of Tuirial Dam, the interpolated raster data was converted into TIN layer using the spatial analyst tool in ArcGIS 10.4. This method is widely used for the estimation of sediment volume (Shiferaw and Abebe, 2021; Mekonnen *et al*., 2022). By using raster calculator minus tool, the initial (2016) reservoir bed elevation was subtracted from the current (2023) reservoir bed elevation to compute the total sediment accumulated during the course of time.

### 3.6.7 Trap efficiency of Tuirial dam

The quantity of inflow sediment that is deposited at the dam is known as trap efficiency (TE) (Brune, 1953; Verstraeten and Poesen, 2001). For the virtue of the reservoir sediment trap, the weight of sediment must be modified in order to find out sediment deposited at the reservoir. Again, to avoid underrate of sediment deposited at the reservoir, the discharge of sediment from the dam must be adjusted, which is common in any reservoir unless the water level is constant (Verstraeten and Poesen, 2001). There are various methods available for computing the TE of a reservoir. However, inflow capacity of reservoir was employed to compute trap efficiency as there is no universally accepted scientific method for TE (Moges *et al*., 2018). While in Brown model, ratio of the watershed area to capacity of reservoir was used to compute TE. This method is one of the most commonly used empirical approaches for small reservoirs when the river is ungauged (Verstraeten and Poesen, 2001). Assuming that the incoming flow equivalent to discharge in large reservoirs, disregarding evaporation and leakage prompt the water level shrinkage would lead to disparity in the amount of sediment estimation in reservoirs (Brown, 1943). In this study, the estimation of trap efficiency was performed by applying Brown's approach as illustrated in Equation 3.17.

$$\text{TE}\ (\%) = 100\left[1 - \frac{(1)}{\left(1 + 0.0021D \times \frac{(C)}{(A)}\right)}\right] \tag{3.17}$$

Where, TE (%) is trap efficiency, C is Tuirial Dam storage capacity ($m^3$) and A is watershed area ($km^2$). D is a constant value depending on the soil texture size ranges from 0.046 to 1. The soil texture was identified using the Indian Society of Soil Science (ISSS) soil mixture classification system. The soil texture confine to more than 70 per cent is considered as fine sediment. Hence, D = 0.046 is fine sediment (Gill, 1979).

### 3.6.8 Dry bulk density

Computation of dry bulk density is necessary in order to find out the sediment yield at the Tuirial reservoir. The undisturbed soil samples were collected from the basin, and dried for two days as per the standard procedure to measure the dry bulk density. The weight of sediment sample was measured and the weight of instrument was subtracted from the total weight. Then the dry bulk density was computed using the Equation 3.18.

$$\mathrm{dBD} = \frac{\mathrm{NW}[\mathrm{SW} - \mathrm{IW}]}{\mathrm{IC}} \tag{3.18}$$

Where, dBD is dry bulk density, *NW* is net weight (kg), *SW* is sediment weight (kg), *IW* is instrument weight (kg) and *IC* is instrument capacity (litre)

### 3.6.9 Estimation of sediment yield (Sy) and specific sediment yield (SSy)

The sediment yield (Sy) was computed using Equation 3.19. The specific sediment yield (SSy), was computed using Equation 3.19. The average dry bulk density (dBD) and trap efficiency (TE) of Tuirial dam was estimated as 1397 kg/m$^3$ and 57.50% respectively.

$$\mathrm{SY} = \frac{\mathrm{SV} \times \mathrm{dBD}}{TE \times \mathrm{T}} \tag{3.19}$$

Where, *SY* is Sediment Yield (ton/km$^2$/yr$^{-1}$), *SV* is Silt Volume (ton/m$^3$), *dBD* is dry Bulk Density (ton/m$^3$), *TE* is Trap Efficiency (%), *T* is duration of Tuirial dam operation

$$\mathrm{SSY} = \frac{\mathrm{SY}}{\mathrm{A}} \tag{3.20}$$

Where, *SSY* is Specific Sediment Yield (ton/km$^2$/yr$^{-1}$), *SY* is Sediment Yield (ton/yr$^{-1}$), *A* is Watershed area (km$^2$)

### 3.6.10 Rate of sediment accumulation

To compute the rate of sediment accumulation in Tuirial dam Equation 3.21 was used.

$$\mathrm{RS} = \frac{SV}{\mathrm{T}} \tag{3.21}$$

Where RS is rate of sediment ($m^3/yr^{-1}$), *SV* is Silt Volume ($ton/m^3$), T is duration of Tuirial dam function (yr)

### 3.6.11 Estimation of sediment thickness

The distribution of sediment thickness in the Tuirial reservoir was computed from Bathymetry survey elevation point data and extracted DEM elevation points data. It was interpolated using local polynomial function (LPF). Again, the interpolated data was converted into raster and reclassified using conversion tools and spatial analyst tools. From the initial bed level in the year 2016 to the bed level of 2023 the interpolated raster layer was subtracted using raster minus tools, to obtain the sediment deposited at the reservoir bed. Finally, at the same points of bathymetry survey, the elevation raster data of sediment deposited was extracted using Equation 3.16.

### 3.6.12 Economic life time of Tuirial dam

The rate of siltation at the Tuirial dam was assumed to be constant due to ungauged river channel and without control measure of sediment within the watershed (Haregeweyn *et al*., 2012; Shiferaw and Abebe, 2021). The Tuirial dam functional lifespan was computed using the Equation 3.22 as illustrated by various scientific investigations (Moges *et al*., 2018; Haregeweyn *et al*., 2012; Shiferaw and Abebe, 2021; Mekonnen *et al*., 2022).

$$\mathrm{LE} = \frac{\mathrm{RSC}}{\mathrm{RS}} \tag{3.22}$$

Where, LE is Economic life time (yr), RSC is Current Reservoir Storage Capacity ($m^3$), RS is Rate of sediment ($m^3/yr^{-1}$).

## 3.7 Analysis of morphometry in Tuirial watershed

Pioneering Horton (1932, 1945) works concentrated in stream number, stream length, drainage density, and channel frequency. Strahler (1952, 1964) adjusted the Horton works to perform further analysis like stream order, form factor ratio, bifurcation ratio,

relief basin, circularity ratio, stream length ratio. Likewise, other various researchers developed the new parameters like elongated ratio, relief ratio (Schumm, 1956), relative relief ratio (Melton, 1958), hypsometric integration (Pike and Wilson, 1971), ruggedness number (Patton and Baker, 1976), hypsometric curve (Kouli et al, 2007), and gradient ratio (Sreedevi *et al*. 2009).

Earlier, the river basin and sub-watershed level of the drainage characteristics were performed by conventional methods at global scale. The advancement of information technologies in geographic information system and spatial remote sensing data (RS and GIS) provide a powerful tool for computation and assessment of various hydrological characteristics at global level. Systematically using geo-spatial approach to perform morphometric analysis of drainage basin has been conducted by various researchers (Rao, 2015; Sreedevi *et al*. 2009). Their result revealed that, morphometric analysis using remote sensing and geographic information system provides the principle information of landform, hydrogeological features of the watershed. The advantage of geo-spatial approach has low in capital investment, expenditure and time saving. In this study, the Tuirial river basin, the linear, areal and relief morphometric parameters were computed by applying pioneering worked out equations with geospatial data and GIS techniques (Table 3.1).

Table 3.1 Details of morphometric parameters and their equations

| Category | Morphometric Parameter | Formula | References |
|---|---|---|---|
| Linear features | Stream order (U) | Hierarchical rank | Horton (1945) |
| | Stream number ($N_u$) | $N_u = N_1+N_2+\ldots+N_n$ | Horton (1945) |
| | Stream length ($L_u$) | $L_u = L_1+L_2+\ldots+L_n$ | Horton (1945) |
| | Mean stream length ($L_{sm}$) | $L_{sm} = L_u/N_u$ | Horton (1945) |

| | | | |
|---|---|---|---|
| | Stream length ratio ($L_{ur}$) | $L_{ur} = L_u/L_u - 1$ | Horton (1945) |
| | Bifurcation ratio ($R_b$) | $R_b = N_u/N_u + 1$ | Schumm (1956) |
| | Bifurcation ratio ($R_{bm}$) | $R_{bm}$ = average | Horton (1945) |
| | Basin length (km) | ArcGIS | |
| Relief features | Maximum basin height (m) (H) | ArcGIS | |
| | Minimum basin height (m) (h) | ArcGIS | |
| | Basin relief (m) (R) | R = (H - h) | Schumm (1956) |
| | Relief ratio (Rr) | $Rr = R/L_b$ | Schumm (1956) |
| | Relative relief ($R_{hp}$) | $R_{hp} = R/A$ | Smith (1935) |
| | Dissection index ($D_i$) | $Di = R_{hp}/R_a$ | Dove Nir, (1957); Singh and Dubey (1994) |
| | Gradient ratio ($G_r$) | $Gr = (a - b)/L_s$ | Sreedevi et al., (2005) |
| | Ruggedness number ($R_n$) | $Rn = R \times D_d$ | Schumm (1956) |
| | Hypsometric integration (HI) | Elmean-Elmin/Elmax-Elmin | Pike and Wilson (1971) |
| Areal features | Basin area (A) ($km^2$) | ArcGIS | |
| | Basin perimeter (P) (km) | ArcGIS | |
| | Drainage density ($D_d$) | $D_d = L_u/A$ | Horton (1945) |
| | Stream frequency ($F_s$) | $F_s = N_u/A$ | Horton (1945) |
| | Length of overland flow ($L_o$) | $L_o = D_d/2$ | Horton (1945) |

| | | | |
|---|---|---|---|
| | Constant channel Maintenance ($C_m$) | $Cm = 1/D_d$ | Schumm (1956) |
| | Form factor ($F_f$) | $F_f = A/L_b^2$ | Horton (1932) |
| | Circulatory ratio ($R_c$) | $R_c = 4\pi A/P^2$ | Miller (1953) |

Where, $N_u$ = number of stream segments, $L_u$ = total stream length of order (u), $L_{u-1}$ = the total stream length of its next lower order, $N_{u+1}$ = number of segments of the next higher order, $R_l$ = stream length ratio, $R_b$ =bifurcation ratio, H = highest elevation, h = lowest elevation, $B_h$ = basin relief, $L_b$ = basin length, R = basin relief, A = basin area, $R_{hp}$ = relative relief, $R_a$ = absolute relief, a = the elevation at the source of the river, b = is the elevation at mouth of the river, L= is the length of main stream, $D_d$ = Drainage density, P = perimeter of basin.

### 3.8 Conclusion

To fulfill this thesis a numbers of robust research methods were incorporated. For the estimation of total soil loss, revised universal soil loss equation (RUSLE) is employed. Secondly, siltation volume at Tuirial dam is estimated by bathymetry survey for the initial 2016 year and the present year 2023. In addition, to identify highly erosion influencing factor among the linear, areal and relief aspects were computed by pioneering works of morphometry parameters.

# CHAPTER – 4

# GEO-ENVIRONMENTAL SETTINGS

## 4.1 Geographical background of Tuirial watershed

Tuirial river basin covers an area of 1414.26 $km^2$ of land and lies between longitudes 92°42′ E – 92°52′ E and latitudes 23°26′ N – 23°52′ N. Tuirial watershed falls in the topographical sheets 83H/3, 83D/14A, 83D/14B, 83D/15, 83D/16, 84A/12, 84A/13, 84A/14, 84A/15, 84E/1, 84E/2, and 84E/3 generated by Survey of India such at 1: 50,000 scale. Tuirial River basin is divided into three watersheds such as upper Tuirial, middle Tuirial and lower Tuirial. The highest elevation of the area is about 1690 m above MSL and 23 m above MSL at the lowest. The different spot heights of the topography are highlighted in figure 4.1. It also forms the district boundary between Kolasib and Aizawl districts in the eastern side. In the lower course of the river, the biggest Tuirial hydel project in Mizoram was constructed. Tuirial Hydro Power Station is medium head storage scheme to harness the hydro power of Tuirial River and located at Saipum village of Kolasib Districts of Mizoram. The installed capacity of the Station is 60 MW and design head of 53 meters (https://neepco.co.in/power-generation/hydro-power/tuirial-hydro-power-station). In Tuirial watershed widely found four types of soil such as Loamy soil, Fine loamy, Fine loamy to loamy skeletal, Loamy skeletal, Coarse loamy (Barman et al., 2020; Lawmchullova and Rao, 2024). Within the watershed, there are 68 settlements with one city being existed, of which 33 and 35 settlements are in the western and eastern sides of the Tuirial river, respectively (Figure 4.2).

## 4.2 Road transport

Along the water divide line, there is well-developed road network. The Serkhan-Bagha road extends up to Saipum village, While NH-6 travels from Aizawl to Serkhan along the western water division line, the Serkhan-Bagha road continues up to Saipum village. NH-306A runs from Saipum to New Vervek, and NH-2 runs from New Vervek to Khanpui village along the eastern water division line. From Seling to Baktawng, NH-2

runs. Again, the PWD concrete road connects Baktawng and Hmuifang along the southern water divide line. The World Bank road connects the village of Hmuifang with Aizawl along the side of the national highway. The NH-306 runs perpendicularly from Khanpui to Aizawl. The present scenario of the ongoing road construction between Aizawl to Saitual district has significant impact of soil erosion due to high surface run-off. Huge volume of sediment influx is noticed at the main river due to improper earth spoil dumping site. Consequently, this would cause the ecosystem of riparian, shallow water along the river; especially siltation accumulation will decrease the reservoir capacity with the useful lifespan of Tuirial hydro-power dam.

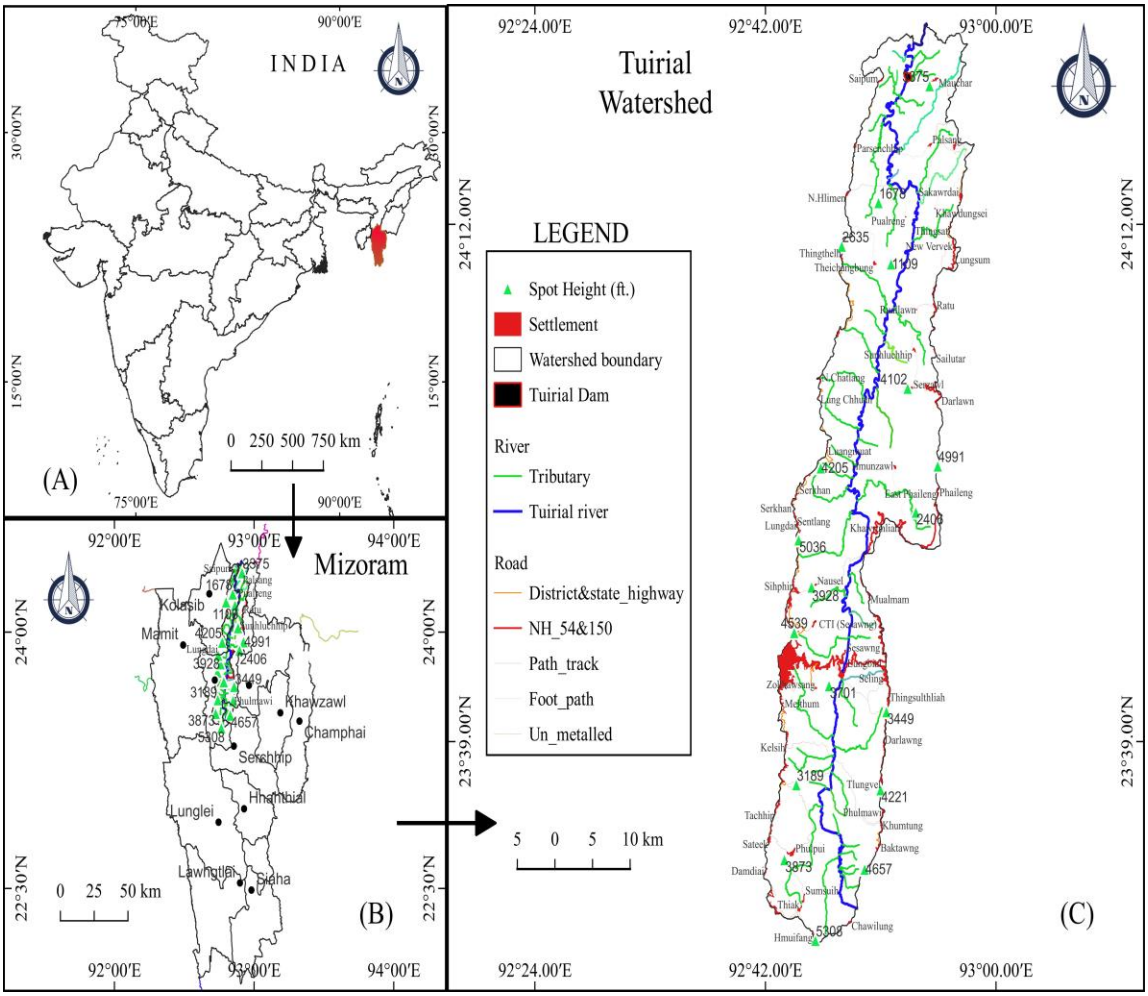


Figure 4.1: Location of study area

### 4.3 Drainage

The river is about 117 kilometers long. It originates from Chawilung hills at an elevation of 1080 meters (62 km from Aizawl). It flows northward to join the Barak river in Assam. Important perennial streams like Lungdai lui, Tuisen lui, Keitum lui, Tuiritai lui and Hachhe lui join Tuirial river before it joins the confluence of Barak river in Cachar district of Assam. The river has a total of 51 tributaries, 30 of which confluence on the western side and 21 on the eastern side. The sub-watersheds exhibit varying drainage pattern like, trellis, dendritic, sub-dendritic and parallel, of which dendritic pattern is predominant as the region is controlled by physiographic conditions and the neo-tectonic activity (Lawmchullova and Rao, 2024).

The Tuirial river has been divided into eight orders as per Horton stream ordering, of which the main Tuirial River is classified as $8^{th}$ order of the hierarchical system of streams. The Tuirial watershed was counted for 7273 streams, of which 882 streams fall in sw7 and 277 streams found in sw12 sub-watersheds to contribute the highest and lowest stream frequency, respectively. The total stream length of the watershed decreases with the increase in the stream order as per the law of Strahler (1952). But, in Horton (1932) stream ordering, one river is assigned as one order with no segment, because each river has origin and outlet, whereas in Strahler stream order it is shortening the main stream length because more than one stream confluences form the bigger stream order, then it forms the main river. The middle Tuirial watershed stream length constitutes $1^{st}$ stream order of 47.26 per cent, $2^{nd}$ order 22.85 per cent, $3^{rd}$ order 13.36, $4^{th}$ order 6.34 per cent $5^{th}$ order 4.93 per cent, $6^{th}$ order 2.02 per cent and $7^{th}$ order of 3.24 per cent of the total stream length. The $7^{th}$ order stream length (115.63 km) is higher than that of the $6^{th}$ (72.01 km) as the similar result highlighted by Iqbal and Sajjad due to variation of slope, topographic and lithological conditions.

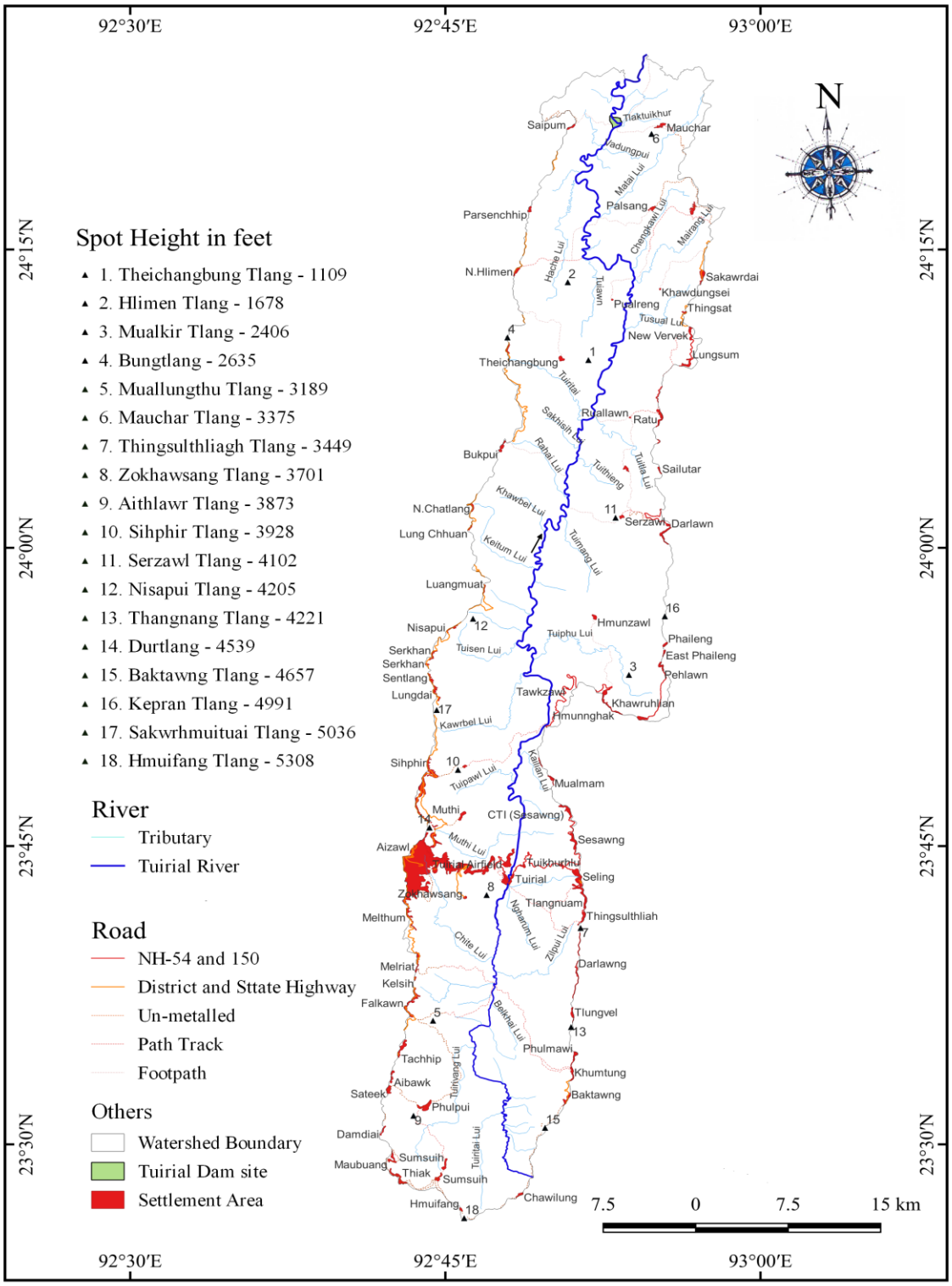


Figure 4.2: Distribution of settlements, roads and spot heights in the study area

Table 4.1 Stream-order, stream frequency and stream length of Tuirial drainage

| Watersheds | Lower | | Middle | | Upper | | Total | |
|---|---|---|---|---|---|---|---|---|
| Stream order | Length (km) | Stream (no.) | Length (km) | Stream (no.) | Length (km) | Stream (no.) | Length (km) | Stream (no.) |
| 1 | 1506 | 467.08 | 1691.52 | 5286 | 1660.94 | 5536 | 4858.46 | 11289.08 |
| 2 | 355 | 228.41 | 816.831 | 1299 | 732.54 | 1107 | 1904.38 | 2634.41 |
| 3 | 116 | 136.95 | 478.516 | 481 | 369.03 | 347 | 963.54 | 964.95 |
| 4 | 45 | 78.61 | 226.362 | 142 | 185.53 | 88 | 456.89 | 308.61 |
| 5 | 12 | 23.38 | 176.168 | 47 | 93.11 | 22 | 281.28 | 92.38 |
| 6 | 10 | 60.57 | 72.0096 | 10 | 67.29 | 11 | 149.30 | 81.57 |
| 7 | 1 | 2.44 | - | - | 22.51 | 3 | 23.51 | 5.44 |
| 8 | 4 | 44.93 | 72.0359 | 5 | 75.76 | 9 | 151.80 | 58.93 |

### 4.4 Climatic condition in Tuirial watershed

Tuirial watershed is not much different from other parts of Mizoram in climate. The region experiences warm and humid climate of tropical rain-forest. The climatic condition of this region is divided into four seasons as per Indian Meteorological Department (IMD) classification viz., winter (December - February), spring (March – April), Monsoon (June-September), autumn (October – November). The climatic condition is determined by climatic variables such as rainfall, temperature, humidity, sunshine, wind, air and evaporation of the region. Consequently, this climatic factors are the agents of soil erosion

### 4.4.1 Rainfall

The average rainfall received in Tuirial watershed is around 1500 mm annually. The rainfall received at Tuirial watershed is influenced by tropical cyclone, thunderstorms and convectional rainfall. The season-wise spatial distribution of rainfall at various rainfall gauge stations are highlighted in figure 4.4. The least rainfall occurred in winter season is about 14 mm/month. The temperature starts rising at the onset of spring and also thunderstorms and cyclones which bring more rainfall during the pre-monsoon season of around 133 mm/month. The southwest monsoon is the main source of rainfall in this region. The area receives most of the rainfall during the monsoon season in early months of June. The highest rainfall occurred in monsoon season in a year, is around 237 mm/month (Fig 4.3). During the retreating monsoon, it receives about 70 mm/month of rainfall. The figure 4.5 indicates the spatial distribution of rainfall throughout the year in Tuirial watershed. The western highland and southern part of the watershed are relatively higher rainfall than the north-eastern and low valley.

Among the climatic factors, rainfall has significant impact on soil erosion. Raindrops detach loose soil particles and absorb soil mass due to limitation of infiltration, thus it transports them from origin to new places by surface run-off. When run-off occurs, the soil surface is susceptible to water erosion, i.e. erosion due to running water. The erosion process includes three primary stages: detachment, transport, and deposition. At the soil surface, detachment of soil particles from the bulk of the soil body can occur due to raindrop impact. The breakdown of soil aggregates upon wetting, and the scouring force of surface runoff. The rate of detachment during water erosion depends on the degree to which the soil surface is covered by vegetation, plant residues, or other protective covers, (i) the soil strength, (ii) the rainfall intensity, and (iii) the velocity of the surface runoff.

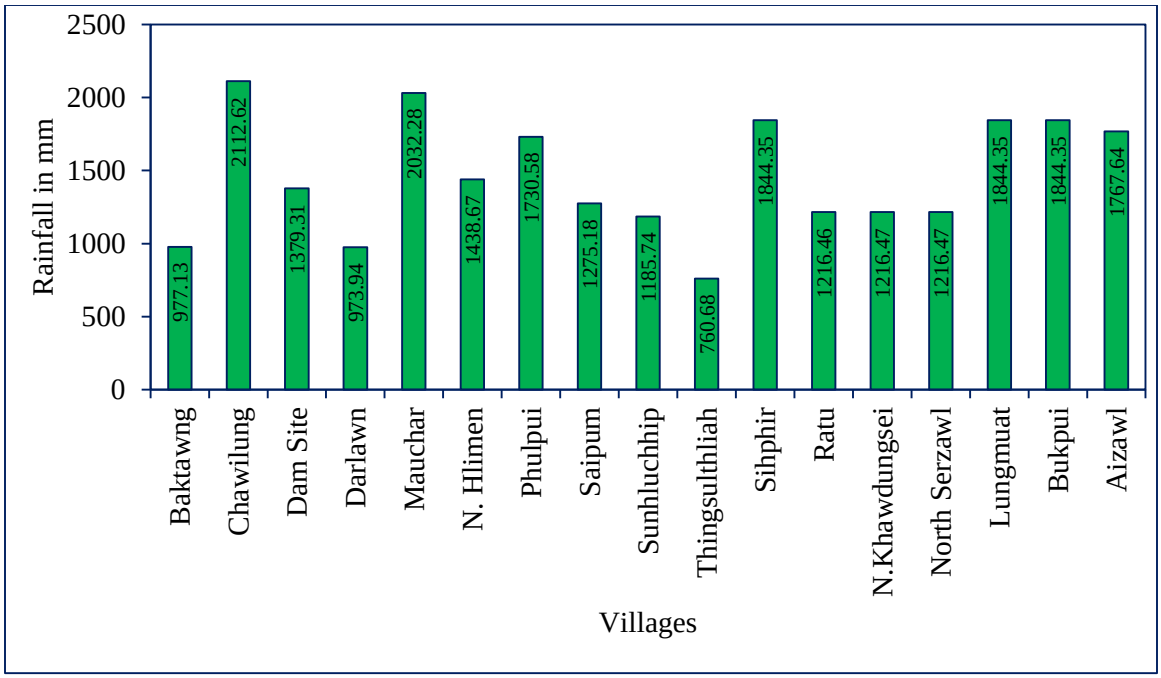


Figure 4.3: Village-wise rainfall received in Tuirial watershed (Source: NASA POWER)

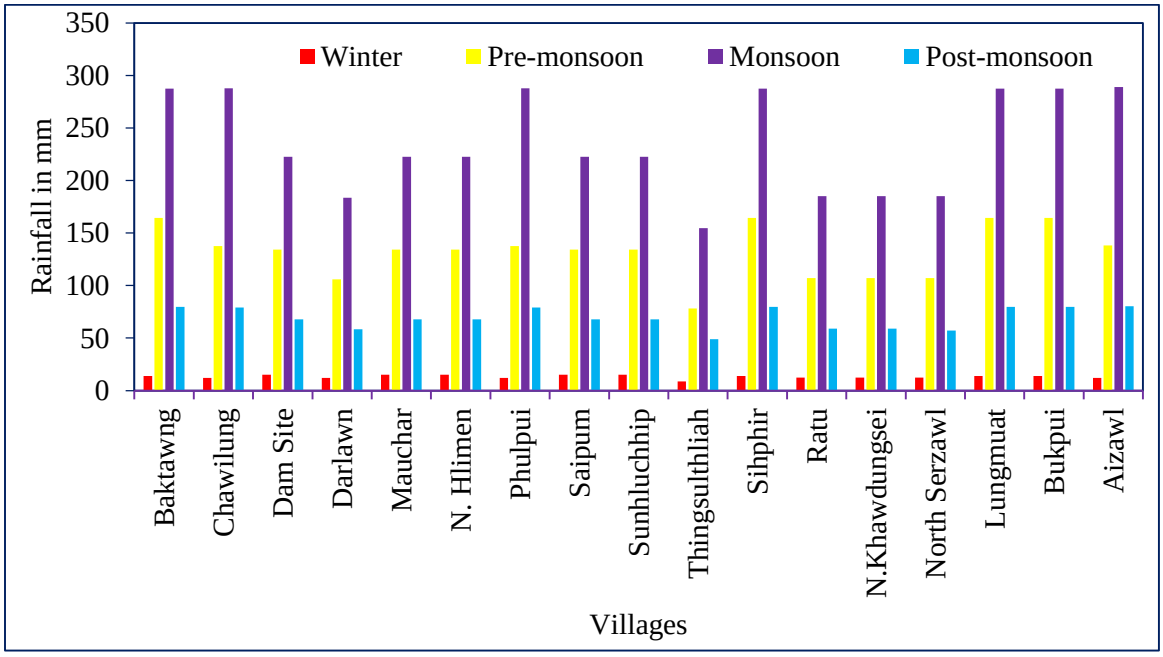


Figure 4.4: Season-wise rainfall distribution in Tuirial watershed (Source: NASA POWER)

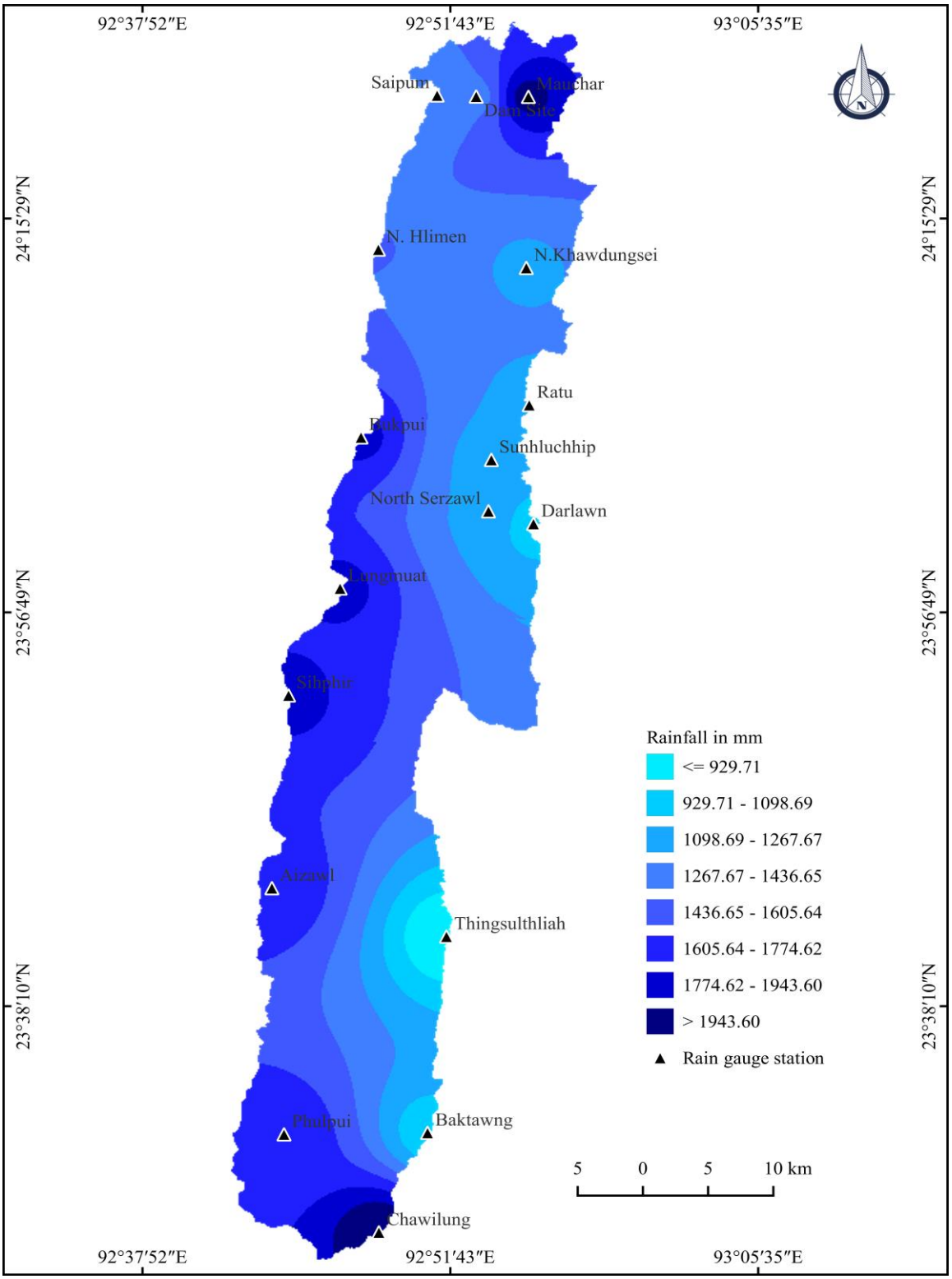


Figure 4.5: Spatial distribution of rainfall in Tuirial watershed

### 4.4.2 Temperature

The Tuirial watershed falls under humid tropical and mild climatic region. The upper parts of the hills are relatively cool during the summer, while the lower reaches are relatively warm and humid. Storms break out during March-April, just before or around the summer. The maximum average temperature in the summer is 26.43 ºC while in the winter the minimum average temperature is below 10 degree ºC. The four months between November and February are winter in Mizoram which is followed by the spring. The storms come in the middle of April to indicate the beginning of the summer. The four months from June to September are known as the rainy season.

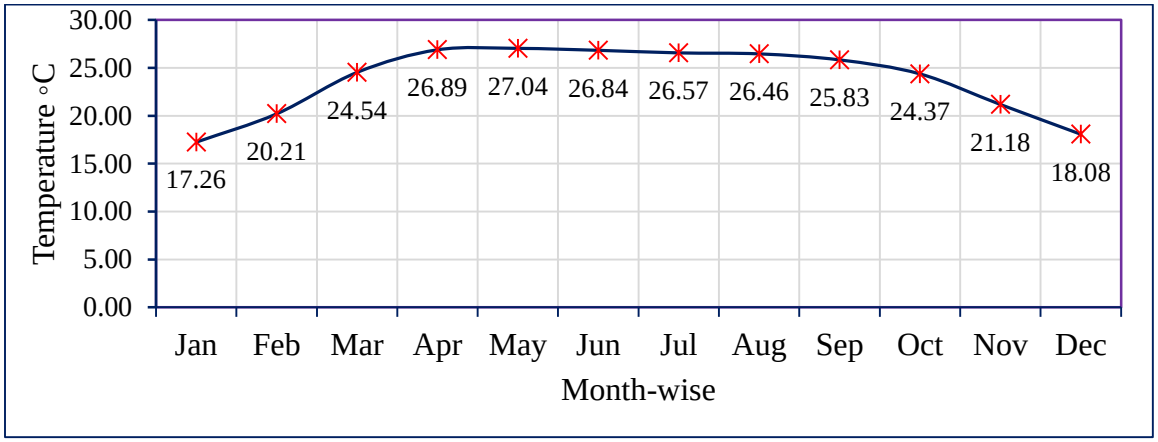


Figure 4.6: Mean monthly temperature in Tuirial watershed (Source: NASA POWER)

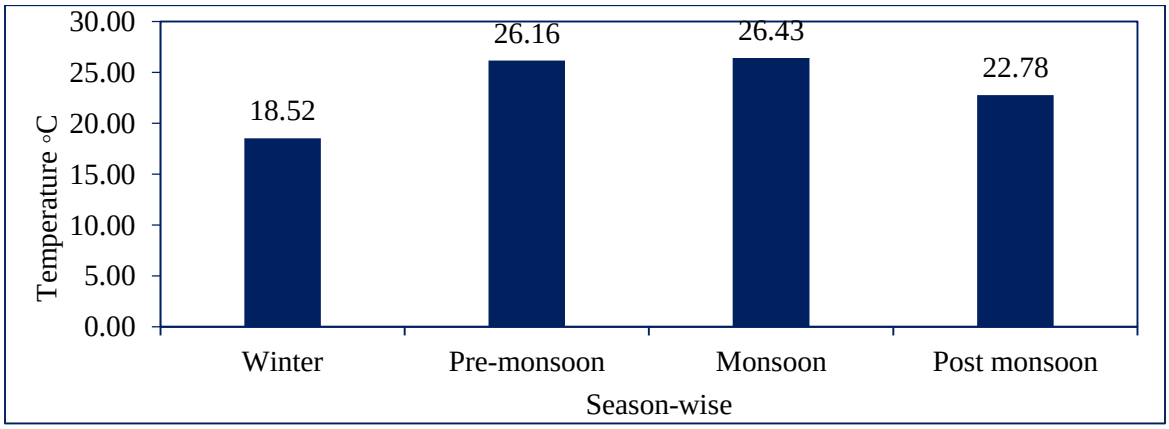


Figure 4.7: Season-wise average temperature experience in Tuirial watershed (Source: NASA POWER).

The climate as at its moderate best in the two autumnal months i.e. October and November the temperature is about 22.78 ºC. The month-wise and season-wise temperature of Tuirial watershed is presented in the figures 4.7 and 4.8.

### 4.4.3 Wind direction

Wind is the horizontal movement of air caused by the uneven heating of the earth by the solar energy. Wind is one of the most influencing factors of climatic condition in a particular region. Wind is the critical significant agent of erosion in semi-arid and arid region, where it does not have significant impact in tropical humid region. However, it is one of the significant determinants of temperature and rainfall in this region. Temperature and rainfall of the Tuirial watershed is determined by the prevailing wind circulation along with the direction. Generally, it is blown from the south to north direction as depicted in the figure 4.8. The average wind speed of the region is 1.50 – 2.50 m/s.

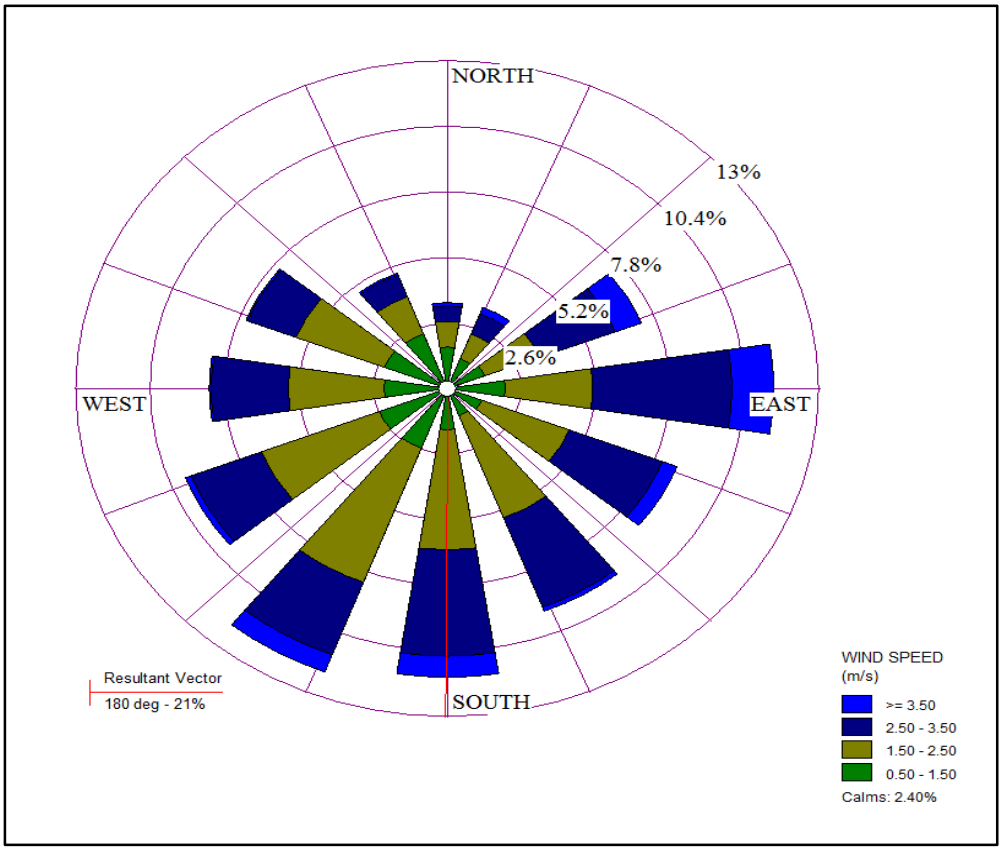


Figure 4.8: Wind direction in Tuirial watershed (Source: NASA POWER)

### 4.5 Elevation

Elevation is the height of land with respect to mean sea level. Generally, at higher elevation is expected more significant run-off and less infiltration (Vijith and Dodge Wan, 2019). Thus, there will be an increase in soil erosion in areas where elevation is higher (Aslam *et al.,* 2021). In fact, the higher elevation not always influence erosion, it must be coherent with rainfall intensity and inclination of slope of the region. As the study area is a mountainous terrain, the highest point within the watershed is 1690 metres, located in the south eastern side of the watershed. Similarly, the steepness of slope with the high intensity rainfall trigger soil erosion at higher elevation and vice versa.

Table 4.2 The elevation of Tuirial watershed along with area and percentage

| Classes | Elevation (metres) | Area ($km^2$) | Area (%) |
|---|---|---|---|
| Very low | < 325 | 534.56 | 37.80 |
| Low | 325 - 630 | 532.92 | 37.68 |
| Moderate | 630 - 935 | 265.87 | 18.80 |
| High | 935 - 1240 | 71.24 | 5.04 |
| Very High | 1240 - 1543 | 9.61 | 0.68 |
| Total | | 1414.19 | 100 |

The elevation of the study area is classified into five equal intervals such as very low, low, moderate, high and very high elevation as depicted in table 4.2. The elevation is low at lower section of the river valley below 325 m is considered as very low, and covers an area of 534.56 $km^2$ which occupies 37.80% of the total geographical area (TGA). The elevation ranges between 325 to 630 m is low which covers an area of 532.92 $km^2$ accounts for 37.68%. Similarly, the elevation ranges between 630 to 935 m is regarded as moderate it extends 265.87 $km^2$ consists of 18.80% of TGA. Again, the elevation ranges from 935 to 1240 m is considered as high class of elevation, which covers an area of 71.24 $km^2$ with 5.04% of TGA. The elevation between 1240 to 1543 m is the very high class which covers an area of 9.16 km2 with 0.68% of TGA. Generally, the higher elevation with steep slope

occurs on both sides of western and eastern water divide line. Then, gradually decreases the steepness of slope with the elevation towards the Tuirial river (Fig 4.9).

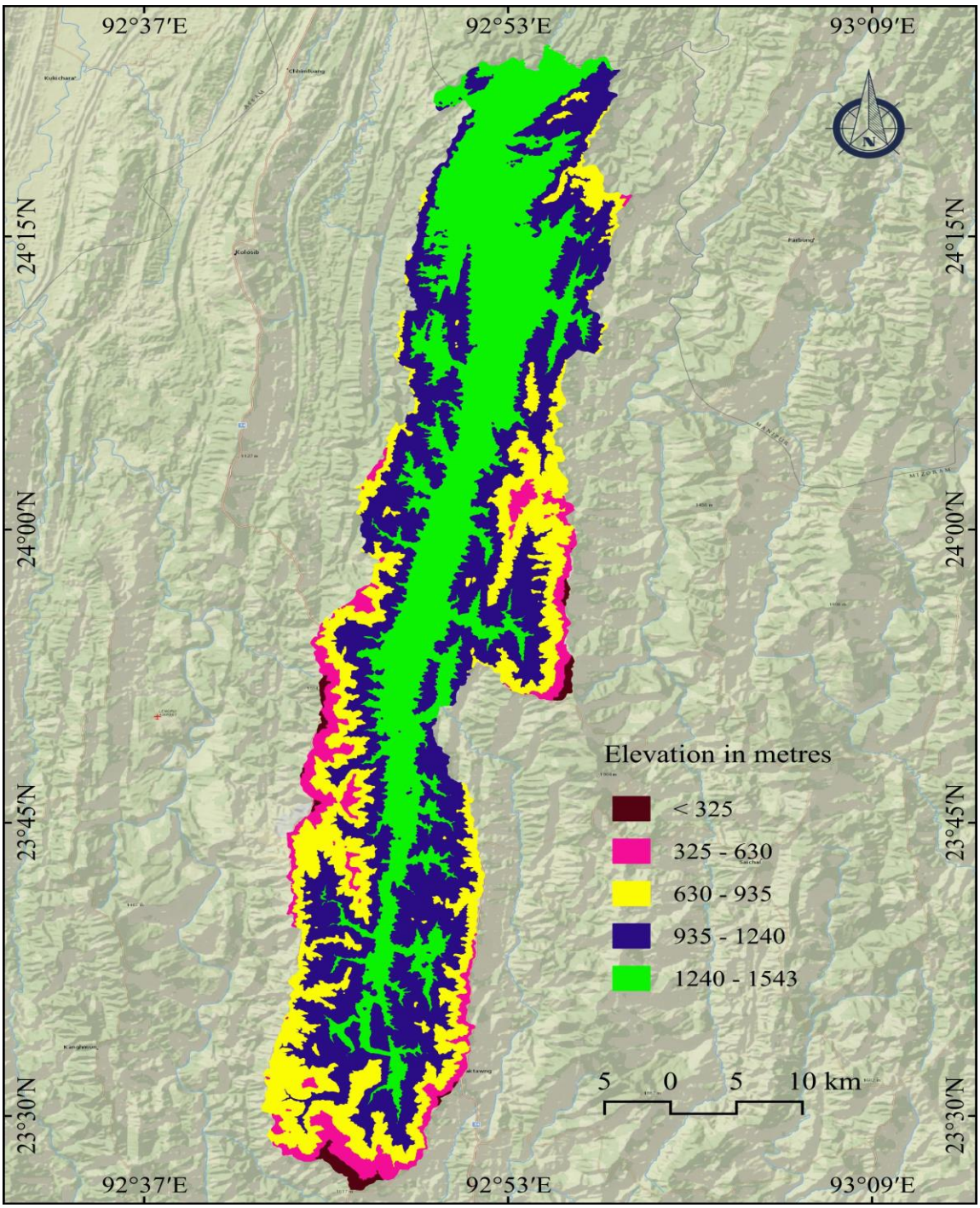


Figure 4.9: The elevation map of Tuirial watershed

## 4.6 Geology

Tuirial river basin consists of sedimentary rocks like sandstone, mudstone, shale-siltstone, clayey, gravel, sand and silt, shale with fossiliferous limestone units which fall under the Bhuban and Bokabil formations of Surma group of the Miocene age (La-Touche,1891; GSI, 2011) (Fig 4.10). The intermixture of varying small to large sized particles which might result in low permeability and high infiltration of the rocks types with excessive surface run-off triggering extreme soil loss. In addition to these major litho-units, the basin is dominated by structural hills with low (<500 m), medium (500-1000 m) and high altitude (>1000 m) which exhibit v-shaped and u-shaped valleys (MIRSAC, 2006). From the analysis of lithological units at Tuirial watershed obtained from Geological Survey of India, Kolkata is presented in Table 4.3 and their spatial distribution in figure 4.11. Only two geological formations found in Tuirial watershed are Bokabil and Bhuban. The Bokabil formation of geology was found in northern part of the watershed covering an area of about 20% of TGA. On the other hand, the Bhuban formation of geology was found in the whole watershed except in the northern part covering 80.5% of the TGA.

Table 4.3 The details of geology and lithological units

| Age | Group Name | Formation | Lithologic units | Area ($km^2$) | Area (%) |
|---|---|---|---|---|---|
| Miocene | Surma | Bhuban | Sandstone, shale, siltstone and conglomerate | 258.84 | 18.24 |
| Miocene | Surma | Bhuban | SST with subordinate siltstone, mudstone, shale | 366.17 | 25.80 |
| Miocene | Surma | Bhuban | Splintery shale with siltstone and conglomerate | 235.84 | 16.97 |
| Miocene | Surma | Bhuban | Sandstone, shale with fossiliferous limestone | 56.742 | 4.00 |
| Miocene | Surma | Bhuban | Grey sandy splintery shale, siltstone and mudstone | 353.68 | 24.92 |
| Miocene | Surma | Bokabil | Thinly bedded shale intercalated SST, siltstone | 110.81 | 7.81 |
| Miocene | Surma | Bokabil | Shale, siltstone and mudstone with sandstone | 31.92 | 2.25 |
| Total | | | | 1414.03 | 100 |

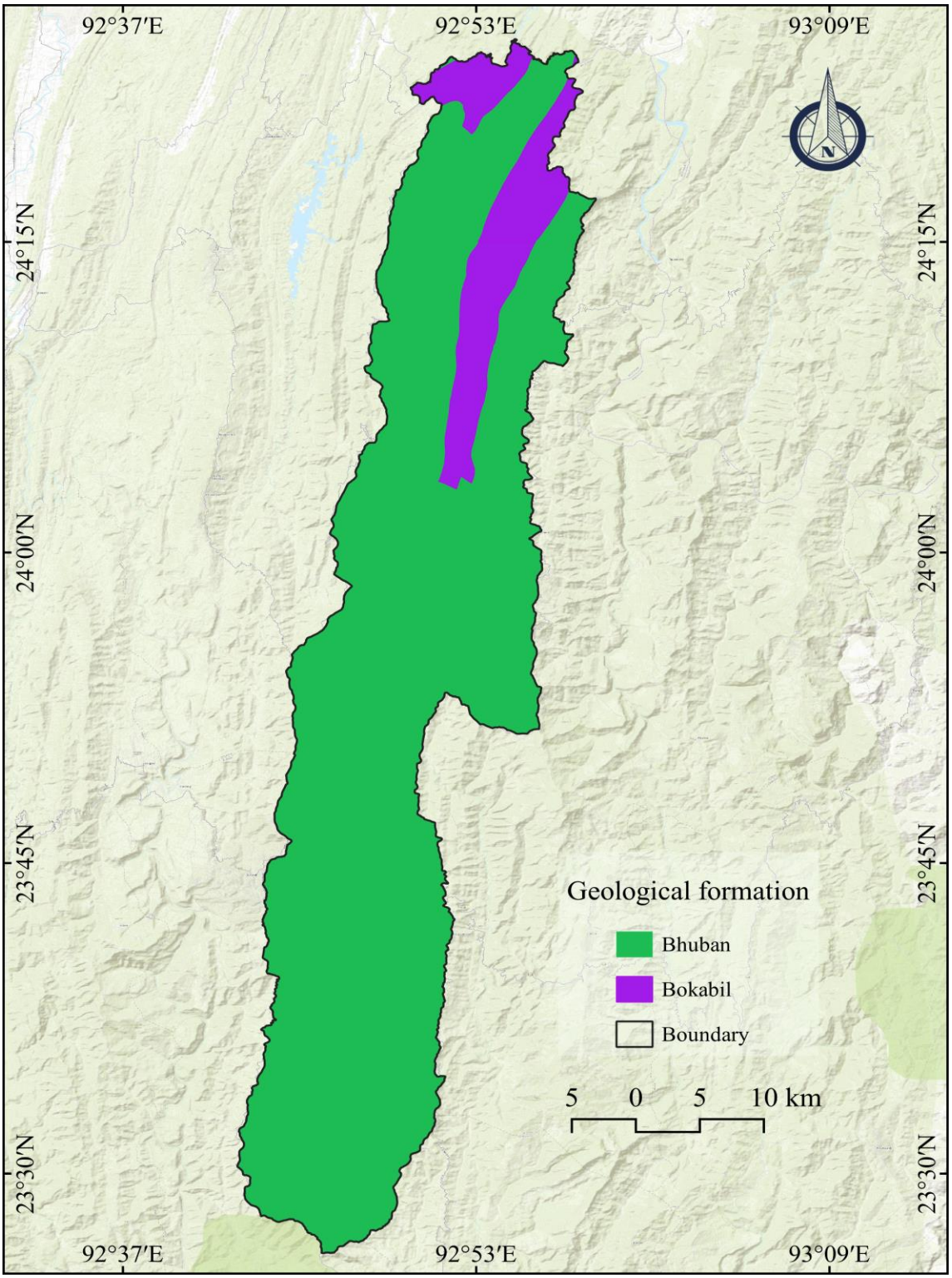


Figure 4.10: The geological formations in Tuirial watershed.

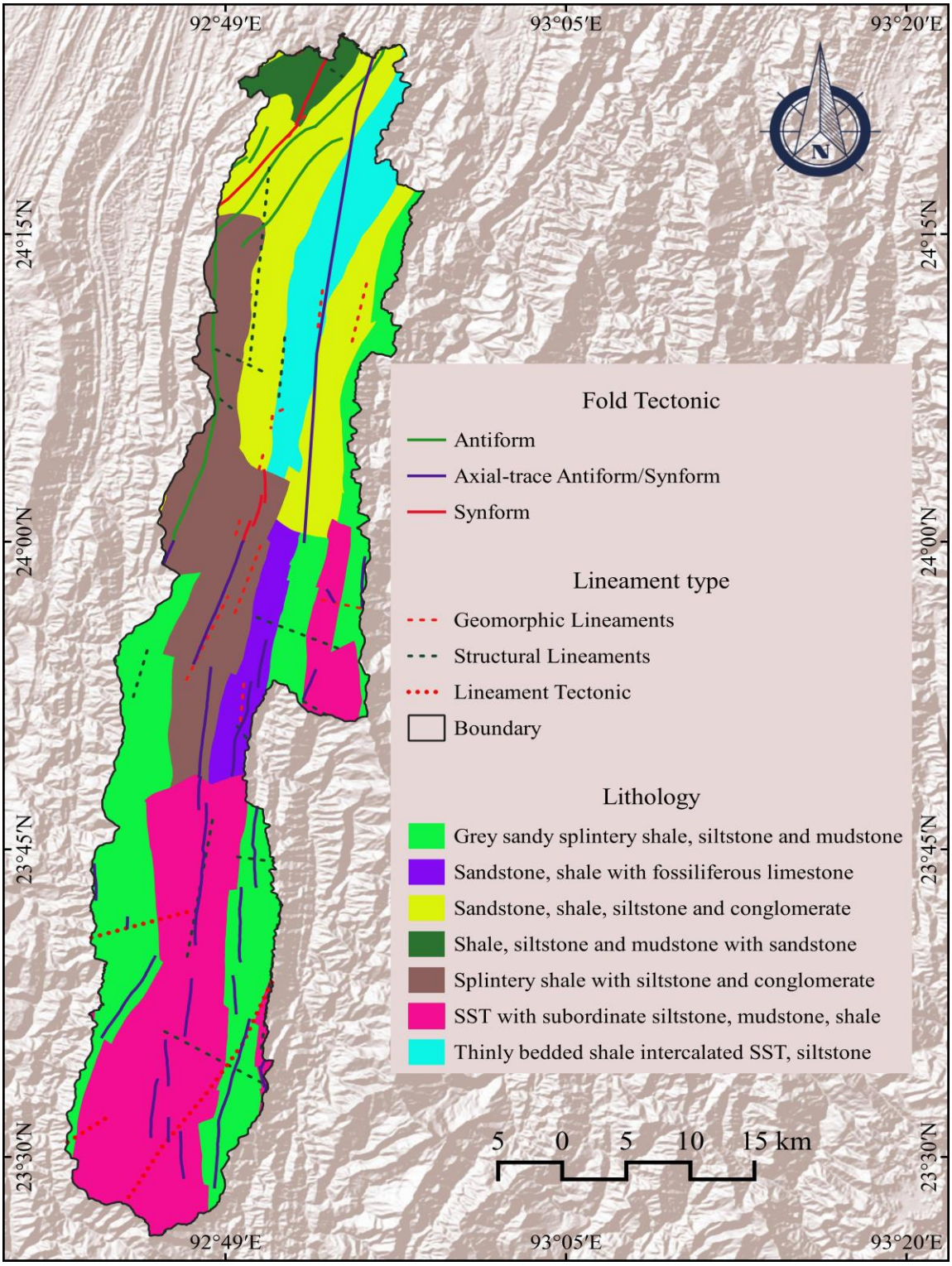


Figure 4.11: The lithological units and geomorphic features map of Tuirial watershed

The lithological units like sandstone with sub-ordinate siltstone, mudstone, shale and grey sandy splintery shale cover the largest area of 50.72% of TGA which are spatially distributed in south, both south-south western and south-south eastern, and also in the eastern side of the watershed. While, shale, siltstone and mudstone with sandstone occupy the lowest area of 2.25% of TGA found in the north western part of the watershed. Antiform, axial-trace antiform and synform are the major fold tectonics found in this watershed. The spatial distribution of details of lithological units, faults, fractures and lineament are depicted in figure. 4.11

### 4.7 Geomorphology

Geomorphology is the study of the process of the formation of landforms and sediments on the Earth's surface. In addition, geomorphology is the analytical description of landscape and the mechanisms responsible for their transformation (Bloom, 1979). The formations could be a result of surface processes triggered by water, air, ice, volcanic eruptions, landslides, earthquakes etc. These landforms are prone to changes, which could be either a slow or sudden process. Generally, all landforms in a particular region reflect a close relationship between the underlying lithology and the operating geological processes.

Table 4.4 The geomorphic features found in the Tuirial watershed

| SI.No. | Geomorphic features | Area (km2) | Area(%) |
|---|---|---|---|
| 1 | Antiformal Hill | 476.39 | 33.57 |
| 2 | Ridge | 289.76 | 20.41 |
| 3 | Highly Dissected Hills and Valleys | 240.77 | 17.32 |
| 4 | Moderately Dissected Hills and Valleys | 303.77 | 21.40 |
| 5 | Synformal Valley | 39.33 | 2.77 |
| 6 | Valley | 57.11 | 4.02 |
| 7 | Water bodies - River | 6.88 | 0.48 |
| Total | | 1414.03 | 100 |

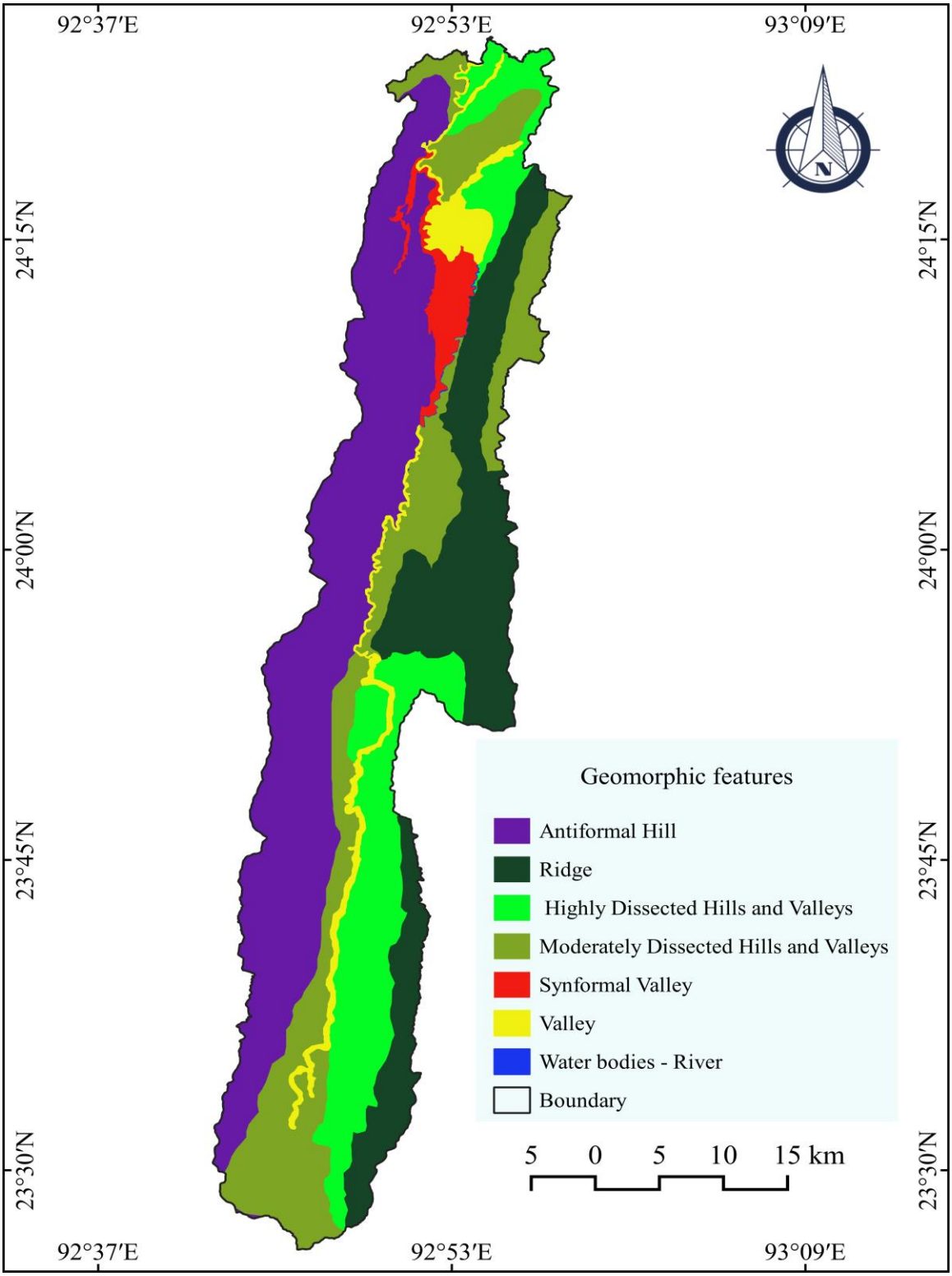


Figure 4.12: Spatial distribution of geomorphic features in the Tuirial watershed

Various landforms spatially distributed in the whole watershed, which are antiformal hills, ridges, highly dissected hills, moderately dissected hill and valleys, synformal valley, valley and water bodies (Fig. 4.12). Synformal valley found in the middle northern part of the watershed, whereas, antiformal hills spread toward south-north direction along the western part of the watershed. Similarly, the water bodies and valleys were found in the middle of watershed. Antiformal hill covering the largest area of 33.57% in TGA. Consequently, moderately dissected hills with valleys, ridge and highly dissected hills with valleys covers 21.40%, 20.41% and 17.32% of the TGA, respectively. The lowest area covers by water bodies of which 0.48% of the TGA. The detail information of geomorphic landforms is presented in table. 4.4.

### 4.8 Vegetation

The presence of vegetation in an area significantly impacts the susceptibility to soil erosion. Typically, when there is dense vegetation cover, its serves as a robust defense mechanism in reducing the rate of soil erosion by enhancing the infiltration rate and decreasing the volume and velocity of run-off, while the absence of vegetation increases the likelihood of soil loss occurring. Vegetation intercepts rain, reducing its energy and preventing splash erosion. It also slows down runoff, reduces sheet erosion, and anchors and reinforces the soil with its root system. Surface water runoff from vegetated areas is much less than that from bare soil due to combination of surface roughness, infiltration, and interception. Runoff generally does not exceed 10 to 20 percent of the rainfall received in small watersheds covered with trees or grass. Without vegetation, however, this could be as high as 60 to 70 percent. Water moving across a bare soil surface erodes soil and transports particles already detached. Vegetation limits the capacity of flowing water to detach soil particles and transport sediment by decreasing runoff volume, slowing velocity, and protecting the soil surface from flowing water. Plant roots create openings or cracks where roots have decayed, increase surface roughness, lower the density of the soil, and improve the structure of surface soils. This increase in the infiltration rate of rainfall and surface flow increases the moisture content of the soil. Plant roots also physically anchor the soil from movement induced by gravity, raindrop impact, or surface runoff. Generally,

the NDVI ranges from 0.6 to 1 indicate the presence of dense and thriving vegetation cover. Conversely, a lower NDVI value of 0.1 or below signifies the absence of vegetation cover such as barren land, water bodies, bare soil and built-up land. In addition, moderate value of 0.2 to 0.3 suggests the prevalence of depleted and open forest areas dominated mainly by shrubs and grasslands (Bhandari *et al*., 2012; Gandhi *et al*., 2015).

Table 4.5 Vegetation coverage of Tuirial watershed

| Classes | NDVI Values | Area (km2) | Area (%) |
|---|---|---|---|
| Very Low | - 0.61 - 0.55 | 69.80 | 4.94 |
| Low | 0.55 - 0.75 | 103.86 | 7.34 |
| Moderate | 0.75 - 0.85 | 548.75 | 38.80 |
| High | 0.85 - 0.89 | 587.62 | 41.55 |
| Very High | 0.89 - 0.99 | 104.24 | 7.37 |
| Total | | 1414.26 | 100 |

In the present study, the vegetation cover is estimated through Sentinel 2 at 10 metres resolution using NDVI formula and pixel values. Based on the NDVI values the present study vegetation is classified into five classes such as very low, low, moderate, high and very high vegetation cover. From the analysis of NDVI value -0.6 to 0.75 signifies very low and low vegetation cover occupies 11.28% of TGA. Medium vegetation covers about 38.80% of TGA. Moreover, the NDVI value 0.85 – 0.89 indicate good vegetation cover and occupies 41.55% of TGA. The NDVI value of 0.89 – 1 indicates the vegetation covers is very dense and it occupies 7.37% of TGA (Table 4.5). Figure 4.13 depicts the spatial distribution of forest within Tuirial watershed. This thematic layer shows medium to dense forest found far away from the settlements and watershed boundary. Healthy vegetation is found in the southern and eastern sides of the watershed.

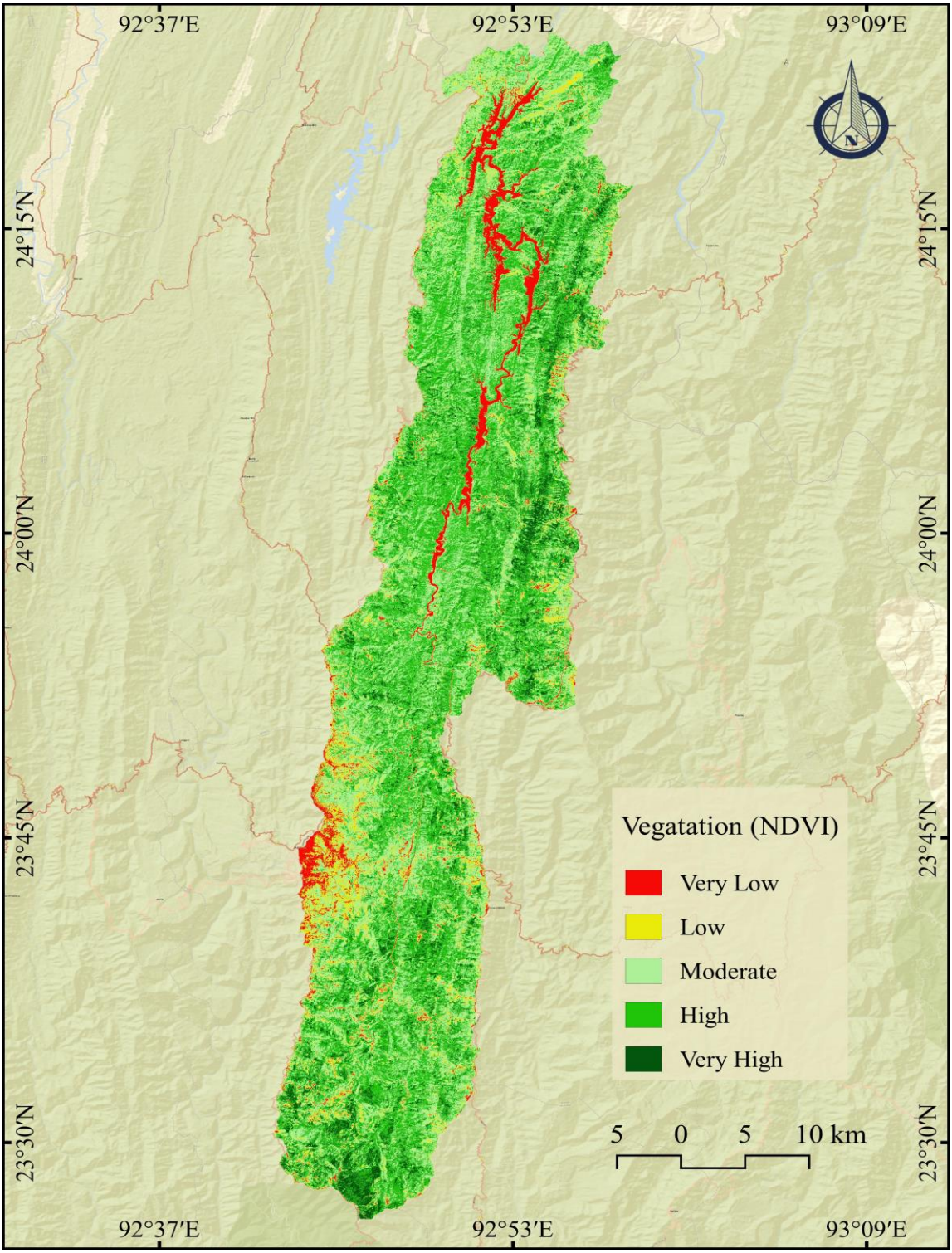


Figure 4.13: Vegetation map of the Tuirial watershed

## 4.9 Conclusion

This chapter comprises the geographical background of Tuirial watershed, climate; rainfall, temperature, wind speed and direction, lithology, geology, geomorphic features and vegetation. Besides that, the transport route and drainage system in the study area was included. This watershed is under the sub-tropical rainforest and temperature is warm and humid. In addition, Bokabil and Bhuban are the two geological formation of Tuirial watershed. Fold, faults, fracture, and lineament are the geomorphic features found in this region. From the analysis of NDVI, healthy vegetation is found distance from the human settlements and built-up land, also closed to the main river.

# CHAPTER – 5

# ESTIMATION OF TOTAL SOIL LOSS IN TUIRIAL WATERSHED

## 5.1 Introduction

The quantification of the rate and magnitude of soil loss is an integral part for the implementation of development and management of watershed. To assess the amount of soil loss, integration of various soil erosion influencing factors viz., land use / land cover, slope-steepness of the basin, soil texture, rainfall intensity, and forest management action are essential. Each of the parameters has different intensity of erosion in terms of location and climatic condition. The accurate assessment of erosion intensity zone would draw more attention of watershed management authority to initiate minimization steps for soil loss along with the sustainable natural forest and ecosystem of that region. In this chapter the amount and the rate of soil loss in Tuirial watershed using revised universal soil loss equation (RUSLE) with the integration of remote sensing and geographic information system are highlighted.

## 5.2 Precipitation erosivity factor (R)

Rainfall erosivity suggest the volume and the rate of soil loss which determined by rainfall and run-off. Generally, rainfall erosivity is directly related to the volume of precipitation received at the river basin. The changes in the characteristics of rainfall intensity and quantity, accelerate soil erosion. The study observed the variation of rainfall from time to time. The years from 1992 to 2022 show the variation in rainfall ranges from 706 mm to 2112 mm (Fig 5.1) whereas the *R*-factor specifies the degree of soil loss that varies from 355.14 to 845.86 MJ.mm $ha^{-1}$ $hr^{-1}$ $yr^{-1}$ with an average value of 1116.77 MJ.mm $ha^{-1}hr^{-1}yr^{-1}$ (Fig 5.2). The spatial distribution of rainfall intensity within the Tuirial basin is highlighted in figure 5.1. Where, highly susceptible to soil loss areas such as Sialsuk, Mauchar and Neihbawi villages are found in the southern, northeastern and western of parts of the basin, respectively. Because this area receives huge volume of rainfall and as it is located the along the edge of water divide, which specify higher chances

of rainfall with high intensity detach loose and unconsolidated soil in those areas, whereas, the eastern side of the basin is receiving low precipitation leading to little chances of soil erosion by rainfall erosivity.

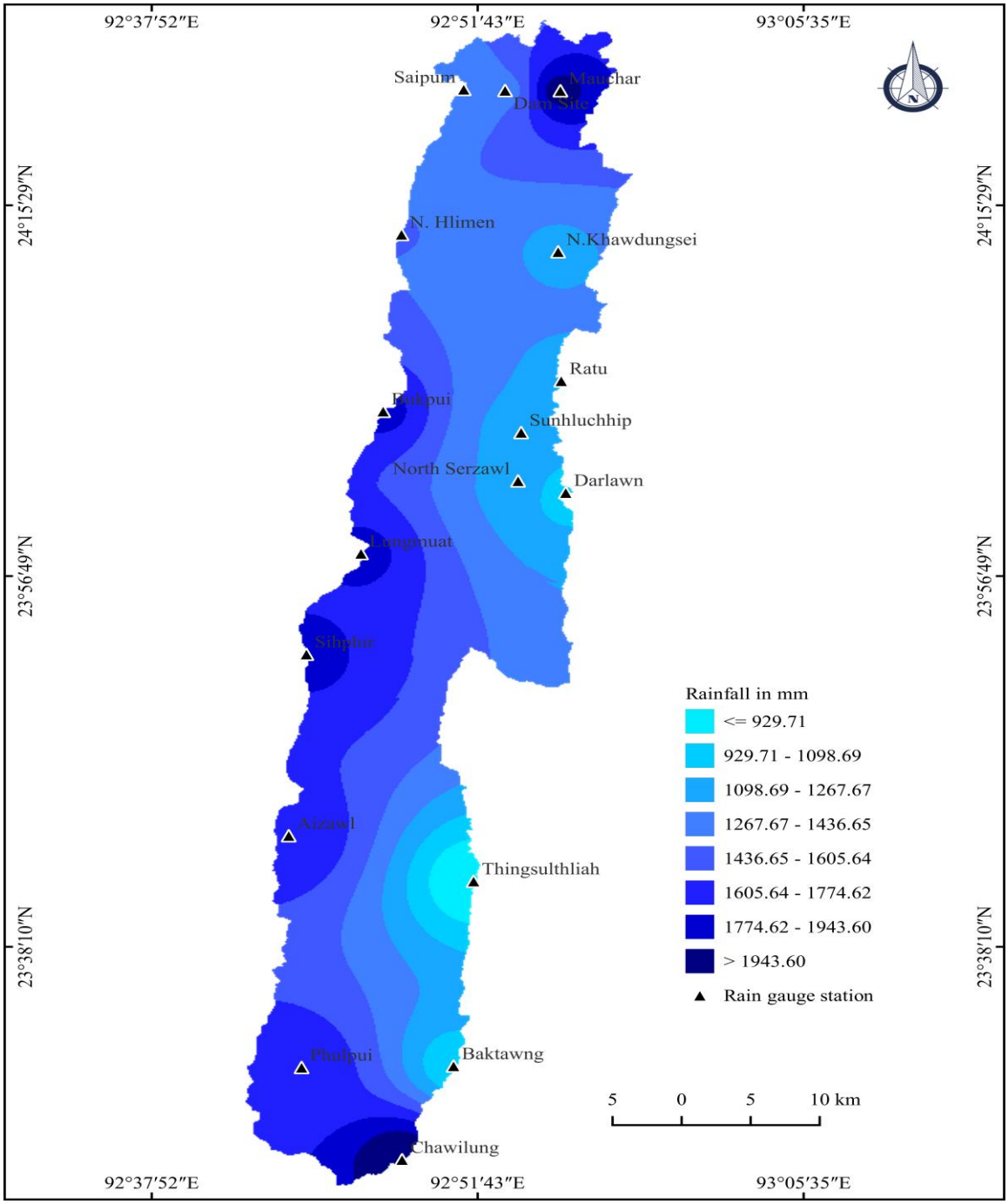


Figure 5.1: Rainfall distribution in Tuirial river basin.

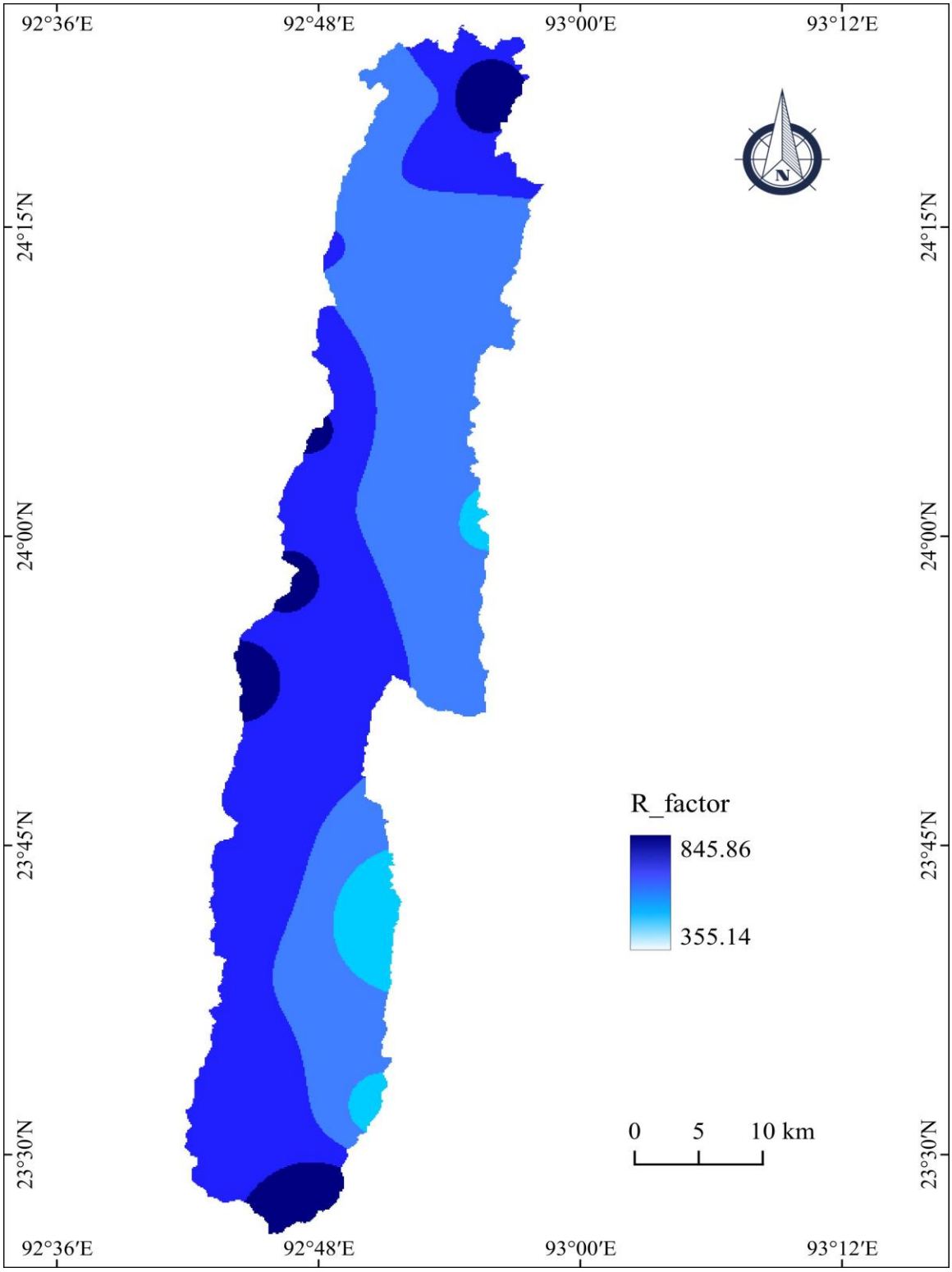


Figure 5.2: Precipitation Erosivity Factor in Tuirial river basin.

### 5.3 Soil erodibility factor (K)

Soil erodibility refers to the composition of soil properties which varies with rainfall and run-off at different soil textures. The rate of erosion is different from one soil to another soil texture, based on the structural composition, permeability and organic matter content (Karaburun, 2010). Fine and medium soil texture are light which are easy to carry away by running water, while coarse and clay particle are heavy with less subjected to erosion. Furthermore, fine texture soil attributed to high clay content with small porosity leads to low infiltration rate. Clay, coarse loamy, fine loamy, and loamy skeletal are the predominant soils found in the Tuirial basin (Fig. 5.3). The soil texture and corresponding K factor values were identified from the soil erodibility values estimated by Barman *et al*., 2020.

The value of *K* varies with soil texture. The *K* value ranges from 0.25 t hr. $MJ^{-1}mm^{-1}$ of clay to 0.66 t hr. $MJ^{-1}mm^{-1}$ of coarse loamy soil texture in the Tuirial basin (Fig. 5.4). This suggests that areas with a higher proportion of coarse loamy soil texture in the Tuirial basin are at a greater risk of soil erosion compared to areas with clay, fine loamy, and loamy skeletal soil textures. It is important to consider the variation in soil erodibility values when implementing erosion control measures in the Tuirial basin.

Table 5.1: Different Soil Textures and K-Factor value

| SI.No. | Soil Texture | K-Factor | Area ($km^2$) | Percentage (%) |
|---|---|---|---|---|
| 1 | Fine Loamy | 0.57 | 953.76 | 67.36 |
| 2 | Loamy Skeletal | 0.54 | 275.86 | 19.48 |
| 3 | Clayey | 0.25 | 66.57 | 4.70 |
| 4 | Coarse Loamy | 0.66 | 119.61 | 8.44 |

The variations in soil erodibility values highlight the need for modified erosion control measures in different areas of the Tuirial basin. By considering the specific soil textures and corresponding *K* factor values, erosion control efforts can be more effectively

targeted and implemented. This approach ensures if resources are utilized efficiently, the erosion can be effectively mitigated across the basin.

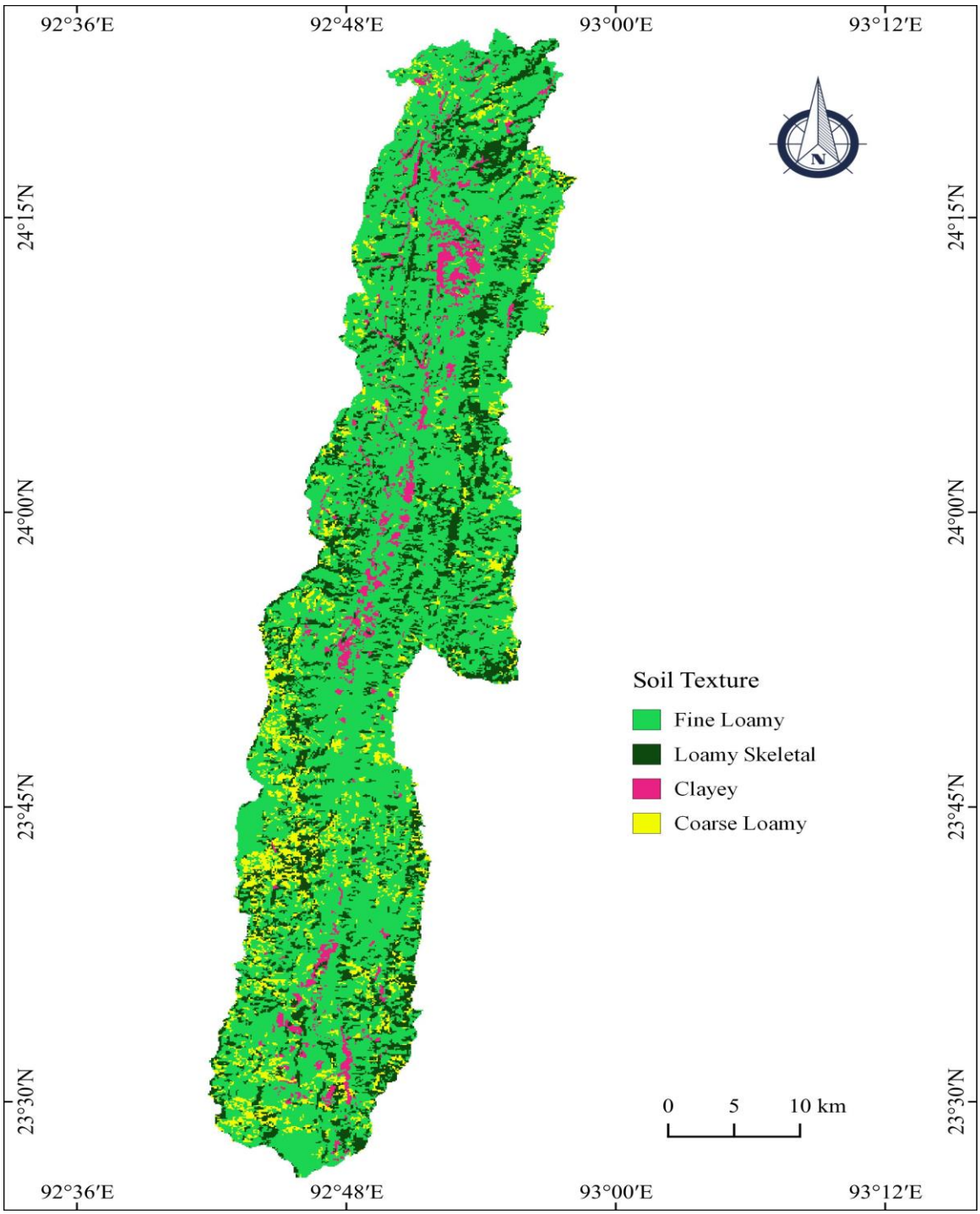


Figure 5.3: Spatial distribution of soil texture in Tuirial river basin.

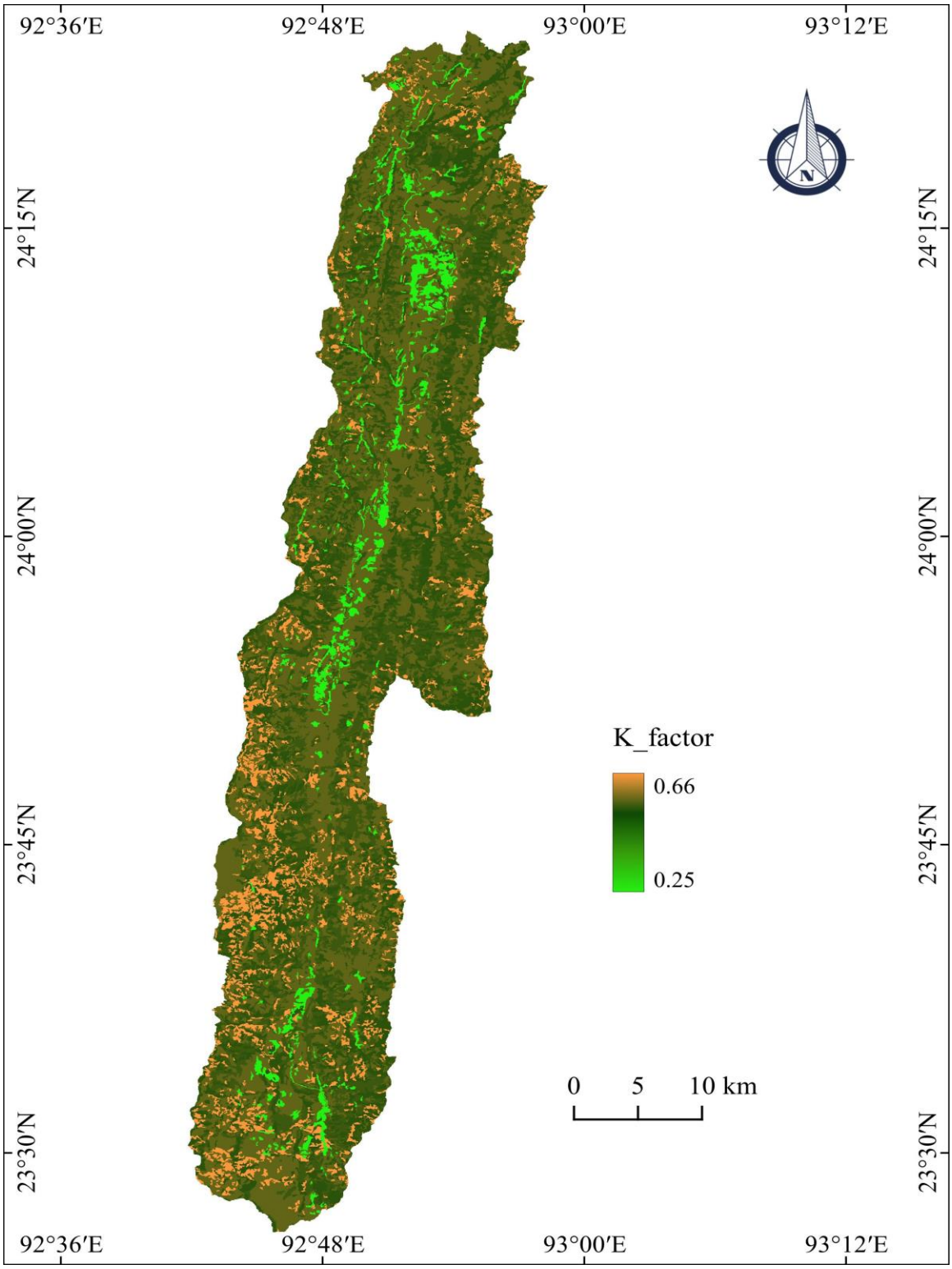


Figure 5.4: Soil Erodibility Factor map of Tuirial river basin.

The study observed that the *K* values differs from 0.51 to 0.66 t ha $MJ^{-1}mm^{-1}$ signifies that the region is moderately susceptible to erosion zone with an average value of 0.45 t ha $MJ^{-1}mm^{-1}$. The different soil textures and their attributed K-factors values are illustrated in table 5.1. A lower value of *K* exhibits that the soil texture is susceptible to low erosion, on the contrary the greater values of soil texture is highly vulnerable to soil loss (Barman *et al*., 2020; Vanlalchhuanga *et al*., 2021; Thakuriah, 2023). The spatial distribution of soil texture within the basin is highlighted in figure 5.3. Fine loamy with the erodibility value of 0.57 t ha $MJ^{-1}mm^{-1}$ covering 67.36 % of the total basin relatively shows equal distribution. While, clay with the erodibility value of 0.25 t ha $MJ^{-1}mm^{-1}$ is seen at the low elevation which covers 4.70 % of the basin. This clay soil is attributed to compact structure with low erosivity after experiencing through mature stage of erosion. Loamy skeletal and coarse loamy soil are found in almost all parts of the watershed with their erodibility value of 0.54 t ha $MJ^{-1}mm^{-1}$ and 0.66 t ha $MJ^{-1}mm^{-1}$ covering an area of about 19.48 % and 8.44 %, respectively (Fig. 5.4).

### 5.4 Steepness and length of the slope factor (LS)

The degree of slope (S) and slope length (L) provide a statistical terrain evaluation of the Tuirial basin. The topographic factor of slope length (L) layer was prepared from the topographic parameters such as $\lambda$ flow accumulation (Fig. 5.6), $\beta$ slope gradient (Fig. 5.7), variable length-slope exponent (Fig. 5.8), slope length (m) (Fig. 5.9), and the steepness of the slope layer was generated from the sin θ of a slope angle (Fig. 5.10). The statistical evaluation of the Tuirial basin includes analyzing the degree of slope (S) and slope length (L). These parameters help in understanding the terrain characteristics and its impact on various aspects such as water flow, erosion, and land stability. The LS factor is integrated using raster calculator in the ArcGIS environment. The flow accumulation thematic layer is generated after the computation of flow direction of the Tuirial basin from ALOS PALSAR DEM using hydrology tools. The flow accumulation thematic layer provides information on the amount of water that will flow through each pixel in the Tuirial basin. This layer is useful for identifying areas of high water flow and potential erosion hotspots. The hydrology tools in ArcGIS support accurate computation of the flow

direction, which is necessary for generating this layer. The spatial variation of the topographic factor (LS) in the Tuirial basin varies from 0 to 16.75 (Fig. 5.11). The basin slope ranges from 0° to 81.34° (Table 5.2), and based on the angle of inclination, found that there is severe soil loss (Fig. 5.5). The LS factor is a key parameter in determining the potential areas of soil erosion, with higher values indicating areas of greater risk. The combination of high flow accumulation values and steep slopes in the Tuirial basin suggests that there are significant erosion hotspots that need to be addressed. The computed values of the steepness of slope and the length of slope distance *LS* factor ranges from 0 to 16.75 which indicates medium-length of slope but high in angle of inclination. The spatial distribution of LS factor of the study area is depicted in generated map. The *LS* values nearby zero shows that the area is gently sloping, as the distance between top to bottom of the slope is lengthy. While the area is characterized by steep slope determined high *LS* values due to abrupt alteration in altitude and inclination of slope.

Table 5.2: The degree of slope along with their area coverage.

| SI.No. | Angle (degree) | Area ($km^2$) | Percentage (%) |
|---|---|---|---|
| 1 | 0-10 | 1251.94 | 88.53 |
| 2 | 10_20 | 20.43 | 1.44 |
| 3 | 20-30 | 23.84 | 1.68 |
| 4 | 30-40 | 22.47 | 1.58 |
| 5 | 40-50 | 23.30 | 1.64 |
| 6 | 50-60 | 22.28 | 1.57 |
| 7 | 60-70 | 18.66 | 1.31 |
| 8 | 70-80 | 18.42 | 1.30 |
| 9 | >80 | 12.65 | 0.89 |

The basin topography also determines soil erosion, however it is depending up on the other erosional agents like rainfall and run-off. The steepness and the length of slope of the drainage basin reflect the rate of sedimentation because it exerts the force of run-off energy. If the inclination of slope is more than $30^{\circ}$ surface run-off energy is strong with loose and fragmented materials are subjected to erosion. On contrary the steepness of slope is below $10^{\circ}$ with length of the slope is longer the rate of erosion is diminishing continues till the river. The present study observed that the Tuirial watershed is mostly covering undulating topography, however 88.53 % of the total basin is covered by below $10^{\circ}$ angle of inclination. The variation of degree of slope of the Tuirial basin is depicted in figure 5.5. However, the hilly areas characterized by fragile sedimentary and loose topsoil subjected to erosion and high possibility of landslide. The length of slope is longer towards the low altitude and close to the mouth of the main channel. On the other hand, shorter with steep slope is found nearby the origin of the river. The angle of inclination of the Tuirial drainage basin is divided into nine equal intervals for the synoptic expression of the basin as displayed in table 5.2.

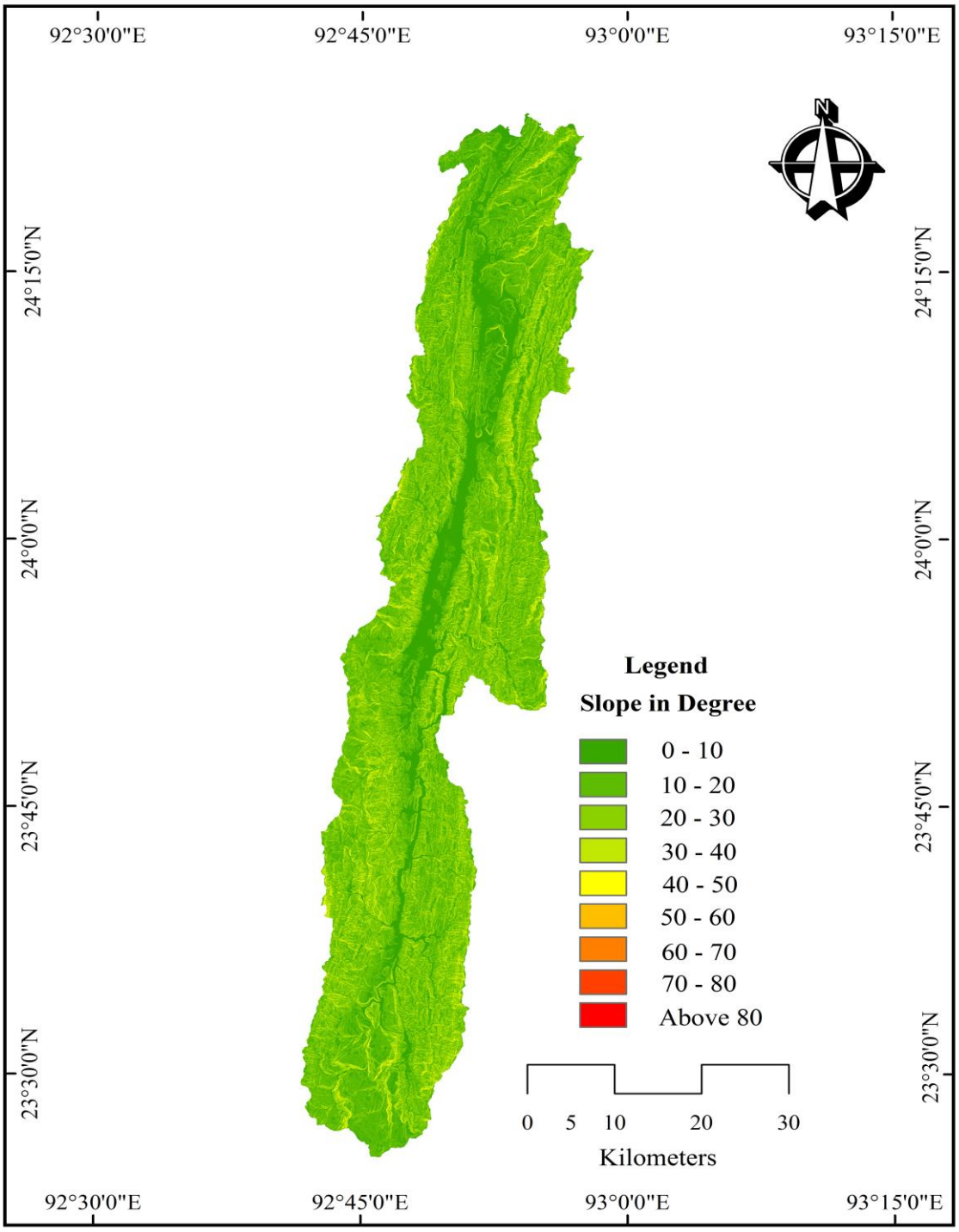


Figure 5.5 Slope map of the Tuirial basin

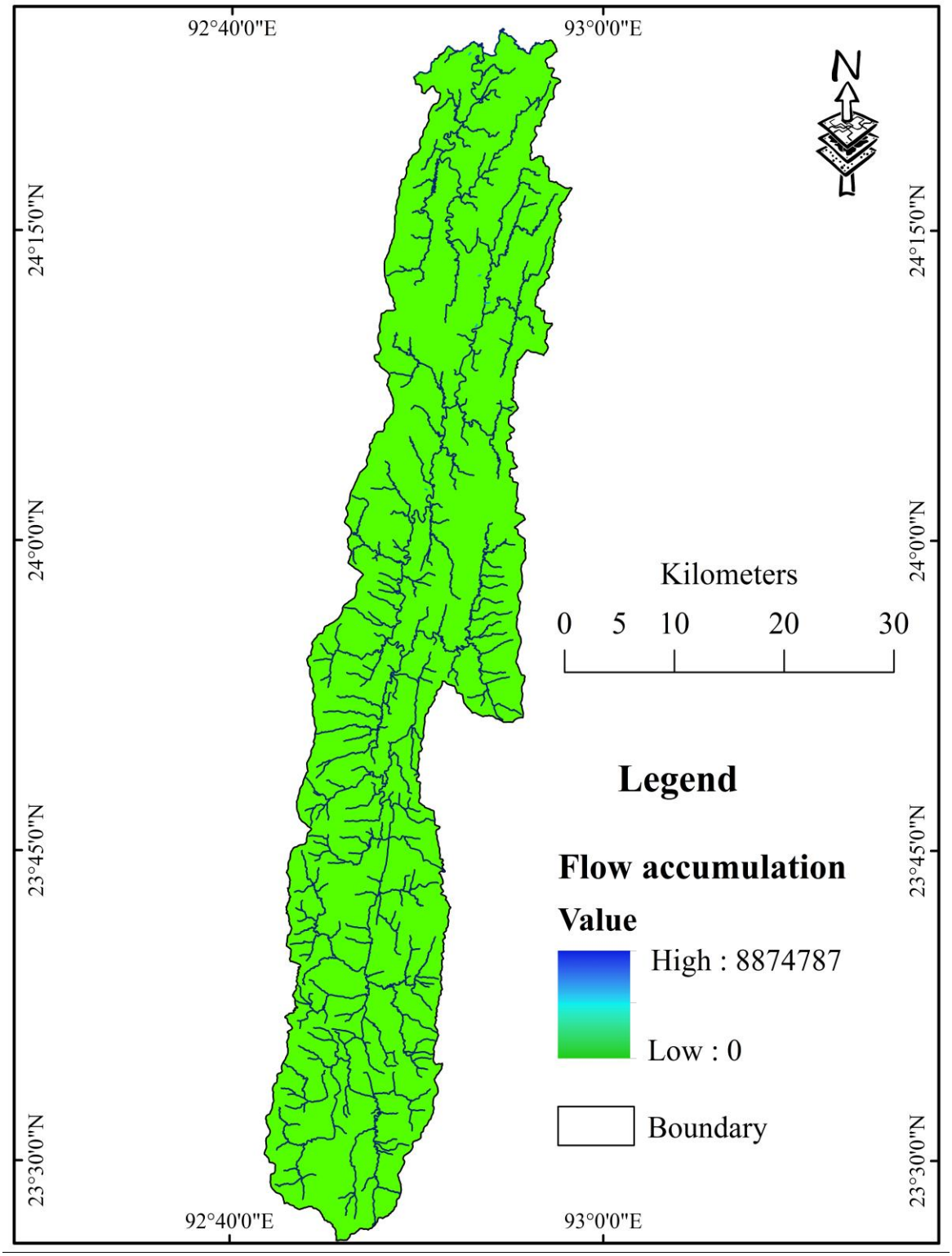


Figure 5.6: Flow Accumulation map

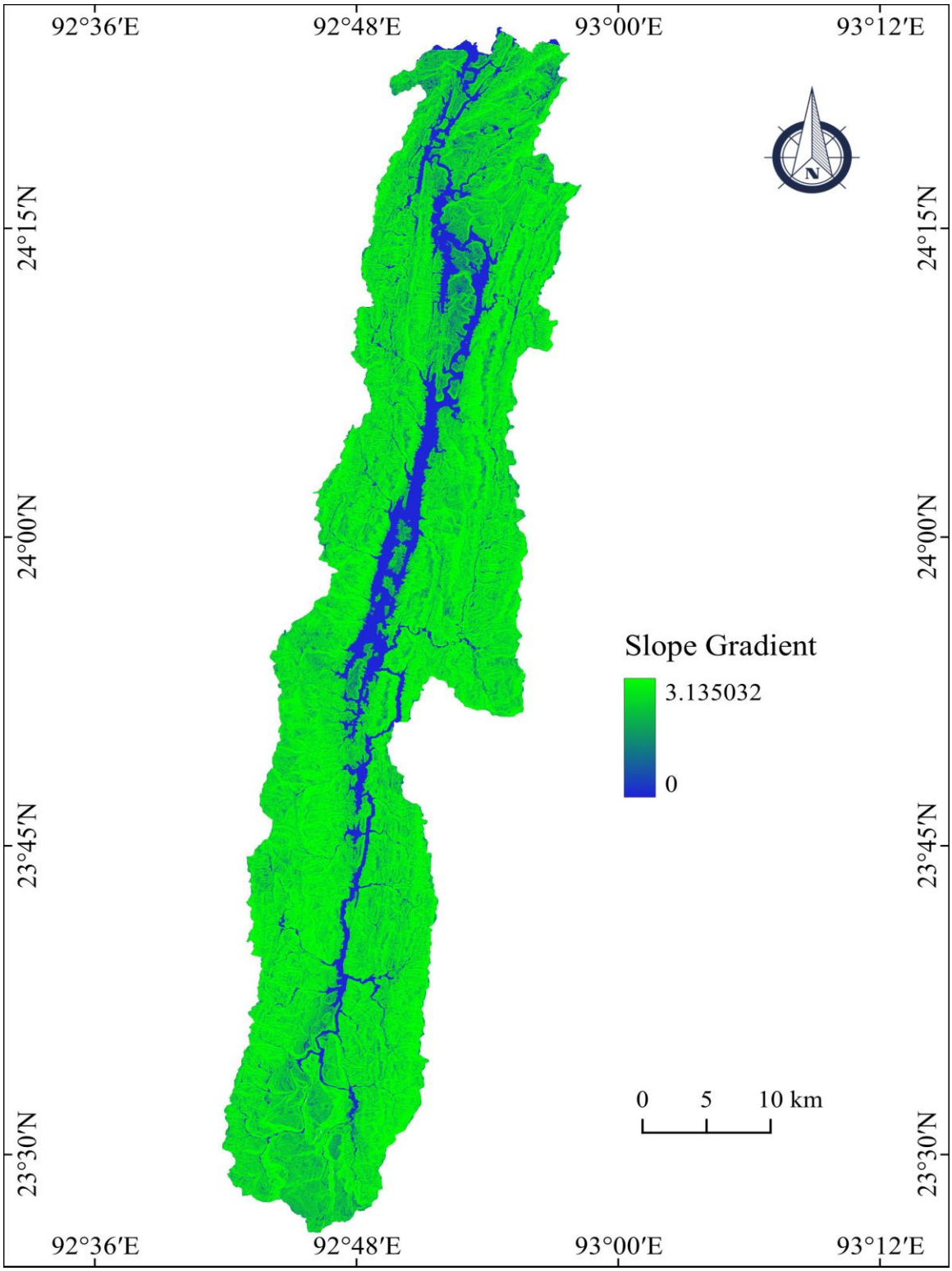


Figure 5.7: Slope Gradient map

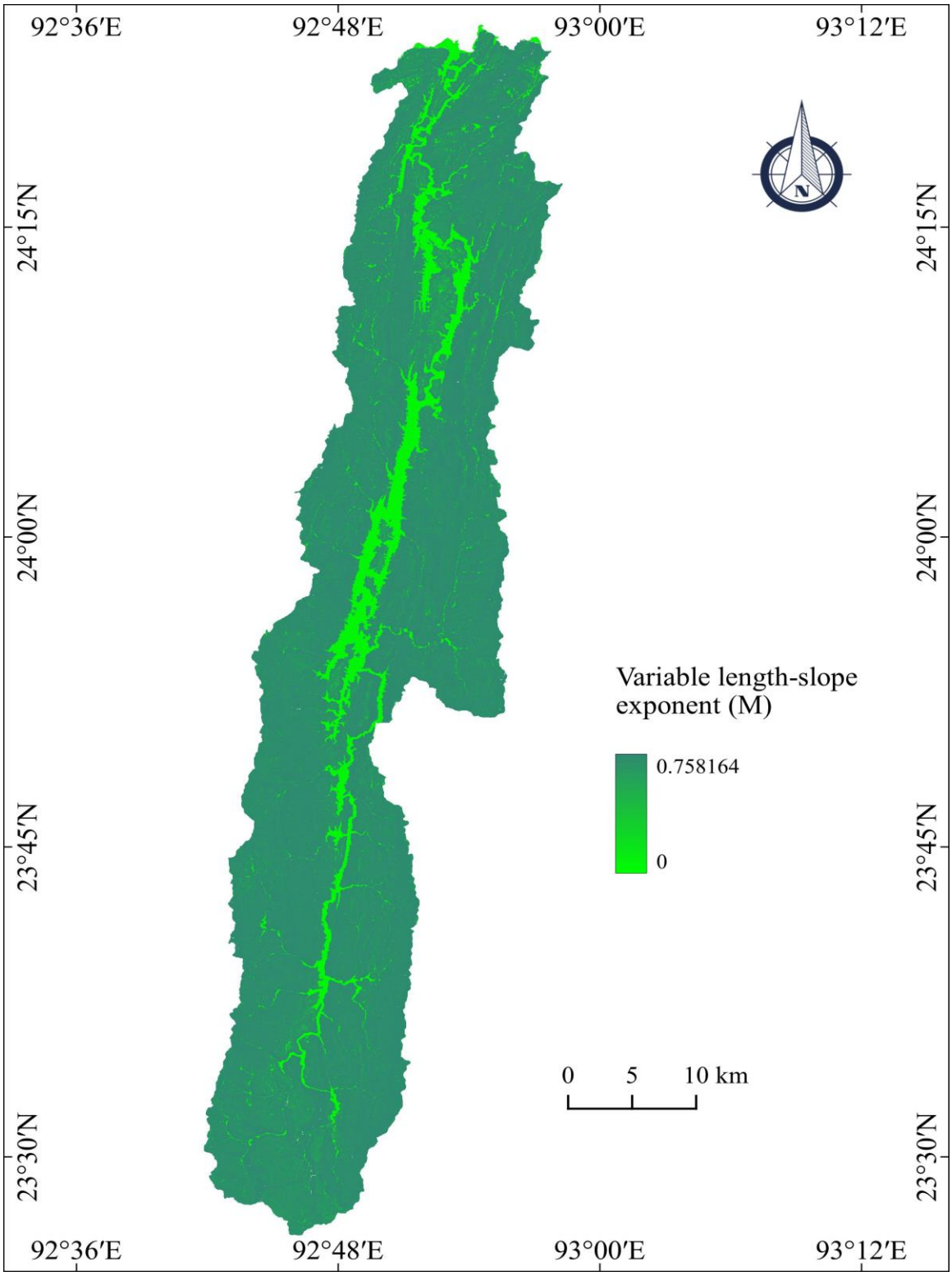


Figure 5.8: Variable length of slope exponent map

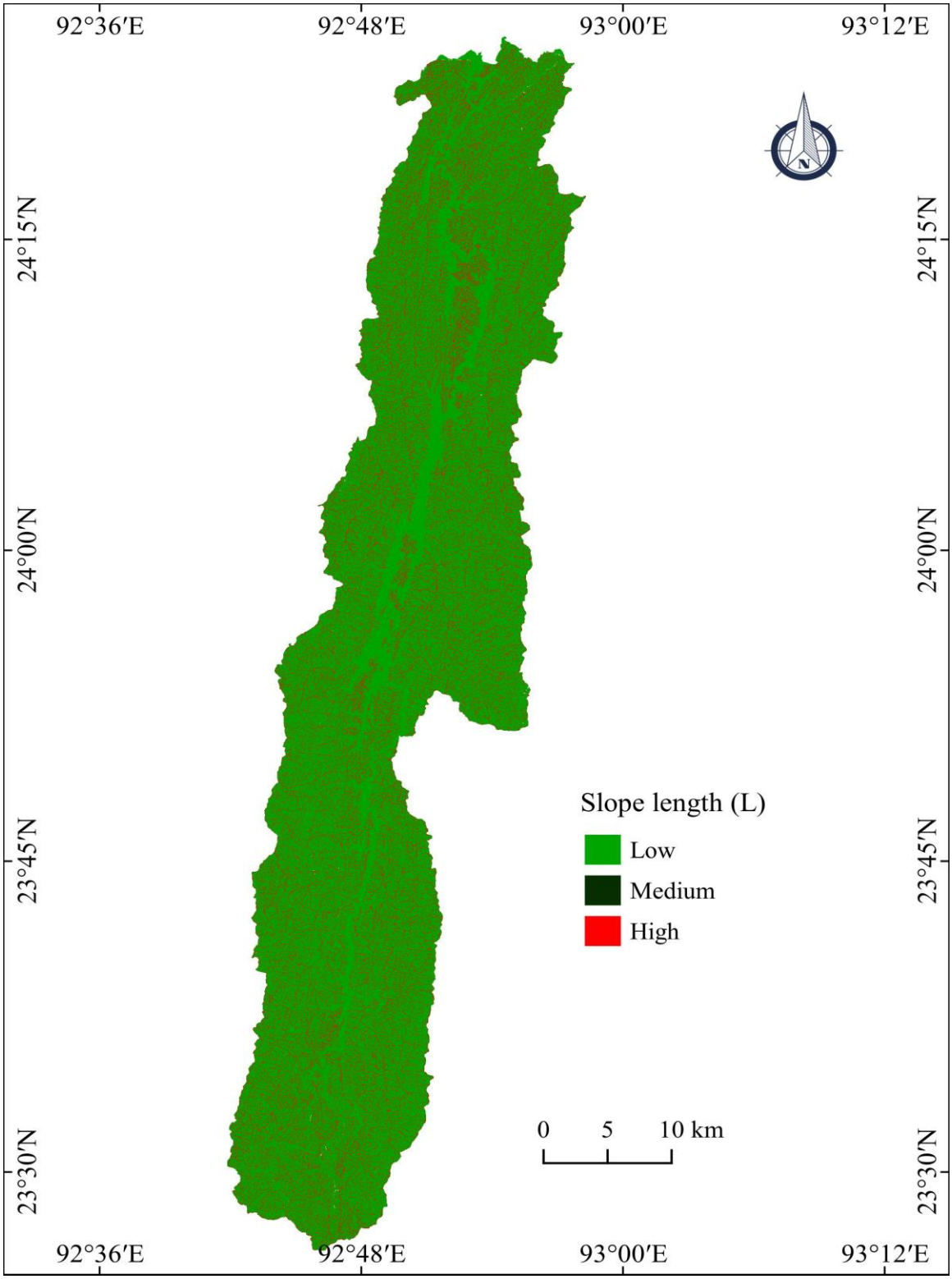


Figure 5.9: Slope Length map

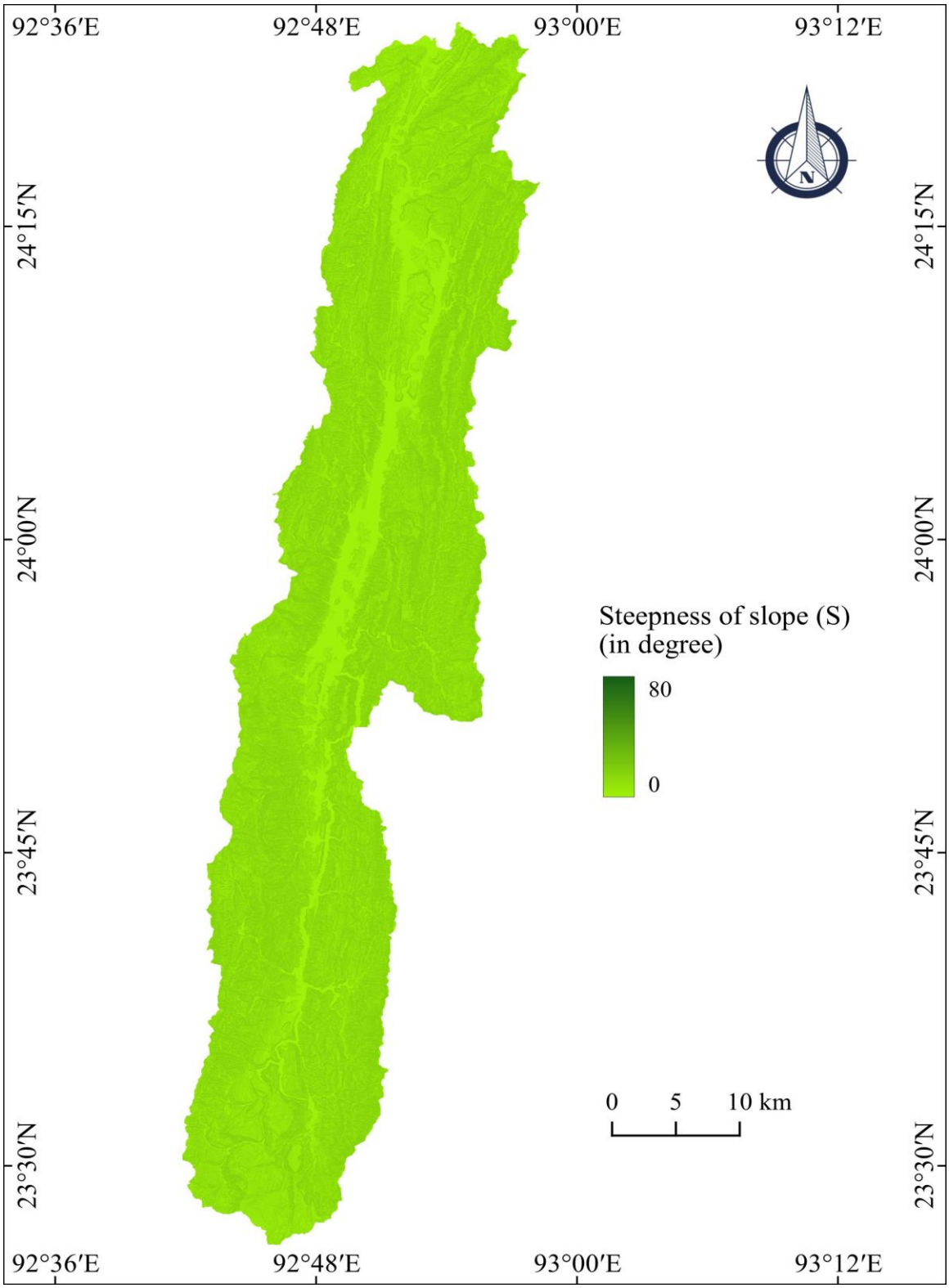

Figure 5.10: Steepness of slope map

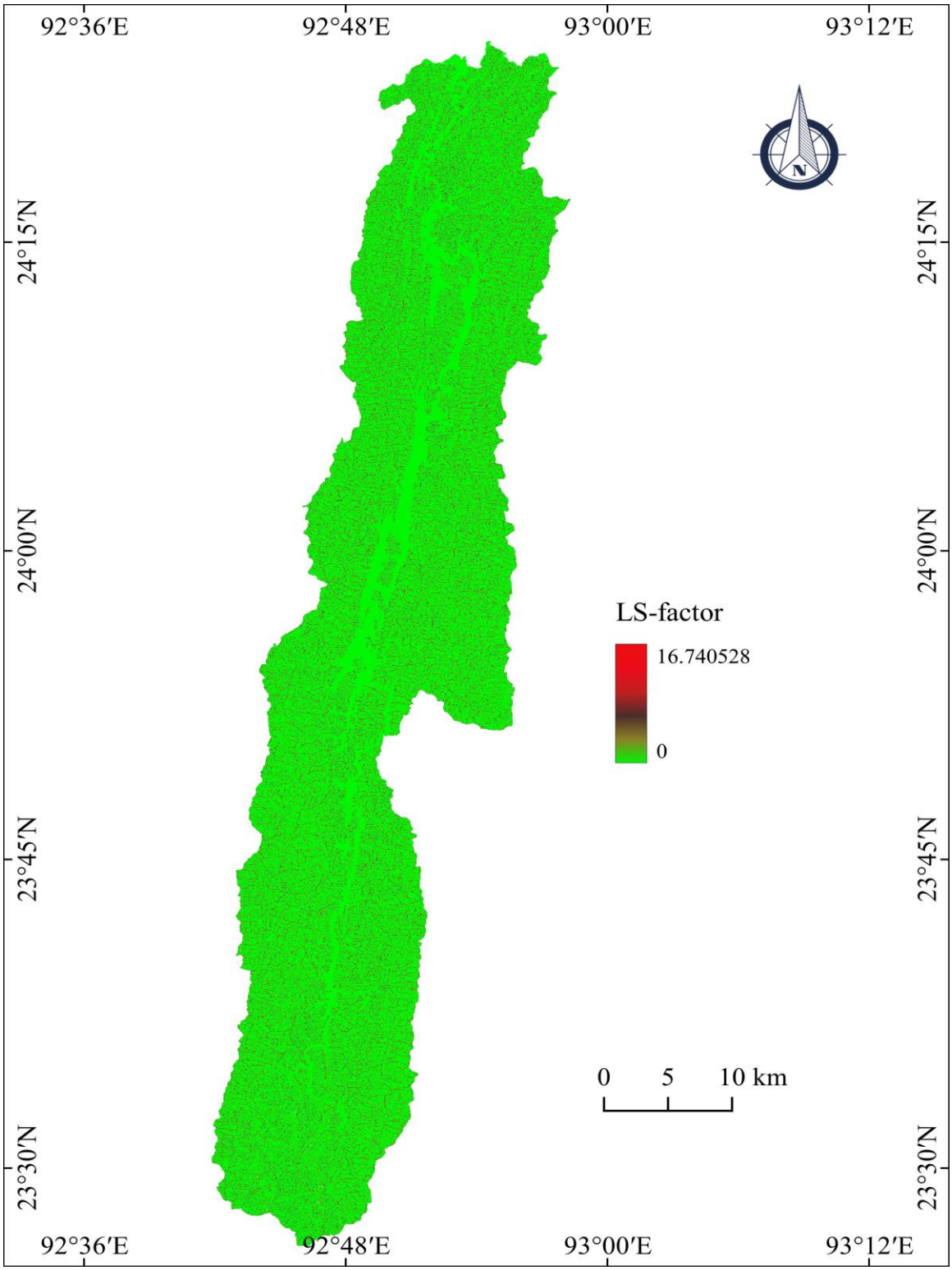


Figure 5.11: LS Factor map

### 5.5 Cover management factor (C)

The cover management and support practice factors are dimensionless parameters in the RUSLE model; both the C and P factors were derived from land use and land cover (LULC) classifications from the Tuirial basin. The supervised image classification by Qgis 3.22 provides accurate and detailed information about the land use and land cover (LULC) in the Tuirial basin. By analyzing the LULC data obtained through supervised image classification, it is possible to assess the impact of different land use practices on soil erosion in the Tuirial basin. This information can aid in implementing effective soil conservation measures and land management strategies to mitigate erosion risks. The degree of soil erosion may vary depending on the land use and land cover of that area. The scale of preservation managing factor (C) ranges from 0.004 to 0.45 with a mean value of 0.16 which indicates low to moderate soil loss under the preservation management. The value close by zero signifies that the preservation practice is good, whereas close to 1 refers to poor practice management (Table 5.3). The study area is classified into eight types of land use and land cover, such as settlements, current cultivation, fallow land, bamboo forest, open, medium, and dense forest, and water bodies (Fig. 5.12). Current cultivation and fallow land constitute of 16.95 % of the total geographical area with having C-factor value of 0.45 and 0.15, respectively. This information specifies current cultivation and fallow land areas are subjected to high erosion due to low cover management which are exposed and directly influenced by rainfall and run-off. While vegetation covering more than 80% of the total geographical area which has significant protection of soil erosion due to indirect impact of rainfall. Built-up land has lower value of C-factor 0.25, which consists of settlement, public recreational facilities, commercial centre and developmental activities places etc. However, these areas are attributed to low infiltration rate due to hard surface and cemented floor along with roads construction subsequent by high run-off, thereby subjected to soil erosion at the low conservation areas. This information is crucial for determining the values of the C and P factors in the RUSLE model, which play a significant role in estimating soil erosion. The C factor value close to zero means well protected, while the value approaches 1 for current and abandoned jhum cultivation (Fig. 5.13).

### 5.6 Conservation management practice factor (P)

The P value ranges between 0 and 1 (Fig. 5.14), where close to zero is good conservation management and close to one is the area of poor conservation management. The P factor value ranges from 0 to 1, with higher values indicating low susceptibility to erosion (Vanlalchhuanga *et al*., 2022; Thakuriah, 2023). The P value serves as an indicator of the effectiveness of conservation measures and land management strategies in mitigating erosion risks. A lower P value suggests that the area has implemented successful conservation practices, while a higher P value indicates a need for improvement in conservation management. In the present study, the P factor values are assigned based on the land use and land cover of the Tuirial basin. The P-values are taken from Barman *et al*., 2020 after the examination of soil erosion susceptible zones at the Upper Tuirial basin. The land use and land cover are classified into eight patterns such as built-up land, current cultivation, fallow land, bamboo forest, open forest, medium forest, dense forest and water bodies. Practice management implementation action taken by forest department and stake holder for minimization of soil loss in Tuirial basin is found to be less. However, the natural forest coverage is quite good, besides this region falls under the tropical rainforest associated with fertile soil favorable for various flora and fauna. Moreover, it can be said that nature re-generates itself without human intervention, but it requires many decades to regenerate after the rigorous exploitation of forest resources. In the present study, various conservation strategies such as contour and terracing, strip crop and underground drainage are neglected that has been suggested by Wischmeier and Smith, 1965 and 1978; Renard *et al*., 1997. This type of practices is found to be limited due to huge capital investment and high labour cost.

Table 5.3 LULC and corresponding factor C and P factors

| SI.No. | LULC | Area($km^2$) | Percentage % | C-Factor | P-Factor |
|---|---|---|---|---|---|
| 1 | Built-up land | 28.46 | 2.01 | 0.25 | 1 |
| 2 | Current Cultivation | 13.31 | 0.94 | 0.45 | 0.5 |
| 3 | Fallow Land | 226.19 | 16.00 | 0.15 | 0.9 |
| 4 | Bamboo Forest | 315.68 | 22.33 | 0.12 | 1 |
| 5 | Dense Forest | 11.22 | 0.79 | 0.004 | 1 |
| 6 | Medium Forest | 659.35 | 46.64 | 0.12 | 1 |
| 7 | Open Forest | 122.96 | 8.70 | 0.1 | 0.8 |
| 8 | Water Bodies | 36.57 | 2.59 | 0.1 | 1 |

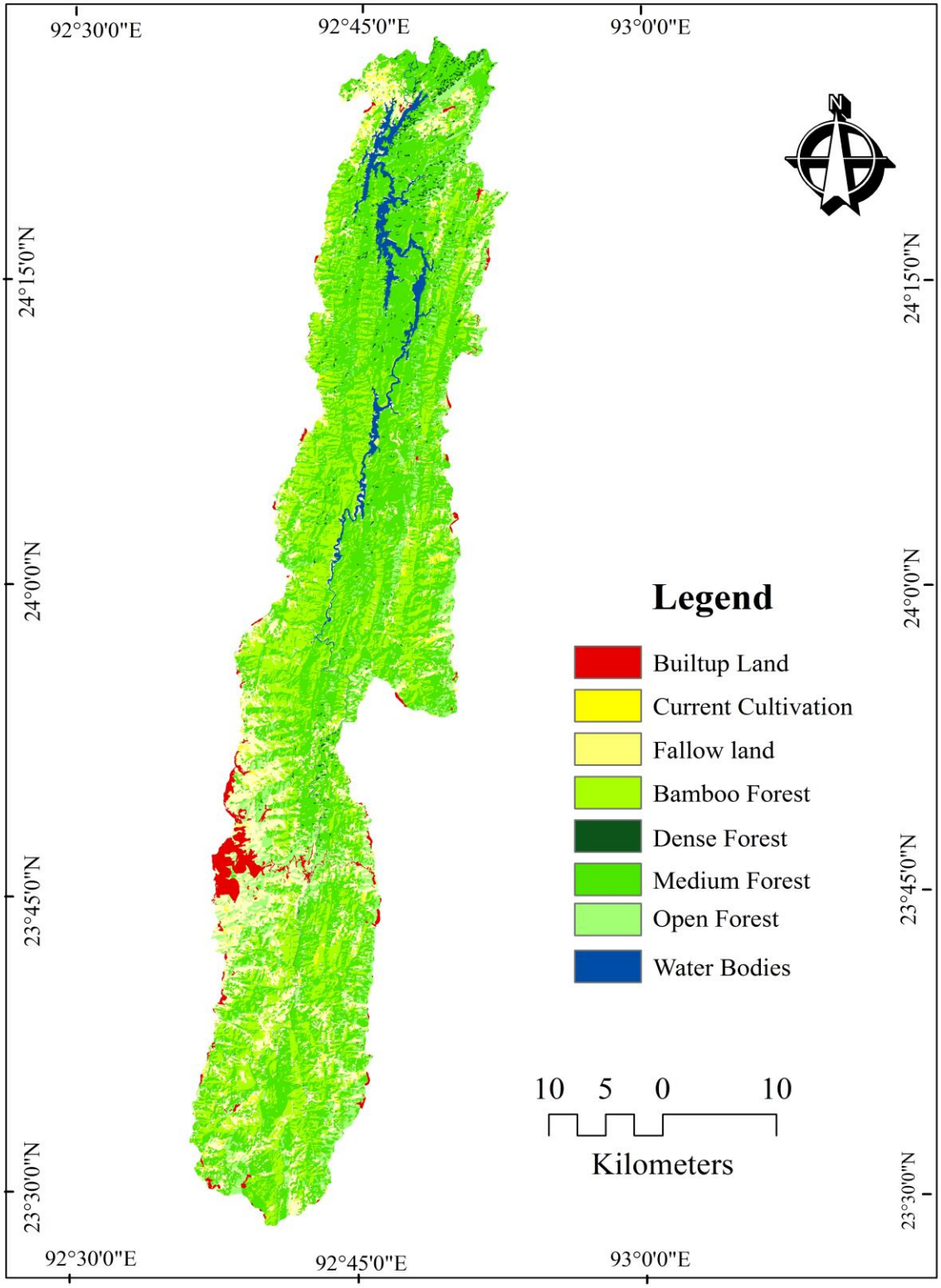


Figure 5.12: Land use and land cover in Tuirial river basin.

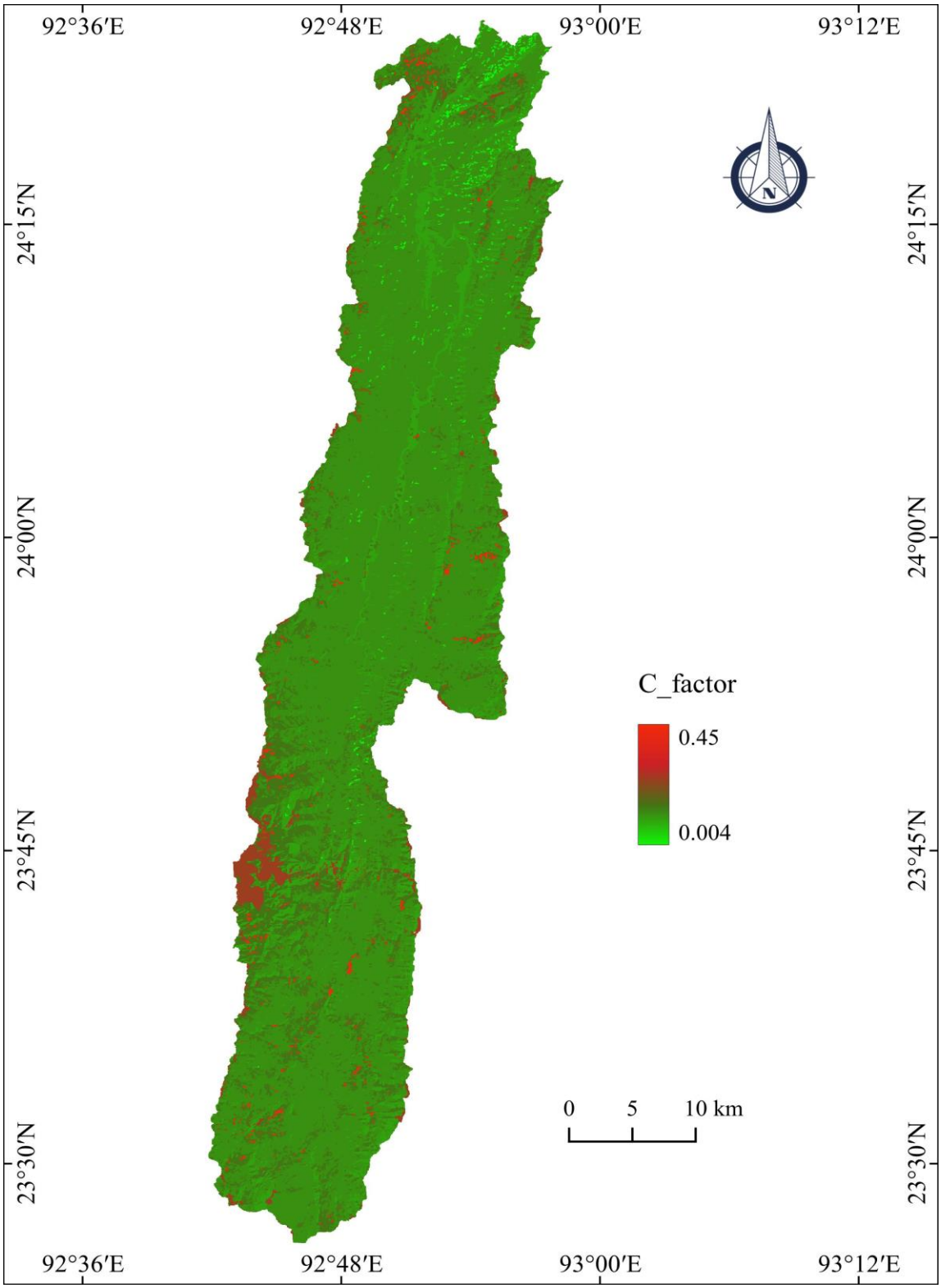


Figure 5.13: Cover Management Factor

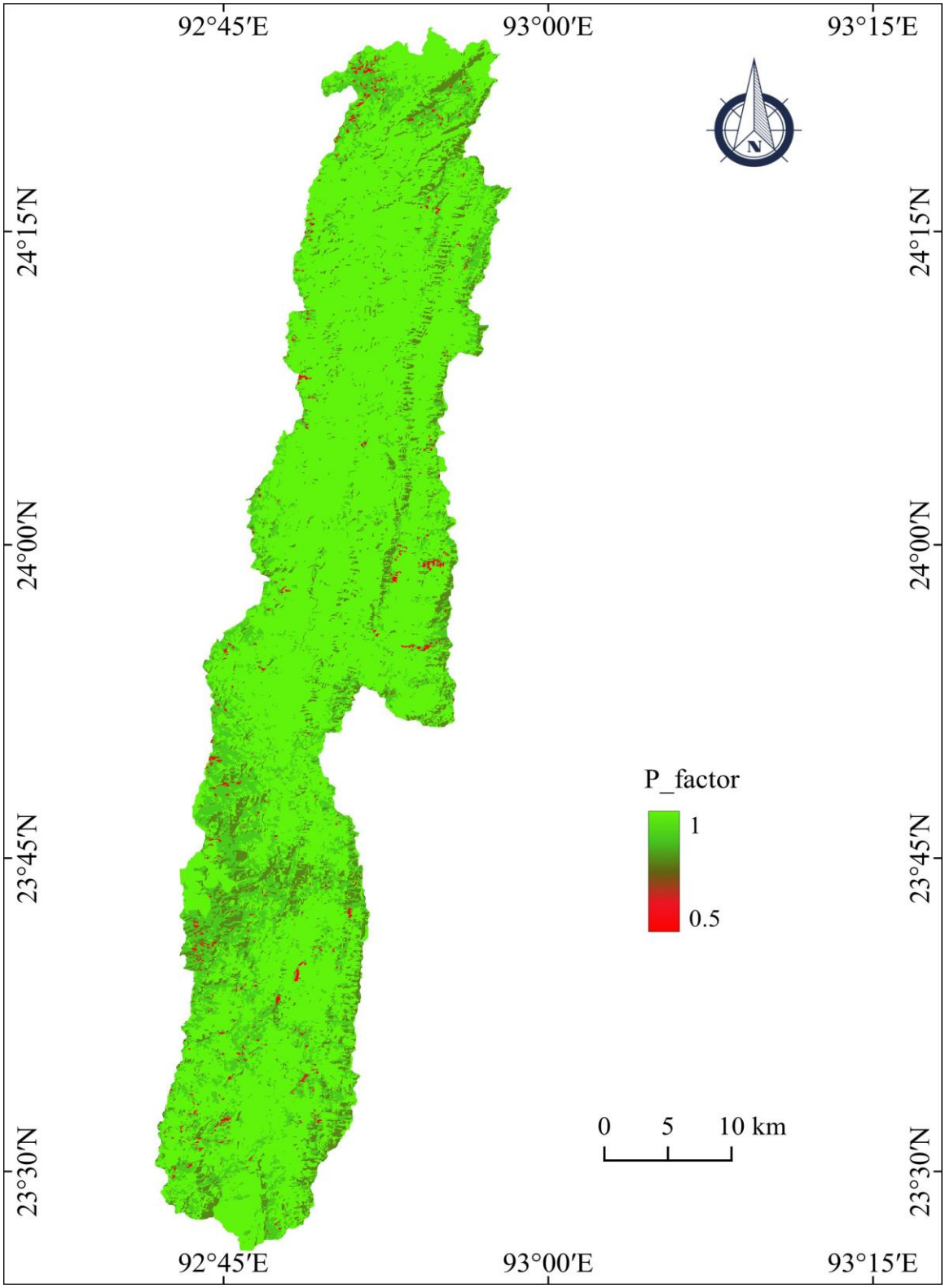


Figure 5.14: Practice Management Factor

### 5.7 Estimated soil loss in Tuirial watershed

The average annual soil loss of the Tuirial river basin was determined using the RUSLE approach, such as precipitation erosivity factors (R), soil erodibility factors (K), topography factors (LS), protection management factors (C), and preservation management factors (P). Precipitation, river flow, surface run-off, wind, and solar energy are some of the variables that cause soil erosion. Rainfall is one of the most significant and triggering factors of all of these variables. It is crucial to accurately measure and to understand the impact of rainfall on soil erosion, as it directly affects the erosivity factor (R) in the RUSLE parameters. The rate of infiltration is determined by the intensity, duration, and volume of rainfall. It also plays a role in determining the amount of water through surface run-off which contributes to soil erosion. Understanding the relationship between rainfall and infiltration can aid in developing effective erosion control strategies and sustainable land management practices. This high surface run-off in Mizoram is primarily due to presence of steep slopes and heavy rainfall. These factors increase the velocity of water flow, leading to greater soil erosion and the loss of fertile topsoil. Implementing measures such as contour ploughing, terracing, and reforestation can help to mitigate the effects of soil erosion caused by high surface run-off in Mizoram. The precipitation erosivity factor of the Tuirial basin ranges from 355 to 845 MJ.mm $ha^{-1}$ $hr^{-1}$ $yr^{-1}$. The average annual rainfall during these periods varies from 1209 to 2104 mm. The soil particles in the Tuirial river basin are likely to be highly susceptible to erosion due to their composition and structure. Additionally, the intense rainfall in the region further exacerbates the surface run-off, leading to high erosion rates. The monsoonal rainfall, with its high intensity and longer duration, resulted in higher surface runoff and also susceptible to soil erosion on hill slopes and floods in the lowland area.

The average annual soil loss of the Tuirial river basin varies from 0 to 1519.52 thousand t $ha^{-1}yr^{-1}$. Seven zones of soil loss were classified into, low (0-1 thousand t $ha^{-1}yr^{-1}$) 125941 ha. slightly (1-5 thousand t $ha^{-1}yr^{-1}$) 112.09 ha. moderate (5-15 thousand t $ha^{-1}yr^{-1}$) 110.54 ha. high (15-30 thousand t $ha^{-1}yr^{-1}$) 358.62 ha. very high (30-60 thousand t $ha^{-1}yr^{-1}$) 471.40 ha. severe (60-90 thousand t $ha^{-1}yr^{-1}$) 540.02 ha. and very

severe (≥120 thousand t $ha^{-1}yr^{-1}$) 12016.10 ha (Table 5.4). Highly susceptible soil loss areas such as barren land, the amount of precipitation, Jhum fallows, agricultural land, and built-up areas, sparse vegetation cover, undulating topography, high in angle of inclination and current cultivation areas are the triggering factors. Among the parameter rainfall erosivity, angle of inclination and slope of the length are the major influencing factors to determine soil loss in hill rain-fed region. In addition, current Jhum and fallow land are also play an important role in soil loss.

Table 1.4: Estimated average annual soil loss of Tuirial River Basin

| SI.No. | Class | Rate of soil loss (thousand t $ha^{-1}yr^{-1}$) | Area (ha.) | Percentage |
|---|---|---|---|---|
| 1 | Very low | 0-1 | 125941.00 | 90.24 |
| 2 | Low | 1_5 | 112.09 | 0.08 |
| 3 | Slight | 5_15 | 110.54 | 0.07 |
| 4 | Moderate | 15-30 | 358.62 | 0.25 |
| 5 | High | 30-60 | 471.40 | 0.33 |
| 6 | Severe | 60-90 | 540.02 | 0.38 |
| 7 | Very severe | >90 | 12016.10 | 8.61 |

The majority of the river basin was categorized as an erosion-free or moderate zone due to the presence of dense vegetation, low terrain, concrete infrastructure, clay, etc. The basin area of 12016 ha (8.61%) was identified as a very severe zone of soil erosion risk. Because of the built-up area, road construction, and current cultivation, exposed bare surfaces on hillslopes accelerate high run-off. The high rate of soil loss in the Tuirial basin was identified in the built-up area, barren land, and current shifting cultivation, including cultivable fallow land. The thick vegetation cover is found on the steep slope, which is inaccessible and difficult for cultivation activities. Generally, the Mizo settlements are located on hill slopes and edges, which contribute to high soil erosion rate along with rainfall and the LS factor. As per the FAO report the average rate of soil loss in the tropical climate is less than 10 t $ha^{-1}yr^{-1}$ (George *et al*., 2021). However, in the current study area,

the average annual soil loss is estimated at 0–1519.52 t $ha^{-1}yr^{-1}$ the upper Tuirial watershed, it is computed at 0–34323.3 t $ha^{-1}yr^{-1}$ (Barman *et al*., 2020) and in the northeastern part of India, at Mahadevpur block, the average soil loss is projected at 0–16843.07 t $ha^{-1}yr^{-1}$ (Vanlalchhuanga *et al*., 2022). the western Ghats of Kerala experiencing the same tropical climate, it has been projected at 0–105.578 t $ha^{-1}yr^{-1}$ (Thomas *et al*., 2018), 0 to 6453 t $ha^{-1}yr^{-1}$ in the lower Kulsi basin of Northeast India (Thakuriah, 2023). Whereas in countries, like Sri Lanka, at the Sabaragamuwa basin, the average annual soil loss is calculated as 0.0–50 t $ha^{-1}yr^{-1}$ (Senanayake *et al*., 2020), and in Malaysia, at the Pansoon sub-basin, it is reported as 0–18473 t $ha^{-1}yr^{-1}$(Yusof *et al*., 2019).

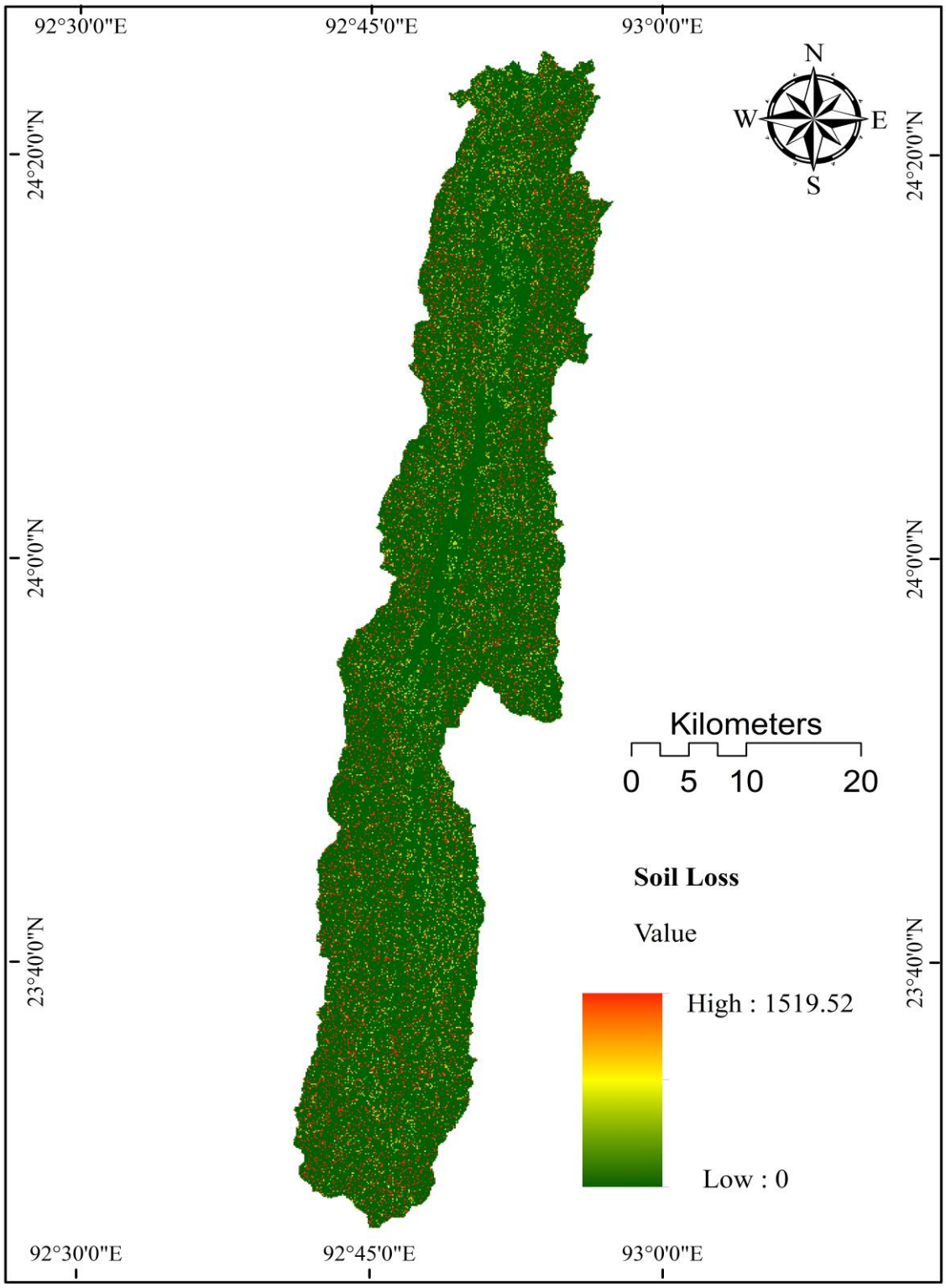


Figure 5.15: Average annual soil loss of Tuirial basin in thousand t $ha^{-1}yr^{-1}$

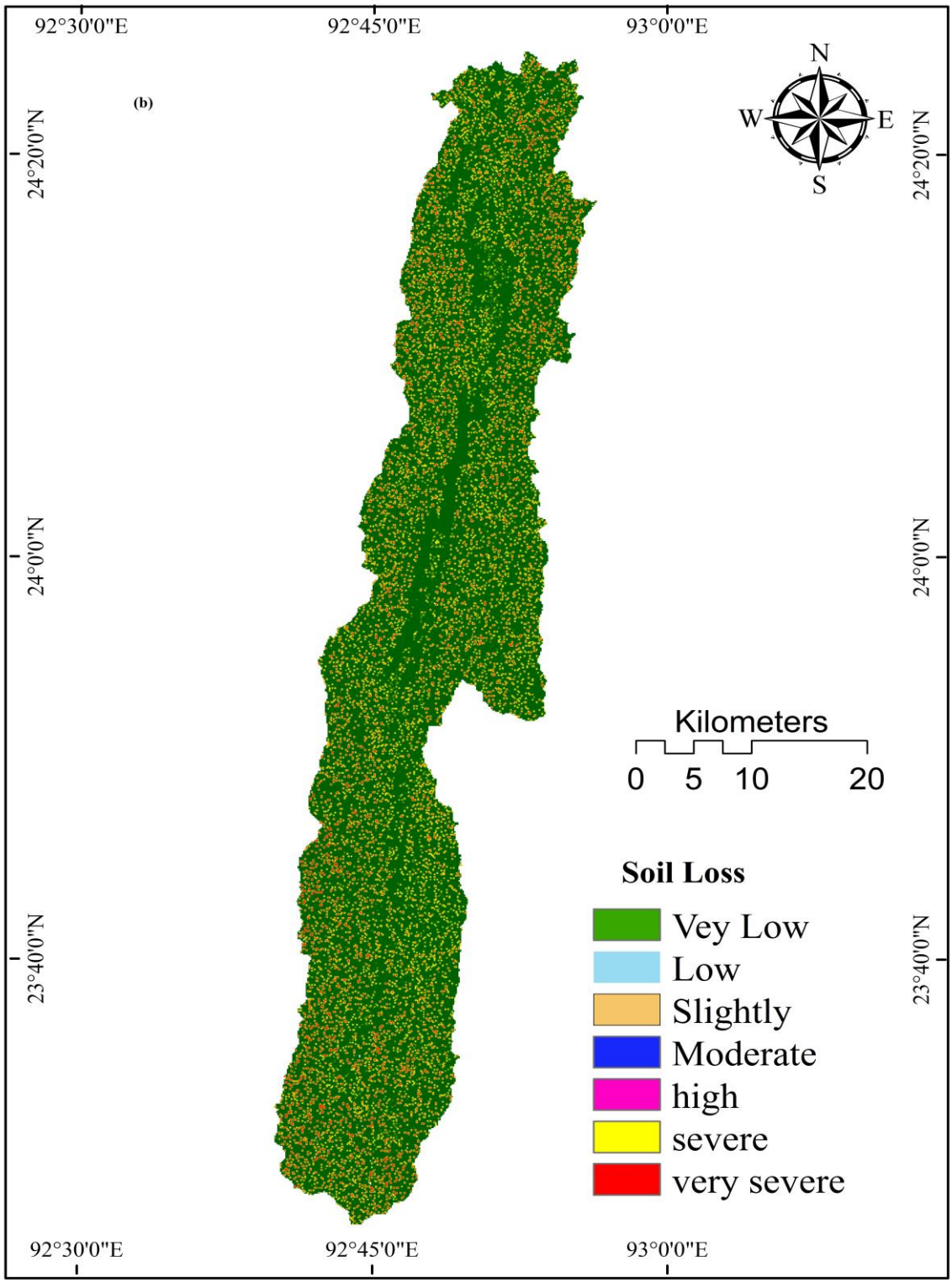


Figure 5.16: Zone wise average annual soil loss of Tuirial basin in thousand t $ha^{-1}yr^{-1}$

The degree of soil erodibility may vary spatially depending on soil texture (Ramesh *et al*., 2023). The *K* value differs from 0.25 t hr. $MJ^{-1}$ $mm^{-1}$ of clay to 0.66 ton/$hr^{-1}$/$MJ^{-1}$/$mm^{-1}$ of coarse loamy soil texture in the Tuirial basin. This suggests that areas with a higher proportion of coarse loamy soil texture in the Tuirial basin are found to be at high risk of soil erosion compared to areas with clay, fine loamy 0.54 ton/$hr^{-1}$/$MJ^{-1}mm^{-1}$, and loamy skeletal soil textures 0.57 ton/$hr^{-1}MJ^{-1}mm^{-1}$. The average annual rainfall received at the basin fluctuated from 1209 to 2104 mm. Similarly, the rainfall erosivity factor also varies based on the amount of rainfall received, as the analysis reveals 974.17–1844.31 MJ/mm/$ha^{-1}$/$hr^{-1}$/$yr^{-1}$. The western side of the basin receives more wind energy than the eastern side because the wind energy is weakened by the hill range, and in this area, rainfall is under the influence of the southwest monsoon. The soil particles in the Tuirial river basin are likely to be highly susceptible to erosion due to their composition and structure. Additionally, the intense rainfall in the region further exacerbates the surface run-off, leading to high erosion rates (Meshram and Sharma, 2018; Arefin *et al*., 2020). The Middle Tuirial river basin slope ranges from 0° to 59° (Table 6), which is divided into four different degrees of slope: 0°-10° (5.16%), mostly found close to the river, denotes low erosion; 10°-20° (5.57%) and 20°-30° (19.06%) gradient of slope shows moderate susceptibility to soil loss; and 30°-59° (70.20%) indicates that more than half of the total basin falls under the high to very high vulnerability to soil loss. In addition, vulnerability of soil loss depends on the angle of slope. The Tuirial basin topographic factor (LS) varies from 0 to 16.75. The LS factor is a key parameter in determining the potential for soil erosion, with higher values indicating areas of greater risk (Lawmchullova and Rao, 2023). The built-up land (0.48%), current cultivation (0.67), fallow land (9.72%), bamboo forest (26.70%), open forest (6.68%), medium forest (52.34%), dense forest (0.42%), and water bodies (2.98%) are the land use and land cover types found in the study area. The C and P factors are dimensionless factors with values range between 0 and 1. The C value nearby zero implies good conservation management, whereas a value at one denotes poor cover management. In the Tuirial river basin, good cover management is found in the areas where natural forest cover, water bodies and fallow land occur, which indicate a low soil risk zone, whereas

low cover management areas such as built-up land and current cultivation are likely to be susceptible to soil erosion (Lawmchullova *et al*., 2024). The P factor value between 0 and 1, with higher values implies low susceptibility to erosion; on the other hand, the values close to zero indicate a high chance of vulnerability of soil loss. The P value denotes the efficiency of cover and land management strategies in minimization of erosion risk.

### 5.8 Conclusion

The severe soil loss in the Tuirial watershed can be attributed to the topographic condition and anthropogenic activities. In addition, the presence of fine to loamy soil in over 80% of the TGA, which further exacerbates the risk of soil loss. The study also observed that the areas where settlements and built-upland experiences severe to extremely severe soil erosion. Excessive rainfall and topographic factors are found to be another influencing factors that determine huge volume of soil loss. The RUSLE model gives an in-depth understanding of spatial distribution of soil erosion patterns in the Tuirial River Basin by precisely analyzing the impact of rainfall erosivity, soil erodibility, and topographic factor (LS) in conjunction with cover management and practise conservation. However, improper drainage system, unplanned cultivation land along with road construction are the immediate increase of siltation and sedimentation process by anthropogenic activities. In addition, the absence of proper implementation of forest conservation measures strategies and management system are the another critical issue in Tuirial watershed.

# CHAPTER – 6

# ESTIMATION OF SILTATION

## 6.1 Introduction

Reservoir sediment is transported by running water and deposited at the reservoir bottom loaded from upstream (Skariah and Suriyakala, 2021). Sedimentation is a continuous process. It has become a major contemporary issue worldwide due to improper management of reservoirs and extensive exploitation of natural forest in the catchment area (Adongo *et al*., 2021). However, the measurement of siltation at the dam does not include statistical models of erosion (Bombino *et al*., 2022). The rate of siltation at the reservoir and the sediment transport index can be computed by measuring sediment pits and using the sediment yield model (Hassan *et al*., 2017; Maina *et al*., 2018). However, the bathymetry survey is the most precise method of evaluation of accumulated sediment at the reservoir than other approaches (Maina *et al*., 2018). These methods determine the sediment thickness at the initial reservoir bed level and the current year of sediment accumulated (Hassan *et al*., 2017).

Tuirial dam has started functioning from 27$^{th}$ October, 2017. It is the largest earth filled-dam within India. The installed capacity of the dam is 60 Mw. The dam is located close to Mizoram-Assam border along the river of Tuirial. Sediment and siltation are the major problems which shortening the dam function over worldwide. Since, Mizoram is the eastern extension of Himalayas, geologically immature and fragile topography along with heavy run-off within the catchment triggering erosion and deposited at the dam. In the present study aimed to estimate the volume of sediment accumulated at the bottom of dam during the last seven years (2016-2023) and the rate of sediment per year using bathymetry survey and pioneering approaches.

### 6.2 Digital elevation model (DEM) and bathymetry survey

Bathymetry survey data showed the current year (2023) bottom topography of dam, and the initial bottom topography of dam was extracted from ALOS PALSAR Dem at 10-meter resolution. The x and y coordinates with the z values from 62 selected points on both bathymetry and Dem survey data are presented in Table 6.1. The difference between the two surveyed elevation surfaces of dam bottom reveals the reduction of bottom elevation in 2023 by 7.92 metres, with the maximum thickness of about 7.2 metres was observed near the entrance of dam, whereas, the minimal change was found along the boundary of the dam.

Table 6.1 Details of Tuirial dam obtained from DEM (2016) and Bathymetry survey (2023).

| SI.No | Latitude | Longitude | Surface Water Level (metres) | Depth (metres) | | Dam Bed level above MSL (metres) | | Sediment Thickness (metres) |
|---|---|---|---|---|---|---|---|---|
| | | | | 2016 | 2023 | 2016 | 2023 | |
| 1 | 24.35409 | 92.88686 | 90.5 | 33 | 27.45 | 48 | 53.55 | 5.55 |
| 2 | 24.35384 | 92.88694 | 90.5 | 42.58 | 40.15 | 38.42 | 40.85 | 2.43 |
| 3 | 24.35363 | 92.88746 | 90.5 | 54.8 | 50 | 26.2 | 31 | 4.8 |
| 4 | 24.35335 | 92.88768 | 90.5 | 24.1 | 22 | 56.9 | 59 | 2.1 |
| 5 | 24.35422 | 92.88803 | 90.5 | 44.51 | 41.7 | 36.49 | 39.3 | 2.81 |
| 6 | 24.35392 | 92.88867 | 90.5 | 47.65 | 41.16 | 33.35 | 39.84 | 6.49 |
| 7 | 24.35546 | 92.88797 | 90.5 | 28.33 | 24.08 | 52.67 | 56.92 | 4.25 |
| 8 | 24.35727 | 92.88911 | 90.5 | 23.31 | 21.3 | 57.69 | 59.7 | 2.01 |
| 9 | 24.35689 | 92.88964 | 90.5 | 35.42 | 32.4 | 45.58 | 48.6 | 3.02 |
| 10 | 24.35573 | 92.88831 | 90.5 | 25.12 | 21.6 | 55.88 | 59.4 | 3.52 |
| 11 | 24.35547 | 92.88887 | 90.5 | 40.91 | 37.8 | 40.09 | 43.2 | 3.11 |
| 12 | 24.35485 | 92.88762 | 90.5 | 45.91 | 40 | 35.09 | 41 | 5.91 |
| 13 | 24.35409 | 92.88762 | 90.5 | 43.76 | 37.8 | 37.24 | 43.2 | 5.96 |

| | | | | | | | | |
|---|---|---|---|---|---|---|---|---|
| 14 | 24.3538 | 92.88691 | 90.5 | 47.77 | 42.5 | 33.23 | 38.5 | 5.27 |
| 15 | 24.35346 | 92.88619 | 90.5 | 47.7 | 41.45 | 33.3 | 39.55 | 6.25 |
| 16 | 24.35313 | 92.88567 | 90.5 | 47.6 | 43.1 | 33.4 | 37.9 | 4.5 |
| 17 | 24.35325 | 92.88517 | 90.5 | 42.58 | 37 | 38.42 | 44 | 5.58 |
| 18 | 24.35367 | 92.88527 | 90.5 | 38.66 | 31.4 | 42.34 | 49.6 | 7.26 |
| 19 | 24.35421 | 92.88593 | 90.5 | 25.31 | 22.65 | 55.69 | 58.35 | 2.66 |
| 20 | 24.35475 | 92.88639 | 90.5 | 17.97 | 10 | 63.03 | 71 | 7.97 |
| 21 | 24.3549 | 92.8867 | 90.5 | 17.97 | 13.1 | 63.03 | 67.9 | 4.87 |
| 22 | 24.35499 | 92.88687 | 90.5 | 17.98 | 15.3 | 63.02 | 65.7 | 2.68 |
| 23 | 24.35526 | 92.88715 | 90.5 | 18.03 | 15 | 62.97 | 66 | 3.03 |
| 24 | 24.35564 | 92.8873 | 90.5 | 19.09 | 18 | 61.91 | 63 | 1.09 |
| 25 | 24.35618 | 92.88804 | 90.5 | 17.13 | 14.4 | 63.87 | 66.6 | 2.73 |
| 26 | 24.35642 | 92.88842 | 90.5 | 19.65 | 19.6 | 61.35 | 61.4 | 0.05 |
| 27 | 24.35626 | 92.88906 | 90.5 | 27.93 | 26.2 | 53.07 | 54.8 | 1.73 |
| 28 | 24.35606 | 92.88963 | 90.5 | 39.84 | 38.2 | 41.16 | 42.8 | 1.64 |
| 29 | 24.35609 | 92.89089 | 90.5 | 22.62 | 22.15 | 58.38 | 58.85 | 0.47 |
| 30 | 24.35719 | 92.89156 | 90.5 | 23.51 | 22.15 | 57.49 | 58.85 | 1.36 |
| 31 | 24.35837 | 92.8918 | 90.5 | 29.37 | 28.9 | 51.63 | 52.1 | 0.47 |
| 32 | 24.35808 | 92.89168 | 90.5 | 29.42 | 28.9 | 51.58 | 52.1 | 0.52 |
| 33 | 24.35808 | 92.89072 | 90.5 | 37.6 | 37.3 | 43.4 | 43.7 | 0.3 |
| 34 | 24.35275 | 92.8889 | 90.5 | 15.74 | 15.4 | 65.26 | 65.6 | 0.34 |
| 35 | 24.35264 | 92.88987 | 90.5 | 10.4 | 10.3 | 70.6 | 70.7 | 0.1 |
| 36 | 24.35352 | 92.88995 | 90.5 | 13.7 | 13.5 | 67.3 | 67.5 | 0.2 |
| 37 | 24.35464 | 92.88998 | 90.5 | 26.65 | 25.32 | 54.35 | 55.68 | 1.33 |
| 38 | 24.35409 | 92.89138 | 90.5 | 11.757 | 11.7 | 69.243 | 69.3 | 0.057 |
| 39 | 24.35319 | 92.89109 | 90.5 | 14.33 | 14 | 66.67 | 67 | 0.33 |
| 40 | 24.35336 | 92.89243 | 90.5 | 13.9 | 13.48 | 67.1 | 67.52 | 0.42 |
| 41 | 24.35421 | 92.89322 | 90.5 | 7.46 | 6.45 | 73.54 | 74.55 | 1.01 |

| | | | | | | | | |
|---|---|---|---|---|---|---|---|---|
| 42 | 24.35586 | 92.89267 | 90.5 | 12.47 | 12.3 | 68.53 | 68.7 | 0.17 |
| 43 | 24.35512 | 92.89154 | 90.5 | 20.43 | 19.63 | 60.57 | 61.37 | 0.8 |
| 44 | 24.35434 | 92.8923 | 90.5 | 18.21 | 17.8 | 62.79 | 63.2 | 0.41 |
| 45 | 24.35534 | 92.89048 | 90.5 | 24.62 | 22.35 | 56.38 | 58.65 | 2.27 |
| 46 | 24.35419 | 92.89069 | 90.5 | 18.49 | 17.52 | 62.51 | 63.48 | 0.97 |
| 47 | 24.35705 | 92.89267 | 90.5 | 17.32 | 15.75 | 63.68 | 65.25 | 1.57 |
| 48 | 24.3561 | 92.89187 | 90.5 | 25.44 | 22.81 | 55.56 | 58.19 | 2.63 |
| 49 | 24.35714 | 92.89069 | 90.5 | 30.67 | 27.9 | 50.33 | 53.1 | 2.77 |
| 50 | 24.35338 | 92.88924 | 90.5 | 24.51 | 21 | 56.49 | 60 | 3.51 |
| 51 | 24.35477 | 92.88906 | 90.5 | 36.78 | 35.7 | 44.22 | 45.3 | 1.08 |
| 52 | 24.35897 | 92.88989 | 90.5 | 11.3 | 10.9 | 69.7 | 70.1 | 0.4 |
| 53 | 24.35816 | 92.88889 | 90.5 | 7.5 | 7.5 | 73.5 | 73.5 | 0 |
| 54 | 24.35514 | 92.8861 | 90.5 | 0 | 0 | 81 | 81 | 0 |
| 55 | 24.35444 | 92.8852 | 90.5 | 0 | 0 | 81 | 81 | 0 |
| 56 | 24.35701 | 92.88791 | 90.5 | 0 | 0 | 81 | 81 | 0 |
| 57 | 24.35772 | 92.8887 | 90.5 | 0 | 0 | 81 | 81 | 0 |
| 58 | 24.35838 | 92.88818 | 90.5 | 0 | 0 | 81 | 81 | 0 |
| 59 | 24.35887 | 92.88884 | 90.5 | 0 | 0 | 81 | 81 | 0 |
| 60 | 24.35375 | 92.89368 | 90.5 | 0 | 0 | 81 | 81 | 0 |
| 61 | 24.35246 | 92.89016 | 90.5 | 0 | 0 | 81 | 81 | 0 |
| 62 | 24.35301 | 92.89225 | 90.5 | 0 | 0 | 81 | 81 | 0 |

Source: Survey by author ($11^{th}$ – $12^{th}$ April, 2023)

### 6.3 Interpolation method

RMSE statistical analysis reveals the Local Polynomial Function (LPF) is the most appropriate method for interpolation, which yields the lowest RMSE value with having the highest positive correlation ($R^2 = 0.80$). The high RMSE value exhibits that the observed and interpolated values are in negative relation (Li and Heap, 2011) whereas; low RMSE value indicates the observed value and predicted value are positively associated. Thus,

using local polynomial interpolation techniques a raster layer of Tuirial dam reservoir was generated. The results of detailed spatial interpolation accuracy assessment along with the RMSE and correlation are presented in Table 6.2.

Table 6.2 Interpolation accuracy assessment of Tuirial dam

| Interpolation Methods | MAE | MSE | RMSE | $R^2$ |
|---|---|---|---|---|
| Ordinary Kriging | 5.48 | 48.79 | 6.98 | 0.74 |
| Local Polynomial Interpolation | 4.58 | 37.77 | 6.14 | 0.80 |
| Inverse Distance Weighted | 6.12 | 67.53 | 8.21 | 0.66 |
| Radial Base Function | 5.43 | 51.30 | 7.16 | 0.73 |

Measured elevation is predicted using geo-statistical tools by four selected spatial interpolation techniques such as radial base, local polynomial, kringing and inverse distance weight interpolation. This technique indicates the correlation between measured elevation and predicted elevation. The analysed measured elevation data plotted on x-axis and predicted elevation data plotted on y-axis. Among the spatial interpolation methods local polynomial interpolation technique yields the highest correlation. The different spatial interpolation techniques are plotted in figure 6.1.

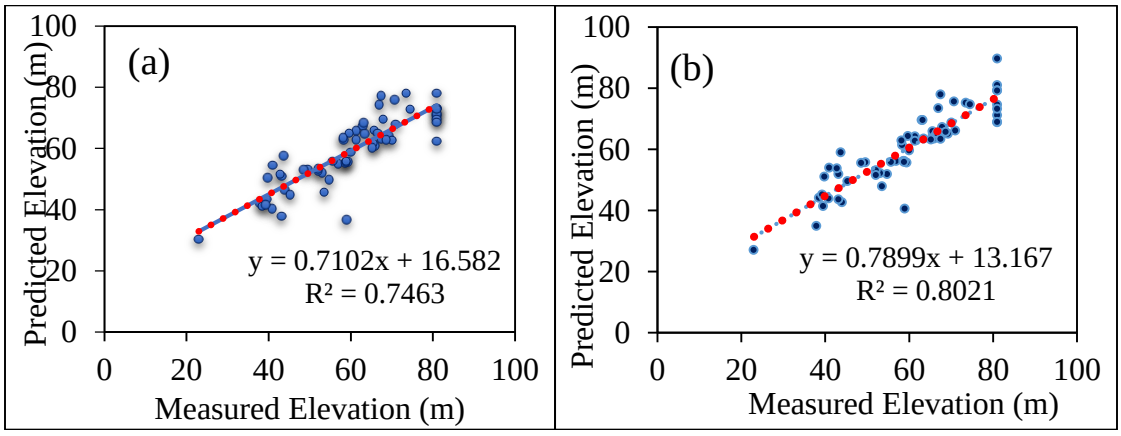

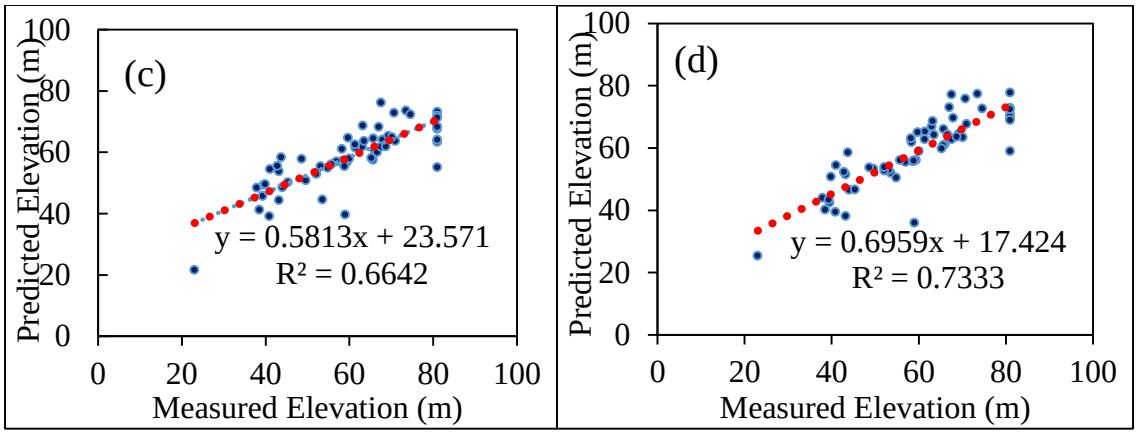


Figure 6.1 Measured vs predicted bottom topography dataset test of Tuirial dam; (a) Ordinary Kringing Interpolation, (b) Local Polynomial Interpolation, (c) Inverse Distance Weight, (d) Radial Base Function

**6.4 Estimation of sediment volume at Tuirial dam**Error! Bookmark not defined.

The amount of sediment deposited was estimated using the variation in Tuirial reservoir capacity between the initial year (2016) and the present year (2023). At an elevation of 90.5 m above mean sea level, the maximum full supply level is 19.87 $Mm^3$, which was computed from the TIN surface volume using 3D analyst tools in Arc-GIS 10.4. Create TIN execution was performed in order to get the surface volume of both 2016 and 2023 years. Then, using spatial interpolation of LPI technique both survey data are interpolated. The initial year layer was subtracted from the current raster layer raster. Thus the volume of sediment yield was estimated. The figure 6.2 indicates the interpolation and create TIN of dam area of the year 2016. Figure 6.3 depicts the interpolation of raster layer and create TIN of dam are of the year 2023. The storage capacity of the Tuirial Dam was 19.87 $Mm^3$ in 2016 and 17.29 $Mm^3$ in 2023. During the past seven years of operation, there has been 2.57 $Mm^3$ (909829.41 tonnes) difference in the storage capacity (Table 6.3). It is noted that the sediment deposition over the last seven years resulted by a drop of 12.96 percent in the total storage volume. The specific sediment yield of Tuirial dam is 0.36 M $m^3/yr^{-1}$. Due to high sediment yield, a huge volume of siltation is deposited in the reservoir, which is influenced by high surface run-off, triggering an influx of loose and fragmented

material due to gravitational force over steep slope. Besides, the traditional shifting cultivation of agricultural practices is the most common influencing factor of soil erosion found in the Tuirial basin. Moreover, the size of the basin also determined the sediment production at the reservoir in other regions. The Tuirial River Basin is more than 1427.92 $km^2$ and is expected to undergo an increased sedimentation process. This can lead to reduced storage capacity of the reservoir and potential impacts the water quality and aquatic ecosystems downstream. Effective soil conservation measures and land use management strategies are essential to mitigate sediment yield in the Tuirial River Basin and protect the reservoir's functionality in the long term. Implementing sustainable land use practices, such as reforestation and terracing, can help to reduce soil erosion and sedimentation in the basin. Additionally, regular monitoring and maintenance of the reservoir can ensure its continued effectiveness in providing water resources for the surrounding communities.

Table 6.3 The details of area, surface and sediment volume obtained by 3Dimensional analysis

| Year | 2D Area($m^2$) | 3D Area($m^2$) | Surface Volume ($m^3$) | Sediment Yield ($m^3$) | SY/Y ($m^3$) |
|---|---|---|---|---|---|
| 2023 | 422438.74 | 443447.5 | 17295827 | 2576350 | 368050 |
| 2016 | 424778.01 | 451013.7 | 19872177 | | |

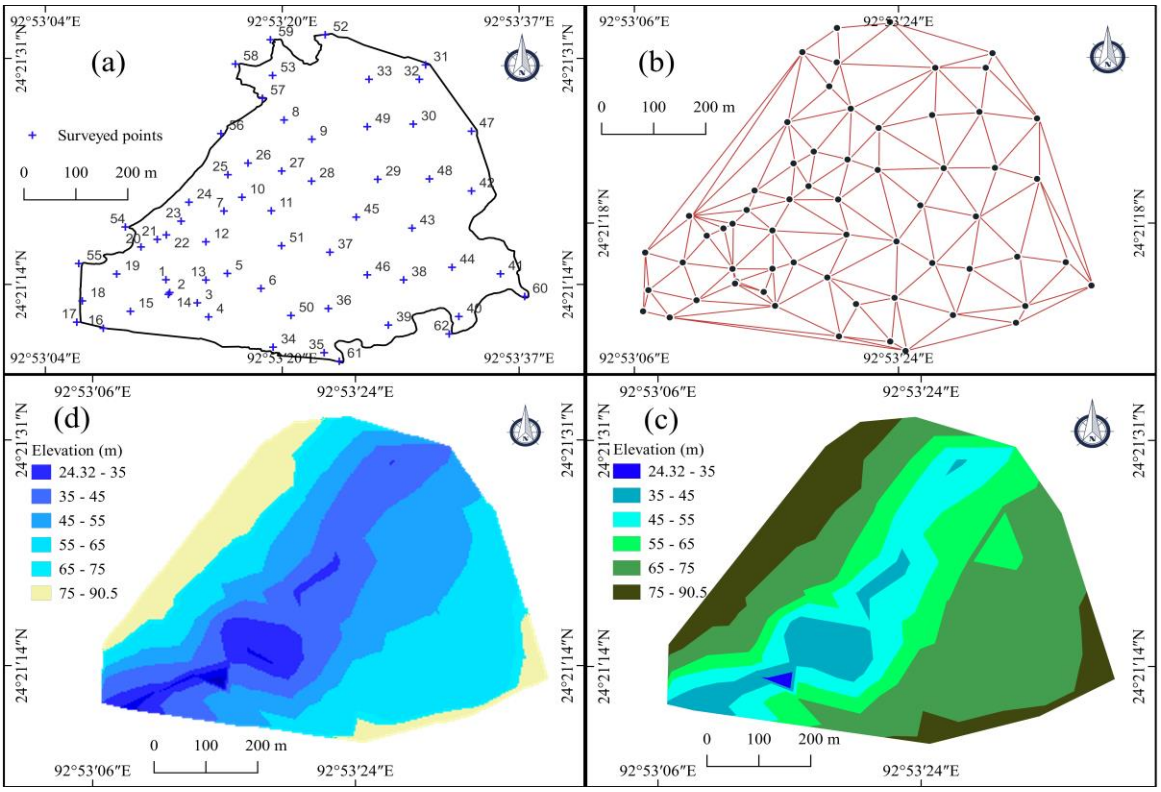


Figure 6.2: (a) Bathymetry survey locations, (b) Triangulation, (c) TIN, (d) Interpolated raster

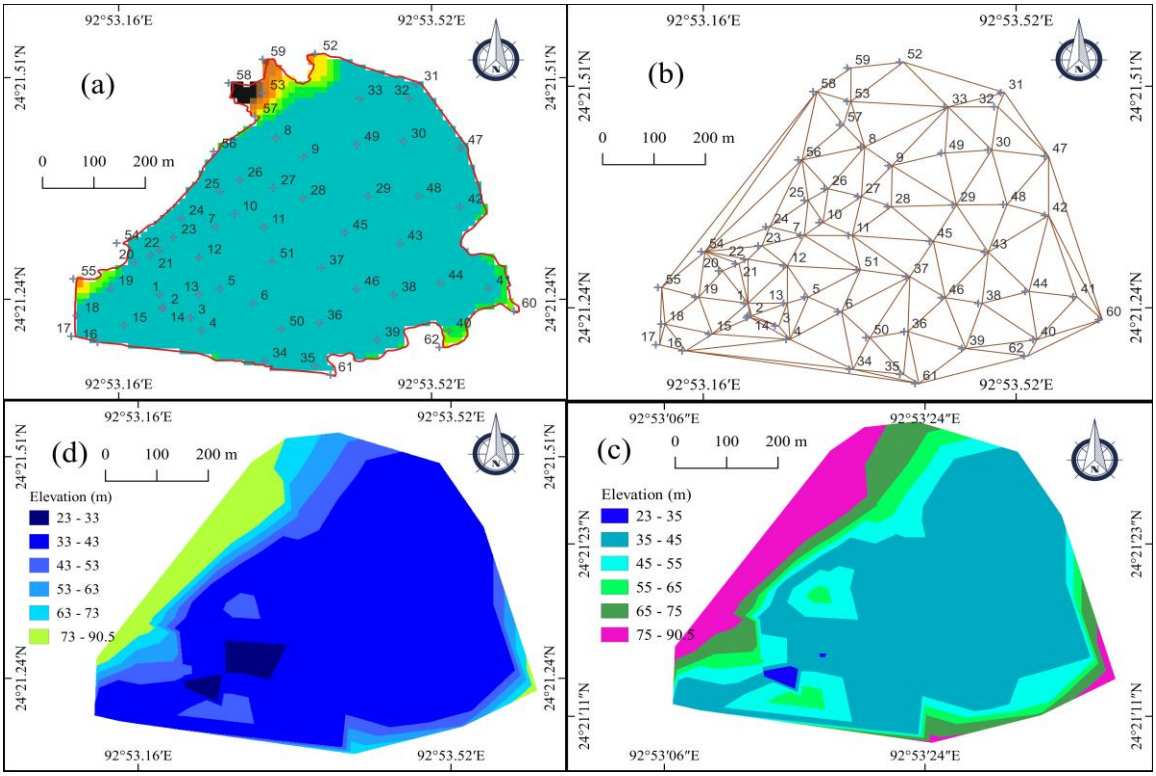


Figure 6.3: (a) Elevation extracted from DEM, (b) Triangulation, (c) TIN, (d) Interpolated raster

**6.5 Sediment distribution and 3D analysis**

As depicted in the 3Dimensional models (DEM) of the dam of the year 2016 before the dam function and after 7 years (2023) of dam operation, the changes in the bottom topography are clearly visible (Fig. 6.5). The three dimensional DEMs specify significant increase of sediment accumulation at the bottom of reservoir, indicating the impact of water flow and sediment transport over time. In 2016 bottom topography, the highest elevation of bottom is about 72 meters, whereas by 2023 the elevation is reduced to 67 meters. The change of about 5 meters may be attributed to the deposition of sediment at the bottom of the dam. This implies within 7 years of dam operation the incoming sediment from streams is 5 meters thick at the bottom. Because the size of the Tuirial basin is large and highly susceptible to soil erosion as the catchment area and geological structure also control sediment inflow at the dam. Understanding the changes in topography over time can also provide valuable insights into potential risks of flooding or structural instability. By

monitoring these changes regularly, authorities can make decisions to mitigate any potential issues and ensure the long-term sustainability of the dam. The computed result showed that the maximum elevation reduction with the thickest sediment is 7.79 meters in the middle of the reservoir. This significant reduction in elevation is crucial for accurately assessing the storage capacity of the reservoir and understanding potential impacts on water availability. Further analysis may be needed to determine the long-term implications of sediment accumulation on water resources in the area. The average sediment deposited at the reservoir bed is 2.25 meters (Table 6.1). Over the last seven years of dam operation, the average depth has decreased by about 2.25 meters. The sediment thickness is uneven, with its maximum at its entrance and the lowest at the middle of the dam. The cross-section of the dam topography shows that the accumulated silt is more on the eastern side than the western part. This may be attributed to rock fall and absorption of the river bank where loose soil exists. Constant inflow of water energy is transporting the fragmented pebbly-gravel and fine silt towards the bottom. Moreover, the wind energy produces wave that highly occur during the pre-monsoon, which attack the soil at the dam edges. The sediment accumulation is greater in the area where the bed was excavated further during the construction of the dam to increase its storage capacity. The distribution and concentration of the sediments are determined by the size of the sediments and the bed level elevation of the reservoir. Figure 6.4 represents three dimensional sediment thicknesses at the Tuirial dam, which exhibit the heavier materials are deposited close to entrance of the reservoir and the lighter sediments are deposited far away from the entrance, as they are controlled by the waves and water currents. While on the eastern side is earth filled and heavier boulders on the top to reduce water pressure where the rate of sediments deposition is low. Additionally, the type of vegetation surrounding the reservoir can also impact sediment flow. The heavier portion of silt was deposited near the entrance, while fine sediment was deposited far away. This demonstrates that the fine dirt part was delivered to the low area of the reservoir even at a slow flow rate, which implies that the live storage zone and the dead storage zone are losing, and the dead storage zone has even greater at loss (Mekonnen *et al*., 2022). It was also found that siltation had greater effects on live storage than it did

on dead storage. Within the watershed, particularly close to the dam, reforestation and sustainable agro-plantations are crucial for managing sediment inflow into the reservoirs. Implementing erosion control measures, such as terracing or buffer strips, can further help reduce sedimentation in the reservoir. These findings highlight the importance of implementing erosion control measures to protect the live storage capacity of reservoirs. Effective management strategies should be prioritized to minimize sedimentation in order to maintain water storage capacity for the long term.

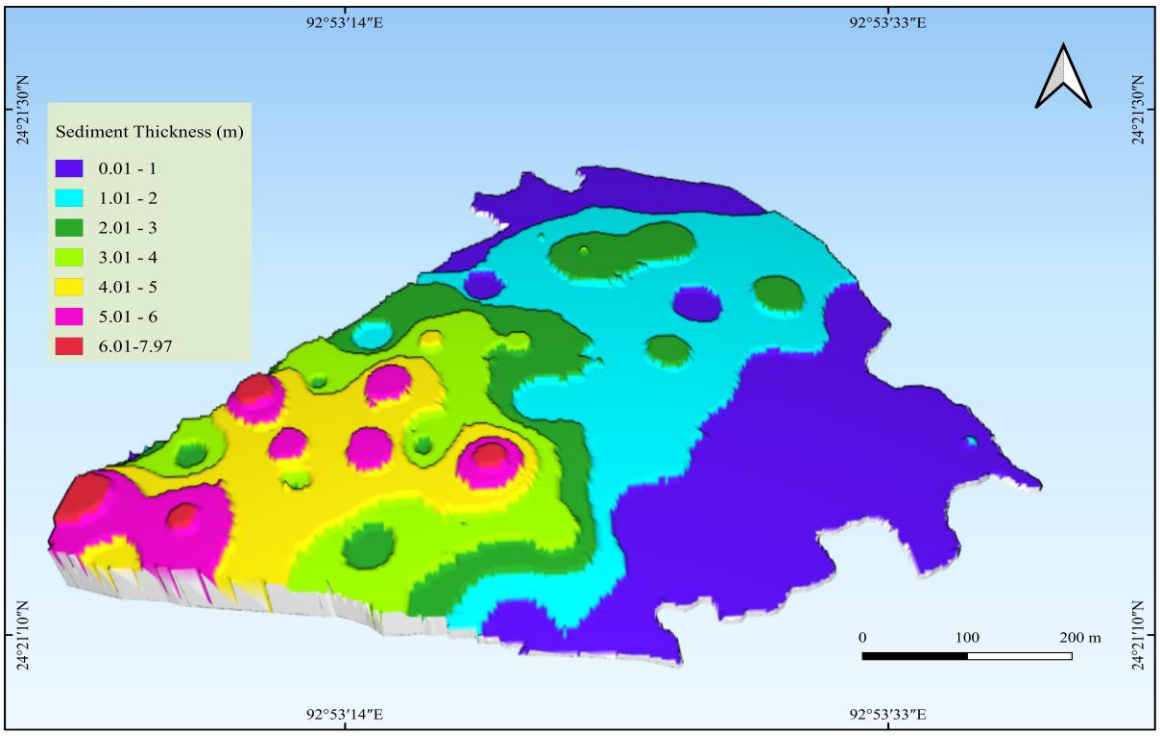


Figure 6.4: Three dimensional representation of spatial distribution of sediment at the bottom

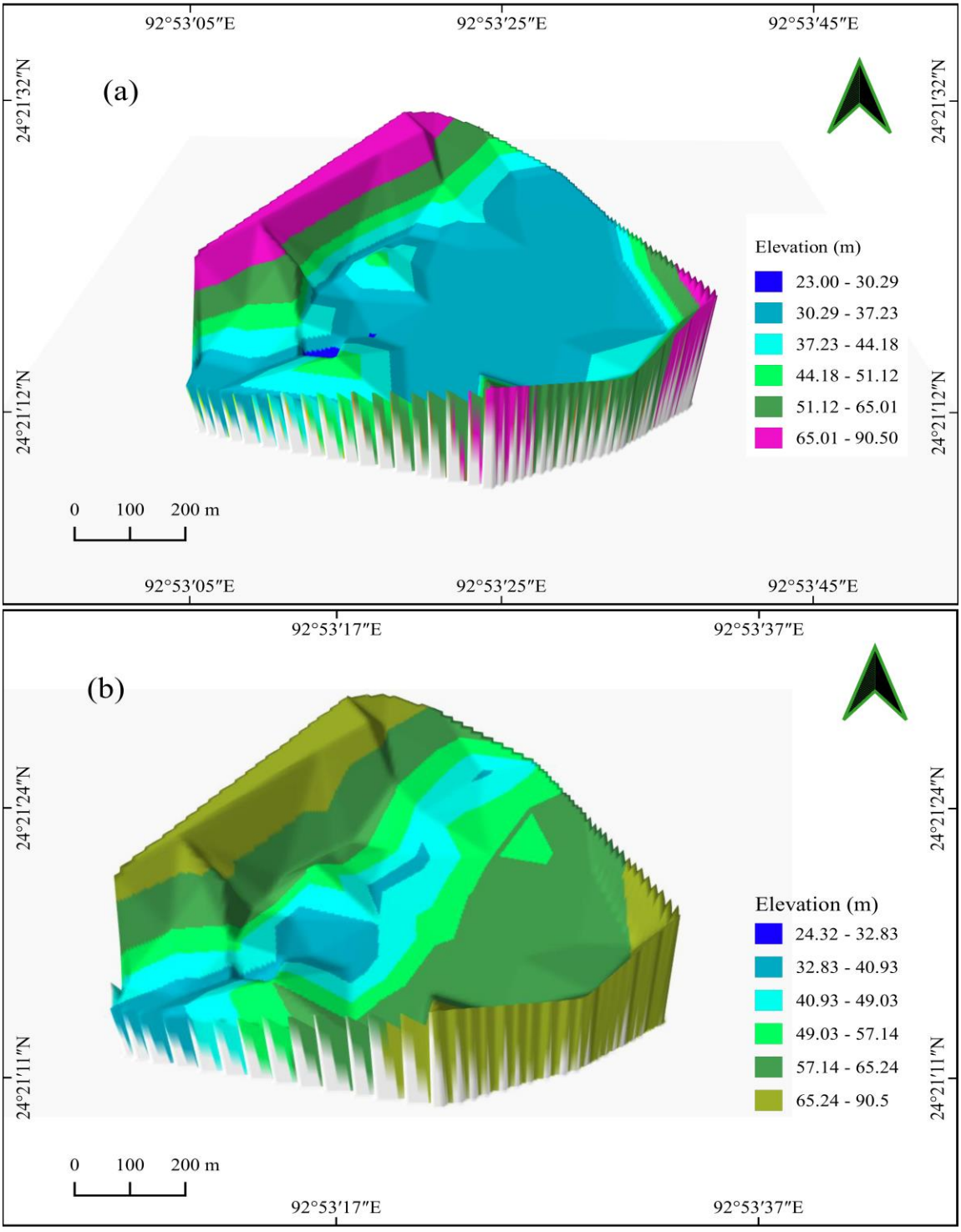


Figure.6.5: Three dimensional representation of the bottom topography of dam; (a) 2016, (b) 2023

## 6.6 Analysis of area-storage-capacity curve

The reservoir storage volume at 5 metres elevation intervals and area (in ha) in the initial year and the current 2023 were estimated using the surface volume and geometry analyst tools. The two surveys that were conducted at different time intervals have revealed the reduction in reservoir storage volume. The change in area storage capacity is induced by the steady loss in reservoir storage capacity due to accumulation of sediment deposits. The reservoir's gross storage capacity was estimated to be 13.97 ha (32.45 $Mm^3$) in 2016 and 12.44 ha (28.83 $Mm^3$) in 2023. The water level at an elevation of 90.5 metres was reduced by 1.52 ha in seven years, from 13.97 ha in the year 2016 to 12.44 ha in the year 2023 due to siltation at the reservoir's original area. The detailed volume of water loss per 5 meters interval of elevation and area of the year 2016 and 2023 is highlighted in Table 6.4Table 6.4 Area and volume of Tuirial dam. In figure 6.5 the area storage capacity of Tuirial dam has been plotted. In This plot exhibits the elevation versus area and volume versus elevation of the original data of the year 2016 and current year 2023. Both curves are deviated toward the top depicting the rising elevation with an increasing the area and capacity of water storage. Similarly, the area and elevation curves are deviated when the elevation is increased due to the variation of area of the year 2016 and 2023.

Table 6.4 Area and volume of Tuirial dam

| 2016 | | | | 2023 | | | |
|---|---|---|---|---|---|---|---|
| Elevation (metres) | Area (ha) | Cumulative area (ha) | Volume of Water ($Mm^3$) | Elevation (metres) | Area (ha) | Cumulative area (ha) | Volume of Water ($Mm^3$) |
| 23.00 | 0.00 | 0.00 | 0.00 | 24.32 | 0.00 | 0.00 | 0.00 |
| 30.16 | 0.19 | 0.19 | 10.74 | 30.16 | 0.02 | 0.02 | 8.78 |
| 35.30 | 1.24 | 1.43 | 11.54 | 35.30 | 0.38 | 0.40 | 11.39 |
| 40.30 | 4.12 | 5.55 | 14.55 | 40.30 | 3.97 | 4.37 | 13.94 |
| 45.40 | 7.72 | 13.27 | 17.97 | 44.40 | 6.56 | 10.93 | 16.53 |
| 51.23 | 8.46 | 21.73 | 20.01 | 51.23 | 8.19 | 19.12 | 19.43 |
| 59.33 | 12.08 | 33.81 | 24.71 | 59.33 | 11.45 | 30.57 | 22.87 |
| 90.05 | 13.97 | 47.78 | 32.45 | 90.05 | 12.44 | 43.02 | 28.83 |

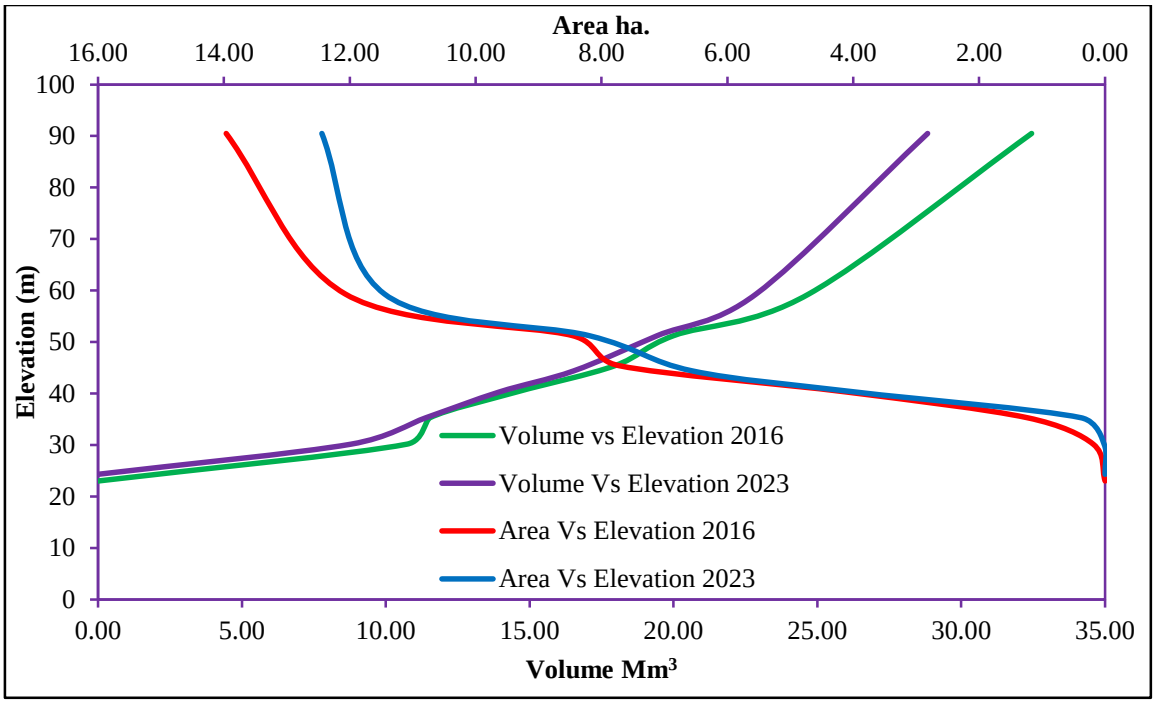


Figure 6.5: Capacity-elevation and area-elevation curves plotted based on the initial year (2016) and the current year (2023) data analysis of Tuirial dam

### 6.7 Longitudinal and latitudinal profile

The longitudinal and latitudinal profiles of the Tuirial dam bottom topography for the initial year of 2016 and the current year of 2023 were measured using the profile tool in Qgis 3.22 software. The raster thematic layer generated by TIN interpolation for both profiles was carried out for the initial year and the current year. During the seven years of dam operation, huge quantity of silt might have accumulated particularly along the Tuirial river's old channel. The huge quantity of silt deposited in the middle of the reservoir is the main reason behind the variation between the longitudinal and latitudinal profiles over the past seven years. From the figure 6.7a, it is visible where the middle part of the reservoir is characterized by flat in the year of 2016. However, figure 6.7b shows that the rising of bottom elevation depicts siltation is accumulated by the year of 2023. The bottom topography of Tuirial dam has become shallow by siltation as highlighted based on the elevation change in figure 6.7c. The deposition of sediment is high in the eastern side of

the dam than the western side. This could be attributed to the occurrence of landslide due to instability of the slope of the river bank.

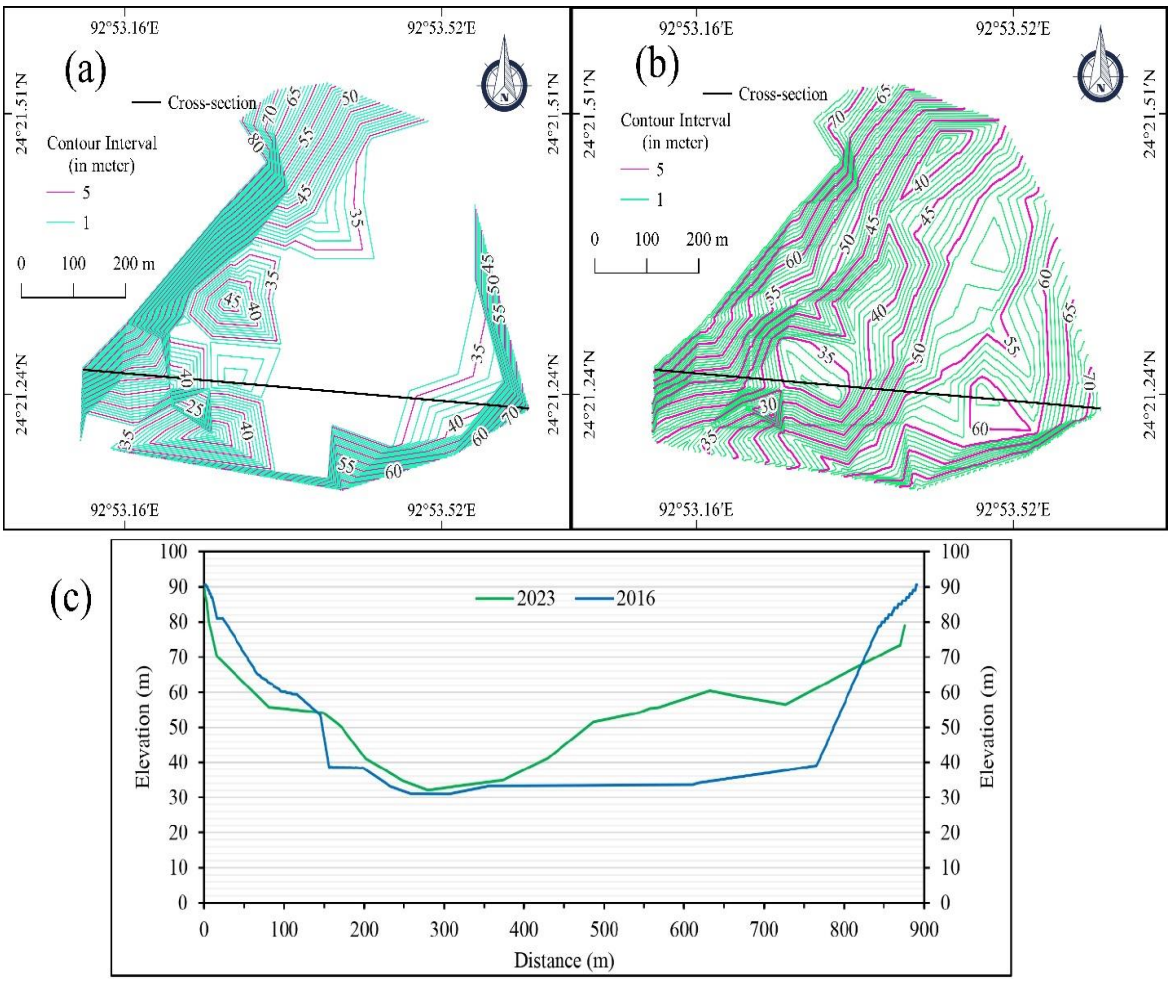


Figure 6.7: Change in the bottom contour configuration of Tuirial dam (a) 2016 and (b) 2023 (c) Cross section showing siltation thickness and water level

### 6.8 Estimation of Tuirial dam useful lifespan

The lifespan of a reservoir is calculated as the time it takes to silt up the dead storage or exhaust 50% of the loading capacity. The lifespan of the reservoir is estimated to be shortened due to the huge volume of sediment deposited at the reservoir. Moreover, the amount of sediment produced by the catchment directly influences the rate of siltation. In this study, the reservoir lifespan was calculated using the economic useful span of reservoir

formula. Based on the amount of sediment deposited at the dead storage level, the reservoir's expected lifespan is about 47 years. The failure of dam before the expected lifespan as it is designed for can be attributed to poor conservation of the watershed, improper soil management, or natural forces. To increase the useful life span of reservoir, proper sediment flush or sediment pits must be installed at the bottom, which can be flushed regularly. On the other hand, monitoring of sediment accumulated at the dam bottom is essential to implement new techniques for removal of the sediment.

### 6.9 Tuirial dam trap efficiency

The reservoir capacity of 19872176.97 $m^3$ (19.87 $Mm^3$) and the watershed area of 1418.61 $km^2$ excluding the Tuirial dam area, the trap efficiency was computed using Equation ((3.17). Hence, the trap efficiency of Tuirial dam is 57.50 per cent which indicates that 57.50 per cent of sediment within the catchment area are trapped or deposited at the bottom of dam and the remaining sediments are deposited before the dam of river bed and outflow from the reservoir. The estimated values of trap efficiency of dams in Ethiopia and Japan range between 83% and 95% (Shiferaw and Abebe, 2021; Tesfaye *et al*., 2023). It is not possible to trap above 70% of the sediment at the dams due to various controlling factors of topography, discharge and flow velocity of rivers.

### 6.10 Bulk density

The estimated dry bulk density of Tuirial reservoir sediment is 1397kg/$m^3$. The bulk density of the Indian reservoirs like Sriramsagar in Telangana state in India ranges between 300 and 1600 kg/$m^3$ (Sultana, 2017) because of the nature of hard rock terrain with granitic-gneiss, whereas, the reservoir Tigray in the northern Ethiopian region ranges from 1010.18 to 1420 kg/$m^3$ (Haregeweyn *et al*., 2006). The lithology of this region is close to the sedimentary rocks of Mizoram. Since Tuirial dam's dry bulk density is lower than that of other reservoirs, it is obvious that the sediment deposit is heavier and increasing more rapidly due to the presence of unconsolidated sedimentary rocks spread extensively in the basin.

## 6.11 Conclusion

The estimation of total sediment, reservoir storage capacity loss, specific sediment yield, sediment yield, trap efficiency, useful lifespan of reservoir, rate of siltation and dry bulk density by the application of RS and GIS, bathymetry survey and scientific methods are found to be useful. The study revealed that the 2.57 $Mm^3$ total amount of sediment deposited and 12.96 per cent reduction in the gross storage capacity during 7 years of dam operation. Also, the useful life span of the reservoir is estimated to be 47 years against the initial design of 100 years. The rate of siltation is estimated at a rate of 368050 $m^3/yr^{-1}$. The dam storage capacity was gradually reduced due to high-rate of infiltration, along with continuously sediment influx at the dam. In addition, the extensive practice of shifting cultivation at the Tuirial watershed even close to the dam site, no proper soil conservation, and high intensity of run-off occurs, which appear to be the major factors contributing to the increased siltation in the Tuirial dam.

# CHAPTER – 7

# MORPHOMETRY OF TUIRIAL WATERSHED

## 7.1 Introduction

Morphometry is quantitatively measuring the surface configuration of land (Clark, 1996). The morphometric study reveals the characteristics of the river catchment, hydrological and geomorphic processes, including the drainage system. Morphometry can be done for linear, relief and areal aspects of the drainage network. These morphometric parameters are associated with different physical and geomorphological aspects of a river basin that have significant impacts either by indirect or direct erosion, which is essential to identify soil loss-prone areas. Understanding the morphometric parameters are of significance for intensity of erosional activities at Tuirial watershed. In addition, it plays a significant role in studies of hydrologic modeling, prioritization of sub-watersheds, soil and water degradation management.

## 7.2 Linear aspects

The morphometric linear parameters provide general information of the geometrical correlation among the stream segments with topographical features and lithological disparities. The linear parameters such as stream order, stream number, stream length, stream length ratio and bifurcation ratio were performed for the detailed analysis of erosional intensity. Earlier the morphometric parameters were computed by conventional methods. The quantitative morphometry analysis was first performed by Horton (1932 and 1945), further, it was modified and simplified by Strahler (1952 and 1964). These newly added parameters are used to analyze the complex nature of landforms and lithological structure. In the present study the stream ordering was done by Horton's stream ranking (1932). The advantage of Horton's stream order over the other method is to extract the exact stream or river length; whereas in other methods the length of streams was distorted due to it has no particular origin. In this research, Tuirial watershed is divided in three

watersheds according to Mizoram Watershed Atlas such as upper, middle and lower. The computed morphometry parameters of the total watershed are presented in the table 7.1.

### 7.2.1 Stream order ($N_u$)

The stream ordering or ranking of the drainage segments is the first step in quantitative analysis of a drainage basin. It is the hierarchical relationship among various stream segments, their discharge and connectivity in a basin. In Tuirial drainage system identified eight stream orders. It was observed in this watershed that the stream segments up to 3rd order are non-perennial type. Moreover, the stream order higher than 4th orders are Perennial type. It is counted as a total of 7123 stream segments of which 5536 stream segments are 1st order, 1107 of 2nd stream order, 347 of 3rd stream order, 88 of 4th order, 22 of 5th order, 11 of 6th order, 3 of 7th order and 9 of 8th order in Upper Tuirial watershed.

Table 7.1 Number of streams in Upper Tuirial watershed.

| Sub-watershed Code | Stream Order | | | | | | | | Total |
|---|---|---|---|---|---|---|---|---|---|
| | 1st | 2nd | 3rd | 4th | 5th | 6th | 7th | 8th | |
| SW-1 | 259 | 67 | 22 | 7 | 1 | 1 | 1 | - | 358 |
| SW-2 | 232 | 67 | 22 | 5 | - | 1 | 1 | 1 | 329 |
| SW-3 | 412 | 93 | 35 | 4 | 1 | 1 | - | - | 546 |
| SW-4 | 433 | 88 | 27 | 10 | 3 | 1 | - | 1 | 563 |
| SW-5 | 620 | 96 | 35 | 9 | 3 | 1 | - | 1 | 765 |
| SW-6 | 520 | 102 | 40 | 9 | 2 | - | - | 1 | 674 |
| SW-7 | 545 | 86 | 42 | 9 | 2 | - | - | 1 | 685 |
| SW-8 | 498 | 91 | 29 | 5 | 2 | - | - | - | 625 |
| SW-9 | 430 | 77 | 21 | 6 | 3 | 2 | - | 1 | 540 |
| SW-10 | 555 | 109 | 21 | 8 | 2 | 3 | 1 | 1 | 700 |
| SW-11 | 492 | 100 | 19 | 10 | 2 | 1 | - | 1 | 625 |
| SW-12 | 540 | 131 | 34 | 6 | 1 | - | - | 1 | 713 |
| Total | 5536 | 1107 | 347 | 88 | 22 | 11 | 3 | 9 | 7123 |

The details sub-watersheds wise and their stream order along with number of streams were presented in table 7.1. The spatial distribution of Upper Tuirial watershed stream order is highlighted in figure 7.1. Consequently, the total watershed is counted as 7273 stream segment of which 5278 stream segments are 1st order, 1298 of 2nd stream order, 428 of 3rd stream order, 144 of 4th order, 49 of 5th order, 11 of 6th order, and 11 of 8th order in Middle Tuirial watershed. The details Middle Tuirial sub-watersheds wise and stream order along with their numbers of streams are presented in table 7.2. The spatial distribution of Middle Tuirial watershed stream order is highlighted in figure 7.2.

Table 7.2 Number of streams in Middle Tuirial watershed

| Sub-watershed Code | Stream Order | | | | | | | | Total |
|---|---|---|---|---|---|---|---|---|---|
| | 1st | 2nd | 3rd | 4th | 5th | 6th | 7th | 8th | |
| SW-1 | 332 | 99 | 21 | 4 | 2 | - | - | - | 458 |
| SW-2 | 190 | 52 | 25 | 3 | 2 | 4 | - | 1 | 277 |
| SW-3 | 528 | 125 | 51 | 12 | 3 | 1 | - | 1 | 721 |
| SW-4 | 231 | 58 | 27 | 8 | 1 | 2 | - | - | 327 |
| SW-5 | 291 | 66 | 25 | 18 | 2 | - | - | 1 | 403 |
| SW-6 | 472 | 116 | 44 | 17 | 6 | - | - | - | 655 |
| SW-7 | 223 | 54 | 22 | 4 | 5 | - | - | 1 | 309 |
| SW-8 | 371 | 102 | 37 | 15 | 3 | - | - | 1 | 529 |
| SW-9 | 399 | 90 | 40 | 14 | 7 | - | - | 1 | 551 |
| SW-10 | 520 | 128 | 50 | 14 | 3 | 2 | - | 1 | 718 |
| SW-11 | 273 | 53 | 29 | 14 | 4 | - | - | 1 | 374 |
| SW-12 | 671 | 150 | 48 | 8 | 2 | 2 | - | 1 | 882 |
| SW-13 | 293 | 79 | 18 | 6 | 3 | - | - | 1 | 400 |
| SW-14 | 484 | 126 | 45 | 7 | 6 | - | - | 1 | 669 |
| Total | 5278 | 1298 | 482 | 144 | 49 | 11 | - | 11 | 7273 |

Table 7.3 Number of streams in Lower Tuirial watershed

| Sub-watershed Code | Order-wise | | | | | | | | Total |
|---|---|---|---|---|---|---|---|---|---|
| | 1st | 2nd | 3rd | 4th | 5th | 6th | 7th | 8th | |
| SW-1 | 300 | 77 | 28 | 10 | 2 | 2 | - | 1 | 420 |
| SW-2 | 495 | 121 | 34 | 18 | 4 | 2 | 1 | 1 | 676 |
| SW-3 | 341 | 84 | 29 | 11 | 6 | 4 | - | 1 | 476 |
| SW-4 | 370 | 73 | 25 | 6 | - | 2 | - | 1 | 477 |
| Total | 1506 | 355 | 116 | 45 | 12 | 10 | 1 | 4 | 2049 |

Furthermore, the total Lower Tuirial watershed is counted as 2049 stream segments of which 1506 stream segments are 1st order, 355 of 2nd stream order, 116 of 3rd stream order, 45 of 4th order, 12 of 5th order, 10 of 6th order, 1 of 7th order and 4 of 8th order. The details Lower Tuirial sub-watersheds wise and their stream order along with number of streams are presented in table 7.3. The spatial distribution of Lower Tuirial watershed stream order is highlighted in figure 7.3. The study observed that the when stream order increases the number of streams are decreasing which is in line with Horton's law of stream order (Horton, 1945). The number of streams depends on the size of the basin and ruggedness of that area. In the Upper Tuirial watershed is identified as highly undulating terrain subsequent by middle Tuirial watershed, although it consists of 14 sub-watersheds which exhibits the size of the basin is bigger than Upper Tuirial watershed of 12 sub-watersheds. Lastly, Lower Tuirial watershed is characterized by low lying terrain with least stream number and smallest basin among the three watersheds of Tuirial.

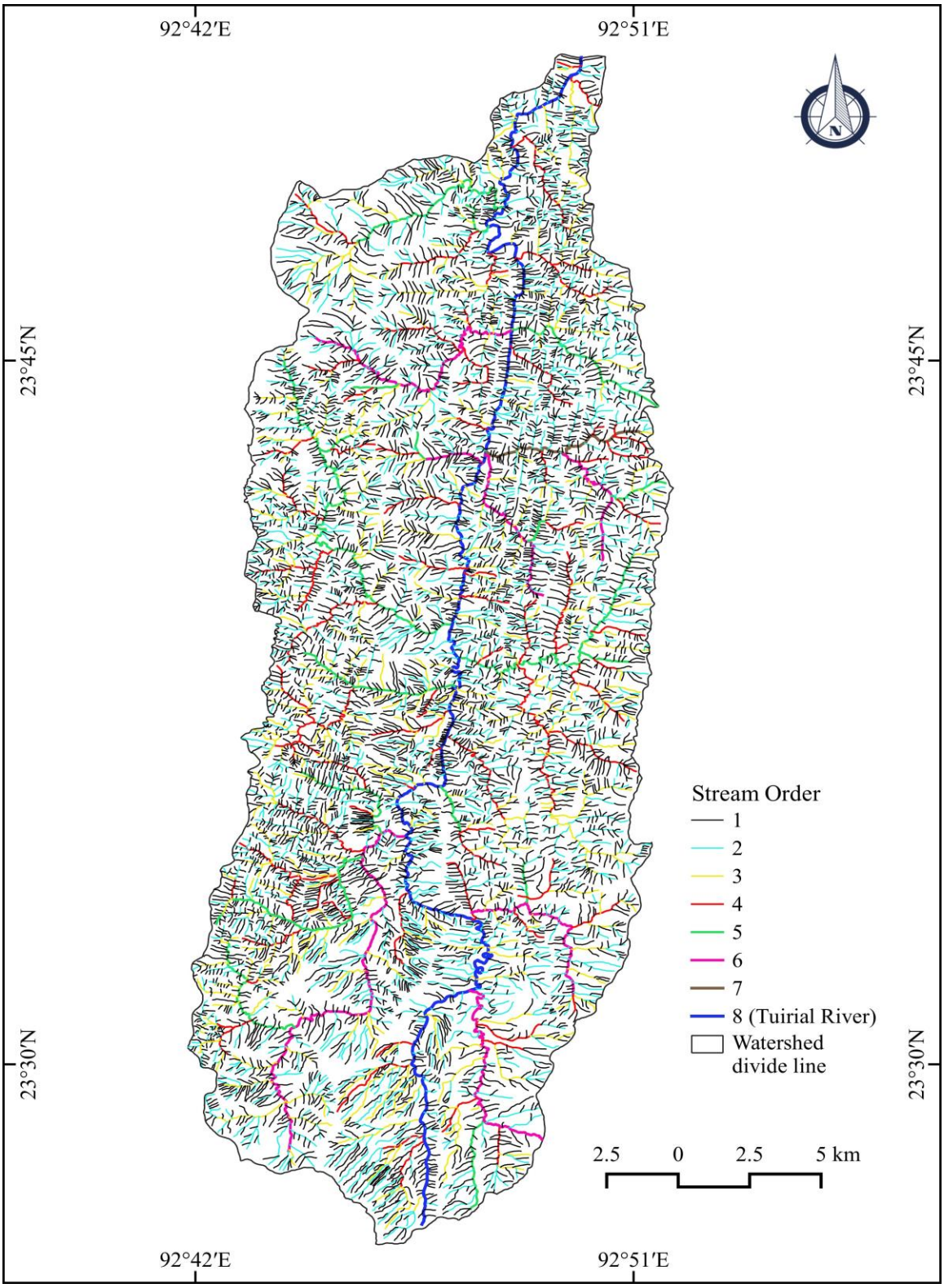


Figure 7.1: Stream-order in Upper Tuirial watershed.

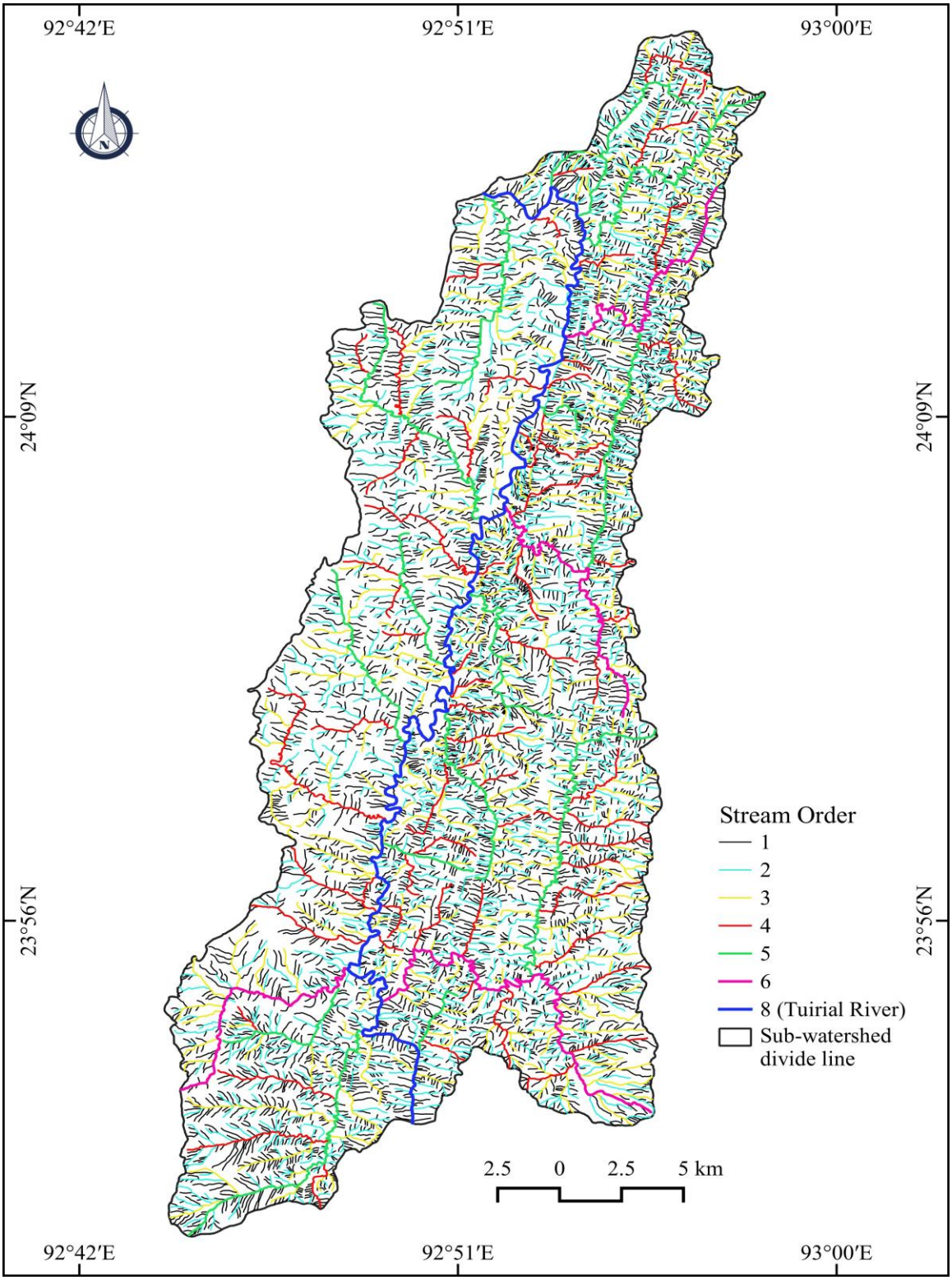


Figure 7.2 Stream-order in Middle Tuirial watershed

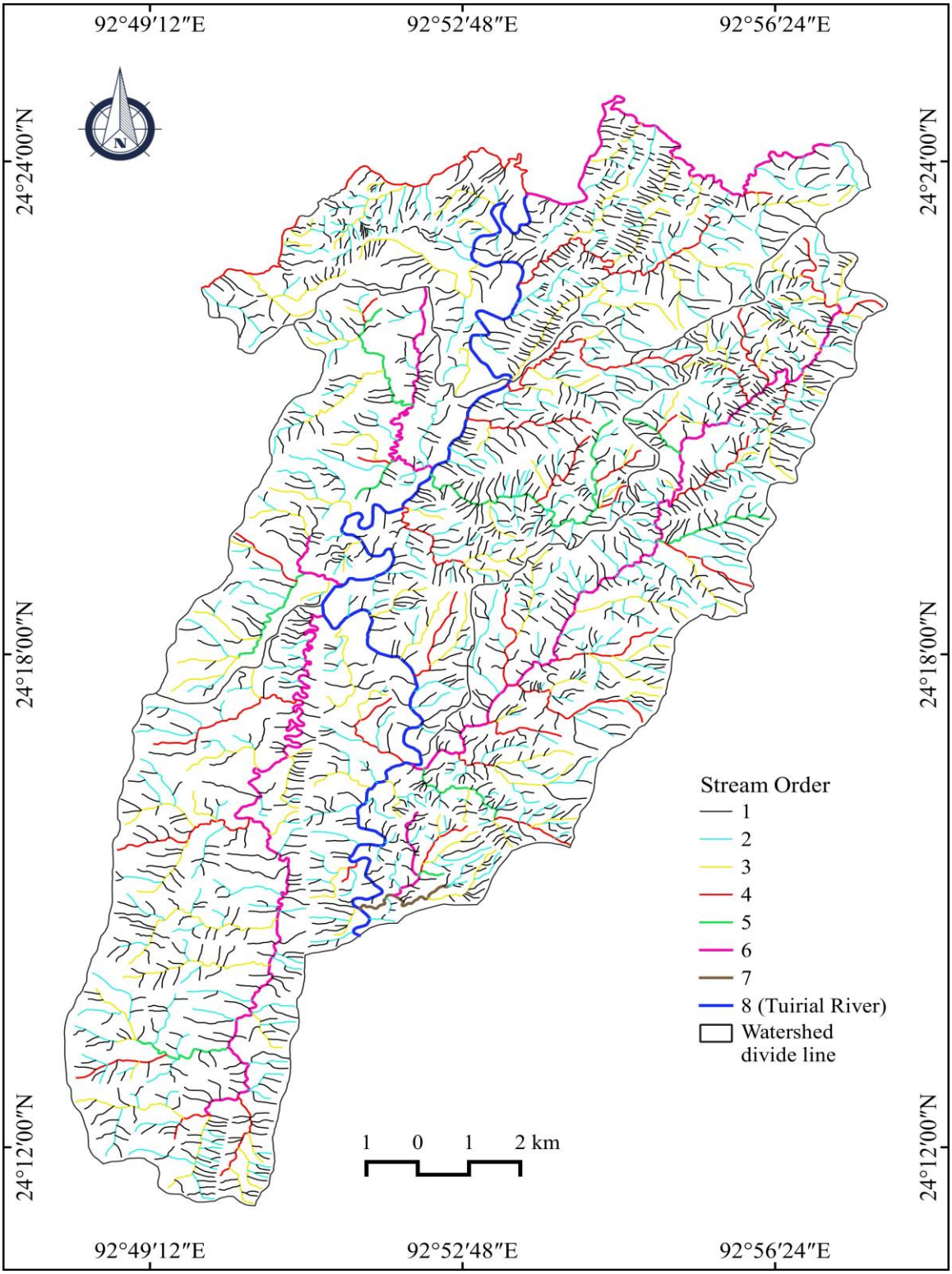


Figure 7.3: Stream-order in Lower Tuirial watershed

### 7.2.2 Stream Length ($L_u$)

Stream length is the total length of each stream order in a basin. In the present study the stream length was computed based on Horton (1945) law. The Horton's law of 'stream lengths' indicates that the mean length of stream segments of the consecutive orders in a basin tend to show a direct geometric relationship. Similarly, the stream length is one of the most critical parameter of morphometry for the understanding of surface run-off characteristics. The study finds out that the total length of first-order streams is 1660.90 km, second-order streams is 732.5 km, third-order streams is 369 km, fourth-order streams is 185.53 km, fifth-order streams is 93.11 km, sixth-order streams is 67.29 km, seventh order streams is 22.15 km and the eight order stream (Main River) is 75.76 km in Upper Tuirial watershed. The $L_u$ values of each sub-watershed and their stream order in Upper Tuirial watershed are given in table 7.4. Similarly, in the Middle Tuirial watershed the total length of first-order streams is 1687.75 km, second-order streams is 815.93 km, third-order streams is 477.28 km, fourth-order streams is 226.36 km, fifth-order streams is 176.17 km, sixth-order streams is 72.01 km, and the eight order stream (Main River) is 115.63 km. The $L_u$ values of each sub-watershed and their stream order in Middle Tuirial watershed are presented in table 7.5.

Furthermore, the Lower Tuirial watershed the total length of first-order streams is 467.08 km, second-order stream is 228.41 km, third-order stream is 136.95 km, fourth-order streams is 78.61 km, fifth-order streams is 23.38 km, sixth-order stream is 60.57 km, seventh-order stream is 2.44 km and eight order stream (Main River) is 44.93 km. The $L_u$ values of each sub-watershed and their stream order in Lower Tuirial watershed is given in table 7.6. The Horton's law states that the length of stream is the highest by first order stream segments. Also, stream order increases with declining stream segment length. Similarly, the study observed that as the stream order increases the stream length of sequential order decreases and this relation between stream order and stream length is called Horton's second law "law of stream lengths". In this study the stream length is classified into three categories such as high, medium and low. The high stream length specifies longer stream length which may be attributed as vulnerable to severe soil loss,

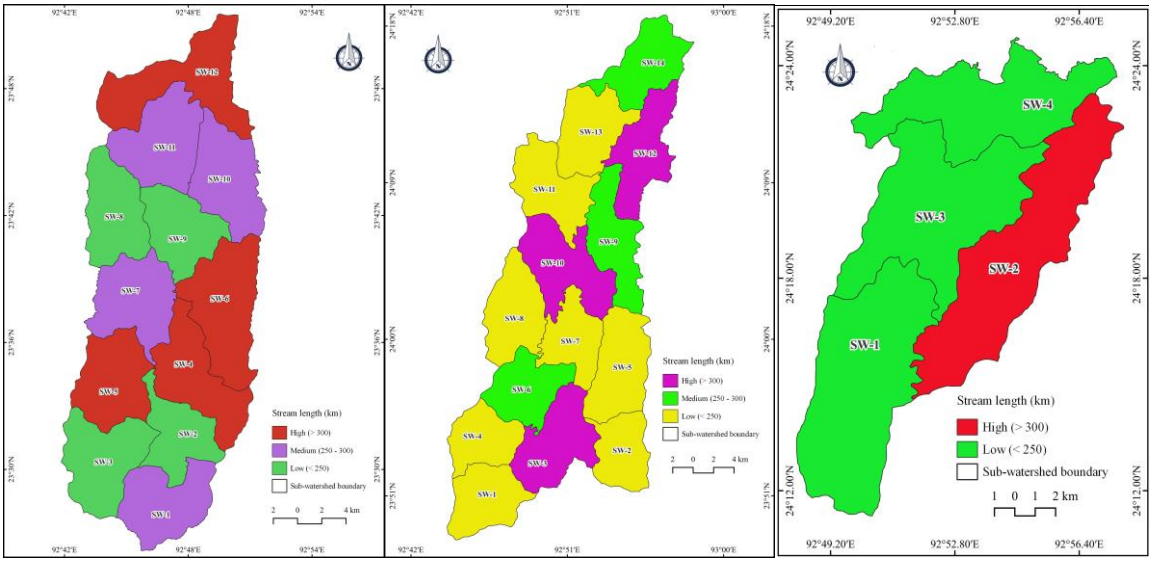


Figure 7.4: Stream length classification of the Tuirial watershed; (a) Upper Tuirial, (b) Middle Tuirial, (c) Lower Tuirial watershed

Table 7.4: Sub watershed-wise stream length ($L_u$) in Upper Tuirial watershed.

| Sub-watershed Code | Stream Order | | | | | | | | Total length (km) | Class |
|---|---|---|---|---|---|---|---|---|---|---|
| | 1st | 2nd | 3rd | 4th | 5th | 6th | 7th | 8th | | |
| SW-1 | 108.98 | 60.58 | 33.90 | 13.98 | 5.18 | 6.78 | 6.01 | - | 235.42 | M |
| SW-2 | 81.32 | 51.69 | 22.95 | 8.05 | - | 6.51 | 9.64 | 5.19 | 185.35 | L |
| SW-3 | 126.69 | 63.86 | 33.93 | 3.22 | 6.21 | 12.19 | - | - | 246.10 | L |
| SW-4 | 136.97 | 61.67 | 25.45 | 17.80 | 3.96 | 7.69 | - | 14.00 | 267.55 | H |
| SW-5 | 166.08 | 59.92 | 33.17 | 21.30 | 14.02 | 6.89 | - | 0.37 | 301.75 | H |
| SW-6 | 162.41 | 68.64 | 40.46 | 28.40 | 13.89 | - | - | 1.75 | 315.54 | H |
| SW-7 | 150.54 | 54.30 | 41.96 | 21.09 | 9.85 | - | - | 11.79 | 289.55 | M |
| SW-8 | 129.92 | 50.93 | 31.41 | 12.41 | 16.15 | - | - | - | 240.83 | L |
| SW-9 | 129.78 | 49.78 | 23.95 | 11.75 | 2.46 | 9.84 | - | 9.45 | 237.02 | L |
| SW-10 | 148.36 | 71.39 | 19.09 | 12.40 | 9.54 | 6.08 | 6.87 | 8.29 | 282.01 | M |
| SW-11 | 148.53 | 58.13 | 22.09 | 17.29 | 3.38 | 11.31 | - | 11.90 | 272.62 | M |
| SW-12 | 171.36 | 81.65 | 40.65 | 17.83 | 8.45 | - | - | 13.03 | 332.98 | H |
| Total | 1660.9 | 732.5 | 369.0 | 185.53 | 93.11 | 67.29 | 22.51 | 75.76 | 3206.71 | |

Table 7.5: Sub watershed-wise stream length ($L_u$) in Middle Tuirial watershed.

| Sub-watershed Code | Stream Order | | | | | | | | Total length (km) | Class |
|---|---|---|---|---|---|---|---|---|---|---|
| | 1st | 2nd | 3rd | 4th | 5th | 6th | 7th | 8th | | |
| SW-1 | 131.29 | 55.09 | 23.95 | 15.26 | 12.09 | - | - | - | 237.68 | L |
| SW-2 | 83.79 | 36.44 | 22.03 | 1.49 | 7.41 | 13.51 | - | 0.43 | 165.09 | L |
| SW-3 | 157.05 | 75.04 | 35.93 | 16.08 | 9.01 | 12.85 | - | 11.73 | 317.70 | H |
| SW-4 | 79.97 | 45.87 | 37.38 | 10.19 | 0.77 | 11.73 | - | - | 185.91 | L |
| SW-5 | 104.42 | 38.79 | 25.41 | 25.33 | 4.26 | - | - | 13.73 | 211.94 | L |
| SW-6 | 131.62 | 67.20 | 45.78 | 26.00 | 19.84 | - | - | - | 290.43 | M |
| SW-7 | 90.22 | 43.56 | 27.21 | 14.50 | 10.43 | - | - | 6.51 | 192.42 | L |
| SW-8 | 107.51 | 59.00 | 36.14 | 18.79 | 11.63 | - | - | 16.29 | 249.35 | L |
| SW-9 | 133.93 | 62.26 | 40.89 | 19.87 | 19.70 | - | - | 18.35 | 295.01 | M |
| SW-10 | 137.24 | 75.32 | 38.69 | 22.24 | 7.19 | 18.07 | - | 8.18 | 306.93 | H |
| SW-11 | 111.91 | 43.53 | 30.67 | 17.09 | 17.82 | - | - | 11.81 | 232.82 | L |
| SW-12 | 171.28 | 81.87 | 46.27 | 15.90 | 10.74 | 15.85 | - | 3.31 | 345.22 | H |
| SW-13 | 108.84 | 61.28 | 29.40 | 11.10 | 13.91 | - | - | 17.51 | 242.05 | L |
| SW-14 | 138.68 | 70.69 | 37.53 | 12.52 | 31.37 | - | - | 7.77 | 298.56 | M |
| Total | 1687.75 | 815.93 | 477.28 | 226.36 | 176.17 | 72.01 | - | 115.63 | 3571.13 | |

Table 7.6: Sub watershed-wise stream length ($L_u$) in Upper Tuirial watershed.

| Sub-watershed Code | Stream Order | | | | | | | | Total length (km) | Class |
|---|---|---|---|---|---|---|---|---|---|---|
| | 1st | 2nd | 3rd | 4th | 5th | 6th | 7th | 8th | | |
| SW-1 | 112 | 55 | 36 | 15 | 2 | 20 | - | 13 | 240 | L |
| SW-2 | 139.66 | 70.73 | 35.34 | 26.60 | 6.90 | 20.05 | 2.44 | 7.30 | 301.72 | H |
| SW-3 | 110.27 | 54.90 | 30.67 | 20.28 | 14.48 | 8.68 | - | 15.45 | 239.27 | L |
| SW-4 | 105.14 | 47.78 | 34.94 | 16.73 | - | 11.84 | - | 9.18 | 216.43 | L |
| Total | 467.08 | 228.41 | 136.95 | 78.61 | 23.38 | 60.57 | 2.44 | 44.93 | 997.4 | |

### 7.2.3 Mean stream length ($L_{sm}$)

The mean stream length is defined as the average stream length which is sum of the stream length ($L_u$) of all orders divided by the total number of stream orders ($N_u$). The mean stream length has significant relationship of drainage characteristics and its basin topographic surface (Strahler, 1964). The shorter mean stream length implies the region is characterized by steep slope along with less permeable rock. Whereas, the longer mean stream length indicates the region is governed by medium to gently sloping areas. In the case of Tuirial basin the gently sloping areas are utilized by agricultural activities which help the surface run-off loading huge amount of sediment resulting land degradation. However, the areas with steep slope have good cover management because of less anthropogenic interference. Even though, the steep slope has high surface run-off but in Tuirial basin eroded material is less due to thick forest cover. The mean stream length is 3.25 km, 2.97 km and 3.47 km in Upper, Middle and Lower Tuirial watersheds, respectively. The observed sub-watershed wise and order-wise mean stream lengths are presented in the Table 7.7, 7.8 and 7.9. The mean stream length of sub-watersheds ranges between 1.35 km and 4.46 km, which exhibit the basin is characterized by highly dissected (Yadav *et al*., 2020). The average stream length of first order streams are the shortest, which implies this first order stream occupied area are characterized by highly dissected. Similarly, it can be said that the increase of stream order reflects the average length of the streams also increases. The mean stream length of Upper Tuirial sub-watersheds ranges from 2.31 km to 4.43 km, the Middle Tuirial sub-watersheds also ranges between 1.35 km and 4.46 km, this can be attributed to some of the sub-watersheds in Middle Tuirial watershed are highly dissected than in the Upper Tuirial watershed. On the other hand, the average stream length ranges between 3.11 km and 4.98 km which indicates the lower Tuirial watershed is characterized by low relief and gently sloping than the Upper and Middle Tuirial watershed.

Table 7.7: Sub watershed-wise Mean stream length ($L_{sm}$) in Upper Tuirial watershed.

| Sub-watershed Code | Stream Order | | | | | | | | Mean Stream Length (Km) |
|---|---|---|---|---|---|---|---|---|---|
| | 1st | 2nd | 3rd | 4th | 5th | 6th | 7th | 8th | |
| SW-1 | 0.42 | 0.90 | 1.54 | 2.00 | 5.18 | 6.78 | 6.01 | - | 3.26 |
| SW-2 | 0.35 | 0.77 | 1.04 | 1.61 | - | 6.51 | 9.64 | 5.19 | 3.59 |
| SW-3 | 0.31 | 0.69 | 0.97 | 0.80 | 6.21 | 12.19 | - | - | 3.53 |
| SW-4 | 0.32 | 0.70 | 0.94 | 1.78 | 1.32 | 7.69 | - | 14.00 | 3.82 |
| SW-5 | 0.27 | 0.62 | 0.95 | 2.37 | 4.67 | 6.89 | - | 0.37 | 2.31 |
| SW-6 | 0.31 | 0.67 | 1.01 | 3.16 | 6.95 | - | - | 1.75 | 2.31 |
| SW-7 | 0.28 | 0.63 | 1.00 | 2.34 | 4.93 | - | - | 11.79 | 3.49 |
| SW-8 | 0.26 | 0.56 | 1.08 | 2.48 | 8.07 | - | - | - | 2.49 |
| SW-9 | 0.30 | 0.65 | 1.14 | 1.96 | 0.82 | 4.92 | - | 9.45 | 2.75 |
| SW-10 | 0.27 | 0.65 | 0.91 | 1.55 | 4.77 | 2.03 | 6.87 | 8.29 | 3.17 |
| SW-11 | 0.30 | 0.58 | 1.16 | 1.73 | 1.69 | 11.31 | - | 11.90 | 4.10 |
| SW-12 | 0.32 | 0.62 | 1.20 | 2.97 | 8.45 | - | - | 13.03 | 4.43 |

Table 7.8: Sub watershed-wise Mean stream length ($L_{sm}$) in Middle Tuirial watershed

| Sub-watershed Code | Stream Order | | | | | | | | Mean Stream Length (Km) |
|---|---|---|---|---|---|---|---|---|---|
| | 1st | 2nd | 3rd | 4th | 5th | 6th | 7th | 8th | |
| SW-1 | 0.40 | 0.56 | 1.14 | 3.82 | 6.05 | - | - | - | 2.39 |
| SW-2 | 0.44 | 0.70 | 0.88 | 0.50 | 3.71 | 3.38 | - | 0.43 | 1.43 |
| SW-3 | 0.30 | 0.60 | 0.70 | 1.34 | 3.00 | 12.85 | - | 11.73 | 4.36 |
| SW-4 | 0.35 | 0.79 | 1.38 | 1.27 | 0.77 | 5.87 | - | - | 1.74 |
| SW-5 | 0.36 | 0.59 | 1.02 | 1.41 | 2.13 | - | - | 13.73 | 3.21 |
| SW-6 | 0.28 | 0.58 | 1.04 | 1.53 | 3.31 | - | - | - | 1.35 |
| SW-7 | 0.40 | 0.81 | 1.24 | 3.62 | 2.09 | - | - | 6.51 | 2.44 |
| SW-8 | 0.29 | 0.58 | 0.98 | 1.25 | 3.88 | - | - | 16.29 | 3.88 |
| SW-9 | 0.34 | 0.69 | 1.02 | 1.42 | 2.81 | - | - | 18.35 | 4.11 |
| SW-10 | 0.26 | 0.59 | 0.77 | 1.59 | 2.40 | 9.03 | - | 8.18 | 3.26 |
| SW-11 | 0.41 | 0.82 | 1.06 | 1.22 | 4.45 | - | - | 11.81 | 3.29 |
| SW-12 | 0.26 | 0.55 | 0.96 | 1.99 | 5.37 | 7.92 | - | 3.31 | 2.91 |
| SW-13 | 0.37 | 0.78 | 1.63 | 1.85 | 4.64 | - | - | 17.51 | 4.46 |
| SW-14 | 0.29 | 0.56 | 0.83 | 1.79 | 5.23 | - | - | 7.77 | 2.74 |

Table 7.9: Sub watershed-wise Mean stream length ($L_{sm}$) in Lower Tuirial watershed

| Sub-watershed Code | Stream Order | | | | | | | | Mean Stream Length (Km) |
|---|---|---|---|---|---|---|---|---|---|
| | 1st | 2nd | 3rd | 4th | 5th | 6th | 7th | 8th | |
| SW-1 | 0.37 | 0.71 | 1.29 | 1.50 | 1.00 | 10.00 | - | 13.00 | 3.98 |
| SW-2 | 0.28 | 0.58 | 1.04 | 1.48 | 1.73 | 10.02 | 2.44 | 7.30 | 3.11 |
| SW-3 | 0.32 | 0.65 | 1.06 | 1.84 | 2.41 | 2.17 | - | 15.45 | 3.42 |
| SW-4 | 0.28 | 0.65 | 1.40 | 2.79 | - | 5.92 | - | 9.18 | 3.37 |

### 7.2.4 Stream Length Ratio ($S_{lr}$)

The stream length ratio is the proportion of average length ($L_u$) of streams in a given order (u) to the mean length of streams in the next lower order ($L_{u-1}$) (Horton, 1945) which tends to be continuous throughout the sequential orders in a basin. The stream length ratio reveals the significant of hydrological characteristics based on the variations of slope and topography of that area (Strahler, 1964). The highest value of mean stream length ratio 7.73 km was obtained from sw-3 at Upper Tuirial watershed, which represents 7.73 km of the 4th order stream equivalent to 1 km of the 5th order stream. Again, the lowest value of mean stream length is 0.38 km of the 5th order streams equal to 1 km of the 6th order streams. Similarly, in the Middle Tuirial watershed the stream length ratio is ranges from 0.56 km to 7.58 km. Table 7.7, 7.8 and 7.9 shows the spatial distribution of stream length ratio of Upper Tuirial, Middle Tuirial and Lower Tuirial sub-watersheds, respectively. Higher the stream length ratio exhibiting the slope of that area is gentle further consequence by mature geomorphic stage. On the contrary, the lower stream length ratio specifies the area of that basin is highly undulating topography in nature. Generally, when the stream length ratio is lowering the order of stream increases. Because, the stream segments are more in the lower order, than in the higher order. The observed values show that the variation of degree of stream order is based on the slope and corresponding topography of each stream order existence area.

Table 7.10: Sub watershed-wise Stream length ratio ($S_{lr}$) in Upper Tuirial watershed.

| Sub-watershed Code | Stream Order | | | | | | | Mean Stream Length (Km) |
|---|---|---|---|---|---|---|---|---|
| | 2/1 | 3/2 | 4/3 | 5/4 | 6/5 | 7/6 | 8/7 | |
| SW-1 | 2.15 | 1.70 | 1.30 | 2.60 | 1.31 | 0.89 | - | 1.66 |
| SW-2 | 2.20 | 1.35 | 1.54 | - | - | 1.48 | - | 1.42 |
| SW-3 | 2.23 | 1.41 | 0.83 | 7.73 | 1.96 | - | - | 2.83 |
| SW-4 | 2.22 | 1.35 | 1.89 | 0.74 | 5.82 | - | - | 2.40 |
| SW-5 | 2.33 | 1.52 | 2.50 | 1.98 | 1.47 | - | - | 1.96 |
| SW-6 | 2.15 | 1.50 | 3.12 | 2.20 | - | - | - | 2.24 |
| SW-7 | 2.29 | 1.58 | 2.35 | 2.10 | - | - | - | 2.08 |
| SW-8 | 2.15 | 1.94 | 2.29 | 3.25 | - | - | - | 2.41 |
| SW-9 | 2.14 | 1.76 | 1.72 | 0.42 | 6.01 | - | - | 2.41 |
| SW-10 | 2.45 | 1.39 | 1.70 | 3.08 | 0.42 | 3.39 | 1.21 | 1.95 |
| SW-11 | 1.93 | 2.00 | 1.49 | 0.98 | 6.69 | - | - | 2.62 |
| SW-12 | 1.96 | 1.92 | 2.49 | 2.85 | - | - | - | 2.30 |

Table 7.11: Sub watershed-wise Stream length ratio ($S_{lr}$)of Middle Tuirial watershed

| Sub-watershed Code | Stream Order | | | | | | | Mean Stream Length (Km) |
|---|---|---|---|---|---|---|---|---|
| | 2/1 | 3/2 | 4/3 | 5/4 | 6/5 | 7/6 | 8/7 | |
| SW-1 | 1.41 | 2.05 | 3.35 | 1.58 | - | - | - | 1.40 |
| SW-2 | 1.59 | 1.26 | 0.56 | 7.49 | 0.91 | - | - | 1.69 |
| SW-3 | 2.02 | 1.17 | 1.90 | 2.24 | 4.28 | - | - | 1.66 |
| SW-4 | 2.28 | 1.75 | 0.92 | 0.61 | 7.58 | - | - | 1.88 |
| SW-5 | 1.64 | 1.73 | 1.38 | 1.51 | - | - | - | 1.04 |
| SW-6 | 2.08 | 1.80 | 1.47 | 2.16 | - | - | - | 1.25 |
| SW-7 | 1.99 | 1.53 | 2.93 | 0.58 | - | - | - | 1.17 |
| SW-8 | 2.00 | 1.69 | 1.28 | 3.10 | - | - | - | 1.34 |
| SW-9 | 2.06 | 1.48 | 1.39 | 1.98 | - | - | - | 1.15 |
| SW-10 | 2.23 | 1.31 | 2.05 | 1.51 | 3.77 | - | - | 1.55 |
| SW-11 | 2.00 | 1.29 | 1.15 | 3.65 | - | - | - | 1.35 |
| SW-12 | 2.14 | 1.77 | 2.06 | 2.70 | 1.48 | - | - | 1.45 |
| SW-13 | 2.09 | 2.11 | 1.13 | 2.51 | - | - | - | 1.31 |
| SW-14 | 1.96 | 1.49 | 2.14 | 2.92 | - | - | - | 1.42 |

Table 7.12: Sub watershed-wise Stream length ratio ($S_{lr}$) in Lower Tuirial watershed

| Sub-watershed Code | Stream Order | | | | | | | Mean Stream Length (Km) |
|---|---|---|---|---|---|---|---|---|
| | 2/1 | 3/2 | 4/3 | 5/4 | 6/5 | 7/6 | 8/7 | |
| SW-1 | 1.91 | 1.80 | 1.17 | 0.67 | 10.00 | - | - | 3.41 |
| SW-2 | 2.07 | 1.78 | 1.42 | 1.17 | 5.81 | 0.24 | 2.99 | 2.24 |
| SW-3 | 2.02 | 1.62 | 1.74 | 1.31 | 0.90 | - | - | 1.39 |
| SW-4 | 2.30 | 2.14 | 1.99 | - | - | - | - | 2.07 |

### 7.2.5 Bifurcation Ratio ($R_b$)

The bifurcation ratio refers to the proportion of number of streams in a particular order to the next subsequent higher stream order in that drainage basin (Schumm, 1956). The bifurcation ratio is computed by dividing the total number of first order streams by the number of second order streams. Similarly, dividing the second order streams by the next higher order, and so on. Bifurcation ratio varies from region to region which reflects the drainage systems developed in uniform lithology tend to display geometrical similarity (Singh *et al*., 1984). The bifurcation ratio controls the drainage complexity and the degree of dissection in a basin. The bifurcation ratio values range between 3 and 5 indicate that the geological structure does not have dominant control and the values greater than 5 indicates that the area is structurally controlled (Strahler, 1957 and 1964). On the other hand, Nag, (1998) stated low values of bifurcation ratio specify decreased structural influence of that basin, while high bifurcation ratio suggests the basin is characterized by elongated shape. However, in this research the bifurcation ratio is classified into three low (<3), medium (3 – 4), and high (>4). The higher values of bifurcation ratios are found to be prone to more erosion because large number of first and second order streams, which accelerate stream flow and transportation energy. On contrary, the low bifurcation ratios are found in the higher order of streams and counted less stream number. The spatial distribution of sub-watershed wise bifurcation ratio is depicted in figure 7.5. The present study observed the Upper Tuirial watershed bifurcation ratio values range between 0.6 and 8.7 with having the mean bifurcation values of 3.29, while in the Middle Tuirial the

bifurcation ratio ranges between 0.5 and 8.3. Table 7.11, 7.12 and 7.13 indicates the bifurcation ratio is consistently greater in number of first order streams in all the sub-watersheds. The drainage development in the Tuirial watershed has been significantly controlled structurally due to tectonic activity, as evidenced by the high bifurcation ratio of 8.33 with a mean of 3.29. The obtained value against Strahler stated specified range of bifurcation ratio, indicating a significant structural mechanism throughout the area. Likewise, sub-basins with low bifurcation values are watersheds that have not been physically altered and do not exhibit any distortion of drainage pattern in that area (Nag, 1998; Thakur *et.al*., 2014). Furthermore, the weighted mean bifurcation ratios ($R_{bmw}$) of Tuirial basin range from 6.90 to 1.02 exhibits the watershed is attributed to variation of lithological, structure and relief.

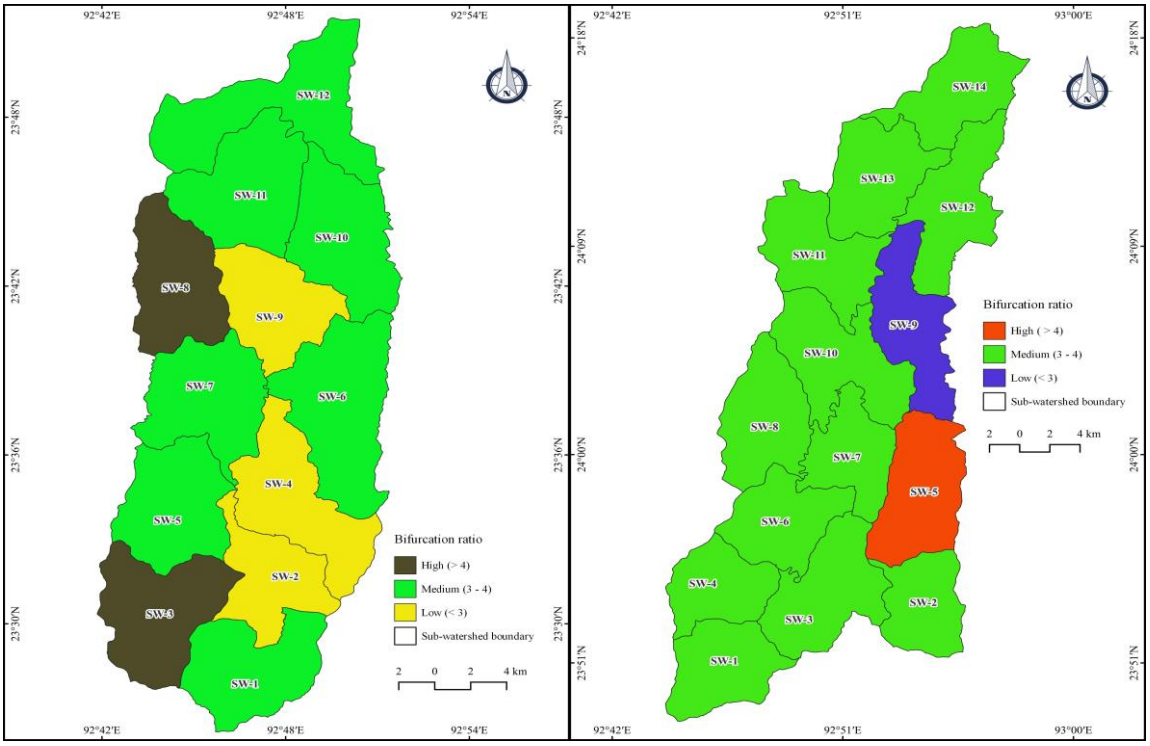


Figure 7.5 Bifurcation ratio in Tuirial watershed; (a). Upper Tuirial, (b). Middle Tuirial basin

Table 7.13: Sub watershed-wise Bifurcation ratio ($R_b$) in Upper Tuirial watershed

| Sub-watershed Code | Stream Order | | | | | | | Mean ($R_b$) | Class |
|---|---|---|---|---|---|---|---|---|---|
| | 1/2 | 2/3 | 3/4 | 4/5 | 5/6 | 6/7 | 7/8 | | |
| SW-1 | 3.87 | 3.05 | 3.14 | 7.00 | 1.00 | 1.00 | - | 3.18 | M |
| SW-2 | 3.46 | 3.05 | 4.40 | - | 0.00 | 1.00 | 1.00 | 2.15 | L |
| SW-3 | 4.43 | 2.66 | 8.75 | 4.00 | 1.00 | - | - | 4.17 | H |
| SW-4 | 4.92 | 3.26 | 2.70 | 3.33 | 3.00 | - | - | 2.87 | L |
| SW-5 | 6.46 | 2.74 | 3.89 | 3.00 | 3.00 | - | - | 3.18 | M |
| SW-6 | 5.10 | 2.55 | 4.44 | 4.50 | - | - | - | 3.32 | M |
| SW-7 | 6.34 | 2.05 | 4.67 | 4.50 | - | - | - | 3.51 | M |
| SW-8 | 5.47 | 3.14 | 5.80 | 2.50 | - | - | - | 4.23 | H |
| SW-9 | 5.58 | 3.67 | 3.50 | 2.00 | 1.50 | - | - | 2.71 | L |
| SW-10 | 5.09 | 5.19 | 2.63 | 4.00 | 0.67 | 3.00 | 1.00 | 3.08 | M |
| SW-11 | 4.92 | 5.26 | 1.90 | 5.00 | 2.00 | - | - | 3.18 | M |
| SW-12 | 4.12 | 3.85 | 5.67 | 6.00 | - | - | - | 3.93 | M |

Table 7.14: Sub watershed-wise Bifurcation ratio ($R_b$) in Middle Tuirial watershed

| Sub-watershed Code | Stream Order | | | | | | | Mean ($R_b$) | Class |
|---|---|---|---|---|---|---|---|---|---|
| | 1/2 | 2/3 | 3/4 | 4/5 | 5/6 | 6/7 | 7/8 | | |
| SW-1 | 3.35 | 4.71 | 5.25 | 2.00 | - | - | - | 3.06 | M |
| SW-2 | 3.65 | 2.08 | 8.33 | 1.50 | 0.50 | - | - | 2.30 | L |
| SW-3 | 4.22 | 2.45 | 4.25 | 4.00 | 3.00 | - | - | 2.56 | L |
| SW-4 | 3.98 | 2.15 | 3.38 | 8.00 | 0.50 | - | - | 2.57 | L |
| SW-5 | 4.41 | 2.64 | 1.39 | 9.00 | - | - | - | 2.91 | L |
| SW-6 | 4.07 | 2.64 | 2.59 | 2.83 | - | - | - | 2.02 | L |
| SW-7 | 4.13 | 2.45 | 5.50 | 0.80 | - | - | - | 2.15 | L |
| SW-8 | 3.64 | 2.76 | 2.47 | 5.00 | - | - | - | 2.31 | L |
| SW-9 | 4.43 | 2.25 | 2.86 | 2.00 | - | - | - | 1.92 | L |
| SW-10 | 4.06 | 2.56 | 3.57 | 4.67 | 1.50 | - | - | 2.34 | L |
| SW-11 | 5.15 | 1.83 | 2.07 | 3.50 | - | - | - | 2.09 | L |
| SW-12 | 4.47 | 3.13 | 6.00 | 4.00 | 1.00 | - | - | 2.66 | L |
| SW-13 | 3.71 | 4.39 | 3.00 | 2.00 | - | - | - | 2.18 | L |
| SW-14 | 3.84 | 2.80 | 6.43 | 1.17 | - | - | - | 2.37 | L |

Table 7.15: Sub watershed-wise Bifurcation ratio ($R_b$) in Lower Tuirial watershed

| Sub-watershed Code | Stream Order | | | | | | | Mean ($R_b$) | Class |
|---|---|---|---|---|---|---|---|---|---|
| | 1/2 | 2/3 | 3/4 | 4/5 | 5/6 | 6/7 | 7/8 | | |
| SW-1 | 3.90 | 2.75 | 2.80 | 5.00 | 1.00 | 1.00 | - | 2.35 | L |
| SW-2 | 4.09 | 3.56 | 1.89 | 4.50 | 2.00 | 2.00 | 1.00 | 2.72 | L |
| SW-3 | 4.06 | 2.90 | 2.64 | 1.83 | 1.50 | 1.50 | - | 2.06 | L |
| SW-4 | 5.07 | 2.92 | 4.17 | - | - | - | - | 2.03 | L |

### 7.2.6 Basin length ($L_b$)

The basin length is the straight line measured distance between the mouth and the source point of main river (Horton, 1932). Basin length is one of the critical parameters of linear features which uses various computed areal parameters. Depending on the basin length the areal parameters result may vary. Similarly, longer the basin length has the least chances of flash flood with scattered sediment deposition along the broader river bank. The longest sub-basin length in the Upper Tuirial watershed is observed in SW-4 with having 13.4 km. While 11.9 km of SW- and 13.9 km of SW-4 in Middle Tuirial and Lower Tuirial are the longest sub-basins, respectively. The observed sub-basin length of Upper, Middle and Lower, in Tuirial watershed is highlighted in tables 7.13, 7.14 and 7.15.

### 7.2.7 Basin perimeter (P)

The basin perimeter is defined as measurement of the circumference of the water divide line extent. The basin perimeter is useful for the exhibition of the shape and size of a river basin (Schumm, 1956). As the basin length, the basin parameter is also useful for various kinds of areal aspects calculation. Similarly, shorter basin parameter exhibits highly vulnerability of flash flood with huge volume of sediment transport down slope by surface run-off. The perimeter of Tuirial sub-watersheds ranges between 28.27 km and 53.20 km which show that the basin is elongated shape along with large volume of sediment deposition at broader river bank. The observed perimeter of sub-basins in upper, Middle and Lower is highlighted in tables 7.13, 7.14 and 7.15 respectively.

### 7.3 Areal aspects

The significant areal aspects such as basin area, basin length, basin perimeter, form factor, elongation ratio, circularity ratio, drainage intensity and compactness co-efficient are calculated in this research. The values obtained from various kinds of aerial parameters are highlighted in the table 7.13 (Upper), 7.14 (Middle) and 7.15(Lower).

Table 7.16. Areal features in Upper Tuirial watershed

| Sub-watersheds | Area (A) $km^2$ | Basin Length (km) | Perimeter (P) (km) | Form factor ($R_f$) | | Elongated Ratio ($R_e$) | | Drainage density ($D_d$) | | Constant channel ($C_c$) | Drainage Texture (T) |
|---|---|---|---|---|---|---|---|---|---|---|---|
| | | | | $Lb^2$ | $\frac{A}{Lb^2}$ | $\frac{1.128\sqrt{A}}{L}$ | $\frac{1.128\sqrt{A}}{L}$ | $\sum l_u$ | $\frac{\sum l_u}{A}$ | $\frac{1}{D_d}$ | $\frac{\sum l_u}{P}$ |
| SW-1 | 42.0 | 7.48 | 32.50 | 55.95 | 0.75 | 7.32 | 0.98 | 235.42 | 5.59 | 0.18 | 11.02 |
| SW-2 | 32.6 | 10.1 | 36.12 | 103.6 | 0.32 | 6.45 | 0.63 | 185.35 | 5.67 | 0.18 | 9.11 |
| SW-3 | 46.0 | 8.92 | 32.96 | 79.57 | 0.58 | 7.65 | 0.86 | 246.10 | 5.35 | 0.19 | 16.57 |
| SW-4 | 47.5 | 13.9 | 42.09 | 194.3 | 0.24 | 7.78 | 0.56 | 267.55 | 5.63 | 0.18 | 13.38 |
| SW-5 | 42.5 | 7.66 | 30.89 | 58.68 | 0.73 | 7.36 | 0.96 | 301.75 | 7.09 | 0.14 | 24.77 |
| SW-6 | 57.1 | 9.92 | 42.15 | 98.41 | 0.58 | 8.53 | 0.86 | 315.54 | 5.52 | 0.18 | 15.99 |
| SW-7 | 44.5 | 7.78 | 37.48 | 60.53 | 0.74 | 7.53 | 0.97 | 289.55 | 6.49 | 0.15 | 18.28 |
| SW-8 | 40.7 | 10.5 | 31.05 | 111.5 | 0.37 | 7.20 | 0.68 | 240.83 | 5.91 | 0.17 | 20.13 |
| SW-9 | 37.0 | 7.91 | 30.05 | 62.57 | 0.59 | 6.87 | 0.87 | 237.02 | 6.39 | 0.16 | 17.97 |
| SW-10 | 45.1 | 11.8 | 34.56 | 140.9 | 0.32 | 7.57 | 0.64 | 282.01 | 6.25 | 0.16 | 20.26 |
| SW-11 | 47.6 | 9.02 | 33.44 | 81.36 | 0.59 | 7.79 | 0.86 | 272.62 | 5.72 | 0.17 | 18.69 |
| SW-12 | 57.9 | 8.23 | 53.32 | 67.73 | 0.86 | 8.59 | 1.04 | 332.98 | 5.75 | 0.17 | 13.37 |

Continued… Table 7.16. Areal features in Upper Tuirial watershed

| Sub-water sheds | Area (A) $km^2$ | Perimeter (P) | Circularity ratio ($R_c$) | | | Drainage frequency ($D_f$) | |
|---|---|---|---|---|---|---|---|
| | | | $P^2$ | $4\pi A$ | $\frac{4\pi A}{P^2}$ | $N_u$ | $\frac{N_u}{A}$ |
| SW-1 | 42.09 | 32.5 | 1056.32 | 528.94 | 0.50 | 358 | 8.51 |
| SW-2 | 32.69 | 36.12 | 1304.65 | 410.85 | 0.31 | 329 | 10.06 |
| SW-3 | 46.00 | 32.96 | 1086.04 | 578.08 | 0.53 | 546 | 11.87 |
| SW-4 | 47.52 | 42.09 | 1771.29 | 597.18 | 0.34 | 563 | 11.85 |
| SW-5 | 42.56 | 30.89 | 954.17 | 534.80 | 0.56 | 765 | 17.98 |
| SW-6 | 57.16 | 42.15 | 1776.52 | 718.33 | 0.40 | 674 | 11.79 |
| SW-7 | 44.58 | 37.48 | 1404.81 | 560.24 | 0.40 | 685 | 15.36 |
| SW-8 | 40.74 | 31.05 | 964.38 | 511.94 | 0.53 | 625 | 15.34 |
| SW-9 | 37.09 | 30.05 | 903.19 | 466.05 | 0.52 | 540 | 14.56 |
| SW-10 | 45.10 | 34.56 | 1194.08 | 566.69 | 0.47 | 700 | 15.52 |
| SW-11 | 47.67 | 33.44 | 1118.52 | 599.06 | 0.54 | 625 | 13.11 |
| SW-12 | 57.95 | 53.32 | 2843.15 | 728.21 | 0.26 | 713 | 12.30 |

Table 7.17. Areal features in Middle Tuirial watershed

| Sub-watersheds | Area (A) $km^2$ | Basin Length (km) | Perimeter (P) (km) | Form factor ($R_f$) | | Elongated Ratio ($R_e$) | | Drainage density ($D_d$) | | Constant channel ($C_c$) | Drainage Texture (T) |
|---|---|---|---|---|---|---|---|---|---|---|---|
| | | | | $Lb^2$ | $\frac{A}{Lb^2}$ | $\frac{1.128}{\sqrt{A}}$ | $\frac{1.128\sqrt{A}}{L}$ | $\sum l_u$ | $\frac{\sum l_u}{A}$ | $\frac{1}{D_d}$ | $\frac{\sum l_u}{P}$ |
| SW-1 | 44.4 | 8.7 | 30.0 | 76.2 | 0.5 | 7.5 | 0.86 | 237.6 | 5.35 | 0.23 | 15.23 |
| SW-2 | 38.1 | 8.1 | 28.2 | 66.1 | 0.5 | 6.9 | 0.86 | 165.0 | 4.33 | 0.18 | 9.82 |
| SW-3 | 56.4 | 6.9 | 41.7 | 48.0 | 1.1 | 8.4 | 1.22 | 317.7 | 5.63 | 0.20 | 17.29 |
| SW-4 | 37.9 | 8.7 | 29.5 | 77.1 | 0.4 | 6.9 | 0.79 | 185.9 | 4.90 | 0.21 | 11.05 |
| SW-5 | 44.9 | 11.9 | 35.3 | 142.5 | 0.3 | 7.5 | 0.63 | 211.9 | 4.72 | 0.19 | 11.40 |
| SW-6 | 56.1 | 7.2 | 35.0 | 52.7 | 1.0 | 8.4 | 1.16 | 290.4 | 5.17 | 0.27 | 18.67 |

| | | | | | | | | | | | |
|---|---|---|---|---|---|---|---|---|---|---|---|
| SW-7 | 51.5 | 7.8 | 36.7 | 61.4 | 0.8 | 8.1 | 1.03 | 192.4 | 3.73 | 0.16 | 8.41 |
| SW-8 | 40.0 | 11.7 | 40.1 | 138.4 | 0.2 | 7.1 | 0.61 | 249.3 | 6.23 | 0.20 | 13.17 |
| SW-9 | 59.9 | 10.7 | 53.2 | 116.0 | 0.5 | 8.7 | 0.81 | 295.0 | 4.92 | 0.16 | 10.34 |
| SW-10 | 49.7 | 10.4 | 47.2 | 109.3 | 0.4 | 7.9 | 0.76 | 306.9 | 6.18 | 0.22 | 15.20 |
| SW-11 | 51.8 | 8.4 | 42.5 | 71.9 | 0.7 | 8.1 | 0.96 | 232.8 | 4.49 | 0.15 | 8.79 |
| SW-12 | 51.9 | 9.6 | 46.8 | 92.5 | 0.5 | 8.1 | 0.85 | 345.2 | 6.64 | 0.21 | 18.85 |
| SW-13 | 51.1 | 9.3 | 36.0 | 86.4 | 0.5 | 8.0 | 0.87 | 242.0 | 4.74 | 0.16 | 11.09 |
| SW-14 | 48.9 | 9.7 | 39.9 | 94.9 | 0.5 | 7.8 | 0.81 | 298.5 | 6.10 | 0.19 | 16.75 |

Continued… Table 7.17: Areal features in Middle Tuirial watershed

| Sub-watersheds | Area (A) $km^2$ | Perimeter (P) | Circularity ratio ($R_c$) | | | Drainage frequency ($D_f$) | |
|---|---|---|---|---|---|---|---|
| | | | $P^2$ | $4\pi A$ | $\frac{4\pi A}{P^2}$ | $N_u$ | $\frac{N_u}{A}$ |
| SW-1 | 44.42 | 30.08 | 904.81 | 558.20 | 0.62 | 458 | 10.31 |
| SW-2 | 38.16 | 28.21 | 795.80 | 479.53 | 0.60 | 277 | 7.25 |
| SW-3 | 56.42 | 41.71 | 1739.72 | 708.99 | 0.41 | 721 | 12.77 |
| SW-4 | 37.97 | 29.58 | 874.98 | 477.15 | 0.55 | 327 | 8.61 |
| SW-5 | 44.95 | 35.36 | 1250.33 | 564.86 | 0.45 | 403 | 8.96 |
| SW-6 | 56.13 | 35.08 | 1230.61 | 705.35 | 0.57 | 655 | 11.66 |
| SW-7 | 51.53 | 36.73 | 1349.09 | 647.55 | 0.48 | 309 | 5.99 |
| SW-8 | 40.01 | 40.16 | 1612.83 | 502.78 | 0.31 | 529 | 13.22 |
| SW-9 | 59.92 | 53.28 | 2838.76 | 752.98 | 0.27 | 551 | 9.19 |
| SW-10 | 49.7 | 47.25 | 2232.56 | 624.55 | 0.28 | 718 | 14.44 |
| SW-11 | 51.87 | 42.56 | 1811.35 | 651.82 | 0.36 | 374 | 7.21 |
| SW-12 | 51.97 | 46.8 | 2190.24 | 653.07 | 0.30 | 882 | 16.97 |
| SW-13 | 51.1 | 36.08 | 1301.77 | 642.14 | 0.49 | 400 | 7.82 |
| SW-14 | 48.95 | 39.95 | 1596.00 | 615.12 | 0.39 | 669 | 13.66 |

### 7.3.1 Basin area (A)

The basin area refers to the total area projected on horizontal plane, which trap overland flow to the channel segments. According to Horton's (1945) Law of stream areas show a geometric relationship between the areas drained by streams of a given order. Basin size helps to estimate the amount of water reaching the main river. The basin size is useful to predict the potential of flooding. The shape of a basin is controlled by the stage of its development. The general shape of a basin appears in its early stage of development and it becomes elongated as the basin is developed. The areal extent of various sub-basins in the Tuirial watershed is presented in the table 7.13 (Upper), 7.14 (Middle) and 7.15 (Lower). It has been observed that the areal extent of all sub-basins range from 32.69 $km^2$ to 59.92 $km^2$.

### 7.3.2 Form factor ($F_f$)

The form factor denotes the proportion of basin area to the square of basin length (Horton, 1932). It is a dimensionless property which shows the shape of a basin useful to predict the overall flow direction (Nag, 1988). The value of form factor ranges between 0 and 1. Where, the value '0' indicates an elongated shape with longer duration of surface run-off. On the other hand, the value 1 exhibits circular shape with high peak flows which leads to flash flood and sediment transportation (Schumm, 1956). The form factor values of Tuirial sub-basins is categorized into three classes such as low (<0.45), medium (0.45 – 0.75) and high (>0.75). Sub-basins such as sw-1, sw-5, sw-7 and sw-12 show high form factor out of 12 sub-basins in Upper Tuirial basin (Fig 7.6a). Similarly, sw-3, sw-6 and sw-7 exhibit high form factor values in Middle Tuirial basin (Fig 7.6b) and sw-4 in Lower Tuirial basin (Fig 7.6c). The above mentioned sub-basins are expected to contribute more erosion based on the shape and circularity of the basin.

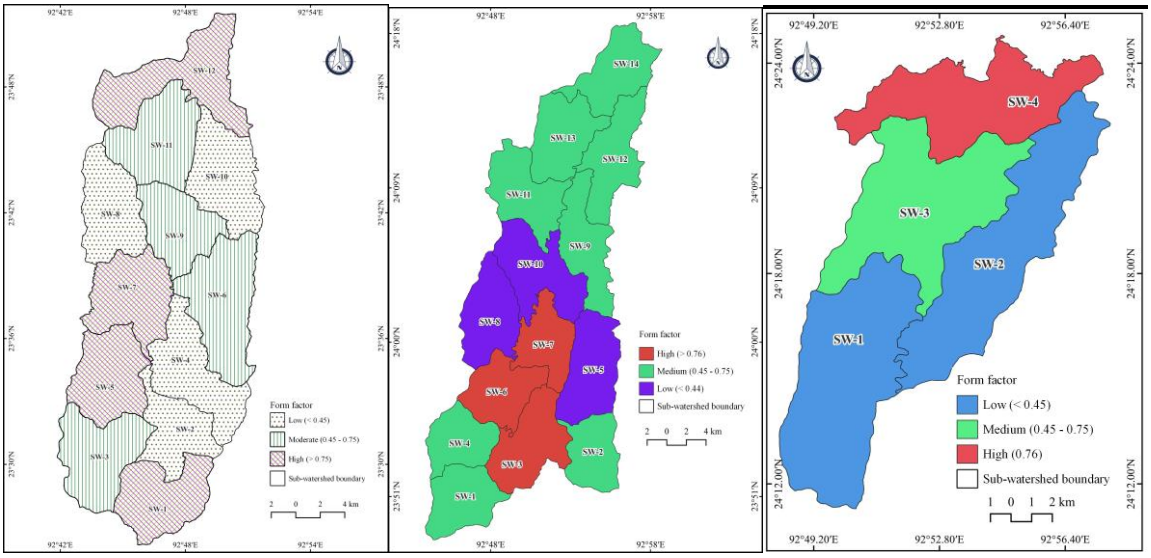


Figure 7. 6: Form factor in Tuirial watershed; (a). Upper, (b). Middle and (c). Lower

### 7.3.3 Circularity Ratio ($R_c$)

The circularity ratio is defined as the proportion of basin area to the area of circle having same outline as the basin (Miller, 1953). The circularity ratio ranges between 0 and 1 with lower and upper limit, respectively. Where higher the circularity implies close to 1, on the other hand, the value nearby zero indicates low circularity ratio. The present study observed that the circularity ratio of Tuirial sub-basins ranges between 0.24 and 0.62, which indicate most of the basins are in elongated to medium circular shape. The general existing research highlighted if the values range between 0.6 and 0.7 signifies the areas are characterized by homogeneous lithology, consequently the values between 0.40 and 0.50 indicate existence of quartzite rocks (Miller, 1953). However, the lithology of Tuirial basin is more or less uniform with sandstones and silt-stones/shales. In this research circularity ratio is classified into three; low (0.24 - 0.39), medium (0.4 – 0.49) and high (> 0.5). The sub-watersheds which have high circularity ratios more than 5 are found only in Middle Tuirial watershed such as sw-1, sw-2, sw-4 and sw-6 which exhibit these sub-basins are expected to produce huge flash flood and more sediment transport towards down surface than other sub-basins. The sub-watershed wise obtained values of circularity ratio and their

classes are presented in table 7.13 (Upper), table 7.14 (Middle), table 7.15 (Lower) and figure 7.7.

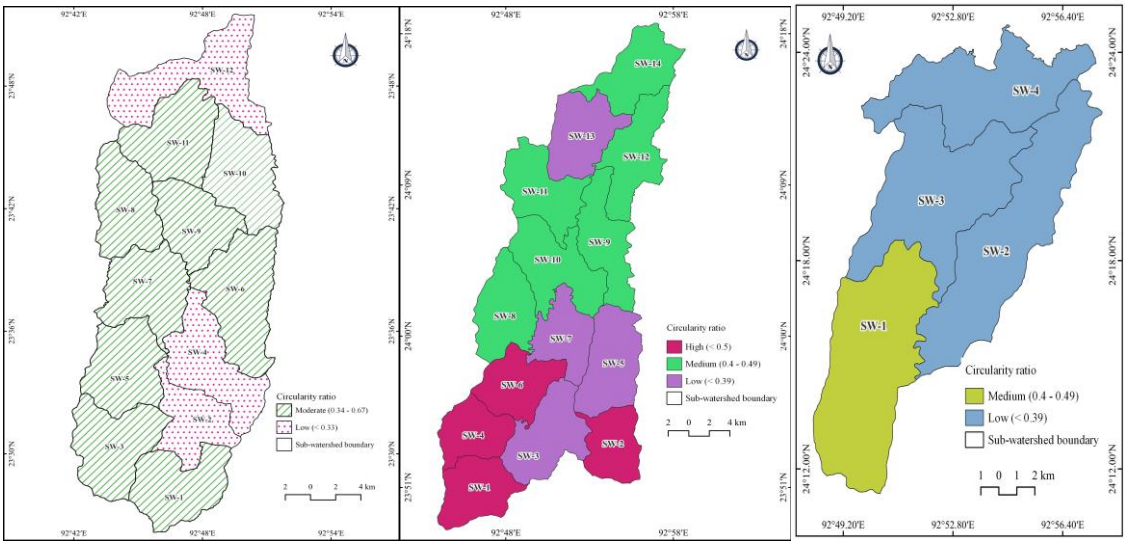


Figure 7.7: Circularity ratio in Tuirial watershed; (a) Upper, (b) Middle and (c) Lower

Table 7.18: Areal features of Lower Tuirial watershed

| Sub-water sheds | (A) Area km$^2$ | Basin Length (Lb) (km) | Basin Perimeter (P) (km) | Form factor ($R_f$) | | Elongated ratio ($R_e$) | | Drainage density ($D_d$) | | Constant channel Maintenance ($C_c$) | Drainage Texture (T) |
|---|---|---|---|---|---|---|---|---|---|---|---|
| | | | | $Lb^2$ | $\frac{A}{Lb^2}$ | $1.128\sqrt{A}$ | $\frac{1.128\sqrt{A}}{L}$ | $\sum l_u$ | $\frac{\sum l_u}{A}$ | $\frac{1}{D_d}$ | $\frac{\sum p}{P}$ |
| SW-1 | 55.00 | 13.51 | 39.81 | 182.52 | 0.30 | 8.37 | 0.62 | 253 | 4.60 | 0.22 | 10.55 |
| SW-2 | 51.62 | 17.62 | 49.27 | 310.46 | 0.17 | 8.10 | 0.46 | 309.02 | 5.99 | 0.17 | 13.72 |
| SW-3 | 49.52 | 9.16 | 46.22 | 83.91 | 0.59 | 7.94 | 0.87 | 254.73 | 5.14 | 0.19 | 10.29 |
| SW-4 | 38.62 | 3.86 | 45.35 | 14.90 | 2.59 | 7.01 | 1.82 | 225.62 | 5.84 | 0.17 | 10.51 |

Continued… Table 7.18: Areal features in Lower Tuirial watershed

| Sub-watersheds | Area (A) ($km^2$) | Perimeter (P) | Circularity ratio ($R_c$) | | | Drainage frequency ($D_f$) | |
|---|---|---|---|---|---|---|---|
| | | | $P^2$ | $4\pi A$ | $\frac{4\pi A}{P^2}$ | $N_u$ | $\frac{N_u}{A}$ |
| SW-1 | 55.00 | 39.81 | 1584.75 | 691.15 | 0.44 | 420 | 7.64 |
| SW-2 | 51.62 | 49.27 | 2427.59 | 648.61 | 0.27 | 676 | 13.10 |
| SW-3 | 49.52 | 46.22 | 2136.45 | 622.27 | 0.29 | 476 | 9.61 |
| SW-4 | 38.62 | 45.35 | 2056.99 | 485.31 | 0.24 | 477 | 12.35 |

### 7.3.4 Elongation Ratio ($R_e$)

The elongated ratio is defined as the proportion of the diameter of a circle having the same area of the basin and maximum length of basin (Schumm, 1956). Elongated ratio is the significant measurement of the shape of drainage basin for the prediction of the rate of water discharge. The circular basins likely to have flash flood whereas, elongated basin shape has longer time spend to discharge. The value of elongated ratio is valuable for the prediction of flood during the monsoon season. Generally, elongated ratio values range between 0.60 and 1. The elongated ratio of basins which range between 0.60 and 0.80 typically characterize the areas with high relief. On the other hand, the values close to 1 are the areas with circular shapes and low relief. The elongation ratio values from the previous studies are further clustered into circular basins (>0.9), oval shaped basins (0.8-0.9) and elongated (0.7) (Strahler, 1964). High elongated ratios specify the controlling consequence of thrusting and faulting in a basin (Strahler, 1964). However, in the present study, elongated ratio is classified into three classes based on obtained values such as low elongation (>0.9), medium elongation (0.79 – 0.89) and highly elongation (<0.71). Sub-watersheds such as sw-2, sw-4, sw-8 and sw-10 have highly elongated basins in the Upper Tuirial watershed. Similarly, sub-basins such as sw-5 and sw-8 are having highly elongated basins in the Middle Tuirial watershed. Furthermore, sub-watersheds sw-1, sw-2 and sw-4 are characterized by highly elongated basins in the Lower Tuirial watershed. The above mentioned sub-basins are expected to contribute low erosion and less sediment transport

than the other sub-basins which are characterized by circular and oval shaped basins due to long duration of transportation of sediment. The results of computed elongated ratio of Tuirial sub-basins are presented in the Table 7.13 (Upper), 7.14 (Middle) and 7.15 (Lower). As a whole the Tuirial river basin with the elongated ratio value 0.34 designates highly elongated nature with high relief and steep slopes.

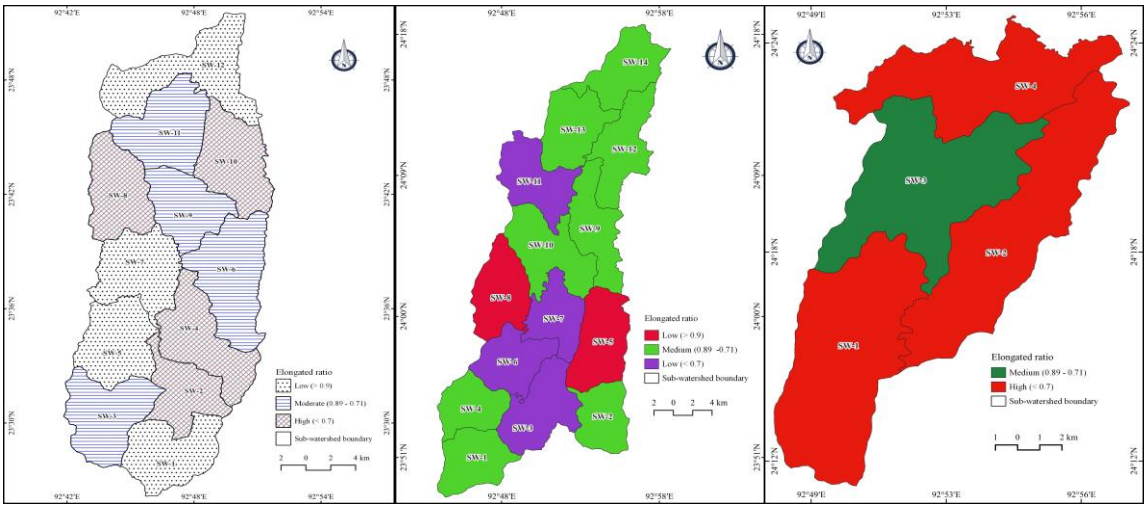


Figure 7.8: Elongated ratio in Tuirial watershed; (a) Upper, (b) Middle and (c) Lower

### 7.3.5 Drainage frequency ($D_f$)

According to Horton (1932) the stream frequency is the proportion of total number of stream segments in each order to the area of particular sub-basin (Horton, 1945). The stream frequency is expressed as numbers of stream segments present per square kilometre of that area. Higher the stream segments more vulnerable to soil erosion. In this research Tuirial watershed drainage frequency is classified into three classes based on the obtained Df values such as low (<10), medium (10 – 15) and high (>15). The Tuirial basin has high stream frequency with an average value of 5.56 stream segments per square kilometer of that area. However, sub-basins such as sw-5, sw-7, sw-8 and sw-10 are having more than 15 streams per $km^2$ in the Upper Tuirial watershed. However, sw-12 is the only sub-basin having more than 15 streams per $km^2$ in the Middle Tuirial watershed, while in Lower Tuirial watershed no sub-basin has high stream frequency due to presence of low and gently sloping land than the Upper and Middle Tuirial watersheds. The above mentioned

sub-basins show high stream frequency which are characterized by undulating terrain, dissected and neo-tectonic activity controlling the drainage pattern of those basins. The observed value of various stream frequency at different sub-basins are highlighted in table 7.13 (Upper), 7.14 (Middle) and 7.15 (Lower). Similarly, the sub-basin wise drainage frequency is illustrated in figure 7.9.

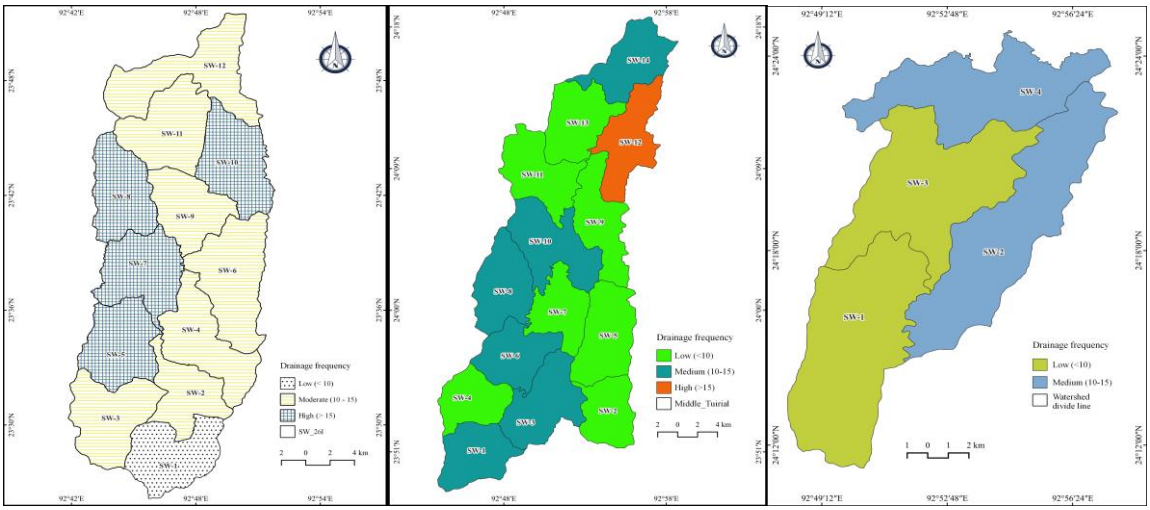


Figure 7.9: Drainage frequency in Tuirial watershed; (a) Upper, (b) Middle and (c) Lower

### 7.3.6 Drainage Texture ($D_t$)

The drainage texture ($D_t$) is defined as the proportion of the number stream segments of all orders within the basin to the perimeter of the basin. The drainage texture varies from region to region depending on the topography of the basin. The drainage texture ($D_t$) from 0 to 4 specifies the texture is coarse, consequently, the $D_t$ values between 4.0 and 10.0 indicate the texture is intermediate the $D_t$ values from 10 to 15 signifies the texture is fine and the $D_t$ values above 15.0 implies the texture is ultrafine (bad land topography) (Smith, 1950; Doornkamp and King, 1971). Drainage texture is the measurement for closeness of spacing of channels which mainly depends on climate, geology, rainfall, soils, vegetation, rate of infiltration, relief and the stage of geomorphic development of a basin area. In the present study Tuirial watershed drainage texture is classified into three classes based on their texture such as intermediate, fine and ultra-fine texture. The sub-basins in the Upper Tuirial watershed like sw-1, sw-4 and sw-12 are characterized by fine texture,

sw-2 is considered as intermediate texture, while sw-3, sw-5, sw-6, sw-7, sw-8, sw-9, sw-10 and sw-11 are regarded as ultra-fine texture which indicates susceptible to erosion (Fig 7.10b). Consequently, sw-1, sw-3, sw-6, sw-10, sw-12 and sw-14 are considered as ultra-fine texture in the Middle Tuirial watershed (Fig 7.10b). Basically, the sub-basins characterized by ultra-fine texture are decreasing toward the lower watershed. The obtained drainage texture of various sub-basins in Tuirial watershed is highlighted in table 7.13 of Upper Tuirial watershed, table 7.14 Middle Tuirial watershed and table 7.15 Lower Tuirial watershed.

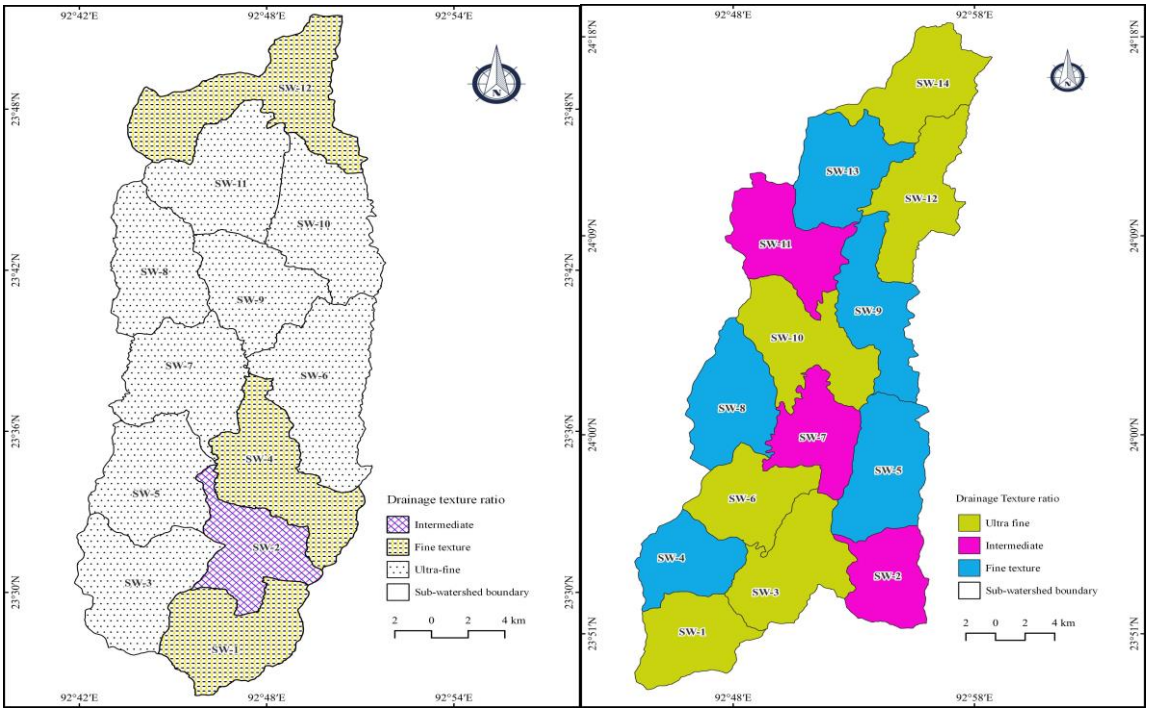


Figure 7.10: Drainage texture in Tuirial watershed; (a) Upper, (b) Middle

### 7.3.7 Drainage density ($D_d$)

Drainage density is defined as the proportion of total length of all stream orders to the area of that basin (Horton, 1945). Drainage density is controlled by the regional climate, vegetation, topography, the formation of rock and the tectonic activity (Nag, 1998). The basin with low drainage density is characterized by low relief, thick vegetation, hard resistant –permeable rock and coarse drainage texture. On the other hand, the basin with

mountainous terrain indicate highly active tectonic activity, fragile loose soil structure and fine drainage texture (Nag, 1998; Strahler, 1964). The obtained drainage density from various sub-basin is illustrated in table 7.13 of Upper Tuirial watershed, table 7.14 of middle Tuirial watershed and table 7.15 of Lower Tuirial watershed. The average Tuirial basin drainage density is 5.25 km/km$^2$ which specify the region is controlled by highly terrain with severe tectonic disturbed area. The study reveals that the all the sub-basin of Upper Tuirial watershed is characterized by high-drainage density, succeeding by middle Tuirial (Fig 7.11a), further it is declining towards the low land in lower Tuirial watershed (Fig 7.11b). This implies higher drainage density and expected to generate more soil erosion and sediment transport towards the low land. The pioneering studies by Strahler (1964) stated the basin with high drainage density is characterized with scarce vegetation cover. However, the present study areas witnesses the region with thick vegetation which is against Strahler's statement which implies drainage density is highly influenced by time and regional climatic differentiation. In the present research the drainage density reveals that it is characterized by permeable soils, soft sedimentary rocks such as sandstones, siltstones and shales of Bhuban formations with narrow valleys, dense vegetation cover and high relief.

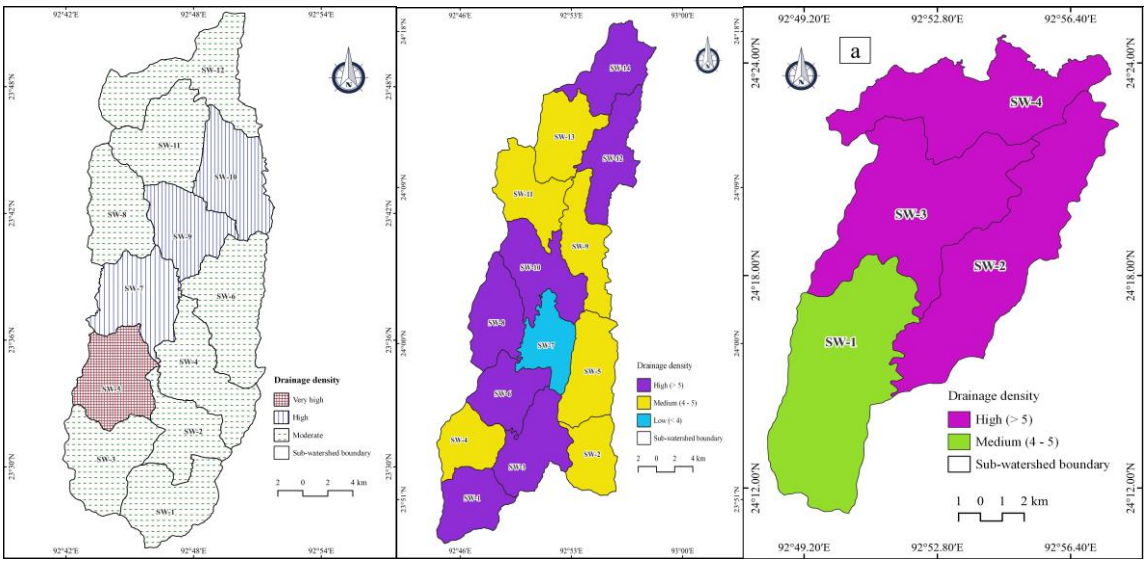


Figure 7.11: Drainage density in Tuirial watershed; (a) Upper, (b) Middle and (c) Lower

### 7.3.8 Constant of channel maintenance (Cc)

Constant of channel maintenance refers to the area of river basin needed to maintain per unit length of stream channel and Cc is the reciprocal of drainage density (Schumm, 1956). The significant of this Cc is to provide a minimum area requirement for the development of length of channel to prevent further deterioration of that area. In the present study, the values of constant of channel maintenance range from 0.17 to 0.77 which implies that 0.17 km/km$^2$ is required to maintain further erosion by surface run-off. The obtained constant channel maintenance is divided into three classes such as extremely require (ER) maintenance (<0.15 km/km$^2$), highly required (HR) maintenance (0.15 – 0.20 km/km$^2$) and moderately required (MR) maintenance (>0.20 km/km$^2$). In the Upper Tuirial watershed, the 20% sub-basins are ER and 80 are attributed as HR. Similarly, in the Middle Tuirial watershed it has been identified 8%, 42% and 50% of sub-basins attributed as ER, HR and MR, respectively. Furthermore, 25% and 75 of Lower Tuirial sub-basins are considered as MR and HR, respectively. Overall, in Tuirial watershed 10%, 64% and 26% of sub-basins are ER, HR and MR maintenance respectively. The study reveals that the area of Cc value specifies, Tuirial basin is controlled by structures, local lithology and humid tropical climate.

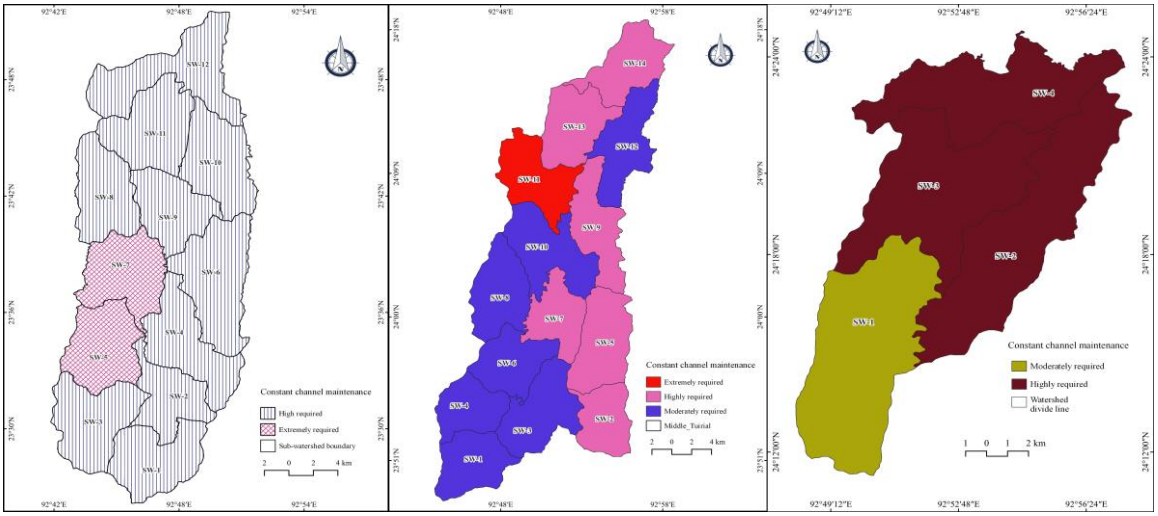


Figure 7. 12: Constant channel maintenance in Tuirial watershed; (a) Upper, (b) Middle, (c) Lower

### 7.3.9 Length of overland flow ($L_o$)

It is the independent parameter which affects the hydrologic and physiographic development of drainage basins (Schumm, 1956). It is a reciprocal relationship to the average slope of the channel and synonymous with length of sheet flow to a large extent. The length of overland flow is defined by the length of flow path, projected to horizontal, non-channel flow from point on the drainage divide to a point on the adjacent stream channel. This refers to the length of run of rainwater on the ground surface before it is localized into definite channels (Horton, 1945). The obtained values of length of overland flow in Tuirial watershed in Upper Tuirial watershed is 0.08, slightly higher in Middle Tuirial watershed with the $L_o$ value of 0.1, and higher in Lower Tuirial watershed of 0.19. Generally, it can be said that $L_o$ increases toward the lower course of stream. In the Upper course of Tuirial river basin the length of overflow land is about 0.08 km, which specifies the surface run-off flow path is short with less infiltration but expected to be high rate of erosion due to high relief and steep slope. The obtained land overflow land values are presented in table 7.13 of Upper Tuirial watershed, table 7.14 of middle Tuirial watershed and table 7.15 of Lower Tuirial watershed.

## 7.4 Relief aspects

The relief aspects involve the height related measurements in a watershed indicate that the potential energy of a drainage system, intensity or rate of erosion and transmissibility of rock debris (Madhuri, *et al*., 2012). The relief and the steepness of the terrain have the obvious effect on the rate of surface run-off, infiltration into the sub-surface and channel flow. The values of computed relief aspects such as basin elevation, basin relief, relief ratio, relative relief, ruggedness number and dissection of sub-watershed wises of Tuirial watershed are highlighted in tables 7.16, 7.17 and 7.18 respectively.

Table 7.19: Relief features in Upper Tuirial watershed

| Sub-watersheds | Area (A) $Km^2$ | Basin length (Km) (Lb) | Basin elevation | | Basin relief (R) | | Relief Ratio ($R_r$) | Relative Relief ($R_{ph}$) | Dissection Index ($D_i$) |
|---|---|---|---|---|---|---|---|---|---|
| | | | Highest Elevation (H) | Lowest Elevation (h) | $R = H - h$ (m) | R/1000 (km) | $\frac{R}{Lb}$ | $\frac{R}{A}$ | $\frac{R_{hp}}{R_r}$ |
| SW-1 | 42.09 | 7.48 | 1559 | 280 | 1279 | 1.28 | 0.17 | 0.030 | 0.18 |
| SW-2 | 32.69 | 10.2 | 1321 | 209.47 | 1111.53 | 1.11 | 0.11 | 0.034 | 0.31 |
| SW-3 | 46.00 | 8.92 | 1445 | 354.08 | 1090.92 | 1.09 | 0.12 | 0.024 | 0.19 |
| SW-4 | 47.52 | 13.9 | 1353 | 196.08 | 1156.92 | 1.16 | 0.08 | 0.024 | 0.29 |
| SW-5 | 42.56 | 7.66 | 1093 | 208.94 | 884.06 | 0.88 | 0.12 | 0.021 | 0.18 |
| SW-6 | 57.16 | 9.92 | 1224 | 193.97 | 1030.03 | 1.03 | 0.10 | 0.018 | 0.17 |
| SW-7 | 44.58 | 7.78 | 906 | 192.03 | 713.97 | 0.71 | 0.09 | 0.016 | 0.17 |
| SW-8 | 40.74 | 10.6 | 1161 | 221.51 | 939.49 | 0.94 | 0.09 | 0.023 | 0.26 |
| SW-9 | 37.09 | 7.91 | 1067 | 179.52 | 887.48 | 0.89 | 0.11 | 0.024 | 0.21 |
| SW-10 | 45.10 | 11.9 | 924 | 165.35 | 758.65 | 0.76 | 0.06 | 0.017 | 0.26 |
| SW-11 | 47.67 | 9.02 | 1335 | 161.9 | 1173.1 | 1.17 | 0.13 | 0.025 | 0.19 |
| SW-12 | 57.95 | 8.23 | 1295 | 147.79 | 1147.21 | 1.15 | 0.14 | 0.020 | 0.14 |

Continued…Table 7.19: Relief features in Upper Tuirial watershed

| Sub-watersheds | Gradient ratio ($G_r$) | | | | | Ruggedness number ($R_n$) | | |
|---|---|---|---|---|---|---|---|---|
| | Elevation of the source of river (a) | Elevation of the mouth of river (b) | $a-b$ | Longest river length (L) | $\frac{a-b}{L}$ | $D_d$ | R | $\frac{R \times D_d}{1000}$ |
| SW-1 | 1073 | 291 | 782 | 6 | 130.13 | 5.59 | 1279 | 7.15 |
| SW-2 | 387 | 209.51 | 177.49 | 5.2 | 34.19 | 5.67 | 1111.53 | 6.30 |
| SW-3 | 1076 | 437 | 639 | 12 | 52.41 | 5.35 | 1090.92 | 5.84 |
| SW-4 | 221 | 196.41 | 24.59 | 14 | 1.76 | 5.63 | 1156.92 | 6.51 |
| SW-5 | 811 | 209.35 | 601.65 | 6.9 | 87.36 | 7.09 | 884.06 | 6.27 |
| SW-6 | 1032.02 | 195.07 | 836.95 | 14 | 60.24 | 5.52 | 1030.03 | 5.69 |
| SW-7 | 208.92 | 192.16 | 16.76 | 12 | 1.42 | 6.49 | 713.97 | 4.64 |
| SW-8 | 1012 | 221.73 | 790.27 | 16 | 48.94 | 5.91 | 939.49 | 5.55 |
| SW-9 | 194.02 | 179.65 | 14.37 | 9.5 | 1.52 | 6.39 | 887.48 | 5.67 |
| SW-10 | 179.42 | 165.37 | 14.05 | 8.3 | 1.70 | 6.25 | 758.65 | 4.74 |
| SW-11 | 179.4 | 162.2 | 17.2 | 12 | 1.45 | 5.72 | 1173.1 | 6.71 |
| SW-12 | 164.83 | 148.05 | 16.78 | 13 | 1.29 | 5.75 | 1147.21 | 6.59 |

Table 7.20: Relief features in Middle Tuirial watershed

| Sub-watersheds | Area (A) $km^2$ | Basin elevation | | Basin relief (R) | | Relief Ratio ($R_r$) | Relative Relief ($R_{ph}$) | Dissection Index ($D_i$) |
|---|---|---|---|---|---|---|---|---|
| | | Highest Elevation (H) | Lowest Elevation (h) | $R = H - h$ (m) | R/1000 (km) | $\frac{R}{Lb}$ | $\frac{R}{A}$ | $\frac{R_{hp}}{R_r}$ |
| SW-1 | 44.42 | 1474 | 144.747 | 1329 | 0.14 | 0.15 | 0.03 | 0.20 |
| SW-2 | 38.16 | 1474 | 133.998 | 1340 | 0.13 | 0.16 | 0.04 | 0.21 |
| SW-3 | 56.42 | 913 | 133.895 | 779 | 0.13 | 0.11 | 0.01 | 0.12 |
| SW-4 | 37.97 | 1728 | 208.052 | 1520 | 0.21 | 0.17 | 0.04 | 0.23 |
| SW-5 | 44.95 | 1230 | 120.611 | 1109 | 0.12 | 0.09 | 0.02 | 0.27 |
| SW-6 | 56.13 | 1449 | 221.844 | 1227 | 0.22 | 0.17 | 0.02 | 0.13 |
| SW-7 | 51.53 | 1096 | 113.589 | 982 | 0.11 | 0.13 | 0.02 | 0.15 |
| SW-8 | 40.01 | 1123 | 105.773 | 1017 | 0.11 | 0.09 | 0.03 | 0.29 |
| SW-9 | 59.92 | 1200 | 92.952 | 1107 | 0.09 | 0.10 | 0.02 | 0.18 |
| SW-10 | 49.7 | 1175 | 80.446 | 1095 | 0.08 | 0.10 | 0.02 | 0.21 |
| SW-11 | 51.87 | 738 | 81.9 | 656 | 0.08 | 0.08 | 0.01 | 0.16 |
| SW-12 | 51.97 | 839 | 76.081 | 763 | 0.08 | 0.08 | 0.01 | 0.19 |
| SW-13 | 51.1 | 656 | 59.894 | 596 | 0.06 | 0.06 | 0.01 | 0.18 |
| SW-14 | 48.95 | 1039 | 59.309 | 980 | 0.06 | 0.10 | 0.02 | 0.20 |

Continued…Table 7.20: Relief features in Middle Tuirial watershed

| Sub-watersheds | Gradient ratio (Gr) | | | | | Ruggness number | | |
|---|---|---|---|---|---|---|---|---|
| | Longest river length (L) | Elevation of the source of river (a) | Elevation of the mouth of river (b) | $a-b$ | $\frac{a-b}{L}$ | R | $D_d$ | $\frac{R \times D_d}{1000}$ |
| SW-1 | 12.09 | 1127.00 | 145.05 | 981.95 | 81.21 | 1329.25 | 5.35 | 7.11 |
| SW-2 | 13.51 | 834.00 | 134.25 | 699.75 | 51.81 | 1340.00 | 4.33 | 5.80 |
| SW-3 | 11.73 | 147.84 | 136.32 | 11.53 | 0.98 | 779.11 | 5.63 | 4.39 |
| SW-4 | 11.73 | 980.00 | 212.00 | 768.00 | 65.46 | 1519.95 | 4.90 | 7.44 |
| SW-5 | 13.73 | 136.33 | 120.88 | 15.45 | 1.13 | 1109.39 | 4.72 | 5.23 |
| SW-6 | 19.84 | 655.03 | 229.00 | 426.03 | 21.48 | 1227.16 | 5.17 | 6.35 |
| SW-7 | 6.51 | 120.86 | 113.78 | 7.08 | 1.09 | 982.41 | 3.73 | 3.67 |
| SW-8 | 16.29 | 113.78 | 107.01 | 6.77 | 0.42 | 1017.23 | 6.23 | 6.34 |
| SW-9 | 18.35 | 106.98 | 92.95 | 14.03 | 0.76 | 1107.05 | 4.92 | 5.45 |
| SW-10 | 8.18 | 92.94 | 80.71 | 12.24 | 1.50 | 1094.55 | 6.18 | 6.76 |
| SW-11 | 11.81 | 98.30 | 81.88 | 16.42 | 1.39 | 656.10 | 4.49 | 2.94 |
| SW-12 | 3.31 | 80.71 | 76.47 | 4.24 | 1.28 | 762.92 | 6.64 | 5.07 |
| SW-13 | 17.51 | 81.89 | 59.88 | 22.01 | 1.26 | 596.11 | 4.74 | 2.82 |
| SW-14 | 7.77 | 68.56 | 59.88 | 8.68 | 1.12 | 979.69 | 6.10 | 5.98 |

Table 7.21: Relief features in Lower Tuirial watershed

| Sub-watershed | Elevation of the basin | | Basin relief (R) (H-h) | | Relief ratio ($R_r$) | Relative relief ($R_{hp}$) | Dissection index ($D_i$) |
|---|---|---|---|---|---|---|---|
| | Highest elevation (H) | Lowest elevation (h) | $R = H - h$ (m) | R/1000 (km) | $\frac{R}{Lb}$ | $\frac{R}{A}$ | $\frac{R_{hp}}{R_r}$ |
| SW-1 | 728 | 44.21 | 683.79 | 0.68 | 0.05 | 0.012 | 0.25 |
| SW-2 | 798 | 52.04 | 745.96 | 0.75 | 0.04 | 0.014 | 0.34 |
| SW-3 | 699 | 32.93 | 666.07 | 0.67 | 0.07 | 0.013 | 0.18 |
| SW-4 | 725 | 20.95 | 704.05 | 0.70 | 0.18 | 0.018 | 0.10 |

Continued…. Table 7.21: Relief features in Lower Tuirial watershed

| Sub-watershed | Gradient ratio ($G_r$) | | | | | Ruggness number ($R_n$) | | |
|---|---|---|---|---|---|---|---|---|
| | Longest basin length (L) | Elevation of the source of river (a) | Elevation of the mouth of river (b) | $a-b$ | $\frac{a-b}{L}$ | $D_d$ | R | $\frac{R \times DD}{1000}$ |
| SW-1 | 13.51 | 59.58 | 52.15 | 7.43 | 0.55 | 4.60 | 0.68 | 3.15 |
| SW-2 | 17.99 | 59.58 | 52.04 | 7.54 | 0.42 | 5.99 | 0.75 | 4.47 |
| SW-3 | 13.06 | 51.8 | 34.1 | 17.7 | 1.36 | 5.14 | 0.67 | 3.43 |
| SW-4 | 13.31 | 33.2 | 24.9 | 8.3 | 0.62 | 5.84 | 0.70 | 4.11 |

### 7.4.1 Basin relief (R)

Relief of a basin is quantitative measurement the variation between the highest (H) point and the lowest (h) point in a given watershed. Relief of the basin provides certain clues to understand the characteristics of the slope. In general, the high relief exhibits vulnerability to soil loss is high and inverse with low relief. In the present study, it was observed the maximum and minimum elevation in the Tuirial basin is 1559 metres and 20.95 metres, respectively. Thus, the basin is highly susceptible to soil loss. In the Upper Tuirial watershed average relief is 1014.36 metres, and it is 1035.77 metres in Middle Tuirial watershed, then declining its relief towards the lower Tuirial with having the average relief is 700 metres. As a whole, the Middle Tuirial watershed average relief is higher than Upper Tuirial watershed, this indicates the size of the basin controls the average basin relief. The basin relief is divided into three classes such as low (<800m), medium (800 – 1000m) and high (>1000m). As indicated in Figure 7.13 the river source area and the sub-basin whichever touches the water divide line on both west and east sides are attributed to higher relief, while it is low in the valley. The basin relief of Upper Tuirial watershed is presented in tables 7.16, 7.17 and 7.18 respectively.

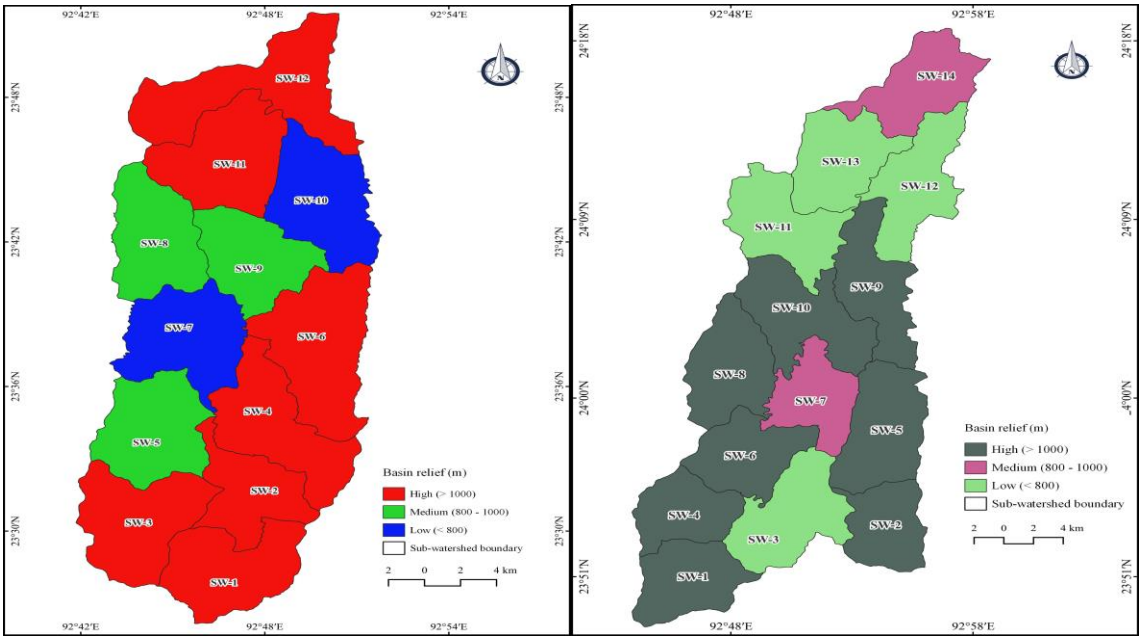


Figure 7.13: Basin relief in Tuirial watershed; (a) Upper (b) Middle

### 7.4.2 Relief ratio ($R_r$)

Relief ratio is the proportion of the elevation difference between the highest and lowest points in a basin to the length of the basin (Schumm, 1956). In other words, relief ratio is expressed as the basin relief per the length of the basin. The relief ratio indicates the overall steepness of the basin; thus it reflects the intensity of erosional processes on the basin slope. In general, the high basin relief ratio exhibits the small basin with high degree of the basin slope and it is reverse with the low relief ratio. The computed relief ratio values of various sub–basins range from 0.06 to 0.17. Figure 7.14a indicates the sub-basins 1, 11 and 12 exhibit high relief ratios with high degree of slope and expected to be susceptible to more soil loss than medium and low relief ratios. Similarly, in the middle Tuirial watershed, the sub-basins such as 1, 2, 4, 6 and 14 show high relief ratio (Fig 7.14b), and only one sub-basin 4 shows high relief ratio (Fig 7.14c). The areas which show low values of relief ratio are characterized by the less resistant rocks in the area like sandstones whereas the areas covered by siltstones and shales coverage show high relief ratio values (Sudheer, 1986 and Sreedevi, 1999).

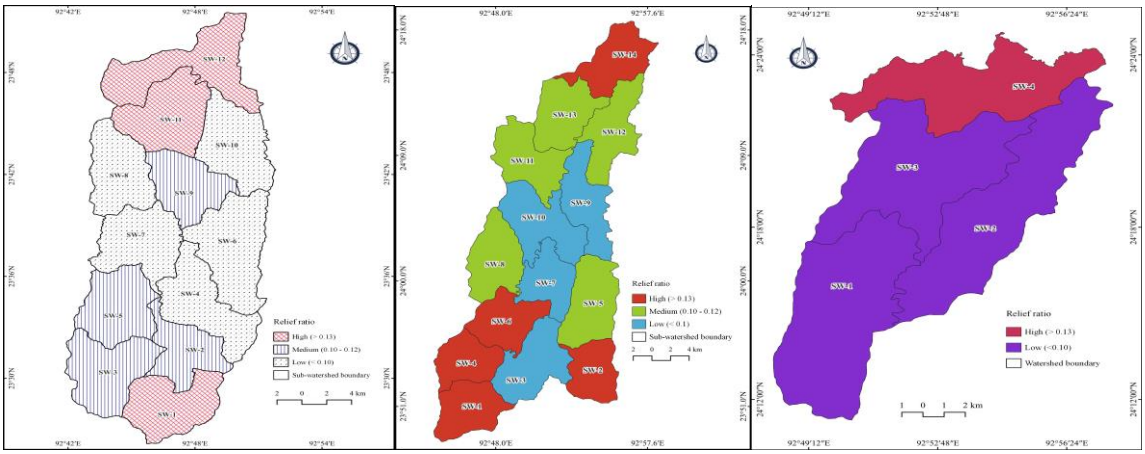


Figure 7.14: Relief ratio in Tuirial watershed; (a). Upper, (b) Middle, (c) Lower

### 7.4.3 Relative relief

Relative relief is defined as the proportion between the basins relief (R) to the basin area of the watershed (Horton, 1945). The low relative relief specifies the gentle slope of the basin. On the other hand, the high relative relief implies the basin is characterized with rugged and steeper slopes. In the present study, the observed relative relief of the Tuirial watershed is 0.027 which exhibits the basin is mature topography. The relative relief of Tuirial watershed is divided into three classes such as low (<0.019), medium (0.02 – 0.024) and high (>0.025). Sub-watershed wise of relative relief is presented in figure (7.15). The average relative relief ratio is 0.023, 0.022 and 0.014 in Upper, Middle and Lower Tuirial watersheds, which indicates the relative ratio decreases from Upper to Lower watershed.

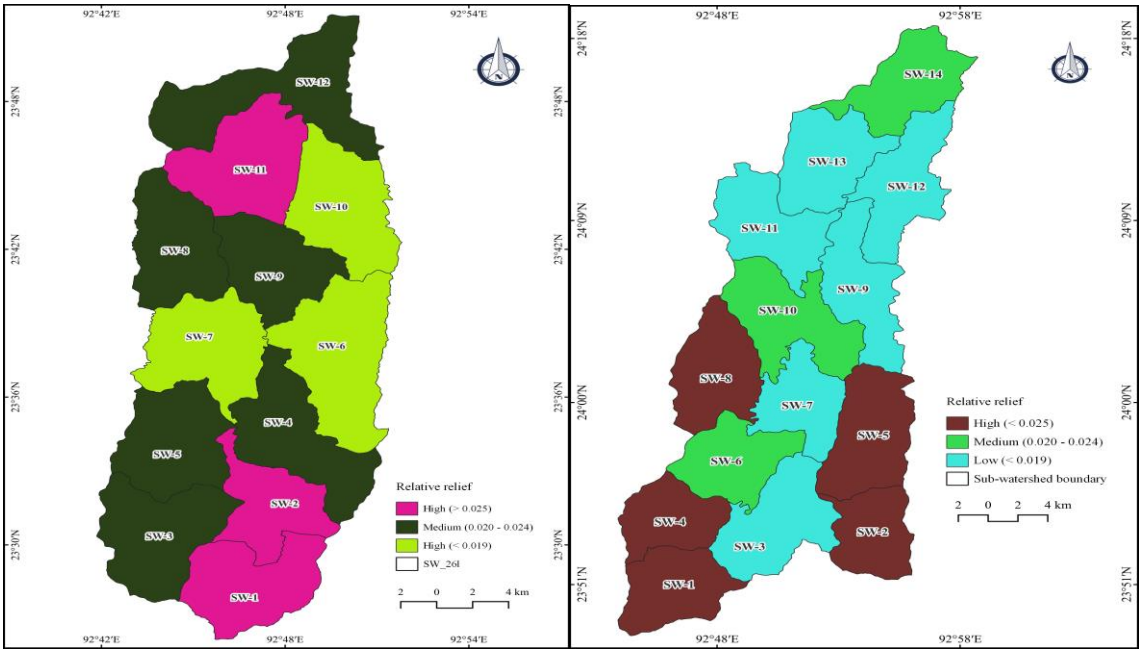


Figure 7.15: Relative relief ratio in Tuirial watershed; (a). Upper, (b) Middle

### 7.4.4 Gradient ratio (Gr)

The Gradient ratio is the proportion of difference between the origin (a) and the mouth (b) altitude of main river channel to the length of main river channel (Ls) of that basin. It is the indicator of channel gradient slope which helps to estimate the run-off volume in a basin (Strahler, 1964). Additionally, it also helps to estimate the degree of sediment transported towards down the river. The observed value of gradient ratios in Tuirial basin varies from 0.4 to 130 which indicates the basin is moderate to high gradient. The sub-basin wise gradient ratio is presented in tables 7.16, 7.17 and 17.8 respectively. The average gradient ratio in Upper Tuirial watershed is 32.20, slightly declines in Middle Tuirial with a value of 16.49 and decreases further by 0.73 in the Lower Tuirial watershed. The gradient ratio of Tuirial watershed is classified into three classes such as low (<10), medium (10 - 50) and high (>50). The sub-basins wise gradient ratio is shown in figures 7.16a (Upper) and 7.16b (Middle).

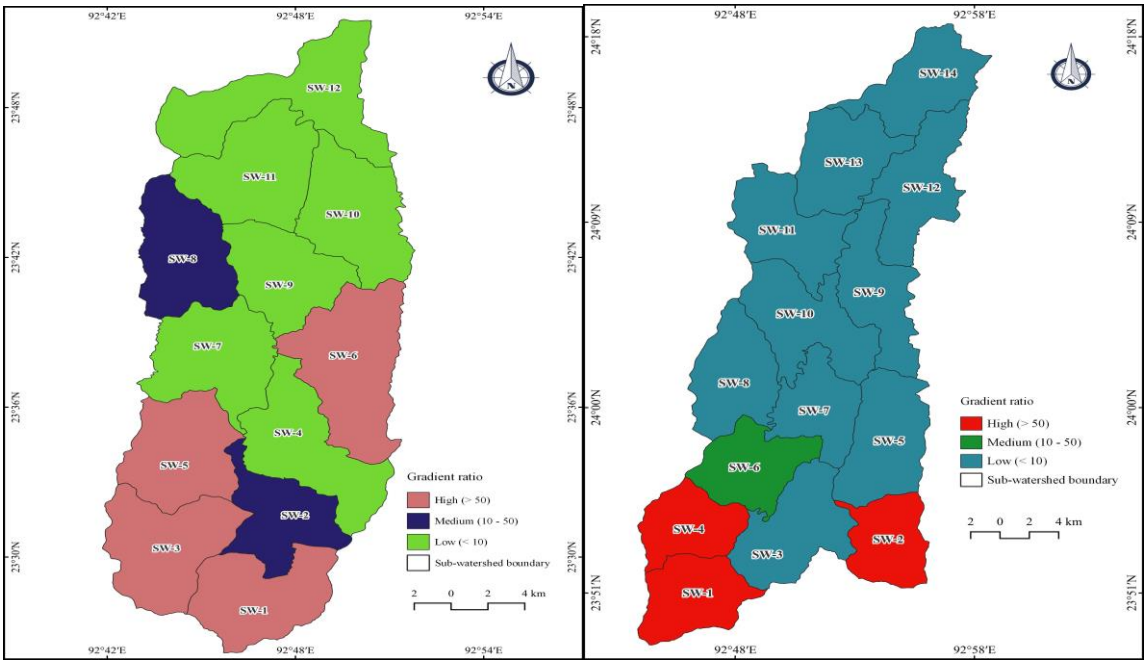


Figure 7.16: Gradient ratio in Tuirial watershed; (a). Upper, (b) Middle

### 7.4.5 Ruggedness number ($R_n$)

The Ruggedness number is a mathematically expressed as the basin relief divided by drainage density of that area. Where, the two parameters must be expressed in same unit (Strahler, 1957). The ruggedness number exhibits the characteristics of the angle of slope, topography of the given area. Low ruggedness number specifies that the river basin is low vulnerability to soil loss whereas, the high in ruggedness number infers that the basin is subjected to highly susceptible to soil loss, due to the physical topography of the basin. In the present study, the obtained ruggedness number varies from 2.8 to 7.1 in basin to basin and even in the sub-basins. The study highlighted the Upper Tuirial watershed is the highly rugged with having 5.97 $R_n$ value, slightly declines to 5.38 in Middle Tuirial watershed and further decreases to 3.78 in the Lower Tuirial watershed, which indicates the Tuirial watershed is highly rugged basin. The high values of Ruggedness number occur when the variables are high and the slope is not only large but long as well in the area (Strahler, 1957). The obtained $R_n$ values of the sub-basins wise are displayed in tables 7.16 of Upper Tuirial, table 7.17 of Middle Tuirial and table 7.18 of Lower Tuirial watershed. In the

present study, the ruggedness number is classified into three classes such as low (<5), medium (5.1 – 5.9) and high (>6). Generally, the ruggedness values decline towards the lower Tuirial watershed which shows erosion is lower in the lower course of the river along and also decline the elevation with ruggedness.

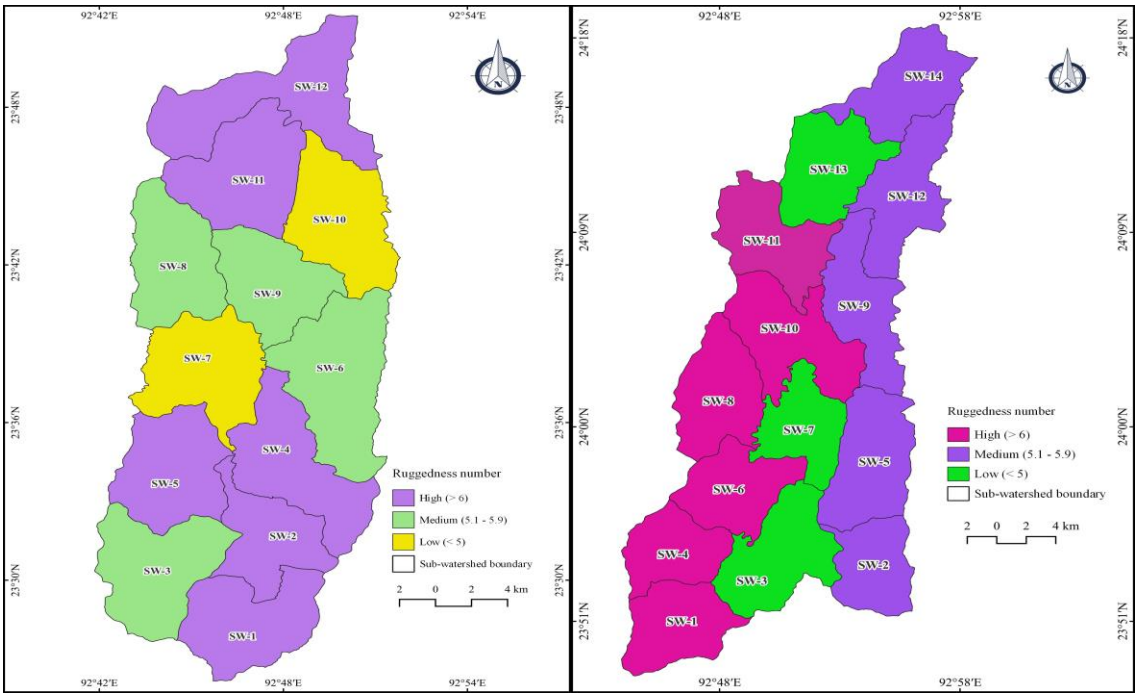


Figure 7.17: Ruggedness index in Tuirial watershed; (a). Upper, (b). Middle

### 7.4.6 Dissection Index (Di)

Dissection index is the proportion between basin relief to the absolute relief of the given area. It exhibits the degree of dissection or vertical erosion of the basin (Singh and Dubey, 1994). The dissection index is also useful index for measuring the stages of cycle of erosion as young, mature and old with the corresponding dissection index values of < 0.2, 0.21 – 0.69 and > 0.7, respectively. The dissection index obtained in the study ranges between 0 and 1. The dissection index value of the study area varies from 0.09 to 0.31. However, it has been classified into three classes based on the obtained $D_i$ values such as low (<0.15) indicating youthful stage of erosion, medium (0.16 – 0.20) specifies late youth stage, and high (>0.21) considered as early mature stage of erosion. The study reveals that

the area is in youth stage to early mature stage of development. In this study it was observed that the Upper Tuirial and Middle Tuirial watersheds show the average $D_i$ of 0.19 (Fig 7.18a and b), however, it increases to 0.22 in Lower Tuirial basin (Fig 7.18c), which signifies the lower course of the river is prone to less erosion and early mature stage of cycle of erosion.

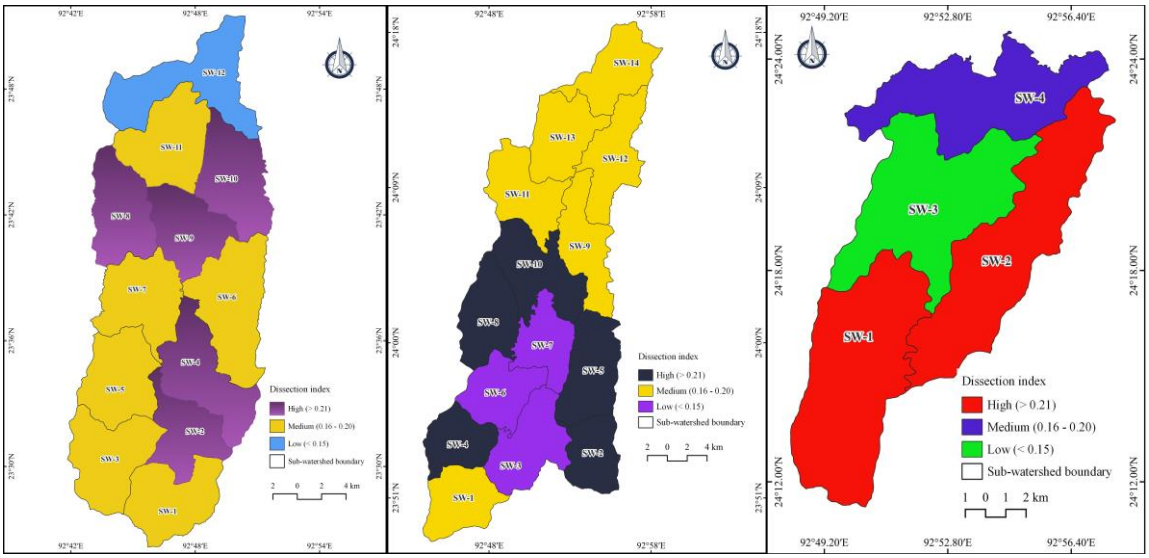


Figure 7.18: Dissection index in Tuirial watershed

### 7.5 Hypsometry curve and Hypsometry integral

The expression of the overall slope and the shape of drainage basin is hypsometry analysis (Langbein, 1947). Later, it was re-defined by Strahler, (1952) as he stated hypsometry implies the relative ratio of that area at different altitudes within the drainage basin. Furthermore, hypsometric curve is the curve relationship between the area and elevation of that basin, which specifies the stages of erosion or landforms at the basin (Strahler, 1952). Generally, hypsometric curve (HC) and hypsometric integral (Hi) are the significant measurements of the stages of erosion or the age of landform within the basin. The shape of hypsometric curve is determined and influenced by different climatic conditions and tectonic activity. The hypsometric curve exhibits the ratio of the amount of land mass has eroded by weathering of that are to the remaining soil mass (Hurtrez *et al*., 1999; Bishop *et al*., 2002). On the other hand, hypsometric integral is computed from the

area under a hypsometric curve and is depicted as percentage. The HC and Hi are classified according to their landforms and stages of erosion such as convex curve and Hi > 0.60 indicates youth stage, which exhibits the basin is highly vulnerable to soil loss. Additionally, S-curve or concave and Hi of 0.30 to 0.60 signifies mature stage of landforms. Lastly, the concave curve with Hi value less than 0.30 specifies old stage of landform (peneplain or monadnock) development. The hypsometric curve plotted from the derived hypsometric integral depicted that the Tuirial watershed has attained the early maturity stage, along with predominant erosional processes involved in landform development.

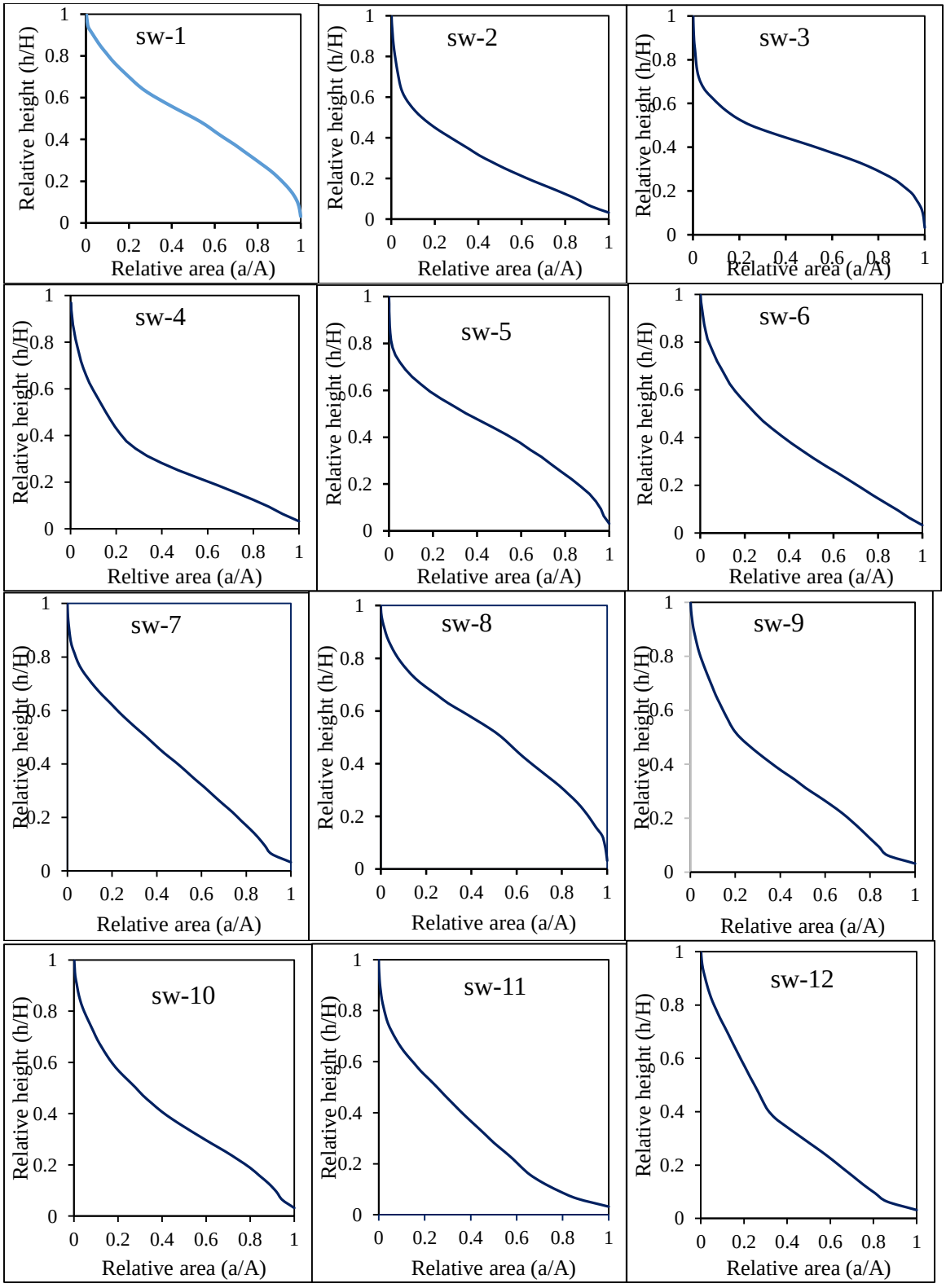


Figure 7.19: Hypsometric curve of sub-watersheds in Upper Tuirial watershed

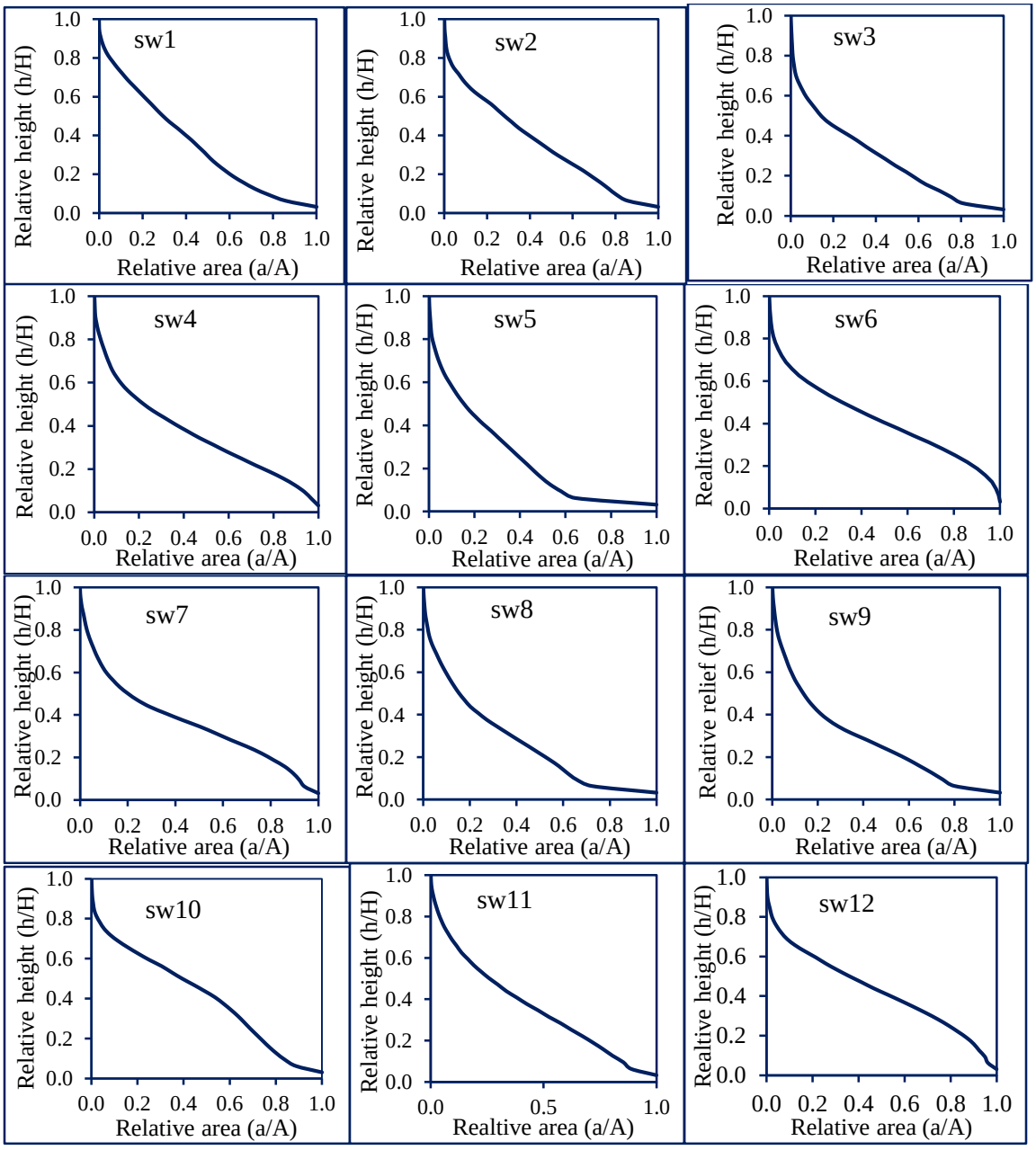


Figure 7.20: Hypsometric curve of sub-watersheds in Middle Tuirial watershed

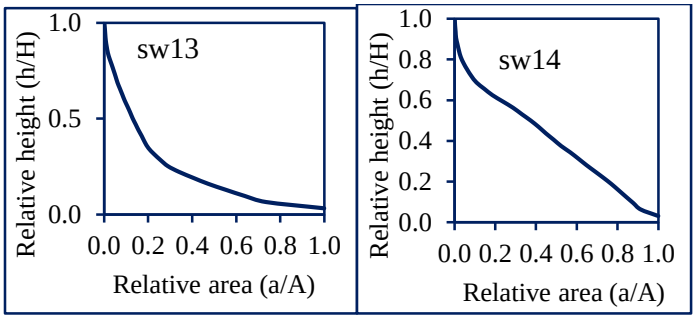


Continued..Figure 7.20: Hypsometric curve of sub-watersheds in Middle Tuirial watershed

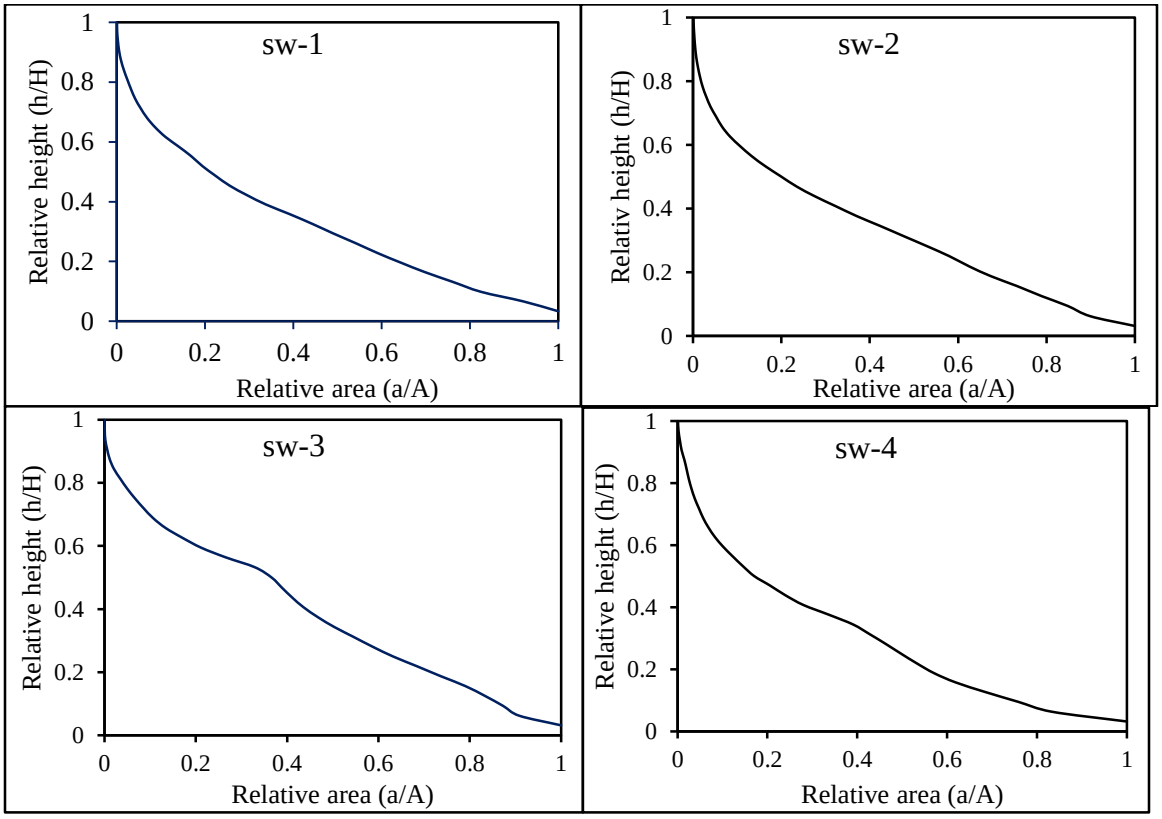


Figure 7.21: Hypsometric curve of subwatersheds in Lower Tuirial watershed

Table 7.22: Hypsometric integral of subwatersheds in Tuirial watershed

| Code | Upper watershed | Middle watershed | Lower watershed | Stages of geomorphic landforms |
|---|---|---|---|---|
| SW-1 | 0.50 | 0.48 | 0.49 | Mature |
| SW-2 | 0.48 | 0.48 | 0.48 | Mature |
| SW-3 | 0.49 | 0.48 | 0.48 | Mature |
| SW-4 | 0.48 | 0.49 | 0.48 | Mature |
| SW-5 | 0.48 | 0.48 | | Mature |
| SW-6 | 0.48 | 0.49 | | Mature |
| SW-7 | 0.47 | 0.48 | | Mature |
| SW-8 | 0.49 | 0.48 | | Mature |
| SW-9 | 0.48 | 0.48 | | Mature |
| SW-10 | 0.49 | 0.48 | | Mature |
| SW-11 | 0.47 | 0.49 | | Mature |
| SW-12 | 0.47 | 0.48 | | Mature |
| SW-13 | | 0.48 | | Mature |
| SW-14 | | 0.48 | | Mature |

The hypsometric integral values obtained for sub-watersheds indicates only one sub-basin (sw-1) from Upper Tuirial watershed attained early maturity, which is found the source of the basin, while all other sub-basins are already reached maturity stage of landform development. This evidence specifies about 98% of the sub-watersheds in this basin have witnessed an active denudation. However, sw-1 is still experiencing early mature stage which exhibits the highest vulnerability to soil loss. The study finds out that the Hi values are not decreasing towards the lower course of river. The low Hi values are found in the lower areas of sub-basin with having low altitude. The sub-basin close to the water divide line yield high Hi value which infer the size and terrain of the basin. Table 7.19 shows the sub-watersheds Hi values of Tuirial watershed and also highlighted the plot of hypsometric curves of Upper Tuirial watershed (Fig 7.19), Middle Tuirial watershed (Fig 7.20) and Lower Tuirial watershed (Fig 7.21).

## 7.6 Conclusion

The morphometric aspects such as linear, areal and relief features are having equal importance to measures severity of erosion status at the watershed level. The morphometric parameters which are associated with different physical and geomorphological aspects of a river basin reveal the nature of soil erosion. In general, the morphometry parameters yield critical significant clues for the detection of soil susceptible to erosion in sub-watersheds. Similarly, the areal morphometry parameters such as basin area, perimeter, drainage density, stream frequency, drainage texture, form factor, circularity ratio, length of overland flow, elongated ratio and constant of channel maintenance show the intensity of erosion in each sub-basin is determined and influenced by the shape and size of the basin. Furthermore, the relief morphometry features such as basin relief, relative relief ratio, relief ratio, gradient ratio, ruggedness number and dissection index having indirect implication on soil erosion. On an average from the computed morphometry parameters the highest influencing soil loss at the Upper Tuirial watershed, followed by Middle Tuirial, and the least by Lower Tuirial watershed.

# CHAPTER – 8

# CONCLUSION AND RECOMMENDATIONS

## 8.1 Conclusion

Soil erosion is the major threat in a hilly terrain characterized by steep slopes with fragile sedimentary terrain in a place like Tuirial watershed in the eastern extension of Himalayan region in Mizoram. The advanced techniques of remote sensing and the tools of geographical information system were used in this study to quantify precisely the total soil loss and to identify severe erosion prone zones in the Tuirial basin.

The present study successfully quantified total soil loss and siltation at Tuirial watershed and Tuirial dam, respectively. In addition, the morphometry of Tuirial river basin encompasses the comprehensive understanding of soil erosion parameters. The study highlights three principal objectives such as; (i) estimation of total soil loss, (ii) assessment of volume of siltation at dam site and (iii) analysis of morphometry of Tuirial basin. A number of methods and models are incorporated and analyzed with the help of remote sensing data and geographic information system (GIS) techniques to accomplish this research. Additionally, field observation; bathymetry and GPS survey were also conducted for measuring the depth of dam and identification of soil erosion zones within the study area. The study mainly focused on soil loss and erosion susceptibility zones with valuable recommendations to minimize the risk and further deterioration of natural environment.

The present study identified areas vulnerable to high severe soil loss in the Tuirial watershed which can be attributed to the increase anthropogenic activities for development such as construction of settlements, road construction, and agricultural system. Similarly, those activities disturb the natural forest cover and soil structure as which resulted in increased vulnerability of soil erosion in this area. In addition, the presence of fine to loamy soil in over 80% of the area, which further exacerbates the risk of soil loss. On the other hand, clay soil occupied close to the major river channel, the compact texture of this soil type provides greater resistance. The study observed that the area experiences severe to

extremely severe soil erosion in several villages, including Hlimen, Bukpui, Thingthelh, North Chaltlang, Lungmuat Nisapui, Serkhan, Lungdai, Sihphir, Nausel, Aizawl, Falkawn, Sateek, Tachhip, Lamchhip, Baktawng, Thingsulthliah, Seling, Saitual, Mauchar, and Ratu. Excessive rainfall and topographic factors are found to be the influencing factors that determine huge volume of soil loss. The RUSLE model gives an in-depth understanding of spatial distribution of soil erosion patterns in the Tuirial River Basin by precisely analyzing the impact of rainfall erosivity, soil erodibility, and topographic factor (LS) in conjunction with cover management. Among the erosion influencing factors rainfall erosivity is the most significant factor due to huge amount of run-off washing and transported loose and unconsolidated fragile material toward the low area in association of removal of forest covers. Similarly, the agricultural system "shifting cultivation" is risk for top soil loss and it is attributed mainly to the unsustainable agricultural practices. Besides that, the absence of proper implementation of forest conservation measures strategies and management system in Tuirial watershed. This information can guide to take effective conservation strategies to mitigate soil loss and protect valuable soil resources in the area. Additionally, the model's ability to identify vulnerable areas allows for targeted interventions that maximize conservation efforts and minimize environmental degradation.

Whereas, reservoir siltation increases with decreased water depth due to sediment deposit which is highly favourable for the growth of aquatic plants, is an issue in water related environments. The estimation of total sediment accumulated, area of reservoir loss and elevation due to silted volume, specific sediment yield, sediment yield, trap efficiency of reservoir, useful lifespan of reservoir, rate of siltation and dry bulk density of sediment at the bottom of reservoir by the application of scientific and empirical methods are found to be useful. Bathymetry survey was used to compute the total sediment volume and the specific sediment yield output for the watershed at micro-level. The bathymetric survey revealed that the total amount of sediment deposited between the years 2016 and 2023 is estimated at 2.57 $Mm^3$, (0.9 tonnes) which represents that 12.96 per cent reduction in the gross storage capacity over the period of seven years of dam function from 19.87 $Mm^3$ in the initial year of 2016 to 17.29 $Mm^3$ in the current year of 2023. Also, the useful life span

of the reservoir is estimated to be 47 years against the initial design of 100 years. It is estimated in this study, that the rate of siltation and annual loss in storage capacity are constant during the last seven years of dam operation at a rate of 368050 $m^3/yr^{-1}$. The dam storage capacity was gradually reduced due to high-rate infiltration of soil texture, the extensive practice of shifting cultivation at the Tuirial watershed even close to the dam site, no proper soil conservation, and high intensity of run-off occurs, which appear to be the major factors contributing to the increased siltation in the Tuirial dam. The sediment inflow, in the vicinity of the dam can be minimized through reforestation and massive sustainable agro-plantation practices to improve the useful lifespan. This type of study by integration of geographical information system, bathymetry with conventional methods is useful to increase the life span of dams worldwide through the monitoring of siltation at regular intervals.

The linear morphometry parameters such as stream order, stream number, stream length, mean stream length, basin length and bifurcation ratio give insight of statistical correlation amongst the stream segments in association with topography and lithological variation of the basin. The variation in stream order and size of the sub-watersheds is determined by structural and physiographic condition of Tuirial basin. The study identified Tuirial river basin is characterized by four drainage patterns, such as trellis, dendritic, sub-dendritic and parallel. However, predominant by dendritic pattern as the region is controlled by physiographic setting and tectonic activity. Similarly, the areal morphometry parameters such as basin area, perimeter, drainage density, stream frequency, drainage texture, form factor, circularity ratio, length of overland flow, elongated ratio and constant of channel maintenance show the intensity of erosion in each sub-basin is determined and influenced by the shape and size of the basin. Furthermore, the relief morphometry features such as basin relief, relative relief ratio, relief ratio, gradient ratio, ruggedness number and dissection index having indirect implication on soil erosion. On an average from the morphometry parameters computed soil loss is found to be high in Upper Tuirial watershed, followed by Middle Tuirial, and the least by Lower Tuirial watershed. The morphometric parameters which are associated with different physical and

geomorphological aspects of a river basin reveal the nature of soil erosion. In general, the morphometry parameters yield critical significant clues for the detection of soil susceptible to erosion in sub-watersheds.

### 8.2 Recommendations

Soil loss and sediment accumulation issues at Tuirial watershed and Tuirial dam have been observed after the systematically analyzing the basin physiographic setting. This problem has both direct and indirect influence on ecosystem, natural life cycle, natural habitat, economic lifespan of dam, losses of forest resources and man-environment relationship. This challenging situation can be primarily attributed to the rapid population growth, further influenced by human intervention on natural forested area. Nevertheless, fragile sedimentary formation of landforms is greatly affected by monsoonal rainfall in this area. Based on the research findings and their implications as well as the field observations, the following recommendations are made for the sustainable management of Tuirial watershed.

1) Highly susceptible erosion prone zones must be treated with appropriate erosion control measures such as re-forestation, vegetative and mechanical practices. Government should execute strict rules and regulation for development and agricultural practices in those areas characterized by more than $45^{\circ}$ angle of inclination of slope. Similarly, restriction of site selection for shifting cultivation land over relatively steep slopes is regarded as the most effective strategy to reduce fragile topsoil and nutrient loss from agricultural land.
2) Shifting cultivation must be transformed into settled farm land to prevent further soil erosion. Shifting cultivation useful economic lifespan is about only one year, it is characterized by extensive clearing and burning of vegetation cover, consequence by exposures of bare land for generating direct influence on rainfall and surface run-off. Immediate elimination of this predominant tribal cultivation system may have significant direct impact on farmer economic activity, so it is unpractical in the present-day. To overcome this problem, in the first year of cultivation,

sustainable agro-forestry such as growing horticultural crops, arecanut plantation, orange plantation, banana plantation etc., must be encouraged while practicing inter-mixed crops. These practices generously aid plants root and body for growing by utilizing the fertility of soil. These types of practices are substantially sustainable for farmer's economic livelihood as well as further degradation of forest area and intensity of erosion.

3) Implementation of cluster farming system is essential for minimization of soil loss. Within the Tuirial watershed, Aizawl is the only city practicing secondary and tertiary economic activity; all other villages are greatly reliant on primary activity. About 34 villages still continued shifting cultivation as dispersion within a village area, which must be clustered at suitable plot of land. Based on the elevation, arrangement of farming system has greatly reduced soil erosion. Suppose on the top of the slope, rearing animal or poultry farming etc., subsequent by agro-forestry plantation and close to the river channel are highly required watering of vegetable area must be implemented. In the meantime, animal waste will be useful for middle and the lower agricultural land to retrieve soil fertility and nutrient provider. On the other hand, practicing of contour farming, mulching, strip cropping and terrace farming along the slope will greatly reduce surface run-off energy and sustain nutrient and soil fertility.
4) Besides the agricultural land, these types of land use such as settlement, road construction, recreational centres and other developmental activities excessively produced run-off due to compact soil texture, consolidated topsoil, cemented pavement and concrete, asphalt base block top prohibit infiltration generate huge amount of surface run-off transported unconsolidated fragmented material and sediment in and around those developmental activities down toward the low land and river channel. To prevent this high surface run-off with no proper channel, proper drainage should be laid and constructed alongside of roads and settlement areas.

5) The construction of house, quarrying sites, road construction and other developmental activities must require removal of huge landmass of topsoil, earth spoil are dumped immediate to nearby construction sites which are fragile and easily washed away by surface run-off and flash flush transported toward the lowland and river bank reduces volume of water due to huge amount of sediment accumulation. Selection of proper earth spoil dumping site is required for minimization of soil erosion. The low lying area with distance from the river is suitable for earth spoil dumping site.
6) Buffer zone must be initiated for the protection and reserved forest areas mainly on steep slopes. Besides the conservation of natural vegetation, suitable methods like re-forestation or afforestation ought to be carried out at severely soil loss zones. Similarly, prohibition of developmental undertakings at the protected areas to maintain sustainable ecosystem which plays an important role to control erosion.
7) To prevent high surface run-off from the settlement areas, generation of roof top harvesting is the most common and less financial investment. This region receives abundant rainfall under the direct influence of south-west monsoon. Thus, proper rainwater harvesting techniques will definitely reduce soil erosion from surface run-off. There are various types of surface run-off harvesting systems like construction of check dams at regular intervals considering slope and other topographic factors, retention ponds, infiltration basin, rainwater recharge well along the Tuirial river channel. Basically, it is not only preventing soil loss but also maintain the water quantity of the river throughout the year.
8) Soil and conservation department, environment and forest department, climate change cell, integrated water management department and national rural livelihood department from the government bodies must check regular interval at those sensitive zones of erosion.
9) Cooperation of non-government organizations, village leaders, stake holders and local farmer is essential to prevent further soil erosion within the Tuirial watershed. In addition, it is necessary to provide financial assistance from the government for

the construction, maintenance of erosion and sediment control such as terrace, contouring stripping, plantation, check dams and retaining etc.

10) It is essential extensive awareness campaigns programmes regarding the importance and benefit of controlling soil erosion and sedimentation through the outreach programmes, like conducting workshops, training, and organizing seminars. Besides that, through the public awareness, which may yield major alteration because people are the eyes witness experiencing land degradation in their day to day observation.
11) On both sides of the main channel of Tuirial river, 200 metres buffer zone must be implemented to maintain the volume of water throughout the year. Furthermore, this buffer zone will act as controlling factor of greater influx of sediments at Tuirial river towards the dam.
12) Measurement the volume of sediment accumulation at the bottom of Tuirial dam is required at regular intervals for obtaining valuable information of reservoir storage capacity and live storage dead.
13) Construction of sediment trap before reaching the dam is essential for preventing further accumulation of sediment. In addition, generation of sediment pits is required for flushing the accumulated sediment at the bottom of dam.

## References


Abboud, I.A., Nofal, R.A., 2017. Morphometric analysis of wadi Khumal basin, western coast of Saudi Arabia, using remote sensing and GIS techniques. Journal of African Earth Sciences, 126, 58–74. https://doi.org/10.1016/j.jafrearsci.2016.11.024.

Acharya, T. D., Subedi, A., Yang, I. T., & Lee, D. H. (2017). Combining water indices for water and background threshold in Landsat image. In *Proceedings* (Vol. 2, No. 3, p. 143). MDPI.

Adongo, T. A., Abagale, F. K., & Agyare, W. A. (2021). Modelling and forecasting reservoir sedimentation of irrigation dams in the Guinea Savannah Ecological Zone of Ghana. *Water Practice & Technology*, 16(4), 1355-1369.

Adornado, H. A., Yoshida, M., & Apolinares, H. A. (2009). Erosion vulnerability assessment in REINA, Quezon Province, Philippines with raster-based tool built within GIS environment. *Agricultural Information Research*, *18*(1), 24-31

Agnihotri, D., Kumar, T., & Jhariya, D. (2021). Intelligent vulnerability prediction of soil erosion hazard in semi-arid and humid region. Environment, Development and Sustainability, 23(2), 2524-2551.

Al-Abadi, A. M. A., Ghalib, H. B., & Al-Qurnawi, W. S. (2016). Estimation of soil erosion in northern Kirkuk governorate, Iraq using rusle, remote sensing and gis. *Carpathian journal of earth and environmental sciences*, *11*(1), 153-166.

Ali, M. I., Dirawan, G. D., Hasim, A. H., & Abidin, M. R. (2019). Detection of changes in surface water bodies urban area with NDWI and MNDWI methods. *International Journal on Advanced Science Engineering Information Technology*, *9*(3), 946-951.

Ambade, B., Sethi, S. S., Kurwadkar, S., Kumar, A., & Sankar, T. K. (2021). Toxicity and health risk assessment of polycyclic aromatic hydrocarbons in surface water, sediments and groundwater vulnerability in Damodar River Basin. *Groundwater for Sustainable Development*, 13, 100553.

Amini Najafabadi, M., Fatahi Nafchi, R., Salami, H., Vanani, H. R., & Ostad-Ali-Askari, K. (2023). Effect of different managements with drip irrigation (tape). *Applied Water Science*, 13(2), 37.

Arabameri, A., Pradhan, B., Pourghasemi, H.R., Rezaei, K., 2018. Identification of erosion prone areas using different multi-criteria decision-making techniques and GIS. Geomatics, *Natural Hazards and Risk* 9(1), 1129–1155.

Arefin, R., Mohir, Md.M.I., Alam, J., 2020. Watershed prioritization for soil and water conservation aspect using GIS and remote sensing: PCA-based approach at northern elevated tract Bangladesh. *Applied Water Science*, 10, 91.

Arabkhedri, M., Heidary, K., & Parsamehr, M. R. (2021). Relationship of sediment yield to connectivity index in small watersheds with similar erosion potentials. *Journal of Soils and Sediments*, *21*(7), 2699-2708.

Arnold, J. G., Srinivasan, R., Muttiah, R. S., & Williams, J. R. (1998). Large area hydrologic modeling and assessment part I: model development 1. JAWRA *Journal of the American Water Resources Association*, 34(1), 73-89.

Arulbalaji, P., & Padmalal, D. (2020). Sub-watershed prioritization based on drainage morphometric analysis: a case study of Cauvery River Basin in South India. *Journal of the Geological Society of India*, 95, 25-35

Asfaw, D., & Workineh, G. (2019). Quantitative analysis of morphometry on Ribb and Gumara watersheds: Implications for soil and water conservation. *International Soil and Water Conservation Research*, 7(2), 150-157.

ASF data. Advanced Land Observing Satellite-1 Phased Array Type L-band Synthetic Aperture Radar (ALOS PALSAR) [Internet]. Available from: https://search.asf.alaska.edu/#/?dataset=ALOS&zoom=7.492&center=92.813,22.918&polygon=POLYGON((92.657%2024.0031,93.0085%2024.0031,93.0085%2024.2953,92.657%2024.2953,92.657%2024.0031))&resultsLoaded=true&granule=ALPSRP256820470-L2.2

Beaurue of Indian Standards. 1972. *Indian Standard Soil Classification System (ISSCS).* p. 14.

Bhavsar, M. M., & Gohil, K. B. (2015). Review on study of reservoir sedimentation by remote sensing technique. *International Journal for Innovative Research in Science & Technology*, *1*(12), 251-254.

Blanco, H., & Lal, R. (2008). *Principles of soil conservation and management* (Vol. 167169). New York: Springer.

Barman, B. K., Rao, K. S., Sonowal, K., Prasad, N. S. R., & Sahoo, U. K. (2020). Soil erosion assessment using revised universal soil loss equation model and geo-spatial technology: A case study of upper Tuirial river basin, Mizoram, India. *AIMS Geosciences*, *6*(4), 525-545.

Bakis R, Bayajit Y, Ahmady DM, Cabuk SN (2021) Analysis and comparison of spatial rainfall distribution applying different interpolation methods in the porsuk river basin, Turkey. *Eskisehir Tech Univ J Sci Technol B-Theoretical Sci* 9(1):1–14.

Bhattacharya, R.K., Chatterjee, N.D., Das, K., 2019. Multi-criteria-based sub-basin prioritization and its risk assessment of erosion susceptibility in Kansai–Kumari catchment area, India. *Applied Water Science*, 9, 76.

Bishop, M., Shroder, J., Bonk, R. and Olsenholler, J. (2002) Geomorphic Change in High Mountains: A Western Himalayan Perspective. *Global Planetary Change*, 32, 311-329.

Bilal, A., Dai, W., Larson, M., Beebo, Q. N., & Xie, Q. (2017). Qualitative simulation of bathymetric changes due to reservoir sedimentation: A Japanese case study. *Plos one*, *12*(4), e0174931.

Bleu, P. (2003). Threats to Soils in Mediterranean Countries. *Document Review. Sophia Antipolis:Plan Bleu Centre d'activités régionales*.

Bombino, G., Barbaro, G., D'Agostino, D., Denisi, P., Labate, A., & Zimbone, S. M. (2022). A method for estimating stored sediment volumes by check dam systems at the watershed level: example of an application in a Mediterranean environment. *Journal of Soils and Sediments*, 22(4), 1329-1343

Brown CB (1943) Discussion of Sedimentation in reservoirs. In: Witzig J (eds) *Journal of the Hydrology Division* ASCE 69:1493–1500.

Brune, G. M. (1953). Trap efficiency of reservoirs. *Eos, Transactions American Geophysical Union*, *34*(3), 407-418

Chalise, D., Kumar, L., Shriwastav, C. P., & Lamichhane, S. (2018). Spatial assessment of soil erosion in a hilly watershed of Western Nepal. *Environmental Earth Sciences*, *77*, 1-11.

Chatterjee S, Krishna AP, Sharma AP (2014) Geospatial assessment of soil erosion vulnerability at watershed level in some sections of the Upper Subarnarekha river basin, Jharkhand, India. *Environmental Earth Science* 71: 357–374.

Chauhan, N., Paliwal, R., Kumar, V., Kumar, S., & Kumar, R. (2022). Watershed prioritization in Lower Shivaliks Region of India using integrated principal component and hierarchical cluster analysis techniques: A case of upper Ghaggar Watershed. *Journal of the Indian Society of Remote Sensing*, 50(6), 1051-1070.

Choudhari, P.P., Nigam, G.K., Singh, S.K., Thakur, S., 2018. Morphometric based prioritization of watershed for groundwater potential of Mula river basin, Maharashtra, India. *Geology, Ecology and Landscapes* 2(4), 256–267.

Copernicus Open Access Hub. Sentinel 2C Satellite image [Internet]. Available from: https://scihub.copernicus.eu/dhus/#/home.

Dabral, P. P., Baithuri, N., & Pandey, A. (2008). Soil erosion assessment in a hilly catchment of North Eastern India using USLE, GIS and remote sensing. *Water Resources Management*, *22*, 1783-1798.

Darama, Y., Selek, Z., Selek, B., Akgul, M. A., & Dagdeviren, M. (2019). Determination of sediment deposition of Hasanlar Dam using bathymetric and remote sensing studies. *Natural Hazards*, *97*, 211-227.

Dadoria, D., Tiwari, H. L., & Jaiswal, R. K. (2017). Assessment of reservoir sedimentation in Chhattisgarh State using remote sensing and GIS. *International Journal of Civil Engineering and Technology*, *8*(4), 526-534.

Dewangan, C. L., & Ahmad, I. (2020). Assessment of reservoir sedimentation and identification of critical soil erosion zone in Kodar reservoir watershed of Chhattisgarh state, India. In *Applications of Geomatics in Civil Engineering: Select Proceedings of ICGCE 2018* (pp. 203-214). Springer Singapore.

Darama, Y., Selek, Z., Selek, B., Akgul, M. A., & Dagdeviren, M. (2019). Determination of sediment deposition of Hasanlar Dam using bathymetric and remote sensing studies. *Natural Hazards*, *97*, 211-227.

Dabral PP, Baithuri N, Pandey A (2008) Soil erosion assessment in a hilly catchment of North Eastern India using USLE, GIS and remote sensing. Water Resource Management 22: 1783–1798.

Das B, Paul A, Bordoloi R, et al. (2018) Soil erosion risk assessment of hilly terrain through integrated approach of RUSLE and geospatial technology: a case study of Tirap District, Arunachal Pradesh. *Model Earth System Environment* 4: 373–381.

Debelo, G., Tadele, K., & Koriche, S. A. (2017). Morphometric analysis to identify erosion Prone areas on the upper Blue Nile using Gis (Case Study of Didessa and Jema Sub-Basin, Ethiopia). International Research Journal of Engineering and Technology, 4(8), 1773-1784.

Dutta, S. (2016). Soil erosion, sediment yield and sedimentation of reservoir: a review. *Modeling Earth Systems and Environment*, *2*, 1-18.

Dutal, H., Reis, M., (2020). Determining the effects of land use on soil erodibility in the Mediterranean highland regions of Turkey: a case study of the Korsulu stream watershed. *Environment Monitoring Assessment*, 192(3), 1-15.

El-Sersawy, H. (2005). Sediment deposition mapping in Aswan High Dam reservoir using geographic information system (GIS). In *Ninth International Water Technology Conference, IWTC9,* Sharm El-Sheikh, Egypt. 239–247.

Endalew, L., & Mulu, A. (2022). Estimation of reservoir sedimentation using bathymetry survey at Shumburit earth dam, East Gojjam zone Amhara region, Ethiopia. Heliyon 8 (12), e11819 (2022).

El Jazouli, A., Barakat, A., Ghafiri, A., Moutaki, S.E., Ettaqy, A. and Khellouk, R. 2017. Soil erosion modeled with USLE, GIS, and remote sensing: a case study of Ikkour watershed in Middle Atlas (Morocco). Geoscience Letters 4(1): 25.

Ebrahimi Gatgash, Z., & Sadeghi, S. H. (2023). Prioritization-based management of the watershed using health assessment analysis at sub-watershed scale. *Environment, Development and Sustainability*, 25(9), 9673-9702.

FAO, 2015. Status of the World's Soil Resources: Main Report. Food and Agricultural Organization of the United Nations (FAO). Accessed 22 May, 2024.

FAO, 2020. Global Symposium on Soil Erosion. Food and Agricultural Organization of the United Nations (FAO). Accessed 22 May, 2024.

Farhan, Y., & Anaba, O. (2016). Watershed prioritization based on morphometric analysis and soil loss modeling in Wadi Kerak (Southern Jordan) using GIS techniques. *International Journal of Plant & Soil Science*, 10(6), 1-18.

Fenta, A.A., Yasuda, H., Shimizu, K., Haregeweyn, N., Woldearegay, K., 2017. Quantitative analysis and implications of drainage morphometry of the Agula watershed in the semi-arid northern Ethiopia. *Applied Water Science,*

Gautam, V. K., Gaurav, P. K., Murugan, P., & Annadurai, M. J. A. P. (2015). Assessment of surface water Dynamicsin Bangalore using WRI, NDWI, MNDWI, supervised classification and KT transformation. *Aquatic Procedia*, *4*, 739-746.

Gelagay, H. S. (2016). RUSLE and SDR model based sediment yield assessment in a GIS and remote sensing environment; a case study of Koga watershed, Upper Blue Nile Basin, Ethiopia. *Hydrology Current Research*, *7*(2), 239.

George JK, Kumar S, Hole RM (2021) Geospatial modeling of soil erosion and risk assessment in indian Himalaya region-A study of Uttarakhand state. *Environ Adv* 4:100039.

Ghashghaie, M., Eslami, H., & Ostad-Ali-Askari, K. (2022). Applications of time series analysis to investigate components of Madiyan-rood river water quality. *Applied Water Science*, 12(8), 202.

Ghimire, M., Timalsina, N., & Zhao, W. (2023). A Geographical approach of watershed prioritization in the Himalayas: a case study in the middle mountain district of Nepal. *Environment, Development and Sustainability*, 1-34.

Guo, H., Jiapaer, G., Bao, A., Li, X., Huang, Y., Ndayisaba, F., & Meng, F. (2017). Effects of the Tarim River's middle stream water transport dike on the fractional cover of desert riparian vegetation. *Ecological Engineering*, 99, 333-342.

Gill, M. A. (1979). Sedimentation and useful life of reservoirs. *Journal of Hydrology*, *44*(1-2), 89- 95

Godwin, M. A., Gabriel, S., Hodson, M., Wellington, D. (2011). Sedimentation impacts on reservoir as a result of land use on a selected catchment in Zimbabwe. *International Journal of Engineering Science and Technology*, *3*(8), 6599–6608

GSI, (2011). Geology and Mineral Resources of Manipur, Mizoram, Nagaland and Tripura. Geological Survey of India, Miscellaneous Publication No. 30 Part IV, 1(2), 36-39.

Hassan, R., Al-Ansari, N., Ali, A. A., Ali, S. S., & Knutsson, S. (2017). Bathymetry and siltation rate for Dokan Reservoir, Iraq. Lakes & Reservoirs: *Research & Management*, 22(2), 179-189.

Haregeweyn, N., Melesse, B., Tsunekawa, A., Tsubo, M., Meshesha, D., & Balana, B. B. (2012). Reservoir sedimentation and its mitigating strategies: a case study of Angereb reservoir (NW Ethiopia). *Journal of Soils and Sediments, 12*, 291-305.

Hailu, M. B., Mishra, S. K., & Jain, S. K. (2023). Sediment yield modelling and prioritization of erosion-prone sub-basins in the Tekeze watershed, Ethiopia. *Environment, Development and Sustainability*, 1-16.

Haokip, P., Khan, M. A., Choudhari, P., Kulimushi, L. C., & Qaraev, I. (2022). Identification of erosion-prone areas using morphometric parameters, land use land cover and multi-criteria decision-making method: geo-informatics approach. *Environment, Development and Sustainability*, 24(1), 527-557.

Harsha, J., Ravikumar, A.S., Shivakumar, B.L., 2020. Evaluation of morphometric parameters and hypsometric curve of Arkavathy river basin using RS and GIS techniques. *Applied Water Science*, 10, 1–15.

Hema hc, Govindaiah S, Lakshmi Srikanth & Surendra, H. J. (2021). Prioritization of sub-watersheds of the Kanakapura Watershed in the Arkavathi River Basin, Karnataka, India-using Remote sensing and GIS. *Geology, Ecology, and Landscapes*, 5(2), 149-160.

Hembram, T. K., & Saha, S. (2020). Prioritization of sub-watersheds for soil erosion based on morphometric attributes using fuzzy AHP and compound factor in Jainti River basin, Jharkhand, Eastern India. *Environment, Development and Sustainability*, 22(2), 1241-1268.

Horton, R. E. (1945). Erosional development of streams and their drainage basins; hydrophysical approach to quantitative morphology. *Geological society of America bulletin*, 56(3), 275-370.

Iqbal, M., & Sajjad, H. (2014). Watershed prioritization using morphometric and land use/land cover parameters of Dudhganga Catchment Kashmir Valley India using spatial technology. *Journal of Geophysics and Remote Sensing*, 3(115), 2169-0049.

Iradukunda, P., Sang, J. K., Nyadawa, M. O., & Maina, C. W. (2020). Sedimentation effect on the storage capacity in lake Nakuru, Kenya. *Journal of Sustainable Research in Engineering*, *5*(3), 149-158.

Issa, I. E., Al-Ansari, N., Knutsson, S., & Sherwany, G. (2015). Monitoring and evaluating the sedimentation process in Mosul Dam Reservoir using trap efficiency approaches. *Engineering*, *7*(4), 190-202.

Jagannathan, S., & Krishnaveni, M. (2021). Longitudinal sediment profiling and capacity lost in reservoir using multidate Sentinel-2 images. *Journal of the Indian Society of Remote Sensing*, *49*, 317-323.

Jain, S. K., Kumar, S., & Varghese, J. (2001). Estimation of soil erosion for a Himalayan watershed using GIS technique. *Water Resources Management*, *15*, 41-54.

Kothyari, U. C. (1996). Erosion and sedimentation problems in India. *IAHS Publications-Series of Proceedings and Reports-Intern Assoc Hydrological Sciences*, *236*, 531-540

Kumar, R., Naqvi, H. R., Devrani, R., Deshmukh, B., & Huang, J. C. (2022). Sediment yield assessment, prioritization and control practices in Chambal River basin employing SYI model. *Journal of the Geological Society of India*, *98*(11), 1585-1594.

Kabite, G., & Gessesse, B. (2018). Hydro-geomorphological characterization of Dhidhessa River basin, Ethiopia. *International Soil and Water Conservation Research*, 6(2), 175-183.

Kadam, A., Karnewar, A. S., Umrikar, B., & Sankhua, R. N. (2019). Hydrological response-based watershed prioritization in semiarid, basaltic region of western India using frequency ratio, fuzzy logic and AHP method. *Environment, Development and Sustainability*, 21, 1809-1833.

Kadam, A. K., Kale, S. S., Umrikar, B. N., Sankhua, R. N., & Pawar, N. J. (2022). Assessing site suitability potential for soil and water conservation structures by using modified micro-watershed prioritization method: geomorphometric and geomatic approach. *Environment, Development and Sustainability*, 1-25.

Kaur, M., Singh, S., Verma, V. K., & Pateriya, B. (2014). Quantitative geomorphological analysis & land use/land cover change detection of two sub-watersheds in ne region of Punjab, India. *The International Archives of the Photogrammetry, Remote Sensing and Spatial Information Sciences*, 40, 371-375.

Krishnan, A., & Ramasamy, J. (2022). Morphometric assessment and prioritization of the South India Moyar river basin sub-watersheds using a geo-computational approach. *Geology, Ecology, and Landscapes*, 1-11.

Kulimushi, L. C., Choudhari, P., Maniragaba, A., Elbeltagi, A., Mugabowindekwe, M., Rwanyiziri, G., ... & Singh, S. K. (2021). Erosion risk assessment through prioritization of sub-watersheds in Nyabarongo river catchment, Rwanda. *Environmental Challenges*, 5, 100260.

Kumar, D., Dhaloiya, A., Nain, A. S., Sharma, M. P., & Singh, A. (2021). Prioritization of watershed using remote sensing and geographic information system. *Sustainability*, 13(16), 9456.

Kumar, R., Naqvi, H. R., Devrani, R., Deshmukh, B., & Huang, J. C. (2022). Sediment yield assessment, prioritization and control practices in Chambal River basin employing SYI model. *Journal of the Geological Society of India*, 98(11), 1585-1594.

Kurwadkar, S., Sethi, S. S., Mishra, P., & Ambade, B. (2022). Unregulated discharge of wastewater in the Mahanadi River Basin: Risk evaluation due to occurrence of polycyclic aromatic hydrocarbon in surface water and sediments. *Marine Pollution Bulletin*, 179, 113686.

Kumar, A., Singh, S., Pramanik, M., Chaudhary, S., Maurya, A. K., & Kumar, M. (2022). Watershed prioritization for soil erosion mapping in the Lesser Himalayan Indian basin using PCA and WSA methods in conjunction with morphometric parameters and GIS-based approach. *Environment, Development and Sustainability*, 1-39.

Kenye, A., Sahoo, U. K., Singh, S. L., & Gogoi, A. (2019). Soil organic carbon stock of different land uses of Mizoram, Northeast India. *AIMS Geosciences*, (1), 25-40.

Kisan, M. V., Khanindra, P., Narayan, T. K., & Kumar, T. S. (2016). Remote sensing and GIS based assessment of soil erosion and soil loss risk around hill top surface mines situated in Saranda Forest, Jharkhand. *Journal of Water and Climate Change*, *7*(1), 68-82.

La Touche, T. H. D. (1891). Record of Geological Survey of India. Geological Survey of India (GSI), 24(2).

Li, J., & Heap, A. D. (2011). A review of comparative studies of spatial interpolation methods in environmental sciences: Performance and impact factors. *Ecological Informatics*, 6(3-4), 228-241.

Lawmchullova, I., & Rao, U. B. (2023). Soil loss modelling in Himalayan region; A case of Tuirial Basin, Mizoram. *Advance online publication*.

Lawmchullova, I., & Rao, C. U. B. (2024). Estimation of siltation in Tuirial dam: a spatio-temporal analysis using GIS technique and bathymetry survey. *Journal of Sedimentary Environments*, 9(1), 81-97.

Langbein, W.B. (1947) Topographic Characteristics of Drainage Basins. *USGS Water Supply Paper*, 947-C. 157 p

Maina, C. W., Sang, J. K., Mutua, B. M., & Raude, J. M. (2018). Bathymetric survey of Lake Naivasha and its satellite Lake Oloiden in Kenya; using acoustic profiling system. *Lakes & Reservoirs: Research & Management*, 23(4), 324-332.

Markose, V. J., & Jayappa, K. S. (2016). Soil loss estimation and prioritization of sub-watersheds of Kali River basin, Karnataka, India, using RUSLE and GIS. *Environmental monitoring and assessment*, *188*, 1-16.

Markose, V. J., & Jayappa, K. S. (2016). Soil loss estimation and prioritization of sub-watersheds of Kali River basin, Karnataka, India, using RUSLE and GIS. *Environmental monitoring and assessment*, *188*, 1-16.

Mandal, D., & Sharda, V. N. (2013). Appraisal of soil erosion risk in the Eastern Himalayan region of India for soil conservation planning. *Land Degradation & Development*, *24*(5), 430-437.

Mekonnen, Y. A., Mengistu, T. D., Asitatikie, A. N., & Kumilachew, Y. W. (2022). Evaluation of reservoir sedimentation using bathymetry survey: a case study on Adebra night storage reservoir, Ethiopia. *Applied Water Science*, *12*(12), 269.

Meshram, S. G., & Sharma, S. K. (2017). Prioritization of watershed through morphometric parameters: a PCA-based approach. *Applied Water Science*, 7, 1505-1519.

Meshram, S. G., & Sharma, S. K. (2018). Application of principal component analysis for grouping of morphometric parameters and prioritization of watershed. In Hydrologic Modeling: Select Proceedings of ICWEES-2016 (pp. 447-458).

Meshram, S. G., Singh, S. K., Meshram, C., Deo, R. C., & Ambade, B. (2018). Statistical evaluation of rainfall time series in concurrence with agriculture and water

resources of Ken River basin, Central India (1901–2010). Theoretical and applied climatology, 134, 1231-1243.

Miller, V. C. (1953). A quantitative geomorphic study of drainage basin characteristics in the Clinch Mountain area, Virginia and Tennessee (Vol. 3). New York: Columbia University.

MIRSAC, (2006). Natural Resources Mapping of Kolasib District, Mizoram using Remote Sensing and GIS, A project report. Mizoram State Remote Sensing Center, S&T, Planning Dept. Mizoram, 28.

Morgan, R. P. C., Quinton, J. N., Smith, R. E., Govers, G., Poesen, J. W. A., Auerswald, K., ... & Styczen, M. E. (1998). The European Soil Erosion Model (EUROSEM): a dynamic approach for predicting sediment transport from fields and small catchments. *Earth Surface Processes and Landforms: The Journal of the British Geomorphological Group*, 23(6), 527-544.

Moges, M. M., Abay, D., & Engidayehu, H. (2018). Investigating reservoir sedimentation and its implications to watershed sediment yield: The case of two small dams in data-scarce upper Blue Nile Basin, Ethiopia. *Lakes & Reservoirs: Research & Management*, *23*(3), 217-229.

Mulu, A., & Dwarakish, G. S. (2015). Different approach for using trap efficiency for estimation of reservoir sedimentation. An overview. *Aquatic Procedia, 4*, 847-852.

NASA Power. Daily rainfall data [Internet]. Available from: https://power.larc.nasa.gov/data-access-viewer/

Naqvi, H. R., Mallick, J., Devi, L. M., & Siddiqui, M. A. (2013). Multi-temporal annual soil loss risk mapping employing revised universal soil loss equation (RUSLE) model in Nun Nadi Watershed, Uttrakhand (India). *Arabian journal of geosciences, 6*, 4045-4056.

Nir, D. (1957). The ratio of relative and absolute altitudes of Mt. Carmel: a contribution to the problem of relief analysis and relief classification. *Geographical Review*, 47(4), 564-569.

Neepco. Tuirial Hydro Power Station Features [Internet]. Available from: https://neepco.co.in/power-generation/hydro-power/tuirial-hydro-power-station

Ozsahin E, Duru U, Eroglu I (2018) Land Use and Land Cover Changes (LULCC), a Key to Understand Soil Erosion Intensities in the Maritsa Basin. Water 10: 335.

Pandey, A., Mathur, A., Mishra, S. K., & Mal, B. C. (2009). Soil erosion modeling of a Himalayan watershed using RS and GIS. *Environmental Earth Sciences*, *59*, 399-410.

Pimentel, D. (2006). Soil erosion: a food and environmental threat. *Environment, development and sustainability*, *8*, 119-137.

Prasannakumar V, Shiny R, Geetha N, Vijith H (2011) Spatial prediction of soil erosion risk by remote sensing, GIS and RUSLE approach: a case study of Siruvani river watershed in Attapady valley, Kerala, India. *Environmental Earth Science*, 64:965–972.

Prasannakumar V, Vijith H, Abinod S, et al. (2012) Estimation of soil erosion risk within a small mountainous sub-watershed in Kerala, India, using revised universal soil loss equation (RUSLE) and geo-information technology. *Geoscience Frontier* 3: 209–215.

Pathare, J. A., & Pathare, A. R. (2021). Watershed prioritization for soil and water conservation in Darna River basin: a PCA approach. *Sustainable Water Resources Management*, 7(4), 49.

Patton, P. C., & Baker, V. R. (1976). Morphometry and floods in small drainage basins subject to diverse hydrogeomorphic controls. *Water Resources Research*, 12(5), 941–952.

Pike, R. J., & Wilson, S. E. (1971). Elevation–relief ratio, hypsometric integral and geomorphic area–altitude analysis. *Geological Society of America Bulletin*, 82, 1079–1084.

Patil, R. A., & Shetkar, R. V. (2015). Sediment deposition in Koyna Reservoir by integrated bathymetric survey. *IJRET: International Journal of Research in Engineering and Technology*, *4*(11).

Rãdoane, M., & Radoane, N. (2005). Dams, sediment sources and reservoir silting in Romania. *Geomorphology*, *71*(1-2), 112-125.

Rawat, J. S., & Rawat, M. S. (1994). Accelerated erosion and denudation in the Nana Kosi watershed, Central Himalaya, India. Part I: sediment load. *Mountain Research and Development*, 25-38.

Rokni, K., Ahmad, A., Selamat, A., & Hazini, S. (2014). Water feature extraction and change detection using multi-temporal Landsat imagery. *Remote sensing*, *6*(5), 4173-4189.

Raymo, M. E., & Ruddiman, W. F. (1992). Tectonic forcing of late Cenozoic climate. *nature*, *359*(6391), 117-122.

Rawat, J. S., & Rawat, M. S. (1994). Accelerated erosion and denudation in the Nana Kosi watershed, Central Himalaya, India. Part I: sediment load. *Mountain Research and Development*, 25-38.

Rahaman SA, Aruchamy S, Jegankumar R, et al. (2015) Estimation of annual average soil loss, based on RUSLE model in Kallar watershed, Bhavani basin, Tamil Nadu, India. *ISPRS Ann Photogram Remote Sens Spat Inf Sci* 2: 207–214.

Renard KG, Foster GA, Weesies DK, et al. (1977) Predicting Soil Erosion by Water: A Guide to Conservation Planning with Revised Soil Loss Equation (RUSLE). Handbook No. 703, Department of Agriculture, Washington DC, USA, 384.

Renard KG, Foster GR (1983) Soil conservation: principles of erosion by water. In: Dregne HE, Wills WO (Eds.), Dry land Agriculture, American Society of Agronomy, Soil Science Society of America, Madison, WI, USA, 155–176.

Rabiei, J., Khademi, M. S., Bagherpour, S., Ebadi, N., Karimi, A., & Ostad-Ali-Askari, K. (2022). Investigation of fire risk zones using heat–humidity time series data and vegetation. *Applied Water Science*, 12(9), 216

Ramesh, A., & Ostad-Ali-Askari, K. (2023a). Effects of magnetized municipal effluent on some physical properties of soil in furrow irrigation. *Applied Water Science*, 13(1), 26.

Ramesh, A., & Ostad Ali Askari, K. (2023b). Effect of effluent and magnetized effluent on Manning roughness coefficient in furrow irrigation. *Applied Water Science*, 13(1), 21.

Rao, C. U. B., (2015). Estimation of Sediment Yield Rate in the Lower Tlawng watershed, Mizoram, *Geographic Journal of GAM*, 10, 1-11

Renard, K.G., Foster, G.R., Weesies, G.A., McCool, D.K., Yorder, D.C., 1997. Predicting soil erosion by water: a guide to conservation planning with the revised universal loss equation (RUSLE). U.S. Department of Agriculture. Agriculture Handbook 703, 404.

Saaty, T., 1980. The Analytic Process: Planning, Priority Setting, Resources Allocation. McGraw, New York.

Saha, R., Chaudhary, R. S., & Somasundaram, J. (2012). Soil health management under hill agroecosystem of North East India. *Applied and Environmental Soil Science*, *2012*.

Sarkar, D., Mondal, P., Sutradhar, S., Sarkar, P., (2020). Morphometric analysis using SRTM-DEM and GIS of Nagar River Basin, Indo-Bangladesh Barind Tract. *Journal of the Indian Society of Remote Sensing*, 48, 597–614.

Scholes, R., Montanarella, L., Brainich, A., Barger, N., ten Brink, B., Cantele, M., Erasmus, B., Fisher, J., Gardner, T., Holland, T.G., Kohler, F., Kotiaho, J.S., Maltitz, G.V., Nangendo, G., Pandit, R., Parrotta, J., Potts, M.D., Prince, S., Sankaran, M., Willemen, L., 2018. IPBES: Summary for policymakers of the assessment report on land degradation and restoration of the intergovernmental science-policy platform on biodiversity and ecosystem Services. Bonn, Germany.

Schumm, S. A. (1956). Evolution of drainage systems and slopes in badlands at Perth Amboy, New Jersey. *Geological society of America bulletin*, 67(5), 597-646.

Senanayake S, Pradhan B, Huete A, Brenan J (2020) Assessing soil Erosion hazards using land-use change and landslide frequency ratio Method: a case study of Sabaragamuwa Province, Sri Lanka. *Remote Sensing* 12:1483.

Sharma, S., & Mahajan, A. K. (2020). GIS-based sub-watershed prioritization through morphometric analysis in the outer Himalayan region of India. *Applied Water Science*, 10(7), 1-11.

Shelar, R. S., Shinde, S. P., Pande, C. B., Moharir, K. N., Orimoloye, I. R., Mishra, A. P., & Varade, A. M. (2022). Sub-watershed prioritization of Koyna river basin in India using multi criteria analytical hierarchical process, remote sensing and GIS techniques. *Physics and Chemistry of the Earth, Parts A/B/C*, 128, 103219.

Shiferaw, M., & Abebe, R. (2021). Reservoir sedimentation and estimating dam storage capacity using bathymetry survey: A case study of Abrajit Dam, Upper Blue Nile basin, Ethiopia. *Applied Geomatics*, 13(3), 277-286.

Singh, L. K., Jha, M. K., & Chowdary, V. (2017). Multi-criteria analysis and GIS modeling for identifying prospective water harvesting and artificial recharge sites for sustainable water supply. *Journal of Cleaner Production*, 142, 1436–1456.

Skariah, M., & Suriyakala, C. D. (2021). Gauging of sedimentation in Idukki Reservoir, Kerala (1974–2019), and the impact of 2018 Kerala floods on the reservoir. *Journal of the Indian Society of Remote Sensing*, *49*(9), 2103-2112.

Shukla, S., Jain, S. K., Kansal, M. L., & Chandniha, S. K. (2017). Assessment of sedimentation in Pong and Bhakra reservoirs in Himachal Pradesh, India, using geospatial technique. *Remote Sensing Applications: Society and Environment*, *8*, 148–156

Smith, G. H. (1935). The relative relief of Ohio. Geographical review, 25(2), 272-284.

Sultana Q (2018). Useful Life of a Reservoir and its Dependency on Watershed Activities. *Agriculture Research Technology Open Access J* 8:1-9.

Stoner, W. D., Stark, B. L., VanDerwarker, A., & Urquhart, K. R. (2021). Between land and water: Hydraulic engineering in the Tlalixcoyan basin, Veracruz, Mexico. *Journal of Anthropological Archaeology*, 61, 01264.

Sreedevi, P.D., Owais, S., Khan, H.H., Ahmed, S., 2009. Morphometric analysis of a watershed of South India using SRTM data and GIS. *Journal of the Geological Society of India*, 73, 543–552.

Strahler, A. (1964) Quantitative Geomorphology of Drainage Basins and Channel Networks. In: Chow, V., Ed., Handbook of Applied Hydrology, McGraw Hill, New York, 439-476.

Sutradhar, H., 2020. Assessment of drainage morphometry and watersheds prioritization of Siddheswari River Basin, Eastern India. *Journal of the Indian Society of Remote Sensing*, 48, 627–644.

Strahler, A.N. (1952) Hypsometric (Area-Altitude) Analysis of Erosional Topography. *Geological Society of America Bulletin*, 63, 1117-1141.

Tesfaye, A. T., Moges, M. A., Moges, M. M., Worqlul, A. W., Defersha, D. T., & Wassie, A. B. (2023). Reservoir sedimentation evaluation using remote sensing

and GIS approaches for the reservoirs in the upper Blue Nile Basin. *Sustainable Water Resources Management*, *9*(1), 23.

Tessema YM, Jasinska J, Yadeta LT, et al. (2020) Soil loss estimation for conservation planning in Welmel Watershed of the Geale Dawa basin, Ethiopia. *Agronomy* 10: 777.

Thakuriah, G. (2023). GIS-based revised universal soil loss equation for estimating annual soil erosion: a case of lower Kulsi basin, India. *SN Applied Sciences*, 5(3), 81.

Thomas J, Joseph S, Thrivikramji KP (2018) Assessment of soil erosion in a tropical mountain river basin of the southern Western Ghats, India, using RUSLE and GIS. *Geoscience Frontier*, 9:893–906.

Thomas, J., Joseph, S., Thrivikramji, K. P., Abe, G., & Kannan, N. (2012). Morphometrical analysis of two tropical mountain river basins of contrasting environmental settings, the southern Western Ghats, India. *Environmental Earth Sciences*, 66, 2353-2366.

Umrikar, B. N. (2017). Morphometric analysis of Andhale watershed, Taluka Mulshi, District Pune, India. *Applied Water Science*, 7, 2231-2243.

UN, 2015. Sustainable development. Department of Economic and Social Affairs, United Nations (UN). Accessed 22 May, 2024.

Uzuner, Ç., & Dengiz, O. (2020). Desertification risk assessment in Turkey based on environmentally sensitive areas. *Ecological Indicators, 114*, 106295.

Valdiya, K. S. (1985). Accelerated erosion and landslide-prone zones in the central Himalayan region. *Environmental regeneration in Himalaya: concepts and strategies/edited by JS Singh*. 122–138.

Vanlalchhuanga, R. K. J., Moharana, P., Kumar, N., Sharma, R. P., Das, B., Roy, P. D., & Ray, S. K. (2022). Modelling and mapping of soil erosion in the north-eastern

frontier Himalayan ranges of India using remote sensing and GIS. *Journal of Soil and Water Conservation*, 21(4), 345-353.

Verheijen, F. G., Jones, R. J., Rickson, R. J., & Smith, C. J. (2009). Tolerable versus actual soil erosion rates in Europe. *Earth-Science Reviews*, *94*(1-4), 23-38.

Verma, N., Patel, R. K., & Choudhari, P. (2023). Watershed prioritization for soil conservation in a drought prone watershed of Eastern India: Tel River Basin, Odisha. *Geology, Ecology, and Landscapes*, 7(4), 405-418.

Verstraeten, G., & Poesen, J. (2000). Estimating trap efficiency of small reservoirs and ponds: methods and implications for the assessment of sediment yield. *Progress in Physical Geography*, *24*(2), 219-251.

Wilkinson, B. H., & McElroy, B. J. (2007). The impact of humans on continental erosion and sedimentation. *Geological society of America bulletin*, *119*(1-2), 140-156.

Wischmeier WH, Smith DD (1978) Predicting rainfall erosion losses: a guide to conservation planning. Agriculture Handbook no 537. US Department of Agriculture, Science and Education Administration, Washington, DC, USA, p 163

Withanage, N. S., Dayawansa, N. D. K., & De Silva, R. P. (2014). Morphometric analysis of the Gal Oya River Basin using spatial data derived from GIS. *Tropical Agriculture Research*, 26(1), 175-188.

Wuepper, D., Borrelli, P., & Finger, R. (2020). Countries and the global rate of soil erosion. *Nature sustainability*, *3*(1), 51-55.

Wulandari, D. A., Legono, D., Darsono, S. (2015). Evaluation of deposition pattern of Wonogiri reservoir sedimentation. *International Journal of Civil & Environmental Engineering IJCEE-IJENS*, *15*(2), 15–20.

Yao, L., Wei, W., Yu, Y., Xiao, J., & Chen, L. (2018). Rainfall-runoff risk characteristics of urban function zones in Beijing using the SCS-CN model. *Journal of Geographical Sciences*, 28(5), 656–668.

Yusof NF, Lihan T, Idris WMR, Rahman ZA, Mustapha MA, Yusof MAW (2019) Prediction of soil erosion in Pansoon Sub-basin, Malaysia using RUSLE integrated in geographical information system. *Sains Malays* 48(11):2565–2574.

Zonunsanga, R. (2016). Estimation of Soil loss in Teirei watershed of Mizoram by using the USLE Model. *Science and Technology Journal*, *4*, 43-47.

PLATE 1


Photo A

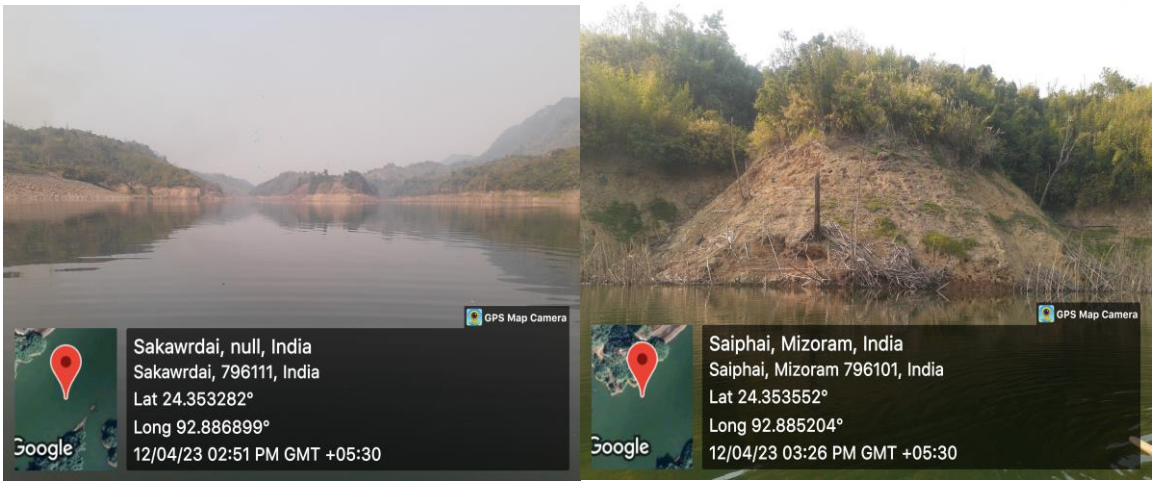


Photo B

Photo A: Bathymetry survey conducted at Tuirial Dam

Photo B: Both side of the dam eroded by water

PLATE 2

Photo A

Photo B

Photo A: Tuirial dam taken from earth filled

Photo B: Spillway along with elevation bench mark

PLATE 3

Photo A

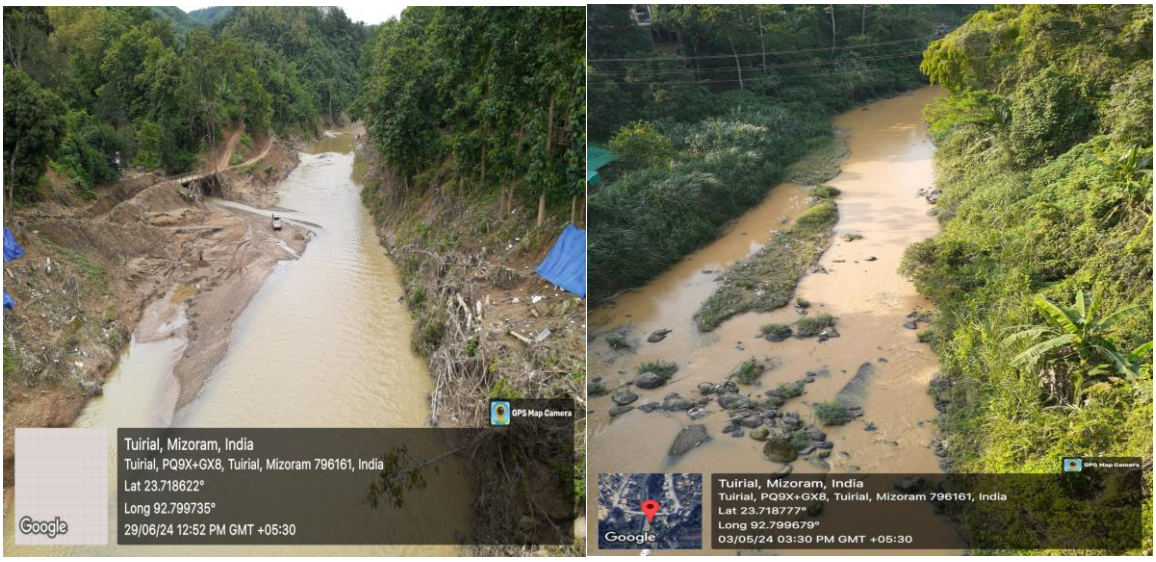


Photo B

Photo A: Tuirial river during the warm season

Photo B: Tuirial river during the monsoon season, depicting sediment transport down the river.

PLATE 4

Photo A


Photo B

Photo A: Improper earth spoil due to road construction

Photo B: Steep slope cut for road construction which later consequence by landslide

PLATE 5


Photo: GPS survey at the source of Tuirial river close to Chawilung village

BIO-DATA OF THE CANDIDATE

Name : Imanuel Lawmchullova

Father's name : Lalzawmliana

Mother's name : Lalrimawii

Gender : Male

Date of Birth : 25th December, 1996

Marital Status : Married

Religion : Christian

Address : Diakkawn, Kolasib-790681

Mobile : 9366337554 / 8413822043

Email : lawmchullova@gmail.com

Academic Profile:

| Class | Board of Examination | Year of Passing |
|---|---|---|
| X | M.B.S.E | 2012 |
| XII | M.B.S.E | 2014 |
| B.A. | Mizoram University | 2017 |
| M.Sc. | Mizoram University | 2019 |
| NET | UGC | 2019 & 2022 |
| UGC-NET-JRF | UGC | 2022 |

## PARTICULARS OF THE CANDIDATE

| | | |
|---|---|---|
| NAME OF THE CANDIDATE | : | IMANUEL LAWMCHULLOVA |
| DEGREE | : | DOCTOR OF PHILOSOPHY |
| DEPARTMENT | : | GEOGRAPHY AND RESOURCE MANAGEMENT |
| TITLE OF THE THESIS | : | ESTIMATION OF SOIL LOSS IN TUIRIAL WATERSHED |
| DATE OF ADMISSION | : | 28th AUGUST, 2021 |
| APPROVAL OF RESEARCH PROPOSAL | | |
| 1. DRC | : | 21st MARCH, 2022 |
| 2. BOS | : | 27th MAY, 2022 |
| 3. SCHOOL BOARD | : | 10th JUNE, 2022 |
| MZU REGISTRATION NO. | : | 3189 OF 2014 |
| Ph. D. REGISTRATION NO. & DATE | : | MZU/Ph. D./1793 OF 28.08.2021 |
| EXTENSION (IF ANY) | : | NIL |

(PROF. BENJAMIN L. SAITLUANGA)

HEAD OF DEPARTMENT

GEOGRAPHY AND RESOURCE MANAGEMENT

# ABSTRACT

# ESTIMATION OF SOIL LOSS IN TUIRIAL WATERSHED

**AN ABSTRACT SUBMITTED IN PARTIAL FULFILLMENT OF THE REQUIREMENTS FOR THE DEGREE OF DOCTOR OF PHILOSOPHY**


**IMANUEL LAWMCHULLOVA**

**MZU REGISTRATION NO.: 3189 of 2014**

**Ph.D. REGISTRATION NO.: MZU/Ph.D. /1793 of 28.08.2021**




**DEPARTMENT OF GEOGRAPHY AND RESOURCE MANAGEMENT**

**SCHOOL OF EARTH SCIENCES AND NATURAL RESOURCE MANAGEMENT**


**MARCH, 2025**

Soil erosion is a natural process that continues depending on natural factors and is accelerated by anthropogenic factors. Soil erosion occurs naturally when soil particles are disintegrated, transported, and deposited at different places by various erosion agents like wind, running water, surface run-off and solar energy. Soil erosion is one of the environmental problems globally which affect soil fertility, agricultural production, siltation in water bodies. The Eastern Indian Himalayan region as a whole is experiencing serious problem of soil erosion and the rivers flowing through this region carries huge quantities of sediments and finally discharge into the Bay of Bengal. Mizoram is an eastern extension of the Himalayas, as it is a mountainous and moist tropical rain-fed region the amount of soil loss and sediment deposit is expected to be huge on the slope area and river bed respectively. The sediment load in the rivers increased due to loss of forest cover, intense exploitation of other natural resources, severe monsoonal precipitations and the fragile river catchments of low water retention capacity.

Geologically the region is very weak and fragile due to presence of loose sedimentary rocks mostly composed of sandstone, siltstone and shales. Anthropogenic activities such as deterioration of forest, expansion of agricultural land construction of road from forest cover, shifting cultivation (locally known as Jhum) on steep slopes, rapid urbanization and other developmental activities integrate with high rainfall, poor soil conservation and high soil erosivity effect by shallow soil depths, un-consolidation of soil deposited are the main reasons for the high rate of soil loss. Each year, due to soil erosion, million tons of soil is eroded off mostly from agricultural lands in mountainous terrain. There are several studies carried out in the region that report shifting cultivation to be the principal source of soil erosion.

Despite knowing the significant issues of soil erosion and siltation, there has been lack of adequate comprehensive research on estimate of total soil loss at sub-watershed level and silted at reservoir with minimization of the strategic action planning. Therefore, a precise and timely assessment is essential for understanding the spatial distribution, degree and amount of erosion and siltation with developing effective control measures. However, the actual field measurements at hilly terrain and mountainous region is

impossible due to huge capital investment and time consuming along with lack of labour. In addition, the recorded data for run-off, and sediment influx is not readily available at the watershed level since most of the river basins are still ungauged. Even though, the absence of erosion and siltation volume recorded with various limitations, the present study try to fill this knowledge gap, generating synoptic information of soil loss and siltation through the application of geospatial technology and bathymetry survey in a watershed. The advancement of remote sensing and geographic information system based approaches, the present study attempts to assess soil erosion comprehensively. Furthermore, this study was intended to provide reliable, cost effective, and spatially explicit information on erosion and siltation in a watershed. This valuable insight into the complex processes and problems will be helpful for sustainable watershed management that focuses on the formulation of feasible erosion and siltation mitigation plans, strategic land use planning, and appropriate land and water management policies.

The present study aimed estimation of total soil loss at Tuirial watershed, Mizoram using bathymetry survey, soil and erosion model integration of geo-spatial data in geographic information system (GIS) along with other pioneering formula. The study aims to achieve the following specific objectives:

1. To estimate the total soil loss at Tuirial watershed
2. To estimate the siltation level at Tuirial dam
3. To analyze the morphometry of Tuirial watershed
4. To suggest the remedial measures of soil loss and siltation level at watershed and dam.

Tuirial watershed covers an area of 1414.26 $km^2$ and geographic location between longitudes 92°42′E–92°52′E and latitudes 23°26′N–23°52′N. Tuirial watershed is divided into three watersheds such as upper Tuirial, middle Tuirial and lower Tuirial. This river demarcates between Aizawl and Kolasib districts in the eastern side. The lower course of the river, nearby Saipum village the biggest hydel project in Mizoram was constructed. The

installed capacity of the Station is 60 MW and design head of 53 meters. Loamy soil, Fine loamy, Fine loamy to loamy skeletal, Loamy skeletal and Coarse loamy soil are the common soil texture in Tuirial watershed. Built-upland, current shifting cultivation, fallow land, water bodies, bamboo forest, open forest, medium forest and dense forest are the land use and land cover pattern in Tuirial watershed. Within the watershed, there are 68 settlements with one city being existed, of which 33 and 35 settlements are on the western and eastern side of the Tuirial river, respectively.

The methodology of the present study comprises an extensive collection of geo-spatial data and field survey. The present study is based on primary data viz. bathymetry survey and secondary data viz. geo-spatial data (rainfall, temperature, lithology, geology, geomorphic features, soil texture, satellite imagery, digital elevation model, wind speed and direction). Linear, areal and relief aspects of morphometry are computed through the pioneering developed equations of morphometric parameters for the understanding of relationship between soil erosions and quantitatively measures the earth surface. Total soil loss at Tuirial watershed was analyzed by revised universal soil loss equation model through the integration of soil erodibility factor, rainfall erosivity factor, length and steepness of slope, conservation practise management and cover management factor. Siltation at Tuirial dam was estimated by various scientific methods such as silt volume, rate of siltation, sediment yield, specific sediment yield, dry bulk density, trap efficiency, along with economic life span with the help of geographic information system particularly ArcGIS 10.4, Qgis 3.28, and microsoft excel 2016 version. Thus, the analyze data were interpreted in a meaningful way with the help of graphs and maps.

The present study observed that the *K* value differs from 0.25 t hr. $MJ^{-1}$ $mm^{-1}$ of clay to 0.66 ton/$hr^{-1}$/$MJ^{-1}$/$mm^{-1}$ of coarse loamy soil texture in the Tuirial basin. This suggests that areas with a higher proportion of coarse loamy soil texture in the Tuirial basin are found to be at high risk of soil erosion compared to areas with clay, fine loamy 0.54 ton/$hr^{-1}$/$MJ^{-1}$$mm^{-1}$, and loamy skeletal soil textures 0.57 ton/$hr^{-1}$$MJ^{-1}$$mm^{-1}$. The average

annual rainfall received at the basin fluctuated from 1209 to 2104 mm. Similarly, the rainfall erosivity factor also varies based on the amount of rainfall received, as the analysis reveals 974.17–1844.31 MJ/mm/ha$^{-1}$/hr$^{-1}$/yr$^{-1}$. The Tuirial river basin slope ranges from 0$^{\circ}$ to 81$^{\circ}$ of which 12.74% of total geographical ground cover 10$^{\circ}$ - 81$^{\circ}$ of slope, suggesting high to very high vulnerability to soil loss. In addition, vulnerability of soil loss depends on the angle of slope. The Tuirial basin topographic factor (LS) varies from 0 to 16.75. The LS factor is a key parameter in determining the potential for soil erosion, with higher values indicating areas of greater risk. The built-up land (0.48%), current cultivation (0.67), fallow land (9.72%), bamboo forest (26.70%), open forest (6.68%), medium forest (52.34%), dense forest (0.42%), and water bodies (2.98%) are the land use and land cover types found in the study area. The C and P factors are dimensionless factors with values range between 0 and 1. The C value nearby zero implies good conservation management, whereas a value at one denotes poor cover management. In the Tuirial river basin, good cover management is found in the areas where natural forest cover, water bodies and fallow land occur, which indicate a low soil risk zone, whereas low cover management areas such as built-up land and current cultivation are likely to be susceptible to soil erosion. The P factor value between 0 and 1, with higher values implies low susceptibility to erosion; on the other hand, the values close to zero indicate a high chance of vulnerability of soil loss. The P value denotes the efficiency of cover and land management strategies in minimization of erosion risk.

The study finds that the average annual soil loss of the Tuirial river basin varies from 0 to 1519.52 thousand t ha$^{-1}$yr$^{-1}$. Seven zones of soil loss were classified into, low (0-1 thousand t ha$^{-1}$yr$^{-1}$) 125941 ha. slightly (1-5 thousand t ha$^{-1}$yr$^{-1}$) 112.09 ha. moderate (5-15 thousand t ha$^{-1}$yr$^{-1}$) 110.54 ha. high (15-30 thousand t ha$^{-1}$yr$^{-1}$) 358.62 ha. very high (30-60 thousand t ha$^{-1}$yr$^{-1}$) 471.40 ha. severe (60-90 thousand t ha$^{-1}$yr$^{-1}$) 540.02 ha. and very severe (≥120 thousand t ha$^{-1}$yr$^{-1}$) 12016.10 ha**Error! Reference source not found.**. Highly susceptible soil loss areas such as barren land, the amount of precipitation, Jhum fallows, agricultural land, and built-up areas, sparse vegetation cover, undulating topography, high in angle of inclination and current cultivation areas are the triggering

factors. Among the parameter rainfall erosivity, angle of inclination and slope of the length are the major influencing factors to determine soil loss in hill rain-fed region. In addition, current Jhum and fallow land are also play an important role in soil loss.

The majority of the river basin was categorized as an erosion-free or moderate zone due to the presence of dense vegetation, low terrain, concrete infrastructure, clay, etc. The basin area of 12016 ha (8.61%) was identified as a very severe zone of soil erosion risk. Because of the built-up area, road construction, and current cultivation, exposed bare surfaces on hillslopes accelerate high run-off. The high rate of soil loss in the Tuirial basin was identified in the built-up area, barren land, and current shifting cultivation, including cultivable fallow land. The thick vegetation cover is found on the steep slope, which is inaccessible and difficult for cultivation activities.

The study observed that the reservoir siltation increases with decreased water depth due to sediment deposit which is highly favourable for the growth of aquatic plants, is an issue in water related environments. The estimation of total sediment accumulated, area of reservoir loss and elevation due to silted volume, specific sediment yield, sediment yield, trap efficiency of reservoir, useful lifespan of reservoir, rate of siltation and dry bulk density of sediment at the bottom of reservoir by the application of scientific and empirical methods are found to be useful. The bathymetric survey revealed that the total amount of sediment deposited between the years 2016 and 2023 is estimated at 2.57 $Mm^3$, (0.9 tonnes) which represents that 12.96 per cent reduction in the gross storage capacity over the period of seven years of dam function from 19.87 $Mm^3$ in the initial year of 2016 to 17.29 $Mm^3$ in the current year of 2023. Also, the useful life span of the reservoir is estimated to be 47 years against the initial design of 100 years. It is estimated in this study, that the rate of siltation and annual loss in storage capacity are constant during the last seven years of dam operation at a rate of 368050 $m^3/yr^{-1}$. The dam storage capacity was gradually reduced due to high-rate infiltration of soil texture, the extensive practice of shifting cultivation at the Tuirial watershed even close to the dam site, no proper soil conservation, and high intensity of run-off occurs, which appear to be the major factors contributing to the increased siltation in the Tuirial dam. The sediment inflow, in the vicinity of the dam can be

minimized through reforestation and massive sustainable agro-plantation practices to improve the useful lifespan. This type of study by integration of geographical information system, bathymetry with conventional methods is useful to increase the life span of dams worldwide through the monitoring of siltation at regular intervals.

The linear morphometry parameters such as stream order, stream number, stream length, mean stream length, basin length and bifurcation ratio give insight of statistical correlation amongst the stream segments in association with topography and lithological variation of the basin. The variation in stream order and size of the sub-watersheds is determined by structural and physiographic condition of Tuirial basin. The study identified Tuirial river basin is characterized by four drainage patterns, such as trellis, dendritic, sub-dendritic and parallel. However, predominant by dendritic pattern as the region is controlled by physiographic setting and tectonic activity. Similarly, the areal morphometry parameters such as basin area, perimeter, drainage density, stream frequency, drainage texture, form factor, circularity ratio, length of overland flow, elongated ratio and constant of channel maintenance show the intensity of erosion in each sub-basin is determined and influenced by the shape and size of the basin. Furthermore, the relief morphometry features such as basin relief, relative relief ratio, relief ratio, gradient ratio, ruggedness number and dissection index having indirect implication on soil erosion. On an average from the morphometry parameters computed soil loss is found to be high in Upper Tuirial watershed, followed by Middle Tuirial, and the least by Lower Tuirial watershed. The morphometric parameters which are associated with different physical and geomorphological aspects of a river basin reveal the nature of soil erosion. In general, the morphometry parameters yield critical significant clues for the detection of soil susceptible to erosion in sub-watersheds.

The study suggests that the highly susceptible erosion prone zones must be treated with appropriate erosion control measures such as re-forestation, vegetative and mechanical practices. Government should execute strict rules and regulation for development and agricultural practices in those areas characterized by more than $45^{\circ}$ angle of inclination of slope. Similarly, restriction of site selection for shifting cultivation land

over relatively steep slopes is regarded as the most effective strategy to reduce fragile topsoil and nutrient loss from agricultural land.

The study also recommend that the shifting cultivation must be transformed into settled farm land to prevent further soil erosion. Shifting cultivation useful economic lifespan is about only one year, it is characterized by extensive clearing and burning of vegetation cover, consequence by exposures of bare land for generating direct influence on rainfall and surface run-off. Immediate elimination of this predominant tribal cultivation system may have significant direct impact on farmer economic activity, so it is unpractical in the present-day. To overcome this problem, in the first year of cultivation, sustainable agro-forestry such as growing horticultural crops, arecanut plantation, orange plantation, banana plantation etc., must be encouraged while practicing inter-mixed crops. These practices generously aid plants root and body for growing by utilizing the fertility of soil. These types of practices are substantially sustainable for farmer's economic livelihood as well as further degradation of forest area and intensity of erosion.

Implementation of cluster farming system is essential for minimization of soil loss. Within the Tuirial watershed, Aizawl is the only city practicing secondary and tertiary economic activity; all other villages are greatly reliant on primary activity. About 34 villages still continued shifting cultivation as dispersion within a village area, which must be clustered at suitable plot of land. Based on the elevation, arrangement of farming system has greatly reduced soil erosion. Suppose on the top of the slope, rearing animal or poultry farming etc., subsequent by agro-forestry plantation and close to the river channel are highly required watering of vegetable area must be implemented. In the meantime, animal waste will be useful for middle and the lower agricultural land to retrieve soil fertility and nutrient provider. On the other hand, practicing of contour farming, mulching, strip cropping and terrace farming along the slope will greatly reduce surface run-off energy and sustain nutrient and soil fertility.

The construction of house, quarrying sites, road construction and other developmental activities must require removal of huge landmass of topsoil, earth spoil are

dumped immediate to nearby construction sites which are fragile and easily washed away by surface run-off and flash flush transported toward the lowland and river bank reduces volume of water due to huge amount of sediment accumulation. Selection of proper earth spoil dumping site is required for minimization of soil erosion. The low lying area with distance from the river is suitable for earth spoil dumping site.

Soil and conservation department, environment and forest department, climate change cell, integrated water management department and national rural livelihood department from the government bodies must check regular interval at those sensitive zones of erosion. Cooperation of non-government organizations, village leaders, stake holders and local farmer is essential to prevent further soil erosion within the Tuirial watershed. In addition, it is necessary to provide financial assistance from the government for the construction, maintenance of erosion and sediment control such as terrace, contouring stripping, plantation, check dams and retaining etc.

The study also suggests that the implementation of 200 metres buffer zone on both sides of the main channel of Tuirial river, to maintain the volume of water throughout the year. Furthermore, this buffer zone will act as controlling factor of greater influx of sediments at Tuirial river towards the dam. Measurement the volume of sediment accumulation at the bottom of Tuirial dam is required at regular intervals for obtaining valuable information of reservoir storage capacity and live storage dead. Construction of sediment trap before reaching the dam is essential for preventing further accumulation of sediment. In addition, generation of sediment pits is required for flushing the accumulated sediment at the bottom of dam.